CRANFIELD INSTITUTE OF TECHNOLOGY

SCHOOL OF MECHANICAL ENGINEERING

Ph.D. THESIS

H.S.M. SALEH

The Influence of Fuel Structure on CO and NO_x Formation in Lean, Premixed, Hydrocarbon Flames

Supervisor : Professor R.S.Fletcher

September, 1978

ABSTRACT

A study is made of the influence chemical structure of fuel has upon combustion performance through tracing the generation of carbon monoxide and oxides of nitrogen in lean, premixed, hydrocarbon-air flames. The study includes both analytical and experimental investigations.

On the analytical side, a kinetic model is developed to predict both CO and NO time-histories in one-dimensional, premixed flames. The model is based upon the assumption of partial equilibrium in the post-flame zone while the fuel oxidation in the main reaction zone is allowed for by using a global oxidation rate equation. NO formation is assumed to be entirely via the Zeldovitch mechanism and to start in the post-flame zone. The utility of the model is judged through comparison between theoretical results and experimental data.

On the experimental side, a simple burner system, supporting a one-dimensional premixed flame was designed and built. All fuels selected for investigation were pure hydrocarbons representing the main hydrocarbon types usually found in practical fuels; namely paraffins, olefins, naphthenes and aromatics. The hydrogen-to-carbon ratio ranged from 1 to 2.67 and the carbon number from 3 to 12. The experiments were performed at 1, 2 and 3 atm pressure levels and 140^{o}C inlet temperature, while the equivalence ratio was in the range 0.6 to 0.9. Flames were sampled for most stable species by a water-cooled stainless steel sampling probe.

The experimental results show that the fuel structure significantly affects CO time-histories in the investigated flames mainly through influencing its generation rather than its burnout. CO burnout is shown to be mainly controlled by radical recombination processes, and the experimentally derived CO global oxidation rate equations are found not to be universally applicable. The results also show that the fuel structure influences prompt NO_x formation within, and very near, the main reaction zone but that it does not influence post-equilibrium NO_x formation if account is taken of differences in the flame temperatures. NO_2 is found to constitute a large percentage of total NO_x measured especially at lower temperature and equivalence ratios.

Comparison between experimental and theoretical results show that the prescribed kinetic model can satisfactorily predict CO levels for different fuels and under different conditions if the fuel oxidation global rate equation is correctly defined for different fuels. On the other hand, agreement between predicted and measured NO profiles has been obtained at atmospheric pressure only. At high pressure, the predicted levels were much smaller than those measured experimentally, and this disagreement is attributed to the fact that proper account is not taken of the NO and NO_2 formation kinetics in the main reaction zone.

ACKNOWLEDGEMENT

The author wishes to express his deepest gratitude to Professor R.S.Fletcher whose stimulating supervision, valuable guidance and encouragement have made the period of this work both rewarding and memorable.

The author is indebted to the Academic Staff of the School for their valuable help. Thanks are due to Mr.Pearman and the Drawing Office Staff.

Many thanks are also due to Mr.R.W.Stutchbury and the Technical Staff in the Departmental Workshop.

Finally, thanks and appreciation are due to Mrs.A.Allen-Rowlandson for typing this thesis.

CONTENTS

CHAPTER FOUR

CHAPTER FIVE

LIST OF TABLES

FIGURES

PLATES

NOTATION

A	frequency factor in the Arrhenius reaction rate constant expression
$A^{`}, A^{``}, a, B, B^{`}, b, c$	constants
C_p	specific heat at constant pressure
$\overline{c}_p$	mean specific heat at constant pressure
D.	diameter
E	activation energy
$E^{`}$	activation energy divided by the universal gas constant
F.B.P.	final boiling point
f	mass fraction
H	enthalpy
ΔH_a	enthalpy of atomization
ΔH_f	standard entalpy of formation per mole of compound
ΔH_r	standard enthalpy of reaction per mole of fuel
ΔH_{res}	resonance energy
ΔH_{rm}	standard enthalpy of reaction per kg mixture
Δh_f	standard enthalpy of formation per kg fuel
Δh_r	standard enthalpy of reaction per kg fuel
I.B.P.	initial boiling point
K_i	equilibrium constant of reaction i
k_i	forward rate constant of reaction i
k_g	global reaction rate constant
M	molecular weight
P	radicals pool
p	pressure

$\bar{R}$	universal gas constant
T	temperature
$\tilde{T_f}$	flame temperature
T_f	temperature at the end of the main reaction zone
T_i	inlet temperature
T_o	temperature at the burner surface
$\tilde{T_o}$	temperature at the end of the preheat zone
T_{th}	theoretical (undissociated) flame temperature
T_w	temperature measured by the thermocouple
ΔT_{rad}	temperature correction for radiation
t	time
u	velocity
X	mole fraction
x	distance along the flame axis
Y	NO yield from fuel nitrogen
Δ	increment of symbol appearing immediately following
ε	thermal emissivity
η	dynamic viscosity
λ	thermal conductivity
ρ	density
σ	Stefan-Boltzman constant
τ	residence time
ϕ	equivalence ratio

Subscripts

e	equilibrium
f	fuel
i	any arbitrary reactant component
i	initial conditions
m	mean value, mixture
o	reference condition

CHAPTER 1

INTRODUCTION

1. INTRODUCTION

For many years attempts have been made to relate the performance of combustion systems to the basic theory. One of the main obstacles in these attempts has been the modelling of the extremely complicated hydrocarbon combustion process. This process involves very rapid reactions occurring at relatively high temperatures which result in the destruction of the original hydrocarbon molecules and the formation of new products. The speed of these reactions depends upon temperature, pressure and the chemical structure of the original fuel molecule.

Differences in chemical structure of hydrocarbons exhibit their effect on the combustion process in several ways. The hydrocarbon. type, or class, can define the bond structure between atoms and hence the conditions necessary for destruction of these bonds in the combustion process. The number of bonds and their type define the heat of formation of fuel, which together with the hydrogen-carbon ratio, decide completely the flame temperature and equilibrium products for a specified initial temperature and pressure. The carbon number defines the size of the hydrocarbons molecule and hence controls the number of intermediate products formed before complete oxidation to final products. The increase of the carbon number also changes the heat of formation and the hydrogen-carbon ratio, and hence causes differences in chemical reaction properties among members of the same hydrocarbon type.

The importance of all these factors to the combustion process has been recognised for many years but as yet there is no means of quantifying their influence. As a consequence, it has become the practice to develop each combustion system to operate with a closely specified fuel and there is little flexibility in operation. Further, nearly all these fuels specificiations call for 'premium' fuels, that is those with high hydrogen-carbon ratio.

Within the last few years the increase in level of usage of liquid fuels in transportation in general, and gas turbines in particular, has led to greater dependence on the poorer, low hydrogen-to-carbon fuel sources, such as residual oils and in the future there will be a need to use tar sands, oil shales and liquid fuels derived from coal. These fuels have to be refined and hydrogenerated to meet both the present fuel specifications and, therefore, the requirements of the present combustors. This will represent a waste of energy and higher cost as refining losses can exceed ten percent. The other alternative is to learn more about the combustion characteristics of low hydrogen-to-carbon fuels so that it becomes possible to design combustion systems which are more flexible in operation and capable of burning these fuels in a clean manner. To create a reasonable balance between these alternatives, better understanding of the effect of fuel properties on combustion process is needed.

Many experimental programmes have been carried out in recent times on model and full-scale combustors to measure the effect of fuel properties, and although some success has been achieved, these programmes have provided very little in the way of basic understanding of direct links with the combustion and emission phenomena. The inherent complexity of the parameters involved prevents simple correlation between cause and effect. Practical correlations obtained are always functions of system design and have to be empirically determined. Adequate predictive techniques for the complex set of phenomenon involved just do not at present exist. In most cases the hydrogen-carbon ratio has been used to correlate fuel composition to performance and pollutants emissions, but this ratio alone cannot account for structural differences among these hydrocarbon compounds, and these are known to affect their combustion kinetics.

One of the difficulties that exist with practical fuels is that each consists of a mixture of an infinite number of pure compounds that belong primarily to the paraffin, olefin, naphthene, and aromatic families. Fuel specifications tend not to be too precise on chemical structure but it is clear that a better understanding of the behaviour of these fuels could be obtained if details of their composition were known. Each can be considered to be made up of mixtures of a limited number of basic hydrocarbon classes.

Apart from the difficulties encountered by the complexity of the chemical mix, the fuel burns over a wide range of conditions in practical combustion systems. In order to study the combustion process, it is obviously much simpler to not only use pure hydrocarbon compounds but also to premix the fuel and air before combustion to ensure that the conditions are homogeneous. Even in this simplified state, however, the reaction kinetics are still very complex.

The main aim of the present study is to investigate the effect of the fuel chemical properties on combustion performance through tracing the history of carbon monoxide (CO) generation and oxidation in different hydrocarbon air-flames. In addition to the importance of carbon monoxide to efficiency, it also represents a major pollutant specie. Little is presently known about carbon monoxide generation except that its history is strongly connected to hydrocarbon oxidation.

In addition to studying CO, the formation of oxides of nitrogen (NO_X) is also considered, with special reference to the influence of fuel type, as it is known that a considerable portion of these oxides (prompt NO_X) is formed near and within the main reaction zone, and that they are strongly influenced by fuel oxidation kinetics.

The study includes both analytical and experimental investigations. On the analytical side, attempts are made to model the CO and NO_X formation characteristics as a function of fuel structure. The success of these models is judged by comparison with experimental results. On the experimental side, a simple burner system supporting one-dimensional, laminar, premixed hydrocarbon-air flames was designed and built. Such a burner permits great simplification in

the combustion flow field which greatly aids analysis. The burner was designed to operate with both liquid and gaseous fuels and the sampling system was designed such that the flames could be probed for stable species at variable distances above the burner port.

The fuels selected for the investigation were all pure hydrocarbons and covered the main classes normally found in practical hydrocarbon fuels. These main classes are paraffins, olefins, naphthenes and aromatics. The carbon numbers of the fuels varied between 3 and 12, while the molar hydrogen-carbon ratio varied between 1 and 2.67. One practical fuel, kerosine, was also investigated to serve as a basis for comparison and assist in being able to make the results useful for practical combustor design.

Experimental runs were performed at pressure levels of one, two and three atmospheres absolute while the mixture inlet temperature for most runs was reasonably constant (410-415^{o}K). Tests were only made with lean mixtures, with the equivalence ratio ranging from 0.55 to 0.9. This range of conditions was selected as it is of general interest in the design of low emission combustors, especially for the gas turbine.

The study concludes with attempts being made to isolate the main points learned from the study that can be useful in the design of combustion systems.

CHAPTER 2

OVERALL OBJECTIVES AND METHOD OF APPROACH

2. OVERALL OBJECTIVES AND METHOD OF APPROACH

The present investigation is an engineering study aimed at producing results which can be applied to gas turbine combustors. It is primarily directed towards achieving a better understanding of the influence of the chemical structure of fuel upon performance and emissions at low power operating conditions, with attempts being made to quantify the effect in a manner which can be useful to design process.

THE MAIN OBJECTIVES can be summarised as follow:

a) By a study of the literature, isolate the main influence that fuel structure might have upon combustion and emission performance.

b) Attempt to produce engineering models to describe the controlling factors

c) Compare predictions from the models with newly-generated data and so refine the models.

The method of approach adopted was to burn premixed, pure chemical compounds and air mixtures over a range of pressure levels and to measure carbon monoxide and oxides of nitrogen profiles above the burner.

CHAPTER 3

HYDROCARBON FUELS AND COMBUSTION

3. HYDROCARBON FUELS AND COMBUSTION

For many years, almost all of the fuels for combustion engines have been derived from petroleum. However, as the world consumption of energy increases and world supply of petroleum decreases, the utilisation of other fuel resources such as coal, shale oil and tar sands will become increasingly important.

Petroleum itself is a complex mixture of large numbers of hydrocarbon compounds varying in physical and chemical properties and ranging from simple-structure gaseous molecules to heavy, tar-like, complex-structure compounds. It also contains various amounts of sulphur, oxygen, nitrogen, sand and water. The carbon percentage varies generally from 83 to 87% and that of hydrogen from 11 to 14%. Practical fuels are produced from petroleum or crude oil according to certain specifications and properties imposed by combustion systems and environmental requirements.

In this chapter, the interest is to briefly review fuel production, classification, specification and in particular to identify the influence of fuel properties upon the factors of interest to this study. These factors include primarily the flame temperature and species concentrations as they are known to control the levels of two chemical species of interest.

3.1 FUEL PRODUCTION AND SPECIFICATION

3.1.1 Important Hydrocarbon Classes in Crude Oil

The hydrocarbon compounds in crude oil belong mainly to the paraffin, naphthene and aromatic families with a smaller percentage of olefins. These families are classified broadly in Table 3.1.

a) Paraffin Family : This family constitutes about 30 to 40% of crude petroleum. Its members have an open chain structure with the general formula C_2H_{2n+2}. The simplest compound in the family is methane CH_4. Higher compounds are formed by replacing the hydrogen atoms by the methyl group (CH_3), and straight or branched chains are formed. Since they are saturated, paraffins are very stable and reaction occurs only by replacement when sufficient energy is available to dissociate the C-H bond.

b) Olefin Family : The olefin family has an open chain structure with the general formula C_nH_{2n}. This group consists of unsaturates, and mono-olefins having one double carbon bond. They are more reactive and combine readily with hydrogen to form paraffins or with oxygen to form smog; for this latter reason their content is limited in jet fuels.

c) Naphthenes : These compounds have a saturated ring structure with the general formula C_nH_{2n}. Although over 25% of crude is made up

Table 3.1 Important Hydrocarbon Classes (Types) in Crude Oil and Fuels Selected for Investigation.

Type or Class	Fuels Selected	H/C Mol.ratio	Carbon Number	Fuel Symbol
PARAFFINS	1.Propane C_3H_8	2.667	3	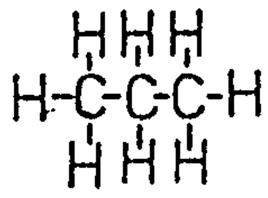
	2.Dodecane $C_{12}H_{26}$	2.167	12	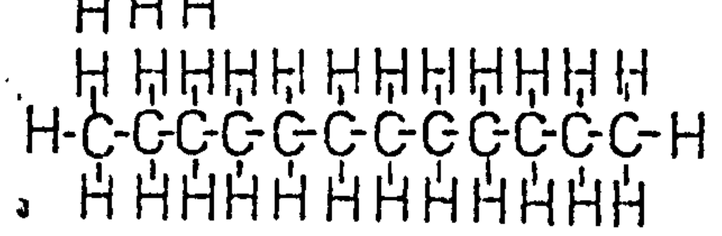
OLEFINS	1.Propene C_3H_6	2.0	3	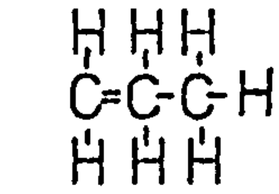
	2.Dodecene	2.0	12	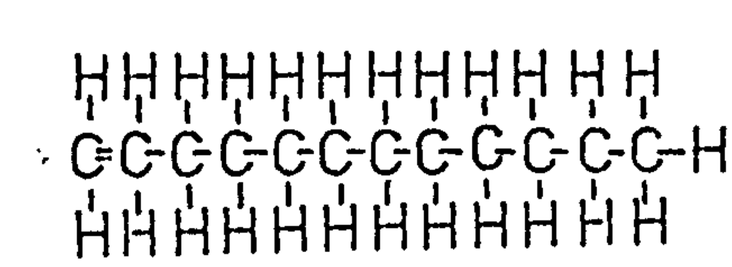
NAPHTHENES	1.Methylcyclo-hexane C_7H_{14}	2.0	14	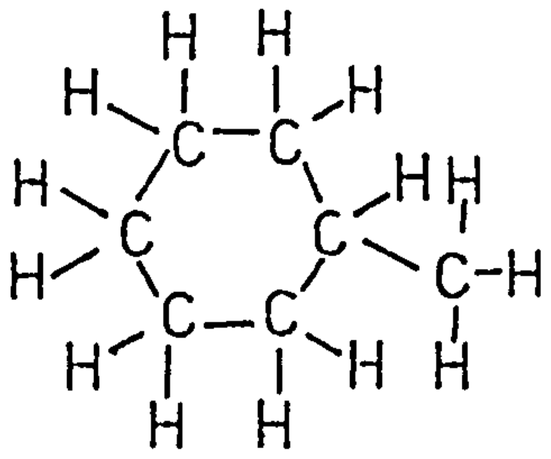
AROMATICS (Benzenes)	1.Benzene C_6H_6	1.0	6	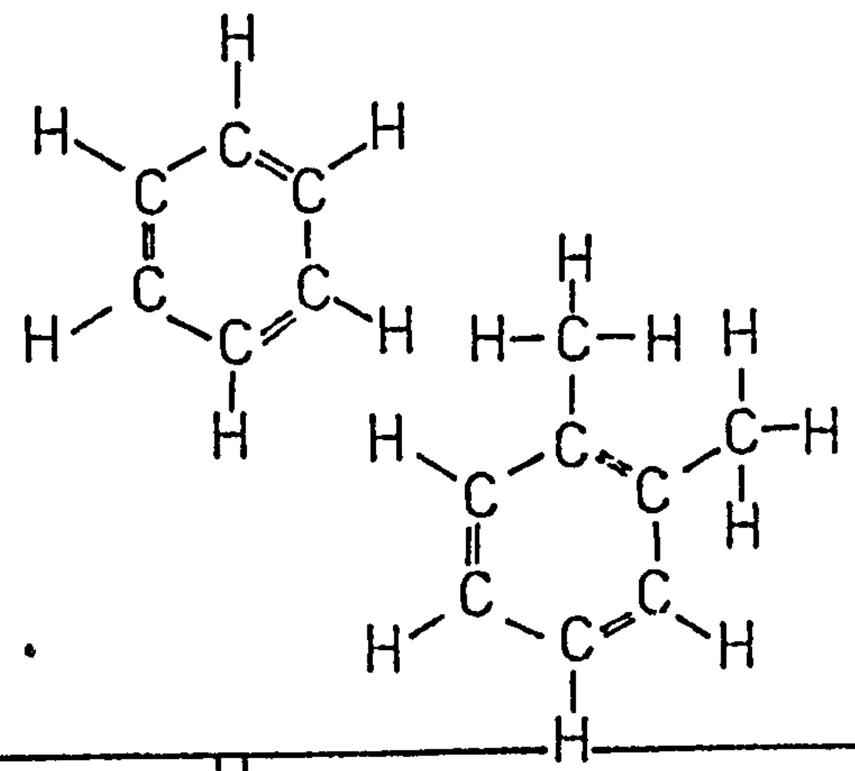
	2.O-xylene C_8H_{10}	1.25	8	
AROMATICS (Double Ring, Partially Hydrogenated)	1.Tetralin $C_{10}H_{12}$	1.2	10	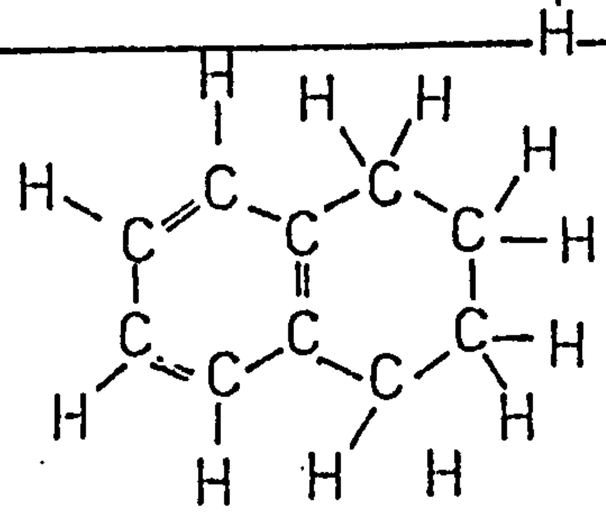
TYPICAL FUEL	Kerosine ($C_{13}H_{255}$)	1.96	—	MIXTURE (56.5% Paraffins 25.5% Naphthenes 17.7% Aromatics)

of naphthenes, apparently such compounds are still derived from either cyclo-hexane or cyclo-pentane with various side chains (usually a paraffin group replacing the hydrogen atom). They are very stable and have higher boiling and freezing points than paraffins and also higher ignition temperatures.

d) Aromatic Family (Benzenes) : Members of this family are unsaturated, ring-structured compounds with the general formula C_nH_{2n-6}. Although unsaturated, these compounds are stable due to large resonance energy involved in the formation of the aromatic ring. This stability causes the higher members of this family to be formed by the addition of side groups rather than ring expansion. When two or more benzene rings are fused or condensed, polycyclic aromatics are formed such as double ring naphthalenes (C_nH_{2n-12}). Aromatics have higher boiling points than other hydrocarbon families and readily produce smoke in burning, thus their content is limited in jet fuels. They also resist autoignition and are used to raise the octane number of gasoline.

3.1.2 Petroleum Refining and Production of Commercial Fuels

After removal of dirt, gases and sands from the crude, it is divided into fractions. In the first stage, separation, the crude is heated and sprayed into a very high tower containing trays at intervals. The temperature gradient in the tower causes the more volatile fractions to be collected in the top trays and the higher boiling point compounds to be condensed in the lower trays. The top fraction is called straight run gasoline followed by higher boiling point products which are classified as kerosine, gas oils, diesel fuels and gas oils (light distillate and heavy gas oils) respectively. The end products are lubrication oils and asphalt.

These straight run products are subjected to some alteration to match the demands made on the required products. This is done through different processes such as conversion by cracking and reforming, and treatment to remove sulphur and other contaminants. Details of these processes are given in many references, see for example References 1 and 2.

3.1.3 Practical Fuel Specifications

As stated before, the fuel is produced from crude oil and processed according to pre-stated specifications. These specifications include factors which could affect combustor performance as well as those affecting fuel storage, handling, safety and environmental conditions. Problems of fuel storage, handling and safety are related to fuel specific gravity and calorific value that control the tank capacity, pour point and viscosity that controls fuel flow in pipelines and the flash point which provides an indication of fire risk in storage.

Combustor performance, on the other hand, is affected by the ability of the fuel to burn completely and liberate most of its heat within the available residence time. Fuel atomisation and evaporation

are affected by viscosity and distillation while combustion time is dependent upon the fuel type which in turn can be defined practically by distillation and the specific gravity. The combustion temperature, however, is a function of the calorific value and the hydrogen content of the fuel as will be seen later.

The environmental requirements play an important role in fuel specifications at present. While some pollutants result from contaminants in fuel such as sulphur and nitrogen, other pollutants such as carbon monoxide, oxides of nitrogen, smoke and soot result from the combustion of the hydrocarbon fuel itself. Environmental legislations, however, restrict the content of contaminant in fuels as well as the percentage of some hydrocarbon classes that do not burn in a clean manner. Aromatics, as an example, that are smoky in burning are usually limited in jet fuels while olefins on the other hand are limited also in jet fuel because they unite with oxygen to form gum, and they are an important factor in smog formation.

Carbon monoxide in particular is dependent on fuel factors as well as on the combustor design and operating conditions. In combustion systems where large residence time is available such as boilers, furnaces, most CO can be oxidized provided there is no excessive cooling of the combustion products. In such combustion systems, slow burning heavy fuels can be used without risking excessive CO emissions. On the other hand, for combustion systems of limited residence time such as gas turbine combustors, only, easy burning light fuels can be used and if it is necessary to use heavy fuels, optimum operating conditions have to be specified to avoid excessive CO emissions; design alterations may also be required.

3.1.4 Kerosine and Future Gas Turbine Fuels

Kerosine is a typical commercial jet engine fuel known as Jet A or Jet A1 and has the specifications shown in Appendix A. It has a relative density of about 0.8 while the flash point is 310.8^{o}K and the boiling range between 423^{o}K and 523^{o}K with an end point of 561^{o}K. The hydrogen content is about 14% and it consists mainly of paraffins and naphthenes. A typical analysis shows it to contain about 56.5% paraffins, 25.5% naphthenes and 17.7% aromatics while the olefin content is about 0.3%. Based upon its hydrogen content, it can be represented by $C_{13}H_{25.5}$, but its physical properties are more equivalent to those of dodecane, $C_{12}H_{26}$. The boiling range for kerosine dictates that its paraffins must have carbon numbers within a range of 9 to 13, naphthenes carbon numbers must be greater than 7, and aromatics between 8 and 13.

Heavy-duty gas turbines also use less volatile fuels such as gas oil which has a relative density of 0.84 and about 13% hydrogen content. Heavier fuels, such as residual fuels of about 11.7% hydrogen content, are also being considered as gas turbine fuels.

In the near future, both aircraft and industrial gas turbines will depend strongly on synthetic fuels from non-petroleum sources. These fuels have a very high percentage of aromatics (40-80%) which means that the hydrogen content will be reduced to about 11%. The hydrogenation of these fuels to meet present fuel specifications will be costly and it may be more economic to use them in their high-aromatic state. Excessive combustion research is required, therefore, to be able to find ways and means of making such fuels more acceptable.

3.2 INFLUENCE OF THE CHEMICAL STRUCTURE OF FUELS ON THEIR COMBUSTION PERFORMANCE AND EMISSIONS

As commercial hydrocarbon fuels are in fact a complex mixture of a large number of individual organic compounds belonging to different classes or types, average properties such as specific gravity, hydrogen to carbon ratio (H/C) and calorific value have long been used to relate fuel combustion performance to its composition. Although some of these average properties, such as H/C ratio, have been useful in correlating performance and pollution parameters such as exhaust smoke levels and combustor wall temperature, it has failed to correlate the emissions of carbon monoxide, oxides of nitrogen and unburned hydrocarbons from both the internal combustion engines and gas turbine combustors as shown in the investigations carried out by Harrington et al (Ref.3) and Butze et al (Ref.4) and co-workers.

This is expected since the combustion performance and species formation depend upon the properties and the structure of the individual compounds forming the fuel. These components cannot be identified simply by defining the H/C ratio as, for example, all olefins and naphthenes have the same H/C ratio although they differ in structure and behave differently in the combustion process. For this reason, a study of the effect of the chemical structure on the combustion performance of individual pure hydrocarbons is more important to the understanding of hydrocarbon fuel combustion. The effect of the chemical structure on the thermochemical properties of pure hydrocarbons which controls the combustion behaviour, and hence flame temperature and exhaust species formation, will be briefly outlined below.

3.2.1 Effect of Chemical Structure on the Thermochemical Properties of Hydrocarbons

The chemical structure of any hydrocarbon can be defined completely by its type, and either the number of carbon atoms (carbon number, n) or the hydrogen-carbon ratio, H/C. The H/C ratio can be calculated from the carbon number for different fuel types as follows; (see Figure 3.1).

$$
\begin{aligned}
H/C &= 2 + 2/n && \text{for paraffins} \\
&= 2 && \text{for olefins and naphthens} \\
&= 2 - 6/n && \text{for aromatics (Benzenes)} \\
&= 2 - 12/n && \text{for naphthalenes}
\end{aligned}
$$

The importnat thermochemical properties which can be affected by the chemical structure are considered below.

a) The Standard Heat of Formations, ΔH_f

It is defined as the net change of enthalpy when one mole of fuel is formed from its elements at standard pressure and temperature. This change of enthalpy is equal to the difference between the energy required to atomize the original molecules of the elements into gaseous atoms, $\Sigma\Delta H_a$, and the energy liberated when carbon-hydrogen or carbon-carbon bonds are formed in the new molecules (bond dissociation energy), $\Sigma D(x\text{-}y)$, where x and y may be carbon or hydrogen atoms. In some cases an additional amount of energy is released during the formation to give more stability to the formed molecule, and this is called the resonance energy ΔH_{res}.

Hence the net heat of formation is given by

$$\Delta H_f = \Sigma\Delta H_a - \Sigma D(x\text{-}y) - \Delta H_{res} \quad \ldots\ldots \quad (3.1)$$

The heat of formation as calculated from equation 3.1 depends strongly upon the carbon-carbon or carbon-hydrogen bonds in the molecule and the type of these bonds. As the carbon number increases the number of bonds increases and the heat of formation decreases, see Figure 3.2. Also, at the same carbon number, the unsaturated compounds, which have multiple carbon-carbon bonds, such as olefins, aromatics and acetylenes, show higher heat of formation per mole than the saturated paraffinic compounds, and this can be attributed to the fact that double and triple carbon-carbon bonds have lower bond energy than the equivalent two and three carbon-hydrogen bonds respectively.

During combustion the fuel molecule is broken down and hence releases again its heat of formation, hence the heat of formation (or the enthalpy of formation) is an important factor in the net heat of reaction of combustion.

b) The Standard Enthalpy of Reaction ΔH_r

It is defined as the enthalpy change when one molecule of fuel at standard state is burned stoichiometrically with gaseous oxygen to produce gaseous CO_2 and liquid water (H_2O) at the same standard conditions of one atmosphere absolute pressure and 298^oK temperature. For the hydrocarbon molecule, C_nH_m the reaction equation will be:

$$C_nH_m + (n + m/4)\ O_2 \rightarrow n\ CO_2 + m/2\ H_2O$$

and the heat of combustion or the standard enthalpy of reaction can be

calculated as follows:

$$\Delta H_r = n(\Delta H_{fCO_2} + \tfrac{1}{2}(m/n)\ \Delta H_{fH_2O}) - \Delta H_{fC_nH_m} \quad \ldots\ (3.2)$$

as $m/n = H/C$

$$\therefore\ \Delta H_r = n(\Delta H_{fCO_2} + \tfrac{1}{2}(H/C)\ .\Delta H_{fH_2O} - \frac{1}{n}\ \Delta H_{fC_nH_m} \quad \ldots\ (3.3)$$

The standard enthalpy of combustion as calculated from equation 3.3 increases with the carbon number and for the same carbon number it increases with the H/C ratio as shown in Figure 3.3.

The standard enthalpy of combustion per kg fuel is given by:

$$\Delta h_r = \frac{1}{12 + H/C}\ (\Delta H_{fCO_2} + \tfrac{1}{2}\ .(H/C)\ .\ \Delta H_{fH_2O} - \frac{1}{n}\ \Delta H_{fC_nH_m}) \ldots\ (3.4)$$

It decreases slightly with the carbon number and for the same carbon number, it increases with the H/C ratio (Figure 3.3).

The heat of combustion per kg of the fuel-air mixture, ΔH_{rm}, is more important than the standard enthalpy of reaction. For stoichiometric combustion of the hydrocarbon C_nH_m with air and assuming all the products are in the gaseous phase at standard conditions, ΔH_{rm} can be expressed approximately by:

$$\Delta H_{rm} = -0.85(3.25 + H/C)/(4 + H/C)\ - 0.028(12 + H/C)\Delta h_{fC_nH_m}/$$

$$(4 + H/C)\quad \text{kcal/kg} \quad \ldots\ (3.5)$$

where $\Delta h_{fC_nH_m}$ is the heat of formation per kg fuel. The first term in equation 3.5 increases with H/C while the second term decreases, but generally the effect of H/C on ΔH_{rm} is very small and ΔH_{rm} decreases slightly as H/C decreases. On the other hand, ΔH_{rm} is directly proportional to the heat of formation per kg of fuel and varies in a similar manner with the carbon number for different hydrocarbon types (see Figures 3.4 and 3.2).

3.2.2 Influence of the Chemical Structure of Fuel on the Adiabatic Flame Temperature

The maximum temperature attainable in an adiabatic flame combustion process is called the adiabatic flame temperature. It is determined by a thermal balance between the enthalpy released by combustion of reactants and the rise in enthalpy of the resulting products. If the enthalpy of products at temperature T is H_T,

then the rise of the enthalpy of products, ΔH_T, is given by:

$$\Delta H_T = H_T - H_{298}$$

$$= \Sigma \overline{c_{p_i}} \cdot f_i . \Delta T \quad \ldots\ldots (3.6)$$

where $\overline{c_{p_i}}$ is the mean specific heat per kg of product i, and f_i is its mass fraction. This change of enthalpy will be equal to the heat or enthalpy of reaction per kg mixture, ΔH_{rm},

$$\therefore \quad T = \frac{\Delta H_{rm}}{\Sigma f_i \overline{c_{p_i}}} + 289 \quad \ldots\ldots (3.7)$$

If all the carbon in a fuel is burned to CO_2 and all the hydrogen to water, H_2O, the temperature of the product is then called the theoretical combustion temperature T_{th}. As the specific heat of H_2O is about twice that of CO_2, O_2 and N_2, then an increase in H/C ratio tends to decrease T_{th}, while the increase in the heat of formation per kg fuel increases ΔH_{rm} which in turn increases T_{th}.

In fact, this temperature is never attained because of the dissociation of both CO_2 and H_2O to carbon monoxide and hydrogen via the reactions:

$$H_2O \rightleftarrows H_2 + \tfrac{1}{2} O_2$$

$$CO_2 \rightleftarrows CO + \tfrac{1}{2} O_2$$

In this case part of the enthalpy available to raise the temperature of the products will be absorbed in CO and H_2 formation and hence a lower combustion temperature is attained which is called, in this case, the equilibrium combustion temperature or the adiabatic flame temperature, T_f. The effect of H/C on T_f is very complicated; since the tendency of dissociation of H_2O is less than that of CO_2, the degree of dissociation decreases as H/C increases and T_f tends to increase, but on the other hand as has been stated before, the increase of H/C increases the mean specific heat of the products of combustion which tends to reduce T_f. Generally, T_f decreases with H/C at the same carbon number as shown in Figure 3.5 where aromatic and olefins possess higher flame temperatures than hydrogen-rich paraffins. The standard heat of formation per kg fuel affects strongly the heat of combustion and hence the flame temperature. Figure 3.6 shows that T_f increases linearly with the heat of formation per kg fuel but different lines are obtained for different fuel types. Figure 3.6, however, suggests

that the heat of formation can be used as an average property of the practical fuel and it can correlate the adiabatic flame temperature within an error of $20^{o}C$. This error is relatively small compared with that which results when H/C is used, as for example, for constant H/C value of 2.0 (olefins and maphthenes) the adiabatic flame temperature varies by about $100^{o}C$. The adiabatic flame temperature can, however, be exactly related to fuel composition by a parameter which is a complicated function in both H/C and the standard heat of formation of the fuel.

The adiabatic flame temperature increases with the equivalence ratio until it reaches its maximum value at slightly rich mixture, then decreases again as shown in Figure 3.7. Increasing the initial mixture temperature tends to increase T_f but this increase in partially suppressed by dissociation effects especially near the stoichiometric point. For the same mixture strength, the flame temperature increases linearly with an increase in the initial temperature, as shown in Figure 3.8. On the other hand, as the pressure increase suppresses dissociation, T_f will increase with the increase in pressure, see Figure 3.7; the pressure effect is dominant only in the range on mixtures near stoichiometric where the flame temperature is highest and hence the degree of dissociation is also high, but for very weak and very rich mixtures the pressure effect is negligible.

3.2.3 Influence of Hydrocarbon Structure on Equilibrium Products of Combustion

When chemical equilibrium is attained in hydrocarbon combustion with air, the major products will be CO_2, H_2O and N_2 as well as O_2 in the case of fuel weak mixtures. At temperatures below $2000^{o}K$, where dissociation is not effective, CO_2, H_2O and O_2 concentrations will depend only on H/C and the equivalence ratio. As the temperature increases, the concentrations of H_2O and CO_2 are reduced due to dissociation. Figures 3.9 and 3.10 show that for different fuels (different H/C ratios) both H_2O and CO_2 increase linearly with ϕ for very weak mixtures (low T_f), but as ϕ increases, T_f increases and dissociation affects CO_2 and H_2O concentration. The rate of increase of both species with ϕ then diminishes.

The concentrations of minor species such as CO, O, OH and H in the equilibrium products of combustion depend on the degree of dissociation and hence on the equilibrium combustion temperature T_f. Figures 3.11 and 3.12 show that the mole fractions of all these species increases with T_f but the dependence seems to vary from one species to the other. OH seems to be less dependent on T_f than the other species while the H atom mole fraction is more strongly affected than the others.

At the same flame temperature and equivalence ratio, the fuel type will affect the concentrations of different species through its effect on the H/C ratio. While there is no effect of the fuel type on O atom, the OH, CO, and H mole fractions are influenced by the fuel type, though it is small. Both OH and H increase with the increase of H/C while CO decreases.

In the case of adiabatic combustion of different fuels at the same conditions (T_i and pressure), the final equilibrium temperature will depend on the fuel structure, see Figure 3.13, and hence the fuel effects on different species may be magnified or reduced. The fuel effect on equilibrium CO mole fraction becomes greater than in the case of constant T_f as shown in Figure 3.14. OH mole fractions are nearly the same for different hydrocarbons except propene which has high T_f and relatively high H/C ratio (see Fig. 3.15). O atom mole fraction in the equilibrium products of adiabatic hydrocarbon-air combustion varies with the fuel structure kind and this variation is completely due to variations in T_f.

Although the adiabatic equilibrium combustion temperature T_f (and associated species concentrations) may be approached in some practical combustors where the pressure and the temperature levels are high, in most cases it is never approached. Even in such cases, the equilibrium concentrations of species such as NO, shown in Figure 3.16, are never attained because their formation involves very slow reactions which need a long time to equilibriate.

For this reason equilibrium calculation, although useful in determining the combustion temperature and the concentrations of major species such as CO_2, H_2O and O_2, are of minor importance to the determination of the level of pollutant species such as NO and CO exhausted from practical combustion system. The study of the kinetics of the combustion process is more important in such cases; the fuel structure may be of greater importance in this case especially in the initial stages of combustion where the original molecule of fuel is destructed to form new products.

3.3 SUMMARY

The foregoing review and discussion can be summarised in the following points:

a) Practical fuels consist of mixtures of hydrocarbon components belonging to different types or classes, and in the present day fuels the presence of some types such as aromatics and olefins is limited due to performance and environmental considerations. In the fuels to be used in future, the percentage of undesirable compounds, such as aromatics, may increase and this may affect the fuel combustion process. The behaviour of different hydrocarbon types during the combustion process needs to be investigated so that combustors can be designed to burn these new fuels in a clean and efficient manner.

b) It is the practice today to relate combustor performance to the average fuel properties, such as H/C ratio, but it seems unlikely that these will adequately reflect the properties of individual compounds present in fuel, hence the resulting correlations will be poor. Correlating parameters must contain the controlling structural parameters such as fuel type, carbon number and heat of formation.

c) The adiabatic combustion or flame temperature, and the associated equilibrium products, depend on the fuel structure. They cannot be simply correlated with the H/C ratio of the fuel; the standard heat of formation per kg of fuel may correlate the adiabatic flame temperature much better, but exact correlating parameters need to be a complex function of both the heat of formation and H/C. Correlation of the species concentrations is more difficult; they depend on T_f as well as on the fuel type and H/C. The equilibrium concentrations of some species such as CO, OH, O and H are more dependent on flame tamperature than on H/C.

d) The equilibrium concentrations are of minor importance to air pollution, as the concentrations of both CO and NO rarely attain their equilibrium value in practical combustor. So the effect of the chemical structure of fuel on combustion kinetics must be studied if a full understanding of the combustion process is to be gained.

CHAPTER 4

CARBON MONOXIDE KINETICS IN LEAN HYDROCARBON-AIR FLAMES

4. CARBON MONOXIDE KINETICS IN LEAN HYDROCARBON-AIR FLAMES

4.1 INTRODUCTION

The level of carbon monoxide in the exhaust of combustion systems is a measure of the combustion inefficiency, and attempts are always made therefore to minimize its level. It is in addition classified as a pollutant species as it is very toxic. For these two reasons it is important that the factors influencing its level are fully understood.

Carbon monoxide (CO) is generated as an intermediary specie during hydrocarbon fuel oxidation in the early stages of the combustion process and then oxidizes slowly in the post flame zone. Although the generation of CO is very fast at high pressure and temperature conditions, it may take a significant time at low pressure, and low temperature conditions. In this case it is particularly important that CO generation and hence hydrocarbon oxidation rates can be quantified in terms of their controlling parameters. Both processes are extremely complex and only fully understood for a few simple fuels such as methane. Next to nothing is known about the details of the kinetic behaviour of the heavier organic fuels which are now more commonly being used.

The purpose of this chapter is to:

i) review the present knowledge of the hydrocarbon combustion and carbon monoxide reactions, and in particular to identify where changes in fuel properties may influence these reactions,

ii) develop a mathematical model which may be used to predict carbon monoxide levels throughout the different zones of a one-dimensional flat flame.

4.2 A REVIEW OF THE HYDROCARBON PYROLYSIS AND CARBON MONOXIDE GENERATION PROCESSES

These are the most complicated kinetic processes in combustion and cannot yet be quantified with any high level of accuracy. Many investigations have been carried out in the past whose common objective was to improve the understanding of the hydrocarbon combustion and develop kinetic models for these processes. An attempt is made below to describe briefly each process and the important work that has been done in the field so far.

4.2.1 Description of Processes

Although fuel oxidation is usually referred to as pyrolysis by combustion engineers, chemically, pyrolysis and synthesis mechanisms are different from the oxidation mechanism. In both cases, however, the reactions may be initiated by decomposition of the original hydrocarbon molecule.

The pyrolysis and synthesis mechanisms are very complicated and are not known with certainty even for the very simple hydrocarbons. In these mechanisms, the radicals formed through decomposition of the original molecules reacts to form ethylene and acetylene chains and further lengthening of these chains leads to the formation of unsaturated radicals. Dehydrogenation of these radicals results in the formation of polyacetylenes, while their reaction via cyclization results in the formation of C_6-C_2 aromatics compounds. Step-wise synthesis of these aromatic compounds leads to the formation of polycyclic organic compounds.

Although many studies have been carried out on hydrocarbon pyrolysis (e.g. Ref. 5 - 7), the details of most reactions involved are not known at the present time.

In the presence of oxygen, the radicals generated from the molecular decomposition of hydrocarbons, react with oxygen to form partially oxidized products. The nature of these products depends strongly on the temperature level. At low temperatures ($T < 1000^{o}K$), the oxidation mechanism is very complicated and the number of intermediate products is very large. It includes the generation of peroxides, hydroperoxides, aldehydes and peracids. Bradley (Ref.8.4) has proposed a low temperature mechanism for the hydrocarbon oxidation. The initiation of the chain reaction is assumed to occur via the reaction

$$RH + O_2 \rightarrow R + HO_2$$

where RH is the parent hydrocarbon molecule and R is a hydrocarbon radical. The reaction path followed by R depends upon the pressure, temperature, mixture composition and fuel structure. A good survey of low temperature hydrocarbon oxidation is given by Baldwin et al. (Ref.9).

At high temperature ($T > 1000^{o}K$), the mechanism differs significantly. The importance of many of the above mentioned intermediary species decreases while other species such as O, H and OH become the dominant chain centres. The dominant chain branching reactions at high temperature are the O_2 - H_2 propagating reactions (reactions (3) - (6) in table 4.1). Although many investigations have been carried out for this condition, the controlling kinetic mechanisms are known only for few hydrocarbons such as CH_4, C_2H_2, C_2H_4 and C_3H_8. Even for these simple hydrocarbons, there are regions of uncertainty, especially in mechanisms and rates of reactions involving intermediate compounds such as CH_3, C_2H, CH_2 and C_2H_5. For higher hydrocarbons, specification of the kinetic mechanisms is not possible at present.

Carbon monoxide is believed to be formed by a mechanism which does not vary with the temperature level and this mechanism is shown schematically below:

$$RH \rightarrow R \rightarrow RO_2 \rightarrow RCHO \rightarrow RCO \rightarrow CO$$

The final step of the reactions, RCO to CO, may occur via thermal decomposition:

$$RCO \rightarrow R + CO$$

or via the reactions:

$$RCO + O_2 \rightarrow RO_2 + CO$$

$$RCO + OH \rightarrow ROH + CO$$

$$RCO + O \rightarrow RO + CO$$

$$RCO + H \rightarrow RH + CO$$

At typical combustion temperatures, the decomposition reaction is considered to be the principle CO formation reaction.

4.2.2 Experimental Studies

Several studies have been made to investigate hydrocarbon combustion and associated CO levels in premixed flames and well-stirred or flow reactors. The most usual method employed has been to trace the combustion species inside the main reaction zone of one-dimensional, flat flames. As this zone is very thin and its thickness inversely proportional to pressure, studies of this kind are usually performed at very low pressures. Species traced depend largely on the sampling and analysing techniques.

Fristrom et al (Ref.10) traced the combustion products inside both the flame and the post-flame zones of a burner operating with C_2 hydrocarbon fuels and at a pressure level of 0.1 atmosphere absolute. The fuel was found to be consumed rapidly after an initial induction period and this consumption to be associated with a related quick consumption in oxygen. Carbon monoxide was found to be generated at a high rate as the fuel was consumed and to reach a maximum at a point where the fuel could be considered to have been completely consumed. The carbon dioxide formed up to the point of complete fuel consumption was slightly higher than half the maximum CO level, while the concentration of water (H_2O) approached its final equilibrium value. Other intermediary organic species also approached their maximum concentrations at the region of maximum fuel removal rate, but decreased in level very quickly and approached zero soon after the fuel was consumed. The results of this study confirmed the fact that the fuel is partially oxidised to CO and H_2O in the early stages of the combustion process.

Porter et al (Ref.11) measured the radical levels in the main reaction zone of premixed CH_4 and C_2H_2 - air flames under 8 mm Hg pressure. They found that, while the hydrocarbon radicals were formed and disappeared very quickly, other radicals such as OH formed equally quickly but their disappearance was much slower. This fact is of great importance to the carbon monoxide reaction rate in the post flame zone as will be shown later. Here again the measured maximum

CO level in lean flames was found to be less than twice the CO_2 level at the same point. They also found that the water concentration reached its maximum at the end of the main reaction zone and then decreased slightly in the post-flame zone. This was attributed to dissociation effects.

Westenberg et al (Ref.12) found, in 0.1 atmosphere C_2H_2 - O_2, C_2H_4 - O_2 and C_2H_6 - O_2 flat flames, that the appearance of OH in the flames preceeded that of O and H atoms. They concluded that the initial fuel attack may be through OH and the resulting radical then reacts with O_2. The maximum CO level in these flames was about twice that of CO_2 at the same point and depended on the flame temperature. The highest maximum CO levels were measured in the hottest flame which suggests that CO generation is more dependant on temperature than the oxidation process. Radicals measured in these flames allowed the evaluation of the rate constant of elementary reactions such as

$$OH + C_2H_6 \rightarrow C_2H_5 + H_2O$$

$$OH + C_2H_4 \rightarrow C_2H_3 + H_2O$$

$$OH + C_2H_2 \rightarrow C_2H + H_2O$$

However, the difficulty of measuring all species involved, hindered the construction of a complete hydrocarbon oxidation model from the experimental data.

Several studies have been also carried out on the combustion of premixed mixtures in stirred and flow reactors. Williams et al, (Ref.13) studied methane combustion in a conical stirred reactor. From their experimental data they were able to derive the following global rate equation for methane combustion to carbon monoxide:

$$\frac{-d(CH_4)}{dt} = 5.3 \times 10^{18} (O_2)^{0.5} (CH_4) (H_2O)^{0.5} e^{-57000/\bar{R}T} \quad .... \quad (4.1)$$

where ( ) denotes concentration in moles per cc and $\bar{R}$ is the universal gas constant.

Another global rate equation was derived for methane oxidation to carbon monoxide by Kozlov (Ref.14) from his experiments on a flow reactor. His rate equation, which is in the form:

$$\frac{-d(CH_4)}{dt} = 7 \times 10^{8} \cdot \frac{1}{T} (CH_4)^{-0.5} (O_2)^{1.5} e^{-60000/\bar{R}T} \quad .... \quad (4.2)$$

gives a lower oxidation rate than equation 4.1. This may be due to the lower temperature and equivalence ratios (0.05 - 0.17) under which the experiments were performed. The dependence of the fuel consumption rate on its concentration was found also to vary with the temperature level.

Methane removal rates have also been studied in turbulent flow reactors (Ref.15) at temperatures ranging from 1100 to 1400^{o}K and equivalence ratios in the range 0.05 to 0.5. The following rate expression was derived from these measurements:

$$\frac{-d(CH_4)}{dt} = 10^{13.2 \pm 0.2} (CH_4)^{0.7} (O_2)^{0.8} e^{-((48,400 \pm 1200)/\bar{R}T)}$$

mole/cc.sec. .... (4.3)

In this work, a very important conclusion was obtained. The reaction rate dependence on fuel concentration was found to vary from phase to phase during fuel consumption. In the early stages and within the induction phase the rate dependence on fuel concentration was negative while in the post-induction phase and during rapid consumption of fuel this dependence was positive. This means that the form of the global rate equations will depend on the region or the phase in which measurements are performed.

In summary, it is very clear that even for the same fuel, the experimental global rate equations as presently derived for hydrocarbon combustion depend upon temperature range, equivalence ratio range and type of apparatus employed. This tends to indicate that care must be taken to ensure that the equations are derived under conditions similar to those for which they are to be applied.

4.2.3 Predictive Models

Two rather different approaches are usually made to the prediction of CO generation in hydrocarbon flames. The first attempts to follow the histories of all species known to take part in the reaction and the other, a more simple and useful approach from the engineering point of view, attempts to follow just the very few species that are considered to control the heat release characteristics. More lately those models have been extended in an attempt to take pollutant species into account.

a) Models of Detailed Hydrocarbon Pyrolysis:

Full model studies have only proved to be successful for very simple hydrocarbons such as methane. These models must detail the early stages of the process known as the ignitions delay period, during which very slow reactions take place with little heat release. Chinitz's (Ref.16), methane model predicts ignition delay times which are very small compared to those measured experimentally. This is attributed to the partial equilibrium assumption made to allow for initial radical concentrations. In the model developed by Bowman et al (Ref.17), for methan oxidation also, the initiation of the reactions occur through high temperature decomposition of methane molecule to CH_3 and H. A similar model has been developed by Sorenson et al (Ref.18) for the ethane reaction.

Chinitz's model (Ref.19) for propane combustion contains kinetic mechanisms for different partially oxidized species. The model is very complex and contains 30 species participating in 69 elementary reactions. Calculations show that after termination of the ingnition delay period, a momentary over production of CO_2 results in a very short period temperature over-shoot. They also show that although the partially cracked fuels require a very short ignition delay, their combustion time is very large and the reaction time for hydrocarbons, generally, is as important as the ignition delay.

The complexity of this model for a relatively simple hydrocarbon suggests that any attempt to accurately model the pyrolysis of heavier hydrocarbons is likely to be unsuccessful today.

b) Simple and Approximate Models:

Several attempts have been made to simplify the oxidation mechanism of higher hydrocarbons. Kollrack et al (Ref.20) have approximated the pyrolysis of C_8H_{16} by three global reactions through which the fuel breaks down to a mixture of partially oxidized products such as HO_2, CO, CH_3, C_2H_4 and H_2CO. These species are then considered to participate in a detailed kinetic mechanism similar to that developed for simple hydrocarbons. A similar model has been proposed by Mosier et al (Ref. 21) for the combustion of JP - 5 fuel (taken as C_8H_{16}). The rate constant of the global reactions in this model have been determined empirically by fitting a rate equation to the experimental ignition delay data. These authors went on to produce a reduced partial equilibrium mechanism consisting of the following reactions:

$$C_8H_{16} + O_2 \rightarrow \widehat{C_8H_{16}}$$

$$C_8H_{16} + OH \rightarrow \widehat{C_8H_{16}}$$

$$C_8H_{16} + H \rightarrow 4C_2H_2$$

$$C_2H_2 + O_2 \rightarrow \tfrac{1}{4}\,\widehat{C_8H_{16}}$$

$$C_2H_2 + OH \rightarrow \tfrac{1}{4}\,\widehat{C_8H_{16}}$$

$$CO + OH \rightleftarrows CO_2 + H$$

where $\widehat{C_8H_{16}}$ is partial equilibrium products with all carbon as CO (excluding CO_2). The temperature rise was assumed to be proportional to CO_2/CO_2e and O_2, H and OH were calculated from equilibrium concentrations and the ratio CO/CO_2e, (where e denotes the final equilibrium value).

Attempts have also been made to produce more simple models. One of the earliest, single global reaction models was produced by Edelman et al (Ref.22) who assumed that the paraffinic fuels break-down to CO and H_2 by the following reaction:

$$C_nH_m + (n/2)\,O_2 \rightarrow nCO + (m/2)\,H_2 \qquad \ldots(1)$$

The fuel oxidation rates are then put in the form:

$$-d(C_nH_m)/dt = k_g\, f(T)\, p^c (C_nH_m)^a\, (O_2)^b\, e^{-E/RT} \qquad \ldots. \quad (4.4)$$

They assumed that the values of a and b were equal to 0.5 and 1.0 respectively and determined E to be equal to 13740 cal/mole. The values of k_g, f(t) and c were determined by comparing the results of this model (used with detailed H_2-O_2 Kinetics) and the detailed kinetic model of propane (Ref.19). The resulting equation was stated to be applicable to a temperature range of 800 to 3000^oK.

It must be mentioned here that, in deriving this equation, the ignition delays of all paraffinic hydrocarbons higher than propane are assumed to be equal (actually they agree only within a factor of 10 as shown in Ref.22). Even if this assumption is accepted, the equation may not be applicable to other hydrocarbon types. The rate equation given in table 4.1 was that used by Edelman et al (Ref.23).

Another global rate equation has been derived by Schefer et al (Ref.24) from experimental measurements of C_3H_8 oxidation rate in a premixed recirculating flow. The activation energy was found to be low and the equation predicts a higher C_3H_8 oxidation rate than is measured at normal combustion temperatures. This may be attributed to the fact that the kinetic parameters of this equation were evaluated at higher temperatures and equivalence ratios than those present in the combustion system where measurements were performed.

4.2.4 Summary

Having reviewed the most important work done in the field of hydrocarbon oxidation kinetics one can come to the conclusions that:

1 - The process is still poorly understood and a lot of work is needed.

2 - Most investigators agree that the main species which are produced from hydrocarbon oxidation are CO, CO_2 and H_2O, and all other organic intermediary species form and disappear very quickly.

3 - Experimentally-derived global fuel oxidation rate equations are dependent on the experimental conditions and are not generally applicable. They have been derived only for a few very simple hydrocarbons.

Table 4.1 Reaction Mechanism and Forward Rate Constants for $CO - O_2 - H_2$ System.

		Reaction	$k_f^* = a_i T^{b_i} e^{-E_i/T}$ $cm^3 \cdot mole^{-1}\ sec^{-1}$			
			a_i	b_i	E_i	Ref.
**	(1)	$C_nH_m + \frac{1}{2}(n+m/2)\ O_2 \rightarrow nCO + (m/2)\ H_2O$	$\frac{d(C_nH_m)}{dt} = -10^{13}\ (T/1111 - 0.5) \cdot p^{-0.815} (C_nH_m)^{0.5}\ e^{-12200/T}$			23
	(2)	$CO + OH = CO_2 + H$	$k_f = 6.76 \times 10^{10}\ e^{T/1102}$			35
	(3)	$O_2 + H = OH + O$	2.2×10^{14}	0.0	8.34×10^3	32
	(4)	$O + H_2 = OH + H$	1.4×10^{14}	0.0	4.75×10^3	32
	(5)	$OH + H_2 = H_2O + H$	2.19×10^{13}	0.0	2.59×10^2	32
	(6)	$OH + OH = H_2O + O$	5.75×10^{12}	0.0	3.93×10^2	32
***	(7)	$O + O + M = O_2 + M$	4×10^{17}	-1.0	0.0	32
	(8)	$H + H + M = H_2 + M$	1.5×10^{18}	-1.0	0.0	32
	(9)	$OH + H + M = H_2O + M$	4.0×10^{19}	-1.0	0.0	32
	(10)	$O + H + M = OH + M$	5.3×10^{15}	0.0	2.78×10^3	32
**	(11)	$O_2 + H + M = HO_2 + M$	2.0×10^{15}	0.0	-5.0×10^2	65
	(12)	$HO_2 + OH = H_2O + O_2$	5×10^{13}	0.0	5.0×10^2	48
	(13)	$HO_2 + H = H_2 + O_2$	2.5×10^{13}	0.0	3.5×10^2	48

* backward rate constant (k_b) is calculated from equilibrium constant.

** see text for rate constants used in the present study.

*** M is the total number of moles per cc.

4 - The detailed kinetic models are very complicated even for very simple hydrocarbons. The only useful instrument available for the heavier hydrocarbons is the simple single global reaction models, but they have yet to be experimentally determined for different fuels and different operating conditions.

5 - The importance of fuel structure in the combustion process has not yet been quantified.

4.3 A REVIEW OF THE CARBON MONOXIDE OXIDATION PROCESS

4.3.1 Description of Process

The carbon monoxide oxidation reaction is slow compared to the fuel reaction rate and therefore relatively easy to investigate experimentally. Many studies have been carried out on this reaction. The results have been expressed both in the form of a global reaction rate equation for CO oxidation in terms of stable species concentrations and also in a form of a kinetic scheme of elementary reactions. Each is considered in turn as well as methods of theoretical predictions.

4.3.2 Experimental Global CO Oxidation Rate Equations

Several experimental investigations have been carried out to study the carbon monoxide oxidation reaction. Due to the difficulty of measuring radicals and atomic species, the carbon monoxide oxidation rate equations have been, in most cases, put in the form

$$\frac{d(CO)}{dt} = -k(CO)^a (O_2)^b (H_2O)^c \; e^{-E/\overline{RT}}$$

Howard et al (Ref.25) reviewed the rate equations derived by many investigators using different burners and reactors, different fuels, different equivalence ratios, different pressures and temperatures over the range 840 - 2360^{o}K. They found that all investigators recommend that a should equal 1.0. The value of b was found to vary between 0.2 and 0.75 with the smaller values for lean mixtures, while the value of c varied between 0.0 and 0.5.

A comparison of CO oxidation rates computed from these different equations (see also Ref.26) shows a large degree of scatter. Although there is some degree of agreement between equations derived from low pressure flat flame experiments and those derived from stirred reactor experiments, rate equations derived from atmospheric flame experiments do not agree so well. These latter rate equations, whether they are derived from flat flames or bunsen flame experiments (Refs. 27 and 28), give very low oxidation rates compared to those calculated from other low pressure equations. This is surprising as carbon monoxide oxidation rate tends to increase with pressure. Fine (Ref.29) has proved that in

post-flame zone of premixed, flat propane-air flames, the carbon monoxide oxidation rate is proportional to $\sqrt{p}$. Howard (Ref.25) has shown that in flat, premixed, atmospheric methane-air flames, the carbon monoxide rate drops sharply in regions far from the luminous or primary flame zone. Experimental results of Singh et al (Ref.26) measured in low pressure C_2H_4 and C_2H_6 - oxygen flames, also show this change in CO oxidation rate especially in lean flames. In low pressure experiments, measurements can be performed in regions very near to the luminous zone (high CO oxidation rate zone), but in atmospheric and higher pressure experiments, measurements are mostly performed in the last stages of the CO burn out zone; this may explain the discrepancy between different global rate equations derived under different pressures as data applies to differing regions of the flames.

Howard et al have combined their own data with that of other investigators to derive the following general global rate equation:

$$\frac{dCO}{dt} = -1.3 \times 10^{14} (CO) (O_2)^{0.5} (H_2O)^{0.5} e^{-30,000/\overline{RT}} \quad .... \quad (4.6)$$

This equation is stated to be applicable in temperature range of 840 to 2360^{o}K but it also fails to predict the carbon monoxide oxidation rate in the last stages of burnout process (where the value of $(CO).(H_2)/(CO).(H_2O)$ approaches the water-gas equilibrium). A two step global mechanism, one to apply near the flame zone and the other to be used in the flame field, has been suggested by the authors to overcome this lack of agreement.

Global rate equations derived in the presence of fuel show a smaller oxidation rate than those derived in its absence (Ref.30). This behaviour can be attributed to the consumption of radicals, especially OH in reaction with fuel and other organic intermediary organic compound rather than in CO burnout and would suggest therefore, that different global rate equations should be used for CO oxidation inside, near and far from the main reaction zone. It also suggests that the fuel structure and hence intermediary species resulting from its oxidation would affect CO oxidation kinetics.

Notice must be taken also of the fact that the global CO oxidation rate equation derived by Singh et al (Ref. 26), differs from all these equations. The CO removal rate derived in that study was a simple first order reaction in CO as given by:

$$\frac{-d(CO)}{dt} = (K \text{ overall}) (CO) \quad .... \quad (4.7)$$

where (K overall) was found to be dependant on the equivalence ratio (greater values for lean mixutres) and fuel structure (greater K overall values for hydrogen rich fuels). It was found also to be proportional to OH concentration measured in the investigated low pressure, flat C_2H_4 and C_2H_6- oxygen flames. As the measurements carried out by Singh are mostly in the region just downstream of the main reaction zone, this

suggests that the fuel effect on CO oxidation extends outside the main reaction zone. The dependance of CO oxidation on fuel structure has been reported also for stirred reactor experiments carried out by Hottle et al (Ref.30) and Williams et al (Ref.13). At positions far from the luminous zone, Fenimore and Jones (Ref.27) found no effect of fuel type on CO burnout. This is to be as expected, for in these later regions the OH concentration is usually near its equilibrium value and, therefore, controlled mostly by temperature.

4.3.3 Elementary CO Oxidation Reactions

Most of the above mentioned investigators support the postulate that the primary path for the removal of CO is the reaction:

$$CO + OH \underset{k_{-2}}{\overset{k_2}{\rightleftharpoons}} CO_2 + H \qquad ...(2)$$

Few investigators have measured the hydroxyl radical in hydrocarbon flames (e.g. Refs. 11, 12 and 31) to determine the rate coefficient of this reaction. Boulch et al (Ref.32), in 1968, have critically reviewed all rate data for this reaction, which showed a large degree of scatter. They recommended the use of the following rate coefficient:

$$k_2 = (5.6 \pm 0.6) \times 10^{11} \; e^{-(1080 \pm 500)/RT} \; cem^3/mole\ sec \qquad ...(4.8)$$

but it was questioned by many investigators. While the experimental results of Singh et al (Ref.26) suggested that the actual value of k_2 must be about 2.7 times that given by Baulch expression, Dryer et al (Ref.33) have shown the non-Arrhenius nature of k_2. On the other hand, when Vandooren et al (Ref.34) used a supersonic molecular beam sampling technique to measure radicals in C_2H_2- O_2 flames, they derived the following Arrhenius type expression for k_2, applicable only for $T > 1000^oK$:

$$k_2 = 2.3 \times 10^{12} \; e^{(-5700/\bar{R}T)} \; cem^3/mole.\ sec. \qquad .... \qquad (4.9)$$

A more recent, non-Arrhenius type expression, has been proposed by Boulch et al (Ref.35) and found wider acceptance, where:

$$k_2 = 6.76 \times 10^{10} \; e^{T/1102} \; cem^3/mole.\ sec. \qquad .... \qquad (4.10)$$

A comparison of the different values of k_2 given by different expressions is shown in Figure 4.1.

In recent studies, Waldman (Ref.36) has suggested that the reaction:

$$CO + O + M \rightleftarrows CO_2 + M$$

can be important, although Fristrom et al (Ref.37) have neglected it on the ground of its slow rate. Other investigators (Refs. 32 and 38)

have shown that this reaction is insignificant in hydrocarbon-air flames where OH concentration is high and could influence only about 1% of total CO oxidation rate.

The hydrogen peroxide radical, HO_2, has been suggested by Westenberg et al (Ref.39) to play a role in CO oxidation via the reaction:

$$CO + HO_2 \rightleftarrows CO_2 + OH$$

This reaction has been also proved to be negligible by Vandooren et al, (Ref. 34).

4.3.4 Predictive Models for CO Oxidation ($CO-O_2-H_2$ Kinetics)

Excluding the fuel pyrolysis itself, the most important processes from the heat release stand point occuring in hydrocarbon combustion are as follow: a) the consumption of oxygen, b) the production of water (H_2O), and c) the production of CO.

The former two processes occur via the very fast $H_2 - O_2$ propagating reactions (Reactions (3) - (6) in table 4.1). Oxygen removal is via reaction (3) while H_2O production is via reactions (5) and (6). The fuel pyrolsis is thought to affect the level of O, H and OH radicals participating in these reactions.

In the final stages of reaction process (zones II and III in Figure 4.2), radical levels are controlled by recombination reactions (Reactions (7) → (13) - table 4.1). Reactions (11) → (13) involving the HO_2 radical have been proved to be very important to the recombination process (Ref.40). In lean flames, Fenimore (Ref.41) suggested that the only important recombination reactions are reactions (11) → (13), and if the reaction rate coefficient k_{11} is very small compared to k_{12} and k_{13} then the whole recombination process will be controlled by reaction (11). Recent measurements of radical levels in lean, sub-atmospheric, flat $CH_4 - O_2 - Ar$ flames (Ref.42) have shown that the most dominant recombination reactions are reactions (9) and (11).

One can make approximations of the $CO - H_2 - O_2$ kinetics by assuming different degrees of equilibration among reactions (3) → (13). Two approaches are commonly used for practical combustors and are discussed below:

(i) Full $O_2 - H_2$ Equilibrium Models:

When all $H_2 - O_2$ reactions shown in Table 4.1 are assumed to be in complete equilibrium, the radical concentrations can be easily calculated from:

CHAPTER FIVE

OXIDES OF NITROGEN FORMATION IN LEAN HYDROCARBON-AIR FLAMES

$$(OH)^2 = K_6^{-1} (H_2O) (O) \quad \ldots\ldots \quad (4.11)$$

$$(O)^2 = K_7^{-1} (O_2) \quad \ldots\ldots \quad (4.12)$$

$$(H)^2 = K_8^{-1} (H_2) \quad \ldots\ldots \quad (4.13)$$

where K_i equals the equilibrium constant of reactions (i) and the stable species can be determined from the mass balance equations. The model proposed by Westenberg (Ref.43) for fuel lean flames is based on this assumption as well as the postulation of instantaneous fuel pyrolysis to CO and H_2. Most heat is assumed to be liberated during the fast fuel pyrolysis and hence the temperature approaches its equilibrium value. In this case the concentrations of all species except CO and CO_2 may be predicted by normal equilibrium calculations. CO concentration after time t could be then given by:

$$(CO)_t = (CO)_e + ((CO)_i - (CO)_e) \cdot e^{-(zt)} \quad \ldots\ldots \quad (4.14)$$

$$\text{where } z = k_2 (OH)_e \left(1 + \frac{(CO)_e}{(CO_2)_e}\right)$$

In this equation, i denotes the initial conditions at t = 0 while e denotes the equilibrium conditions. Such an approach was adopted by Sheppard (Ref.44) to model a gas turbine combustor but he made no attempt to compare theoretical results with experimental data. The oxidation of carbon monoxide as predicted by this model depends strongly on temperature since it controls $(OH)_e$, k_2 and $(CO)_e$ levels. The assumption of constant flame temperature during the whole CO oxidation region will produce a very high oxidation rate for mixtures near stoichiometric, while the assumption of equilibrium concentration for OH will result in low oxidation rates for weaker mixtures than expected since the actual OH concentration in the early stages of CO burnout is several times the equilibrium value.

(ii) Partial Equilibrium Models:

As it has been shown before, radical species such as OH, O and H reach very high levels during the fuel oxidation and then decay slowly in the post flame zone. Determination of the true level of these radicals is very important for CO oxidation process. Many attempts have been made to calculate these levels by approximate methods. Bulewicz et al (Ref.45) have postulated that reactions (3) to (6) could be assumed to be in partial equilibrium or balanced, i.e. the multiplication of the products concentrations of each reaction divided by the multiplication of its reactants concentrations is equal to the equilibrium constant of that reactions as calculated from the local temperature. This state prevails at temperatures near to the maximum flame temperatures (i.e. in zones II and III in Figure 4.2). The individual concentrations, however, need not be equal to the equilibrium

values. Since that study there have been several investigators who validated this hypothesis for H_2 - O_2 - N_2 flames (Ref.46) and CO - H_2 - O_2 - N_2 flames (Ref.47). Other workers (Refs. 26 and 38) have questioned this hypothesis.

Biordi et al (Ref.42), when tracing the radical concentrations in low pressure, flat, premixed CH_4 - O_2 - Ar flames, found that reactions (2) - (6) were balanced only at temperatures very near to the maximum flame temperature. At lower temperatures, inside the main reaction zone, departure from equilibrium was found to vary from one reaction to the other. While reaction (6) is equilibrated within a factor of two or better even at relatively low temperatures, reaction (3) was further away from being equilibrated than any of the others.

If one applies the partial equilibrium assumption to reactions (3) - (6) then

$$(OH) = (K_3K_4)^{\frac{1}{2}} (H_2)^{\frac{1}{2}} (O_2)^{\frac{1}{2}} \quad .... \quad (4.15)$$

$$(O) = (K_3K_5) (H_2) (O_2)/(H_2O) \quad .... \quad (4.16)$$

$$(H) = K_5 (K_3K_4)^{\frac{1}{2}} (H_2)^{3/2} (O_2)^{\frac{1}{2}}/(H_2O) \quad .... \quad (4.17)$$

It is clear that since both O_2 and H_2O are major species in lean flames, the accuracy of the calculations will depend on the accuracy of H_2 concentration. Errors in measuring H_2 concentration can cause the calculated peak value of OH from equation 4.15 to be about 100 times the equilibrium value at equivalence ratios as low as 0.6, while the measured peak OH concentration (Ref.26) or that calculated from detailed kinetic model (Ref.48) at similar conditions is only about 7 times the equilibrium value. It should be mentioned here that the maximum to equilibrium ratio of OH, H and O concentrations increases as the equivalence tatio and the flame temperature decreases (Ref.48).

In theoretical predictions, the H_2 concentration is usually calculated from mass balance equations or the total number of moles constraints. Any small error in the major species concentration or in the total number of moles will greatly affect H_2 concentration.

Keck (Ref.49) avoided this problem by calculating the partial equilibrium products by minimising the free energy function of the system. Unequilibrated species reaction rates, mass balance equations and the change of the total number of moles are included as constraints on the system with the use of Lagrange multipliers. This model has been verified by Morr et al (Ref.50) in a region simulating the dilution zone of a premixed experimental burner but not in the region of fast, CO oxidation near the flame zone.

Several other assumptions have been made by other workers; though they do not represent in themselves complete mathematical models, they can be very useful when onetries to construct a complete mathematical model. They will be referred to in the next section.

4.3.5 Summary

From the above brief review of CO oxidation kinetics one can conclude the following:

1. The experimentally derived global CO oxidation rate equations have proved not to be universally applicable; they are applicable only to conditions for which they have been derived. Different equations have to be used for different regions in the flames.

2. CO oxidation is actually controlled by OH levels in different zones of the flame. Observed CO oxidation rate variations from region to region in the flame can, however, be attributed to variations in OH levels as proved in Singh's experiments. The assumption of constant equilibrium OH level during whole CO oxidation regions leads to false results.

3. Fuel structure affects CO oxidation through its influence on OH levels inside the main reaction zone and very near to it, where OH concentration is well above its equilibrium level. As most CO is actually oxidized in these regions, so the fuel effect can be very important. Few investigators, however, have paid attention to the influence of fuel properties and their results are conflicting. This subject is still to be clarified.

4.4 A MODEL FOR THE HYDROCARBON COMBUSTION IN A FLAT FLAME BURNER

In this section an attempt is made to construct a mathematical model capable of predicting CO levels in premixed hydrocarbon-air flames supported on a flat flame burner. It will consist of a kinetic model and a burner flow model, which will be assumed to be a one-dimensional flow.

4.4.1 Selection of Kinetic Schemes

In spite of the huge amount of work carried out on CO oxidation kinetics, contradictions still arise from time to time among the results of different investigators. The global models, although simple in use, are not too successful; the oxidation process is controlled by OH level which cannot be allowed for by using these models. It is also important to note the conflicting views on the effect of fuel on CO oxidation. These, it is believed, can all be explained if one assumes the model proposed below in which the flame is considered to consist of three zones, see Figure 4.2. In Zone I the fuel is oxidised and excess OH is generated but it reacts with fuel and intermediary organic compounds as well as CO; the rate of consumption of OH by fuel and intermediary compounds in this zone will affect CO oxidation rate. Zone II starts

at the end of the luminous zone and after most fuel is burned. An excess OH level exists in this zone and it is mainly reacting with CO but is also participating in the much slower recombination reactions. Zone III represents the last stage of CO burnout in which OH reached near equilibrium levels; the oxidation rates here are slower than in Zone II. It is believed that such a model can explain the results of all workers, as some tended to work predominantly in Zone II and others, like Fenimore (Ref.27), in Zone III.

It is important to note that this model suggests that if the global scheme is adopted, there should be three models, one for each zone. Further, we can expect fuel properties to exert some influence upon Zones I and II.

The kinetic schemes that will be adopted for different zones in the present study are not new, but are chosen from the literature according to accuracy and reliability. It is intended that further refinement of the mode will be made through compairson between theoretical predictions and experimental measurements.

In Zone I, a global fuel oxidation rate equation is assumed which is similar to that proposed by Edelman (see Table 4.1). As the partial equilibrium assumption is not valid in this zone (Refs. 42 and 51), the OH levels cannot be predicted and CO oxidation can be allowed for in this zone only by the use of a global rate equation for CO oxidation or CO_2 formation. The following equation, which was derived by Hottle et al (Ref.30), for CO_2 formation rate in the presence of fuel (propane),

$$d(CO_2)_{/dt} = 2.9 \times 10^{10} \cdot (CO)\ (O_2)^{0.35} \cdot (H_2O)^{0.4} \cdot e^{-(15,000/\bar{R}T)} \quad \ldots\ (4.18)$$

is used to predict CO_2 levels, and CO is calculated from the conservation of the carbon atom assuming the carbon in fuel is oxidised to CO and CO_2 only.

The partial equilibrium model is assumed to be valid in Zones II and III. Zone II starts at a point where about 95% of the fuel is burned and where the radicals concentrations are maximum. To avoid the calculation of the small H_2 concentration from mass balance equations and for reasons stated before, the radical pool principle (Ref. 41), is adopted here. The trace species (O, H, OH and H_2), though they remain equilibrated among themselves, are assumed to decay towards their equilibrium levels as a pool in Zones II and III. This pool (P) is represented by the weighted sum of the concentrations of these species,

$$(P) = 3\ (H) + 2(O) + 2(H_2) + (OH)$$

and the sum decays at four times the rate of the recombination reaction

irrespective of what they may be. Fenimore (Ref.41) has assumed that the whole recombination process, in lean enough flames, can be through reactions

$$H + O_2 + M \rightleftarrows HO_2 + M \qquad (11)$$

$$HO_2 + X \rightleftarrows HX + O_2 \text{ where } X \equiv O, H \text{ or } OH$$

If a steady state concentration is assumed for HO_2 (i.e. $d\,HO_2/dt = 0$) and if $k_{-11}(M) \ll k_{12}(OH)$, then the decay of O atom can be calculated from the following equation:

$$dy/dt = a\,(y^2 - 1)/(1 + by^{\frac{1}{2}} + c\,y) \quad .... \quad (4.19)$$

where

$$y = (O)/(O)_e ,$$

$$a = 8\,k_{11} \cdot (M) \cdot (O)_e/K_3 ,$$

$$b = 4 \cdot \left(\frac{(O)_e}{(OH)_e} + \frac{(H_2)_e}{(OH)_e} \right) ,$$

$$c = 9 \cdot (H)_e/(OH)_e , \text{ and}$$

(M) = the total number of moles of the system per cc.

The decay rate in this equation is completely controlled by the forward reaction rate coefficient of reaction (11), k_{11}. Instead of using similar equations for other species, they are calculated from the following relations recommended by Thompson et al (Ref.51).

$$\frac{(O)}{(O)e} = \frac{(H_2)}{(H_2)_e} = \frac{(OH)^2}{|(OH)_e|^2} = \frac{(H)^{2/3}}{|(H)_e|^{2/3}} \quad .... \quad (4.20)$$

Carbon monoxide oxidation rate can then be calculated from reaction (2) as follows:

$$-dCO/dt = k_2\,(OH)\,(CO) - k_{-2}\,(CO_2)\,(H) \quad .... \quad (4.21)$$

Other stable species such as CO_2, H_2O, O_2 and N_2 are calculated from the conservation of different atoms in the system (C, H, O and N).

To perform calculations in Zones II and III by the above described model, the initial concentration of O atom at the end of Zone I must be known. It can be calculated from relations 4.15 → 4.17 in connection with the total number of mole and different atoms conservation equation. This may lead to a large error in H_2 concentration (and hence in O atom

concentration) as discussed before and, therefore, O atom is calculated from the following relation recommended by References 52 and 53.

$$(O) = K_2K_3 \frac{(CO)}{(CO_2)} \cdot (O_2) \quad \ldots\ldots \quad (4.22)$$

4.4.2 Modelling of the Burner

The prescribed kinetic models are employed to predict CO levels in laminar flat flames. Laminar flames are usually affected by molecular diffusion and heat conduction in addition to chemical kinetics. While diffusion can affect the slopes of the profiles of the stable species such as CO, H_2O, O_2, CO_2 by about 5 to 20% only, the slopes of the profiles of radicals such as O, H, and OH can be affected more strongly. As all these species are determined by approximate methods, there is little point in introducing complicated diffusion equations in the present model. On the other hand, heat conduction exerts a greater influence due to its effect upon the reactant temperature in the preflame zone and, therefore, on the thickness of this zone.

In considering the level of heat release rate and resulting temperature profiles, flat flames can best be considered to consist of three main zones - the preheat, the luminous and the post-flame zone, (Ref.37). Each zone will be considered in turn and it will be assumed that the flame is one-dimensional (i.e. constant area).

a) Preheat Zone:

The preheat zone extends from the burner port to the luminous zone. Heat release in this zone is negligible but heat is transferred from the luminous zone and causes a temperature rise of the reactants, up to the point where ignition occurs and heat release starts at the upstream edge of the luminous zone.

Following references 37 and 54, if the heat release is neglected then:

$$\frac{d}{dx}\left(\lambda \frac{dT}{dt}\right) = \rho u \cdot \frac{dT}{dx} \sum \frac{f_i C_{pi}}{M_i} \quad \ldots\ldots \quad (4.23)$$

where x = distance along flame axis

λ = thermal conductivity of gas

f_i = mass fraction of species i

M_i = molecular wt. of species i

C_{pi} = specific heat at constant pressure of species i

ρ = density of mixture

u = velocity of mixture normal to the flame front

For a steady one-dimensional flow, the mass conservation equation and the spatial derivatives can be written in the form:

$$\rho_o u_o = \rho u \qquad \ldots\ldots \quad (4.24)$$

$$\frac{d}{dx} = u \frac{d}{dt} \qquad \ldots\ldots \quad (4.25)$$

Assuming no change in the number of moles in this zone, then the velocity is a function of temperature only:

$$u = u_o \frac{T}{T_o} \qquad \ldots\ldots \quad (4.26)$$

The mean specific heat c_{p_m} also replaces the term $\sum \frac{f_i \ C_{pi}}{M_i}$ using the following:

$$c_{p_m} = \frac{1}{T-To} \int_{T_o}^{T} \left(\sum \frac{f_i \ C_{pi}}{M_i} \right) dt$$

If, in addition, one postulates that

$$\frac{\lambda}{c_{p_m}} \ \alpha \ (T)^{0.75}$$

equation 4.21 can be integrated assuming

$$dT/dx = 0 \quad \text{at } T = T_o$$

The resulting equation, in terms of residence time (t) is:

$$dT/dt = (T - T_o) \ (c_{p_m}/\lambda)_o \ \left(\frac{T}{T_o}\right)^{0.25} \cdot (\rho_o \ u_o^{\ 2}) \qquad \ldots\ldots \quad (4.27)$$

where (o) denotes the initial conditions at the burner surface, while the value $(c_{p_m}/\lambda)_o$ is taken equal to that of air at the same temperature. The relation between c_{p_m}/λ and T depends, of course, upon the mixture properties, but for the purpose of the present study the assumption can be considered to be satisfactory.

b) Luminous Zone:

Defined as being the zone from the ignition point to the point where fuel is mostly consumed, it is the zone where main heat release occurs. The ignition point is defined as the point at which heat release becomes measurable. For the purpose of the present study, this point will be considered to be the point where the temperature reaches about $1200^{o}K$ (see Ref.55).

The thickness of the luminous zone is proportional to the inverse of the fuel oxidation rate. In models where instantaneous pyrolysis is assumed, the thickness of this zone is zero, and the temperature rises instantaneously to the value comparable to the kinetic model adopted. For a finite pyrolysis model, temperatures can be calculated from energy equations which implies that the specific enthalpy is constant since the flow energy is very small. Sometimes this is difficult because not all the species are considered or not accurately predicted in this zone.

Approximate methods for temperature calculation inside the reaction zone have been proposed by different investigators. The temperature rise is assumed to be proportional either to CO_2 formation (Ref.21), oxygen disappearance rate (Ref.56) or fuel burning (Ref.37). This latter assumption is adopted here and the temperature rise is calculated from the following relation:

$$\frac{\tilde{T_f} - T}{\tilde{T_f} - \tilde{T_o}} = \frac{f_{fuel}}{(f_{fuel})_o} \qquad \ldots\ldots \quad (4.28)$$

where f_{fuel} is the mass fraction of fuel at temperature T, and $\tilde{T_o}$ and $\tilde{T_f}$ are the temperatures at the commencement and the end of the luminous zone respectively. $\tilde{T_f}$ can be calculated by assuming certain percentage of heat release in the luminous zone. According to Fristrom et al (Ref.37) $\tilde{T_f}$ is about 95% T_f for type of flames investigated in the present study.

c) Post-Flame Zone:

The post-flame zone is often referred to as the CO burnout zone despite the fact that its temperature rise is mainly due to heat release resulting from radical recombination and only partially due to CO burnout. Temperature rise in this zone can be related to CO burnout (Ref.37) or to the decrease of the total number of moles of the system (Ref.52), which results from radical recombination. In the present study the first approach is followed and it is calculated from the following relation:

$$\frac{T - T_f}{\tilde{T_f} - T_f} = \frac{(CO) - (CO)_e}{\tilde{(CO)} - (CO)_e} \qquad \ldots\ldots \quad (4.29)$$

where T_f is the final flame temperature and $\tilde{(CO)}$ is the concentration of CO at the end of the luminous zone.

It should be noted here that in practice, the temperature in the post-flame zone may decrease due to heat losses to the surroundings. In this case, the measured temperatures are often correlated with time and used in the calculation when the results are to be compared with experimental measurements.

4.5 THEORETICAL PREDICTIONS AND COMPARISON OF MODELS

Different kinetic models, including the one proposed in the present study, have been employed to predict CO profiles in different hydrocarbon-air flames. The ability of different models to predict the CO time history, the influence of equivalence ratio and the influence of fuel structure are to be compared.

4.5.1 Calculated CO-Time Histories

The carbon monoxide-time histories as predicted by the different models for an atmospheric propane-air flame of equivalence ratio 0.8 and inlet temperature 400°K are compared in Figure 4.3. In all models the fuel pyrolysis to CO and H_2O are assumed to be instantaneous. CO oxidation rate, as predicted by both the full O_2 - H_2 equilibrium model or the partial equilibrium model proposed by Morr et al (Ref.50), remain constant during the whole post flame region (Zones II and III in Figure 4.2). This contradicts the experimental observations of many investigators, as mentioned before, which show that the CO oxidation rate varies through the region, depending upon the degree of equilibrium of OH. On the other hand, the CO-time history as predicted by the partial equilibrium model proposed for this study seems to follow this logic as the predicted oxidation rate decreases with the residence time in the post flame zone, i.e. as OH decays to its equilibrium level. It should be noted here that excessive initial CO concentration assumed in the calculations does not affect the time history as it is removed very quickly at the initial stages of oxidation (CO oxidation rate as calculated from reaction (2) is proportional to its concentration).

4.5.2 Effect of the Equivalence Ratio

The carbon monoxide levels in different adiabatic propane-air flames, predicted by using full O_2 - H_2 equilibrium model, are plotted in Figure 4.4. The predicted oxidation rates generally decrease with a decrease in the equivalence ratio and this is expected since the OH_e used in calculations decreases. These predictions however, contradict the results of Singh et al (Ref.19) and Ay and Sichel (Ref.49), which suggest higher CO oxidation rates in leaner flames due to higher degrees of OH overshoot (high OH_{max}/OH_e). Also the same kind of trends have been obtained when the partial equilibrium model of Reference 50 was used. This is due to the fact that this model fails to predict the higher degrees of overshoot of radicals.

When the present partial equilibrium model is used, a more acceptable result is obtained. The predicted CO oxidation rate as shown in Figure 4.5, increases at first as the equivalence ratio decreases, but as the equivalence ratio becomes smaller, the temperature decrease causes the oxidation rate to decrease.

4.5.3 Influence of Fuel Structure

Calculations have been made of the carbon monoxide levels after 2 milliseconds residence time in the post-flame zone for different hydrocarbon-air flames at atmospheric pressure and 400°K inlet temperature. If the full O_2-H_2 equilibrium is used, then the results are as shown in Figure 4.6. For each fuel CO level is shown to decrease with an increase in equivalence ratio until a maximum value is reached. It then increases again as the equivalence ratio is further increased. The equivalence ratio at which CO is minimum will be referred to here as ϕ_r and as is shown in Figure 4.6, the CO levels for $\phi > \phi_r$ are equal to the equilibrium values but for $\phi < \phi_r$ they are much higher. Figure 4.6 also shows that the differences in the values of ϕ_r for different fuels (except propene) are very small. As the critical equivalence ratio represents the minimum equivalence ratio at which equilibrium CO level is attained within the characteristic residence time, then the small differences in ϕ_r may indicate that the predicted CO oxidation rate is nearly the same for all fuels. This is to be expected as the fuel affects CO oxidation through its effect upon the super equilibrium concentration of OH and no radical overshoot is considered in this model. The oxidation in this model is only influenced by temperature.

When the present partial equilibrium model is used instead, differences between fuels become relatively bigger, see Figure 4.7, but not too significant. It should be noticed here also that for $\phi > \phi_r$, CO levels for different fuels are comparable to the calculated equilibrium values but not equal to them.

However, in all the above calculations, the CO generation time (fuel oxidation) has not been taken into account. When the global fuel oxidation rate equation of Edelman (Table 4.1) is used in the present model, the fuel oxidation time was found to vary with the equivalence ratio significantly as shwon in Figure 4.8. This has a large influence upon the shape of CO-ϕ relation and the position of ϕ_r as shown in Figure 4.9. It is possible that fuel may produce a significant effect upon CO level if it influences its generation time.

When the same global fuel oxidation rate equation is used with the partial equilibrium model to predict CO levels in propane-air and o-xylene/air flames at the same conditions, the results are surprising. Large difference in the critical equivalence ratio is predicted with o-xylene combustion being faster than propane, as shown in Figure 4.10. O-xylene, of course, is known to be slower in reaction than propane, which means that one cannot use the same global fuel oxidation rate equation for different fuels. Different equations must be needed for different fuels.

4.6 CONCLUDING REMARKS

From the survey it can be concluded that:

1. More has still to be learned about the fuel oxidation and CO generation process.

2. Carbon monoxide oxidation is strongly related to radical recombination processes and the use of approximate O_2-H_2 partial equilibrium models can give satisfactory results in modeling CO oxidation in the post-flame gases if carefully constructed.

3. Fuel oxidation rates exert a strong influence upon CO kinetics especially at low inlet temperatures and very weak mixture conditions. The use of the empirical global fuel oxidation rate equations seems to be the only way to account for this stage in combustion process.

4. These global rate equations for fuel oxidation are not universally applicable. It is suggested that new global models need to be established and expressed in terms of fuel properties, stoichiometry and temperature and pressure ranges to which they can be applied.

5. The influence of fuel structure needs to be extensively investigated. Few investigators have tried to quantify the influence on CO oxidation in the post flame zone but the range of fuels investigated so far has been confined to simple, gaseous, hydrocarbons. Higher hydrocarbons of various types have yet to be considered. The fuel effect is expected to be most dominant in the main reaction zone, and a single global fuel oxidation rate equation is not expected to apply for all fuels, even if they are burning under the same conditions. Different equations must be established for different fuels.

5. OXIDES OF NITROGEN FORMATION IN LEAN HYDROCARBON-AIR FLAMES

5.1 INTRODUCTION

Oxides of nitrogen formed during the combustion process represent a major problem in air pollution. The two major oxides emitted from combustion systems are nitric oxide, NO, and nitrogen dioxide, NO_2, while the total oxides of nitrogen are usually referred to as NO_x. Interplay between NO and NO_2 in the presence of hydrocarbons and sunlight results in the formation of brown smog. NO_2, which has been found in significant concentrations in gas turbine exhaust in recent years, is itself toxic.

Nitric oxide, NO, is usually the major component in NO_x and although NO_2 may be of equal importance in special conditions, all current theories consider NO_2 to form from NO. So in mathematical modeling, the prediction of NO is sufficient except when the NO/NO_2 ratio is required.

In flames and practical combustors burning hydrocarbon fuels in air, nitric oxide can be formed in one of the following ways:

i) Thermal NO
ii) Prompt NO
iii) Fuel NO

Thermal NO usually denotes the NO formed from reaction of nitrogen with oxygen at high temperatures in the latest stages of the combustion process, the "post-flame zone". Its kinetics is well understood and is separable from the complicated hydrocarbon combustion kinetics.

The term "Prompt NO" has been recently introducted to describe the observed NO formation in the main reaction zone, or very near to it, and at temperatures lower than those required for thermal NO to form. Its kinetics is not well understood as it is tightly connected to the hydrocarbon combustion kinetics and involves radicals and transient species whose levels cannot be either exactly measured or calculated at present. The effect of the fuel structure on prompt NO formation via its effect on radical levels, can be of vital importance, and has to be carefully investigated.

Fuel NO is formed from nitrogen released from the nitrogen-containing compounds in the fuel. It is formed at relatively low temperatures during fuel pyrolysis and oxidation (the main reaction zone). When considering future fuels such as residual oils and synthetic fuels from coal which contain nitrogen compounds, the fuel NO may be an important factor in total NO_x emissions.

The purpose of this chapter is to review the present knowledge of the kinetics of the oxides of nitrogen formation as well as predictive

models employed in theoretical calculations. In this review, thermal NO, prompt NO, fuel NO, and NO_2 are dealt with separately. A suitable model is also selected to predict NO_x levels in different premixed, flat, hydrocarbon-air flame and its ability to predict the effect of the fuel chemical structure and the operating conditions is studied.

5.2 THERMAL NO FORMATION

5.2.1 A Review of Thermal NO Kinetics

The mechanism of NO formation has been studied extensively for a long time; a good review of this aspect is given by Bowman (Refs. 57 and 58). The generally accepted mechanism for thermal NO formation in lean and near stoichiometric flames is that originally proposed by Zeldovitch (Ref.59) and consists of the following two reactions:

$$O + N_2 \underset{k_{-14}}{\overset{k_{14}}{\rightleftarrows}} NO + N \qquad \ldots\ (14)$$

$$N + O_2 \underset{k_{-15}}{\overset{k_{15}}{\rightleftarrows}} NO + O \qquad \ldots\ (15)$$

Fenimore and Jones (Ref.60) reported that their kinetic data obtained from premixed, flat, hydrocarbon-air flames agree with the data of Zeldovitch for lean flames and fit the form of his kinetic equation. However, they suggested that reaction (14) only is significant.

Singer et al (Ref.61) used the kinetic data of Zeldovitch (Ref. 59) and derived the following equation to predict NO level in lean premixed propane-air flames:

$$\frac{d\,NO}{dt} = 610 \times 10^2\, [N_2][O_2]^{0.5}\, \left(1 - \frac{[NO]^2}{[NO]_e^2}\right)\, \exp\left(-128000/\bar{RT}\right)(ppm/sec) \qquad \ldots\ (5.1)$$

where [ ] denotes mole fraction and e denotes equilibrium conditions while t is the time in seconds. The predicted NO concentrations from this equation were lower than those measured experimentally by a factor of 2 to 7, and the larger difference was in the case of rich flames. However, the predicted NO rate of generation in positions far from the flame was similar to that measured experimentally and this means that disagreement between predictions and measurements is mainly in the region very near to the flame.

Many other investigators have measured the reaction rate constants for reactions (14) and (15) and these data have been critically reviewed by Baulch et al (Ref.62) who have recommended the values given in Table 5.1.

In near stoichiometric and rich flames, Lavoie et al (Ref.63) found that the reaction:

$$OH + N \underset{k_{-16}}{\overset{k_{16}}{\rightleftarrows}} NO + H \qquad \ldots\ldots \quad (16)$$

can be important if the flames are held at high temperatures for long enough time. The rate constant for this reaction had to be indirectly determined. Campbell (Ref.64) evaluated the ratio of k_{16} to the backward rate coefficient of the following reaction (k_{-3}):

$$H + O_2 \underset{k_{-3}}{\overset{k_3}{\rightleftarrows}} O + OH \qquad \ldots\ldots \quad (3)$$

While Bowman (Ref.58) went on to calculate k_{16} using this value of k_{16}/k_{-3} and the value of k_{-3} measured by Baulch et al (Ref.65) at $300^{o}K$. Bowman also calculated the high temperature value of k_{16} from k_{-16} measured by Flower at al (Ref.66), Duxbury et al (Ref.67) and Bradley et al (Ref.68). He found that k_{16} is independent of temperature and recommended the value of k_{16} given in Table 5.1 which is consistant with those value of k_{16} calculated from transition state theory (Ref.69).

In stirred reactor experiments operated at low temperature ($T < 1500^{o}K$) and low pressure conditions, Bowman et al (Ref.70) found that the measured NO concentrations are about one order of magnitude higher than those predicted, using reactions (14)-(16) and a detailed kinetic mechanism for methane combustion. They supposed that other unknown reactions were responsible for this discrepancy. Malte et al (Ref.71) have proposed a bimolecular mechanism consisting of the following reactions to explain that extra NO formation:

$$N_2O + M \rightleftarrows N_2 + O + M \qquad \ldots\ldots \quad (17)$$

$$N_2O + O \rightleftarrows N_2 + O_2 \qquad \ldots\ldots \quad (18)$$

$$N_2O + O \rightleftarrows 2NO \qquad \ldots\ldots \quad (19)$$

$$N + O + M \rightleftarrows NO + M \qquad \ldots\ldots \quad (20)$$

Table 5.1 Extended Zeldovitch Mechanism and Rate Constants

Reaction	Rate constant (cm^3/mole sec)	Temperature range ^oK	Uncertainty	Ref.
(14) $O + N_2 \rightarrow NO + N$	$1.4 \times 10^{14} Exp(-37960/T)$	2000-5000	± 200%	57
(-14) $N + NO \rightarrow N_2 + O$	1.6×10^{13}	300-5000	± 200% at 2000-5000^oK	62
(15) $N + O_2 \rightarrow NO + O$	$6.4 \times 10^9 .T.Exp(-3150/T)$	300-3000	± 30% (300-1500^oK) ± 200% at 3000^oK	62
(-15) $NO + O \rightarrow N + O_2$	$1.5 \times 10^9 .T.Exp(-19500/T)$	1000-3000	± 30% at 1000^oK ± 200% at 3000^oK	62
(16) $NO + OH \rightarrow NO + H$	1.0×10^{14}	300-2500	± 80%	58
(-16) $NO + H \rightarrow N + OH$	$2.0 \times 10^{14} Exp(-23650/T)$	2200-4500	± 200%	66-68

When this mechanism was proposed, it was thought to be of practical interest only under conditions similar to those present in stirred reactor experiments. It may be important, however, in the low temperature region in lean flames at low pressures.

The importance of N_2O reactions (17)-(20) have been investigated in practical combustors and high temperature regions of flames ($T > 1800^oK$). Fletcher et al (Ref.72), Semerjian et al (Ref.73) and Thompson et al (Ref.51) have shown that reactions involving N_2O are not significant in high temperature conditions such as those existing in gas turbine combustors, turbulent flames and tubular combustors respectively. Sarofim et al (Ref.52) carried out experiments on premixed laminar, flat methane-air flames at temperatures higher than 1800^oK and again showed a negligible effect of reactions involving N_2O on NO formation.

5.2.2 Kinetic Modelling and Theoretical Predictions of Thermal NO

In lean flames only reactions (14) and (15) need to be considered in NO formation. If the N atom concentration is assumed in stationary or steady state, i.e. $\frac{d(N)}{dt} = 0$, then one can write:

$$k_{14}\,(O)(N_2) - k_{-14}\,(NO)(N) = k_{15}\,(N)(O_2) - k_{-15}(O)(NO) \quad \ldots\ (5.2)$$

and

$$(N) = \frac{k_{14}\,(O)(N_2) + k_{-15}(NO)(O)}{k_{-14}(NO) + k_{15}(O_2)} \quad \ldots\ (5.3)$$

where k_i and k_{-i} is the forward and backward reaction rate coefficients of reaction (i). NO formation via reactions (14) and (15) can be written as:

$$\frac{d(NO)}{dt} = k_{14}(N_2)(O) - k_{-14}\,(NO)(N) + k_{15}(N)(O_2) - k_{-15}\,(NO)(O) \quad \ldots\ (5.4)$$

From equation 5.2, 5.3 and 5.4 one can write:

$$\frac{d(NO)}{dt} = \frac{2k_{14}(O)(N_2)\ \left[1 - (NO)^2/K\,(N_2)\,(O_2)\right]}{1 + k_{-14}(NO)/k_{15}(O_2)} \quad \ldots\ (5.5)$$

where $K = k_{-14}\,k_{-15}/k_{14}k_{15}$

In near stoichiometric and rich flames, reaction (16) must be included and if reaction (3) is assumed to be equilibriated then equation 5.5 will tend to 5.6 (Ref.43):

$$\frac{d(NO)}{dt} = \frac{2k_{14}(O)(NO)\left[1 - (NO)^2/K\,(N_2)(O_2)\right]}{1 + k_{-14}(NO)/\left[k_{15}(O_2) + k_{16}(OH)\right]} \quad \ldots\ldots \quad (5.6)$$

The calculation of thermal NO formation rate using equation 5.6 requires the determination of the local values of temperature as well as O_2, N_2, O and OH concentrations. As the thermal NO formation is very slow compared to hydrocarbon combustion and occurs in the late stages of the flame, the concentration of these species can be assumed to be equal to their equilibrium values and the temperature to be equal to the maximum temperature of the flame. NO formation rates calculated this way did show an excellent degree of agreement with measured values taken from the post flame zone of laminar flames (Refs. 61 and 74), turbulent flames (Ref.73) and high pressure combustion vessel (Ref.75).

5.2.3 Effect of Operating Conditions and Chemical Structure of Fuel on Thermal NO Formation

The effect of both the pressure and the temperature on thermal NO formation have been studied by many investigators and it will be referred to briefly here before discussing the effect of the chemical structure of fuel.

i) Effect of flame temperature.

The large activation energy of reaction (14) reflects the strong dependence on temperature of thermal NO formation rate as given by equation 5.6. Moreover, the equilibrium concentration of O atom is a function in temperature (see Section 3.3). This means that as the temperature increases both k_{14} and O atom concentration increases rapidly and excessive levels of thermal NO are formed even for a very small residence time. This is clear in Figure 5.1 where the temperature effect becomes larger at high temperature levels.

ii) Effect of pressure.

As the species concentrations in mole per cc increases linearly with the pressure for the same temperature and mole fractions, then thermal NO formation might be expected to be proportional to pressure. However, in adiabatic flames, although the flame temperature increases with the increase of pressure, the degree of dissociation is reduced as the pressure increases and hence the mole fraction of radials such as O, OH and H decreases. Generally the predicted thermal NO levels, after fixed residence time in adiabatic flames, will be proportional to the pressure raised to the power 0.5 as shown in Figure 5.2.

iii) Effect of the equivalence ratio.

An increase in the equivalence ratio increases the flame temperature of adiabatic flames which results in an increase in O atom concentration (see Chapter 3.3) hence thermal NO formation rate must also increase (Figure 5.3). For non-adiabatic flames of the same flame temperature, thermal NO formation rate decreases with the increase of the equivalence ratio due to reduction in O_2 and hence O atom concentrations.

iv) Effect of fuel structure.

The fuel type affects the adiabatic flame temperature which is the important factor in thermal NO formation. Figure 5.3 shows the predicted thermal NO formed in the post flame zone of different hydrocarbon-air flames after 3 millisecs. All flames are assumed to have the same inlet temperature of $400^{o}K$ while the pressure is 1 atm. The adiabatic flame temperatures as well as the equilibrium concentrations have been calculated using the computer programme developed by Fletcher et al (Ref. 76) and NO was calculated from equations 5.6. It is clear that thermal NO levels are higher for flames burning fuels of higher adiabatic flame temperatures, and differences in thermal NO levels increase with the increase in the equivalence ratio due to temperature increase and increased effect of dissociation which increases the O atom concentration. As expected, thermal NO formed at the same residence time in the post flame zone of different hydrocarbon-air flames under the same conditions correlates well with the standard heat of formation of the fuel as shown in Figure 5.4. This can be attributed to the fact that the adiabatic flame temperature is strongly dependent on the standard heat formation of fuel (see Section 3.3). However, in lean, non-adiabatic, hydrocarbon-air flames of the same equivalence ratio and the same flame temperature, O atom concentration does not depend on the fuel type and hence thermal NO levels produced will be nearly the same for different fuel (Figure 5.5).

Alternatively, it is more practical to consider the effect of fuel type upon thermal NO formation when the temperature rise across the combustor is held constant. Calculations have been made for conditions similar to those that may be experienced in a gas turbine. The inlet temperature is assumed to be constant at a value of $400^{o}K$ while the final temperature is $2200^{o}K$ and the residence time in the post-flame zone is 5 milliseconds. These conditions may be achieved, of course, by ranging the equivalence ratio for different fuels. The effect of fuel type upon thermal NO is shown in Table 5.2.

It is clear that aromatic fuels produce more thermal NO than paraffins. This is due to the fact that aromatics have lower equivalence ratios for the same flame temperature and it has been shown before that for the same flame temperature, NO formation rate increases as the equivalence ratio decreases. There are also differences in thermal NO levels among the members of each hydrocarbon type but generally one can say that fuels of higher heat of formation per unit mass will produce higher thermal NO levels under these conditions.

Table 5.2 Thermal NO Formed After 5 Milliseconds in the Post-Flame Zones of Different Hydrocarbon-Air Flames, T_f = 2200°K, T_i = 400°K and p = 1.0 atm

Fuel	Equivalence ratio for T_f = 2200°K	Thermal NO formed after 5 ms (ppm)
a) Paraffins		
C_3H_8	0.87	77
$C_{12}H_{26}$	0.853	81
b) Olefins		
C_3H_6	0.813	89
$C_{12}H_{24}$	0.845	82
c) Aromatics		
C_6H_6	0.803	94
$C_{18}H_{10}$	0.823	88

5.2.4 Summary

From the above one can conclude the following:

a) Thermal NO formation is controlled by the flame temperature and the corresponding equilibrium O atom concentration which itself is a function of the flame temperature and the equivalence ratio only irrespective of the fuel structure.

b) The fuel structure may influence thermal NO formation through its effect on the flame temperature for constant equivalence ratio operation or through affecting the equivalence ratio for adiabatic combustion of the same inlet and flame temperatures.

The typical levels of this influence are:

(i) for adiabatic flames of the same inlet temperature the effect is very strong especially for equivalence ratios near stoichiometric where small differences in T_f increases thermal NO formation rate lagely. NO levels in this case can be related to the fuel structure by using the standard heat of formation per unit mass of fuel.

(ii) For non-adiabatic flames of the same equivalence ratio, inlet and flame temperatures (or adiabatic flames with varying inlet temperatures), no effect of the fuel structure on thermal NO will be expected.

(iii) For adiabatic flames of the same inlet and flame temperatures but ranging in the equivalence ratio fuel structure influences NO formation but at a much lower extent than in case (i).

5.3 PROMPT NO FORMATION

5.3.1 A Review of Prompt NO Kinetics

NO measurements in the post-flame zone of hydrocarbon-air flames carried out by Singer et al (Ref.61) and Fenimore (Ref.74) have shown that although the measured rate of NO formation agrees with that predicted from equation 5.6, NO levels themselves were higher than those predicted. Fenimore has shown that if NO profiles measured in the post-flame zone are linearly extrapolated back to the position of the burner surface, or zero time point, positive intercepts are obtained which means that NO forms at a very fast rate for a very short time within and very near to the primary reaction zone. Fenimore termed that rapidly formed NO as "prompt NO", and as he observed prompt NO in hydrocarbon flames only, he suggested that prompt NO formation may involve N_2 reaction with hydrocarbon fragments through reactions such as:

$$CH + N_2 \rightleftarrows HCN + N \quad .... \quad (21)$$

$$C_2 + N_2 \rightleftarrows 2CN \quad .... \quad (22)$$

with both N and CN going on to react further to yield NO. The levels of prompt NO measured by Fenimore especially at stoichiometric and slightly rich mixture can be significant even at conditions which are experienced in practical systems, hence numerous investigations have been carried out.

Bowman (Ref.57) made experiments on a shock tube using lean CH_4-O_2-N_2-A_r mxitures and he found that prompt NO formation can be explained by using the extended Zeldovitch mechanism (Reactions (14)-(16)) coupled with the detailed kinetics model of the fuel oxidation. In this case prompt NO formation is explained to be due to acceleration of Zeldovitch mechanism as a result of O atom concentration overshoot rather than due to other kinetic mechanism as suggested by Fenimore (Ref.74). Although Bowman's experimental and theoretical results agree fairly well (Figure 5.6), the agreement between his predicted prompt NO levels and those measured by Fenimore was not so good (Figure 5.7), especially for rich mixtures. This suggested that there is still the possibility of the existence of non-Zeldovitch mechanism which is responsible for prompt NO formation in rich flames.

Sarofim et al (Ref.52) have shown that the prompt NO formation in atmospheric, premixed, flat methan-air flames, of equivalence ratios between 0.89 to 1.15 can be explained to be due to O atom overshoot within and near the main reaction zone. In this study the species profiles have been measured inside the main reaction zone as well as the post flame zone. The O atom concentration has been calculated from measured stable species assuming either O_2-H_2 or O_2-H_2-CO partial equilibrium and NO formation rates have been calculated using equation 5.6. These rates agreed well with those determined from measured NO profiles near the main reaction zone.

Iverach et al (Ref.53) investigated both lean and rich hydrocarbon-air flames supported on a Meker burner at atmospheric pressure and found that although the O atom overshoot could explain prompt NO formation in lean flames, it failed to do this in the case of rich mixtures. They suggested that in rich flames prompt NO formation advanced via a mechanism similar to that proposed by Fenimore (Ref.74) and involving reactions (21) and (22). The very small concentrations of HCN and CN measured in lean flames (Ref.77) rules out the possibility of prompt NO formation via such mechnism at least under lean flame conditions where O atom overshoot may be the major factor in prompt NO formation.

Other investigators, such as Leonard et al (Refs. 38 and 78) reported that the O atom overshoot calculated from measured stable species and the partial equilibrium assumption, could explain prompt NO formation in lean, premixed, flat propane and methane-air flames under 2/3 and 1 atm pressures. Leonard's measurements showed also that the maximum NO

formation rate in lean flames as well as the maximum O atom concentrations falls outside the main reaction zone and this is very important as it suggests that prompt NO formation in lean and slightly rich flames can be treated separately from complicated hydrocarbon kinetics in the main reaction zone.

However, although many investigators now agree that the radical overshoot is responsible for prompt NO formation in lean and slightly rich flames, the non-zero levels of NO measured in the primary reaction zones of these flames remain unexplained.

Some investigators attributed them to the effect of the hot probe tip when inserted into the main reaction zones (Refs. 52 and 53), while others suggest that NO formation is initiated inside the main reaction zone via unknown reaction mechanisms and then it is accelerated due to O atom overshoot. Blauwens et al (Ref.79) suggested that prompt NO formation in lean flames can be via two mechanisms, the first is non-Zeldovitch mechanism involving HCN radical and reactions (21) and (22) and it is effective only in the main reaction zone while the other is the accelerated Zeldovitch mechanism which is effective at the downstream edge of the main reaction zone where the O atom concentration is maximum. The importance of each mechanism depends on temperature, pressure and equivalence ratio. It must be noted that little NO is formed in the flame front in lean flames.

5.3.2 Kinetic Modelling and Theoretical Predictions of Prompt NO

Most predictive models for prompt NO formations in lean flames are based on the assumption that prompt NO is mainly due to O atom overshoot. The involvement of hydrocarbon radicals in rich flames or in the main reaction zone of lean flames makes it difficult to predict prompt NO formed under these conditions. Bowman (Ref.57) and A, et al (Ref.48) used a detailed kinetic mechanism for methane combustion to predict the O atom concentration, while the extended Zeldovitch mechanism(reactions (14)-(16))was employed to predict NO levels at different residence times in the flame. The prompt NO levels were determined by linearly extrapolating the post-flame NO levels to the zero residence time point.

For higher hydrocarbons the detailed fuel kinetic mechanism cannot be employed and the O atom concentrations have to be calculated from approximate partial equilibrium models as those described before (see Section 4.3.3). An example of these models is that proposed by Sarofim et al (Ref.52) based on the assumption that the fuel can be assumed to be instantaneously burned to CO and H_2O and the temperature of this partial equilibrium is calculated from an enthalpy balance. Concentrations of species at this temperature are calculated from partial equilibrium assumption (see Section 4.4) and as the number of moles decreases to its equilibrium value via the recombination reactions, the temperature increases to its maximum value calculated by an enthalpy balance, assuming complete combustion of fuel to CO_2 and H_2O and neglecting dissociation (theoretical T_f). The assumption of the theoretical flame temperature, however, can affect the NO formation

strongly and it is better to use the dissociated adiabatic flame temperature.

Homer et al (Ref.40) used a similar model to predict NO levels in H_2-O_2-N_2 flat flames, and found that NO formation rate is strongly affected by the recombination rate of O atom and suggested that the recombination reactions involving HO_2 radicals must be included. The initial O atom concentration in their study was taken as input, while temperature rise was calculated from the recombination rate. An important result, drawn from Homer's investigation, is that for initial O atom concentrations greater than 0.3% the profiles of nitric oxide become insensitive to the initial levels of the O atom due to the accompanying low temperature. This means that the temperature is still more important than O atom concentration to NO formation, and whatever the levels of O atom inside the main reaction zone it cannot account for any significant NO formation.

Concerning the NO formation inside the main reaction zone, De Soete (Ref.80) has suggested the following empirical formula:

$$\frac{d(NO)}{dt} = k_c (O_2)^b (N_2) (fuel)_{\epsilon} e^{-E_a/\overline{RT}} \quad .... \quad (5.7)$$

where the value of b depends on the oxygen concentration and k_c, E_a were empirically determined. The validity of this equation has been checked in rich flames only and the observation of prompt NO formation in lean flames confirms the invalidity of this equation under these conditions. Experimental study however seems to be the only possible way for prompt NO investigation until a better understanding of the exact mechanism is achieved.

5.3.3. Influence of the Fuel Structure and Operating Conditions on Prompt NO Formation

i) Effect of Pressure and Temperature.

The effect of both pressure and the flame temperature on prompt NO formation has been studied by Heberling (Ref.81). He found that prompt NO has less dependence on temperature than thermal NO in accordance with the findings of Fenimore (Ref.74) and Eberius et al (Ref. 82). The temperature dependence was also found to vary with the equivalence ratio and when it was expressed as a pseudo-Arrhenious activation energy, it ranged from 35 Kcal/mole in lean flames to a minimum of 12 Kcal/mole at ϕ = 1.2 to 16 Kcal/mole at ϕ = 1.4. The pressure dependence was also found to vary with the equivalence ratio, with zero dependence at equivalence ratio of 0.8. At equivalence ratios 1.0 and 1.2, the pressure dependence of prompt NO could be expressed as pressure exponent of 0.2 but at ϕ = 1.4 the pressure dependence was found to be negative. This, however, contradicts the findings of Fenimore (Ref.74) who suggested that the pressure dependence of prompt NO increases as the mixture becomes leaner. Theoretical

predictions of Bawman (Ref.57) also show that prompt NO in lean flames is proportional to the pressure raised to the power 0.5. The situation is not clear. The increase in pressure increases the O atom concentration, in moles per cc, and hence increases prompt NO formation rate but on the other hand, it also increases the recombination rate and causes the O atom concentration to decrease rapidly and hence the time available for prompt NO formation is reduced. Also the profiles of NO, in lean flames, are not straight lines and this may lead to errors in experimental results and causes discrepancy among them. There is a possibility that the pressure affects the flame front NO very strongly and as this NO is not included in the theoretical predictions, it causes lack of agreement between measured and predicted pressure dependence of prompt NO.

ii) Effect of the Chemical Structure of Fuel.

The results of Fenimore (Ref.74) showed that there are differences in prompt NO levels measured in methane and ethylene-air flames of the same equivalence ratios and the same flame temperatures and these differences are more pronounced in rich flames. These differences can be attributed to differences in the chemical structure of fuel. A more specific study of the effect of the chemical structure of fuel has been carried out by Bachmaier et al(Ref.83) who measured prompt NO levels in different, adiabatic hydrocarbon-air flames supported on a Meker burner. For different fuels, prompt NO appears at a certain equivalence ratio which depends on the kind of fuel and as the equivalence ratio increases the prompt NO level increases to a certain maximum value before dropping again to zero level in very rich flames. The rate of variation of prompt NO with the equivalence ratio was found to depend on the fuel structure. The cyclic compounds were found to behave differently from the open chain structured compounds. In lean flames, the prompt NO levels were found to increase with the increase of the carbon number of paraffinic fuels, but for other types only one fuel was investigated from each type and no general conclusion can be derived. These measured differences in prompt NO can be attributed to the differences in the flame temperature or in the chemical structure of the fuel itself or to both. When Eberius et al (Ref.81) compared the prompt NO levels measured in adiabatic CH_4, C_2H_4, C_2H_2 and C_3H_8 - air adiabatic flames of the same flame temperature and equivalence ratio (flame temperature was varied by varying O_2/N_2 ratio), they found differences in prompt NO levels between flames burning different fuels and the levels of differences depended on mixture strength. While both lean propane and acetylene flames produced nearly the same prompt NO levels, rich acetylene flames produced about 50% more prompt NO than propane flames of the same equivalence ratio and flame temperature. Also while lean ethylene flames produced less prompt NO than propane flames, rich ethylene flames produced more prompt NO than propane flames under the same conditions. It was found also that differences of prompt NO levels produced in different lean hydrocarbon-air flames are much smaller than those present under rich mixture conditions. These differences can, however, be attributed to difference in NO formed in the flame front which is the dominant component in prompt NO in rich flames and is greatly affected by hydrocarbon pyrolysis and hence hydrocarbon type. In lean flame this flame front NO is very small and hence small differences in prompt NO were measured among different fuels.

5.3.4 Summary

From the above review one can conclude the following:

i) Prompt NO is formed via two mechanisms: the first is the accelerated Zeldovitch mechanism which is dominant in lean flames, the other is a non-Zeldovitch one which involves hydrocarbon radicals and is dominant in rich flames.

ii) Prompt NO is less dependent on the flame temperature especially in rich flames and there are a lot of contradictions concerning its dependence on the pressure.

iii) Fuel structure affects prompt NO formation through its effect on the flame temperature, super equilibrium concentration of O atom, and the levels of hydrocarbon radicals which contribute to prompt NO formation via the non-Zeldovitch mechanism. However no quantitative information can be derived from the few investigations that have studied this subject. Information about the effect of different fuels on prompt NO formation can only be obtained from experimental investigations, under conditions similar to those under which they are to be practically used.

5.4 FUEL NO

5.4.1 Significance of Fuel Nitrogen to NO Emission

There are a variety of nitrogen-bearing compounds contained in crude oil, residual oils and synthetic fuels. These compounds are categorized as:

i) basic, where the ring-structured organic molecule contains N atoms attached to its side such as pyridines and quinolines, and

ii) non basic, which contain the NH group instead of N atom such as pyrroles, indoles and carbazoles.

In most of these compounds the bond between N atom and the remainder of the organic molecule is much weaker than that which exists in the N_2 molecules and hence N atom can be liberated easily and oxidized to NO. For this reason fuel nitrogen can be an important factor in NO emissions. As an example, residual fuel oil has approximately 0.6% nitrogen and if all this nitrogen is oxidized to NO, it will develop a concentration level of about 12 gm NO/kg fuel or 200 ppm of NO in the exhaust gas of a combustor operating at an air to fuel ratio of 60.

5.4.2 Kinetics of Fuel NO Formation

Several investigations have been carried out to study the formation of NO from fuel nitrogen-containing compounds. It is generally agreed that the generation of NO from fuel N involves an intermediate compound

whose formation kinetics are not known. It is also believed that, in the primary reaction zone and at relatively low temperatures, these intermediate compounds are formed very quickly and react with oxygen containing compounds to form NO levels well above the equilibrium values. These high NO levels decay in the post flame zones at very small rates in lean flames and higher rates in rich flames, which means that the final yield or the percentage of fuel N that converted to NO is higher in lean flames. Fenimore (Ref.84) and de Soete (Ref.81) have proposed a mechanism in which primary fuel nitrogen compounds, Nf, react to form an intermediate compound RN which may be HCN, CN or NH or even N atom. This intermediate compound reacts with an oxygen-containing compound RO to form NO or with NO to form N_2 as shown in the following schematic form:

$$\text{Nf} \rightarrow \text{RN} \begin{cases} + \text{RO} \overset{ka}{\rightarrow} \text{NO} \\ + \text{NO} \overset{kb}{\rightarrow} N_2 \end{cases}$$

Fenimore (Ref.84) found that NO yield can be given by the following equation:

$$Y = \frac{NO}{(Nf)_o} = \frac{X}{(Nf)_o} \left(1 - \exp\left(-\frac{(NO) + (Nf)_o}{2X}\right)\right) \quad \ldots\ldots \quad (5.7)$$

where $(Nf)_o$ = total nitrogen compound in fuel expressed as ppm NO which would be produced if all fuel nitrogen is converted into NO, and X = maximum NO formed when NO formation becomes independant of added Nf. Fenimore suggested also that RO may be taken as OH and X may be taken to be equal to (ka/kb). RO.

A similar empirical correlation has been developed by de Soete (Ref.80) which may be written in the form:

$$Y = \frac{2}{\frac{1}{Y} - \underline{k}_{14}\,(Nf)_o / k_{15}(O_2)^b} - 1 \quad \ldots\ldots \quad (5.8)$$

where b is an empirically determined constant and RN is assumed to be the N atom, while the formation of NO and N_2 are assumed to be via reactions (14) and (15) respectively. In lean flames $k_{15}(O_2) >> k_{14}(Nf)_o$ and so if b is taken to equal 1, the yield Y will be equal to unity, which means complete conversion of fuel nitrogen to NO. The experimental results of de Soete, however, did not support this and the value of b was found to decrease as the oxygen concentration increases, i.e. as the flame becomes leaner.

A mathematical model for prediction of NO formed from fuel nitrogen was developed by Flagan et al (Ref.85) based on the partial equilibrium assumption which includes all possible species that participate in fuel NO formation as well as those usually found in hydrocarbon flames,

(CO, CO_2, H_2O, OH, O, H, O_2 etc.). Calculations showed that all fuel N is instantaneously converted into NO (Y = 1) and then NO decays in the post flame zone. The decay was very small in lean flames. The predicted results were improved upon when some constraints, such as the assumption of zero NO and N levels at the initial conditions, were considered but the model is still inapplicable to very rich and very weak flames.

Leonard et al (Ref.78) reported that the important intermediate in NO formation from fuel nitrogen is HCN, and NO formation in lean flames takes place in the region outside the main reaction zone. HCN, as they proposed, can be determined from the assumption of partial equilibrium of CN/HCN reactions at the edge of the main reaction zone.

However, dealing with NO formation from fuel nitrogen is beyond the scope of the present study. All fuels investigated here are pure, nitrogen-free, hydrocarbons.

5.5 NO_2 FORMATION

Equilibrium calculations show that a very small amount of NO_2 should be present in the products of hydrocarbon combustion. However, recent measurements in model combustors (Refs. 86 and 24) and gas turbine combustors exhaust (Ref.87) show NO_2 levels as high as 50 to 100 percent of the total NO_x in very lean mixture and low temperature conditions. Investigations carried out on premixed flat flames by Fenimore (Ref.88), Merryman et al (Ref.89) and Allen (Ref.90) have shown that large amounts of NO_2 are formed in the early stages of the flame and that amount decreases again outside the main reaction zone. NO_2 was also found to appear in the flame before NO. Merryman et al (Ref.89) have suggested that NO_2 is formed from NO via the reactions

$$NO + HO_2 \rightleftarrows NO_2 + OH \quad .... \quad (23)$$

$$NO + OH \rightleftarrows NO_2 + H \quad .... \quad (24)$$

with reaction (23) being favoured over reaction (24) due to its lower activation energy. The production of NO itself in the main reaction zone was supposed to be via the reactions

$$CN + O_2 \rightleftarrows NO + CO \quad .... \quad (25)$$

$$NH + O_2 \rightleftarrows NO + OH \quad .... \quad (26)$$

Outside the main reaction zone, both the reactions

$$NO_2 + O \rightleftarrows NO + O_2 \quad .... \quad (27)$$

and

$$NO_2 + M \rightleftarrows NO + O + M \quad .... \quad (28)$$

can be responsible for NO_2 consumption. Both Merryman et al (Ref.89) and Fenimore (Ref.88) found that the consumption of NO_2 in oxygen-rich flames measured experimentally is much smaller than that which may be predicted from reactions (27) and (28) while in fuel-rich flames, NO_2 was found to be completely consumed in the post-flame zone. However, the halt in NO_2 consumption in lean flames still needs further clarification. In practical combustors this halt of NO_2 consumption as well as the effect of quenching of reactions due to turbulent mixing of combustion products and cold air, can explain higher NO_2 levels in the exhaust gases. It is important, however, to note that the very high rate of reaction (23) even at room temperature suggests that it may proceed in the sampling probe and the sampling system, and due to the presence of high concentration of HO_2 which results from sudden quenching of O and OH radicals in the probe, the formation of NO_2 may occur in the sampling line. Allen (Ref.90) has also suggested that NO may react with O atom on the probe wall to form NO_2 via the following reaction

$$NO + O \xrightarrow{wall} NO_2 \quad .... \quad (29)$$

For that reason, Tottle et al (Ref.91) have pointed out that the measurements of NO in reacting mixtures, using probe techniques, are subjected to large errors. Until further investigations on NO_2 formation are conducted, preferrably by use of methods other than sampling probe techniques, the NO_2 kinetics will still not be completely understood. On the other hand, whether NO_2 is formed in the flame or in the probe, the measured levels of NO_2 in the early stages of the flame suggest that NO formation starts in the main reaction zone even in very lean flame and it is oxidized completely into NO_2 in this zone. The reconversion of NO_2 to NO downstream the main reaction zone suggests that even in this region NO formation rate measured experimentally must be higher than that calculated from accelerated Zeldovitch mechanism, and NO produced from NO_2 conversion must be taken into account, which is a very difficult job at present. As a consequence, results of experimental measurements are better reported as total oxides of nitrogen, NO_x.

5.6 SELECTION OF MATHEMATICAL MODEL FOR NO PRODICTION IN PREMIXED LEAN FLAMES

This study is interested in lean, premixed, flames burning nitrogen-free hydrocarbons where NO can be formed from atmospheric nitrogen only. In lean flames prompt NO formation through Zeldovitch mechanism is dominant while that portion formed inside the main reaction zone via non-Zeldovitch mechanism is small. The formation of this later NO also involves hydrocarbon fragments which cannot be predicted unless a detailed kinetic model of fuel pyrolysis is employed. This is not possible for the fuels to be investigated in the present study. NO_2

kinetics are connected with NO formation in the main reaction zone and hence cannot be considered in the present theoretical study.

5.6.1 Description of the Kinetic Model

NO formation, whether near or far downstream the main reaction zone, is assumed to be via the extended Zeldovitch mechanism (reactions (14)-(16) in Table 5.1). The prompt NO formation inside the main reaction zone is assumed to be negligible in the investigated lean flames. Based on this assumption, the NO formation rate can be calculated from equation 5.6 and NO profiles can be predicted from integrating this rate equation with respect to residence time in the flame. This equation, however, is to be coupled with the burner flow model and O_2-H_2 partial equilibrium model described in section 4.4 which predicts the temperature, as well as the concentration of O, O_2, N_2 and OH. As the partial equilibrium assumption and hence O atom concentration prediction is assumed to start at the downstream edge of the primary zone, the present model will not detect any NO levels inside the main reaction zone. Typical results of theoretical predictions of NO levels using this model are presented below. Because the global fuel oxidation equations for different fuels are not exactly known, fuel is assumed to burn instantaneously to CO-and H_2O in all these predictions.

5.6.2 Theoretical results

a) Predicted NO versus time histories

Figure 5.8 shows the NO profiles predicted for different propane-air flames at atmospheric pressure and an inlet temperature of 400^{o}K. It is clear that the partial equilibrium model which allows for O atom overshoot, predicts faster NO formation rates than those obtained when assuming O atom concentration to be equal to the final equilibrium value. However, as equilibrium is approached, the NO formation rate decreases and it finally becomes constant and equal to that calculated using equilibrium O atom concentration. Extrapolation of that linear portion of the profile to the zero time point will result in a positive intercept which is considered as prompt NO in this study. However, the prompt NO is affected by the O atom recombination rate which in the present model is controlled by the forward reaction rate coefficient of the reaction (see Chapter 4.4).

$$O_2 + H + M \underset{k_{-11}}{\overset{k_{11}}{\rightleftarrows}} HO_2 + M \qquad \ldots\ldots \quad (11)$$

Values of this rate coefficients as reported in literature, vary by a factor of 6. It is important here to check the effect of k_{11} on NO predicted profiles. As this rate constant has a very weak dependence on the temperature, two extreme constant values of k_{11} have been used to predict NO profiles in a lean propane-air flame of equivalence ratio 0.8. The first value of k_{11} chosen is 2.0×10^5 that was used by Ay et al

(Ref.48) while the other is 1.2×10^{16}, reported in the Leeds tables (Ref.32); the results are shown in Figure 5.9. It is clear that NO profiles and hence prompt NO levels predicted by the present model can be strongly affected by the value of k_{11}. However, a more recent value of k_{11} reported by Fenimore et al (Ref.41) and Biordi et al (Ref.42) show it to be about 5×10^{15} with M, in reaction (11), taken as the total number of moles of the mixture per cc. This is to apply to equivalence ratios around 0.75 and temperature range of $1750 \pm 150^{o}K$. The value will be checked in this study through comparison between experimental and theoretical results.

b) Influence of the Equivalence Ratio

Figure 5.10 shows that for fuel lean benzene-air flames, prompt NO increases with an increase in the equivalence ratio and this agrees well with trends observed by Bachmaier et al (Ref.83).

The measured prompt NO values are smaller than those predicted theoretically because of the fact that Bachmaier's measurements were made with the feed mixture to the burner at ambient temperature while predictions are based on an inlet temperature of $400^{o}K$. For rich flames, as expected, the predicted prompt NO levels are smaller than those measured experimentally due to the fact that this model does not predict flame front NO which constitutes a large percentage of total prompt NO under these conditions. Similar conclusions have been reached by Ay et al (Ref.48) who used a detailed kinetic model for methane combustion, but they did not consider NO formation by non-Zeldovitch mechanisms in the main reaction zone.

c) Influence of the Chemical Structure of Fuel

Figure 5.11 shows prompt NO levels predicted for different hydrocarbon air flames, plotted as a function of the equivalence ratio. All flames are assumed to be adiabatic and the fuel oxidation to CO and H_2O instantaneous. It is clear that higher prompt NO levels are predicted for higher temperature flames and this means that the chemical structure of the fuel affects predicted NO level through its effect on the flame temperature. Differences between prompt NO levels for different fuels are not so pronounced as differences in thermal NO levels shown in Fig.5.3. This may be due to the fact that although the temperature rise increases the rate coefficient in equation 5.6 and the equilibrium O atom concentration, the degree of O atom overshoot ($\frac{(O)_{max}}{(O)_e}$) decreases as the flame temperature increases at the same equivalence ratio (Ref.48) and hence small differences in prompt NO are obtained.

When the flame temperature is kept the same for different hydrocarbon-air flames at the same equivalence ratio, the differences in prompt NO predicted in these flames are negligible as shown in Figure 5.12. This contradicts the results of Eberious et al (Ref.82), who found small differences in prompt NO measured in different hydrocarbon-air falmes of same equivalence ratio and same flame temperature.

These differences can be attributed either to the errors in determining experimental prompt NO in lean flames as discussed before, or due to the flame front prompt NO which cannot be predicted by the present model and which may be affected strongly by the fuel type.

5.7 CONCLUSIONS

From the foregoing review of NO_x formation kinetic and the results of preliminary theoretical predictions, one can conclude the following:

1) Total NO formed in hydrocarbon-air flames consists of thermal NO which is formed in the post-flame zone at high temperature, and prompt NO which is formed within and very near to the primary reaction zone.

2) Thermal NO formation is controlled by the equivalence ratio, the flame temperature and pressure only; the fuel type can affect thermal NO formation in adiabatic flames either through its effect on the adiabatic flame temperature for constant equivalence ratio operation, or through its effect on the equivalence ratio for constant inlet and constant flame temperatures operation. This latter effect is very small.

3) Prompt NO consists of NO formed via the Zeldovitch mechanism (in excess to thermal NO) due to radical overshoot, and NO formed in the main reaction zone via a non-Zeldovitch mechanism and involving hydrocarbon radicals. The first is mainly controlled by temperature and the chemical structure of the fuel affects in the same way as it affects thermal NO. The second reaction, which takes place in the flame front, depends on the fuel pyrolysis and hence it may be strongly influenced by the chemical structure of the fuel, even under constant flame temperature conditions. Differences in prompt NO measured in different, lean hydrocarbon-air flames at the same flame temperature may be attributed to difference in flame front prompt NO. Experimental studies have to be conducted to study the effect of higher hydrocarbons on this flame front NO.

4) The proposed kinetic model can predict only prompt NO formed via Zeldovitch mechanism due to O atom overshoot. It can be applied in lean combustion conditions where flame front NO is assumed to be very small.

5) There is discrepancy among experimental data reported in literature concerning the effect of pressure on prompt NO formation in lean flames.

6) The formation of NO_2 in lean hydrocarbon-air flames is still not fully understood. It may form in the sampling system rather than the flame front. NO_2 is believed to form from NO and the

detection of NO_2 in samples withdrawn from the main reaction zones of very lean flames supports the assumption that NO formation starts in the main reaction zone even in very lean mixture conditions. At present, this flame front prompt NO and its dependence on the fuel and operating condition can only be studied experimentally.

CHAPTER SIX

DESIGN OF TEST FACILITY AND EXPERIMENTAL PROCEDURE

6. DESIGN OF TEST FACILITY AND EXPERIMENTAL PROCEDURE

A test facility had to be designed and built for this research study. It consisted of four main sections: the burner, the fuel-air mixer, the supply system and the gas sampling-analysing system. A layout of the facility is shown in Figure 6.1 while plates 1 - 3 show the details of particular sections; a brief description of each section follows.

6.1 BURNER

The burner used is shown in Figure 6.2 and it is similar to that first developed by Singer et al (Ref.61) but it has the capability to operate at pressures up to 15 atm. The burner port consisted of a stainless steel grid of $\frac{1}{8}$ in. (3.2 mm) squares formed by strips of $\frac{3}{8}$ in. (9.5 mm) high and $\frac{1}{32}$ in. (0.8 mm) thick. This grid was held in an insulated stainless steel tube 6 ins. (152.4 mm) in height which had an internal diameter of 2 ins. (5.08 mm). Layers of glass beads and stainless steel screens were used to smooth the flow inside the burner tube. A thermocouple was inserted along the axis of the burner tube to measure the mixture inlet temperature just below the burner grid.

The burner was enclosed in a 6 ins. (152.4 mm) inner diameter, stainless steel, pressure cylinder equiped with viewing windows on opposite sides. The pressure inside the cylinder was controlled by a restricting orifice placed at the cylinder exit. Ignition of mixture was carried out by a removable igniter inserted into the cylinder side through a pressure sealing connection.

The pressure cylinder was protected from inside by a coaxial air stream which flowed around the flame via a glass-bead calming-bed. The velocity of this secondary air stream was about twenty percent of the cold fuel-air mixture at the burner port.

6.2 MIXTURE SUPPLY AND FLOW CONTROL

The air and fuel were metered and controlled through separate systems, then mixed and supplied to the burner. Both the air and the fuel systems, as well as mixing facilities, were designed such that both gaseous and liquid fuels could be burned.

6.2.1 Air System

Air was supplied to the rig from a pressurised storage tank of adequate capacity. The tank was connected to the combustion and cooling air lines through $\frac{1}{2}$ in. and 1 in. rotameters respectively. The air flow rate could be measured by these meters with an accuracy better than one percent.

After being metered, the combustion air was separated into a main and an atomising line. The atomising air was chosen such that the pressure drop across the fuel atomising-air orifice was sufficient to produce an adequate air velocity. The main combustion air was heated before entering the mixing tube by a 2 kw electric heater. The temperature of the heated air was controlled via a rheostat in the heater circuit. For reasons of safety, the heater was placed far from the mixing point and heating tape was used to compensate for any heat loss from the air piping. All the hot air pipes were made of stainless steel.

6.2.2 Fuel System

Gaseous fuels were supplied to the system directly from gas cylinders, but the liquid fuels were supplied from a nitrogen-pressurised vessel. Small, $\frac{1}{16}$ in. and $\frac{1}{8}$ in. tri-flat, variable area flowmeters were used to meter the liquid and gaseous fuels respectively. The flow rate was calculated using float characteristic curves supplied by the manufacturer. In the case of liquid fuels a calibration check was made by timing the flow under operating conditions. The fuel flow was regulated by means of remote-controlled micro-valves at the meter's inlet and exit.

6.2.3 Evaporating and Mixing Tube

One of the main practical problems in the study was in devising a way to evaporate and regulate the small fuel flows required. The use of an evaporating coil caused heavy oscillation in the fuel line. On the other hand, the use of a pressurised heating coil was unsafe because some fuels had boiling points at high pressures which were well above their self-ignition temperatures, and their vapours could ignite just after leaving the heating coil and mixing with air.

An atomising-vapourising system similar to that used by Calcote (Ref.92) was found to be useful in the present situation. The atomiser (see Figure 6.3) consisted of a $\frac{1}{32}$ in. (0.8 mm) hypodermic tube at the end of the fuel line, surrounded by the $\frac{1}{16}$ in. (1.59 mm) diameter atomising-air orifice. The hypodermic tube was concentric with the $\frac{1}{4}$ in. (6.4 mm) atomising air tube but extended to about 1 mm above the air orifice surface. Fuel was formed as drops or a weak jet at the end of the fuel tube and was atomised by the surrounding high velocity air coming from the air orifice. A pressure drop of 0.7 to 0.8 atm across the air orifice was found to be sufficient to produce an adequate high atomising air velocity.

This simple atomiser was assembled in the mixing tube such that the hot air coming from the air heater mixes with, and evaporates, the atomised fuel. The hot air surrounding the fuel tube caused it to

heat up, such that volatile fuels could vaporise before being atomised. In such cases smaller fuel tubes were used to increase the fuel pressure and hence its boiling point and prevent that evaporation, which might cause oscillations in the fuel line.

The mixing tube itself was an insulated stainless steel tube of 2 ins. (5.08 mm) internal diameter and 4 ins. (101.6 mm) high, and was equipped with a thermocouple. It was connected directly to the bottom of the burner tube.

6.3 GAS SAMPLING AND ANALYSING SYSTEM

6.3.1 Gas Sampling System

The combustion gases were sampled by a probe located on the traversing mechanism, situated on the top of the pressure vessel. The sampling probe was as shown in Figure 6.4. It was a stainless steel probe similar to that used by Sawyer et al (Ref.93) and consisted of a $\frac{1}{4}$ in. (6.4 mm) outer diameter tube with an aerodynamic tip. A convergent/divergent nozzle was drilled through the tip to accelerate the cooling and quenching process. The throat diameter was 0.38 mm which is the minimum diameter necessary to provide sufficient mass flow to operate the gas analysers. The gas carrier was a $\frac{1}{16}$ in. (1.59 mm) hypodermic tube silver-soldered to the probe tip and surrounded by another three hypodermic tubes carrying distilled cooling water to the probe tip. The cooling water returned to the other end of the probe through the annular space between the hypodermic tubes and the outer probe tube. The long $\frac{1}{4}$ in. probe tube was supported by a water-cooled $\frac{5}{8}$ in. (15.9 mm) outer diameter tube which ended at about 8 ins. (203.2 mm) from the probe tip.

The probe was introduced into the pressure vessel through the sliding block which moved horizontally over a $\frac{5}{8}$ x 3 ins. (15.9 x 76.2 mm) slot on the cover plate. The motion of the sliding block and hence the position of the probe across the flame was controlled by a micrometer system. The vertical motion of the probe along the burner axis was controlled by a traversing mechanism which consisted of a threaded bar and a push which was rigidly connected to the probe. Thus the sampling positions in the flame could be measured to an accuracy of 0.25 mm.

6.3.2 Gas Analysing Unit

Combustion gases sampled from the flame were analysed for stable species in a steady-flow analysing system. Main species measured were CO, CO_2, O_2 NO and the total oxides of nitrogen NO_x. In certain tests both H_2 and unburnt hydrocarbon were also measured.

Carbon monoxide (CO) and dioxide (CO_2) were both monitored by Analytical Development Co.Ltd. types 131 and 654 infrared gas analysers respectively. The CO analyser had four ranges: 0-200, 0-2000, 0-1000 and 0-10000 ppm which could be selected by cell division or by switch reset zero. The carbon dioxide analyser had two ranges: 0-5% and 0-20% and could be selected by cell division.

Oxygen concentrations were monitored by a Tyler-Servomex, type OA.250, paramagnetic oxygen analyser. It had three ranges: 0-10%, 0-25% and 0-100% oxygen.

NO and NO_x concentrations were measured by Thermo-Electron, Series 10A chemiluminescent gas analyser. There were eight ranges on the instrument: 0-2.5, 0-10, 0-25, 0-100, 0-250, 0-1000, 0-2500 and 0-10000 ppm with a minimum detectable concentration level of 0.05 ppm.

The total unburned hydrocarbons were measured with an Analysis Automation, total hydrocarbon analyser, model 521. It was based on the flame ionisation detector principle. It had five switched, adjustable ranges from 0-1, 0-10, 0-100, 0-1000 and 0-10000 ppm methane (CH_4).

The hydrogen concentration was measured with a hot-wire analyser which consisted of a thermal conductivity detector associated with a gas chromatographic unit.

6.4 FLAME TEMPERATURE MEASUREMENT

The temperature of the flame gases was measured by a Pt/Pt-Rh thermo-couple with a wire diameter of 0.025 mm. Temperature correction for radiation was applied using the following formula suggested by Kaskan (Ref.94)

$$\Delta T_{rad} = 1.25 \frac{\sigma \varepsilon}{\lambda} T_w^4 \; D^{0.75} \; \left(\frac{n}{\rho v}\right)^{0.25} \quad \ldots \quad (6.1)$$

where

ΔT_{rad}	=	correction in temperature which should be added to the measured value	^oK
ε	=	emissivity of the couple wires	
D	=	bead diameter	m
λ	=	thermal conductivity of hot gases	$J/m^2.s.^oK$
T_w	=	measured temperature	^oK
η	=	viscosity of the hot gases	$N.s./m^2$
v	=	velocity of hot gases	m/s
ρ	=	density of hot gases	kg/m^3
σ	=	Stefan-Boltzman Constant	$W/m^2\ ^oK^4$

It was assumed that the properties of the hot gases were those of air at the same temperature.

In tests where the flame temperatures were higher than 2000^{o}K it was impossible to measure the temperature by this thermocouple and the maximum flame temperature was assumed to be equal to the calculated adiabatic flame temperature.

6.5 EXPERIMENTAL PROCEDURE

The methods used to operate the rig and to measure the chemical species are described in this section.

6.5.1 Burner Operation

The procedure was as follows:

1) The air valve was opened and adjusted to flow according to the required inlet velocity at the burner port. Adjustment of the amount of atomising air was made with a control valve situated at the flowmeter exit.

2) The position of the probe tip relative to the burner surface was checked by fixing the zero of the traverse mechanism scale with the probe tip just touching the burner surface. The probe tip was then raised a safe distance (about 50 mm) above the burner surface.

3) The air heater was switched on and allowed to wait until the air reached a temperature about 20^{o}C higher than the required mixture temperature.

4) During air heating, all the measuring instruments were calibrated. (All analysers were switched on for about 2 hours before use).

5) After the air temperature reached the required value, the fuel valve was gradually opened while the ignitor was switched on and an anchored flame obtained. The igniter was pulled out of the flame and the pressure seal retightened.

6) The flow rates and heater voltage were trimmed to give the required mixture strength and inlet temperature.

7) For high pressure operation, the ignition was carried out at atmospheric pressure before raising the pressure by gradually closing the control orifice exit. The fuel and air flow rates were readjusted at the same time to maintain a stable flame on the burner surface.

6.5.2 Sampling and Analysing Procedure

1) For ambient pressure tests, the vacuum pump on the sampling line was switched on.

2) The heating tape was switched on and present at the required sampling line temperature.

3) The probe was positioned at the highest sampling point from the flame.

4) The sample flow was directed to the required analyser and then its flow rate was controlled. Either the flowmeter on the instrument or that on the sampling line could be used for this purpose.

5) After measuring all the species requried at this sampling position (temperature was measured at that position at the same time), the probe was moved to the next station. Distances between successive sampling points were equal to 2.5 mm in the far post-flame, while near the main reaction zone distances were taken as steps of 1 or 0.5 mm.

6) During sampling, the fuel and air flows were all continuously maintained.

CHAPTER SEVEN

EXPERIMENTAL PROGRAMME AND RESULTS

7. EXPERIMENTAL PROGRAMME AND RESULTS

The conditions over which the experimental programme was carried out are specified and results obtained are summarised. No attempt is made to present a detailed examination of the results in this chapter but the objective is to describe, very briefly, just the general trends in CO, NO, NO_x and prompt NO_x levels that were measured at the many conditions tested. A full analysis of the results is given in the following chapters.

7.1 FUELS SELECTION

The fuels selected for investigation are shown in Table 3.1. They were taken from all the main hydrocarbon families, namely paraffins, olefins, naphthenes and aromatics that are to be found in hydrocarbon fuels. The range of the carbon numbers tested varied from 3 to 12. Higher hydrocarbons than these could not be investigated because of their high boiling points and low ignition temperatures. The hydrogen to carbon ratio (H/C) of the investigated fuels varied from 1 to 2.67.

In addition to those pure hydrocarbons, kerosine, a typical practical fuel was also investigated and served as a basis of comparison. Tests were also carried out on tetralin, a partially hydrogenated aromatic hydrocarbon. The intent was to determine the affect of hydrogenation, often common to synthetic fuels, on the combustion behaviour.

7.2 EXPERIMENTAL CONDITIONS

Experiments were performed over a range of pressure, temperature and fuel-air ratio conditions. The objective was to cover that range which can be found at idle and lower power operating conditions within gas turbine combustors.

Values of these parameters that were selected were:

1) The equivalence ratio ϕ :

... This parameter affects combustion performance and pollutant emission through its influence on the combustion kinetics and thermodynamics. Only fuel lean conditions were tested. In these flames the kinetic reactions are slow and chemical equilibrium is hardly attained within residence times comparable to that available in practical combustors (less than 3 milliseconds). The minimum equivalence ratio tested depended upon the fuel, inlet temperature and pressure.

2) Pressure:

Pressure affects both hydrocarbon and CO oxidation rates as well as NO_x formation. Experimental runs were performed under three different pressurs, 1, 2 and 3 atmosphere absolute. While the one atmosphere runs were necessary for kinetic study, the high pressure runs covered the range present in a gas turbine combustor under idling and low power conditions.

3) Inlet Temperature:

The inlet temperature affects the flame temperature and hence the speed of chemical reactions. The large range of boiling points and self-ignition temperatures of the fuels investigated restricted the choice of a common inlet temperature. An inlet temperature of about 140°C was found to be suitable for different fuels at different equivalence ratios and pressures. Only one fuel (propane) was investigated at different inlet temperatures.

Numerical values of the above parameters chosen for different series of tests are shown in Table 7.1.

Table 7.1 Test Series and Values of Parameters Varied

Series No.	Pressure atm	Inlet Temp ^{o}K	Range of Equiv. Ratio	No. of Fuels	Species Measured
1	1.0	413	0.60 - 0.90	8	CO, CO_2, O_2 (all fuels) NO, NO_x (4 fuels) C_nH_m (3 fuels)
2	2.0	413	0.60 - 0.80	4	CO, CO_2, O_2
3	3.0	413	0.60 - 0.75	9	CO, CO_2, O_2, NO, NO_x
4	1.0	283, 373, 413	0.60 - 0.8	1	CO, CO_2, O_2

7.3 MEASUREMENTS AND RESULTS

For each run of the test series, combustion gases were sampled at different positions above the burner surfaces. Samples were taken along the axis of the flame and assumed to be representative of the flame gases in the same horizontal plane. The validity of this assumption requires a flatness in the velocity and temperature profiles.

7.3.1 Temperature Profiles

Horizontal temperature profiles measured at different distances above the burner port in flat propane and kerosine-air flames are shown in Figures 7.1 and 7.2. It is clear that for both flames, the flatness of temperature profiles was good within the sampled region of the flames (about 0 - 30mm above the burner port).

The measured temperature profiles along the axis for the two flames are presented in Figure 7.3. The maximum temperature was measured to be at a distance of 4 to 4 mm above the burner surface and then found to drop slightly due to heat loss to the surroundings. The temperature drop was higher for richer flames and the maximum drop rate found to be above $40^{o}C/cm$, a typical value observed by many investigators for such type of flames. The temperature values shown in all these figures were not corrected for radiation loss of the thermocouple wires. The temperature overshoot in the case of kerosine flame may be attributed to the catalytic heating of the thermocouple wires inside the main reaction zone.

7.3.2 Concentration Profiles of the Combustion Products

Different stable species concentrations were measured at various positions along the flame axis and are plotted against the time of travel from the burner surface to the sampling point as shown in Figure 7.4. The residence time was determined from the measured distance above the burner surface by use of local gas velocities estimated from the volumetric flow rate and density of the burning gas mixture.

The concentration of oxygen is shown to decrease sharply in the primary flame zone before its rate of decay becomes very slow. On the other hand, carbon monoxide is shown to be formed at a very high rate and to peak just near the point where oxygen consumption drops to a very low rate. It is found to be consumed at a very high rate just beyond the peak point but its rate of consumption decreases in the post-flame region, until it becomes very small at the final stages. Carbon dioxide concentration increases rapidly during CO generaion and high burnout regions, then the rate of its concentration increase, decreases considerably. Peak carbon monoxide concentration was measured to be much lower than the CO_2 concentration at the same point. This contradicts measurements made by some investigations in low pressure flames but confirms measurements made by other investigators for atmospheric flames (Ref.52).

NO_x concentrations are shown to increase at a very high rate in the region just downstream of the luminous zone and then to decrease its rate of formation which becomes nearly constant in the last stages of the post-flame zone. Positive NO_x concentrations were measured in the early stages of the flame, before the high production rate took place.

Similar measurements for different species were carried out for each run of the run series discussed earlier.

7.4 RESULTS OF CO MEASUREMENTS

Wet carbon monoxide concentrations have been calculated from the measured dry-concentration, using the method outlined in Reference 95. The logarithms of these concentrations for different fuels and different equivalence ratios were plotted against the travel time from the burner surface to the sampling point. This was carried out for different pressures.

A typical set of these plots is shown in Figure 7.5 from which it is clear that in propene-air flames the CO generation is greatly affected by the equivalence ratio and with very weak mixtures, the carbon monoxide generation time is considerably large. The CO oxidation rate is shown to increase with decreased equivalence ratio, and this is in accordance with the results of References 26 and 41. The transient CO peaks increase with the equivalence ratio in an approximately linear relation. Although the final CO equilibrium concentration differs by more than 2.5 orders of magnitude when the equivalence ratio is decreased from 0.84 to 0.61, the peak CO levels differ only by a factor of about 2.

The shape of CO profiles depends on the kind of fuel, as shown in Figure 7.6. The generation rate seems to be more strongly affected by the kind of fuel than the oxidation rate does.

CO levels at fixed residence time are plotted as a function of the equivalence ratio in Figure 7.7. As the equivalence ratio ϕ decreases from 0.9, the CO level first decreases to a minimum value before increasing again. This minimum value will be referred to as the critical equivalence ratio, ϕ_r. In some tests, the CO level starts to decrease again on further lowering of ϕ; this was attributed to the slow rate of CO generation at the very low (typically < 0.6) equivalence ratio values.

The value of the critical equivalence ratio is found to decrease as the residence time increases and at positions far from the flame, CO levels are similar to those calculated for equilibrium. The value of ϕ_r is also found to depend on the kind of fuel as shown in Figure 7.8 but the difference between the critical equivalence ratios of various fuels seems to decrease with increased residence time, as presented in Figure 7.9. At longer residence time, CO levels in different hydrocarbon-air flames follow the same trends as those calculated for chemical equilibrium (Figure 7.10).

Similar CO trends were measured at higher pressures and the variations of CO levels with the equivalence ratio for different fuels and a fixed residence time are shown in Figures 7.11 and 7.12. As the pressure increased the carbon monoxide levels were generally reduced, but the value of the critical equivalence ratio decreases slightly as shown in Figure 7.13. The carbon monoxide levels also increase rapidly on both sides of the critical equivalence ratio at high pressures.

7.5 RESULTS OF NO and NO_x MEASUREMENTS

Typical NO and NO_x profiles are presented in Figures 7.14 and 7.15 for two different fuels, and at different equivalence ratios. It is clear that the difference between NO_x and NO levels (NO_2) does not vary too greatly with equivalence ratio. Both NO and NO_x generation was found to take place in two stages, the first stage being characterised by a relatively high production rate. In both stages, the production rate increased with increased equivalence ratio.

Variations of NO_x levels (after 6 ms residence time) with equivalence ratio for different fuels are compared in Figures 7.16 and 7.17 for 1 and 3 atm pressures respectively. Higher levels are generally produced in high temperature flames.

Prompt NO_x values were obtained by linear extrapolation of NO_x profiles in the post-flame zone back to zero time, corresponding to the edge of the primary reaction zone. These values are plotted as a function of the equivalence ratio for different fuels in Figures 7.18 and 7.19. The change of prompt NO_x with the equivalence ratio is smaller than that of total NO_x, but higher temperature flames, generally, produce more prompt NO_x.

A detailed discussion of these general points is given in the following chapters where comparisons are also presented of the predictions obtained by the methods described before with the experimental data.

CHAPTER EIGHT

ANALYSIS AND DISCUSSION OF CARBON MONOXIDE RESULTS

8. ANALYSIS AND DISCUSSION OF CARBON MONOXIDE RESULTS

As shown in the previous chapter, it is convenient to present CO data either as CO concentration versus equivalence ratio ϕ, or as CO concentration versus time. The former method is useful from practical considerations as one is able to quickly observe the value of ϕ which produces the lowest CO level for fixed conditions of fuel, pressure, temperature and combustion time. This value has been termed as ϕ_r, the critical value, and the corresponding CO concentration CO_{min}. In the discussion that follows both are considered; general observations are made about the sensitivity of ϕ_r and CO_{min} to the parameters studied, some observations follow of the influence fuel type has upon the CO formation and oxidation processes and finally, a comparison is made between the measured and predicted CO-time characteristics for the differing fuels.

8.1 EFFECT OF DIFFERENT PARAMETERS ON ϕ_r AND CO_{min}

For a fixed combustion residence time, the value of ϕ_r represents the condition that corresponds to the highest efficiency and lowest emission performance. As CO levels for $\phi > \phi_r$ tend to be little higher than equilibrium values, it can be considered to be the lowest ϕ value at which the characteristic times for CO generation and oxidation are low relative to the reference residence time. It can be expected therefore that ϕ_r will be affected only by parameters which affect CO generation and oxidation kinetics. CO_{min} on the other hand will depend on ϕ_r and also upon the H/C ratio of the fuel, flame temperature and pressure, i.e. both the kinetic and physical properties of the flame.

8.1.1 Influence of the Fuel Structure

Variations in the chemical structure of fuel include variations in type, hydrogen-to-carbon ratio (H/C) and carbon number (n). All these properties are interconnected and their effect is inseparable.

a) Influence of Fuel Type

To evaluate the effect of fuel type, the minimum CO levels and the critical equivalence ratios are mapped for different fuel types. The CO_{min} and ϕ_r for differing fuels of a common class can be represented within a reasonably narrow range. Figure 8.1 shows that at atmospheric pressure and 413^{o}K inlet temperature, the measured minimum CO levels in aromatic flames are about twice as high as those measured in paraffinic flames for a 3 ms residence time burner. Olefins show CO_{min} levels which are slightly lower than those of paraffins.

This same relationship and trends are obtained at higher residence times and pressures, as shown in Figure 8.2. The CO_{min} levels for all types are, however, reduced by about a factor of ten as the pressure is increased from 1 to 3 atmospheres.

Naphthenes, as represented by methylcyclohexane, produce minimum CO levels which are observed to be higher than those of olefins and paraffins but less than aromatics. The minimum CO level of the type of kerosine* tested is observed to be higher than that calculated using the average CO_{min} of each hydrocarbon type and its percentage in kerosine. Better agreement between measured and calculated CO_{min} for kerosine can be obtained if calculations take into account only those compounds which have boiling points comparable to the boiling range of kerosine.

The variation of the critical equivalence ratio is presented in Figure 8.3. It is clear that aromatics and naphthenes possess slightly higher critical equivalence ratios than both olefins and paraffins. It must be noted here that the two former types have stable ring-structured molecules.

b) Influence of Carbon Number

Figures 8.4 and 8.5 show that both the minimum CO levels and the critical equivalence ratios increase as the carbon number of the members of each hydrocarbon type increases. The rate of increase of CO_{min} with the carbon number is greater in the case of aromatics. It must be noticed also that tetralin, a partially hydrogenated aromatic compound, is an exception as its structure is no longer a perfect aromatic ring-compound.

c) Effect of Molar H/C Ratio

This factor is very important as it is generally used in practice to correlate fuel composition to performance and pollution emissions. Figure 8.6 shows that the minimum CO level generally decreases with an increase in H/C ratio. On the other hand, if we consider each individual compound within a fixed fuel type, the trend is different. For aromatic compounds, CO_{min} increases with the increase in H/C. This is due to the fact that higher H/C ratios belong to higher aromatic

---

* Consisting of 56.5% paraffins, 25.5% naphthenes, 17.7% aromatics and 0.3% olefins.

members which possess higher ϕ_r, see Figure 8.7, that tend to increase CO level. In the case of paraffins, CO_{min} decreases with increased H/C ratio due to the decrease in carbon content as well as to the reduction in ϕ_r, (the higher H/C ratios belong to simple molecules of lower carbon number and hence lower ϕ_r).

8.1.2 Influence of Pressure

Figures 8.8, 8.9 and 8.10 show the effect of pressure on both ϕ_r and CO_{min}. The critical equivalence ratio is observed to decrease slowly as the pressure increases. The effect is generally larger for aromatics and higher hydrocarbons. The minimum CO value decreases sharply with the increase of pressure but the rate of decrease becomes smaller at higher pressure levels. At first sight, it is surprising that as the pressure increases from 1 to 3 atm, CO_{min} is reduced by a factor of 10 while CO equilibrium is only reduced by a factor of 1.7 ($\sqrt{3}$).

The effect of pressure can be explained as follows. For a fixed residence time, the pressure level affects two differing factors; firstly, how close the CO_{min} is to equilibrium and secondly, the equilibrium value itself. At low pressures, the CO_{min} is far above equilibrium value and the equilibrium value itself is high. These two factors together produce the large variation measured. At high pressures as ϕ_r decreases only slightly, it is to be expected that CO_{min} will vary as the square root of pressure in the same manner as the equilibrium value.

8.1.3 Influence of Inlet Temperature

Inlet temperature was not varied for more than one fuel, propane, and results, given in Figure 8.11, show that as the inlet temperature is increased, the critical equivalence ratio is reduced. The minimum CO level is also reduced but to a modest extent. At high pressure, where CO_{min} approaches the equilibrium value, the increase of the inlet temperature will result in an increase in the flame temperature and hence CO_{min} will increase unless ϕ_r is reduced substantially.

8.1.4 Summary

The foregoing discussion can be summarised by the following points:

1) Ring compounds (aromatics and naphthenes), show higher critical equivalence ratios and hence higher values of CO_{min} when compared to

open-chain-structured compounds (paraffins and olefins). On the other hand, the unsaturated chain-structured compounds (olefins) possess lower values of ϕ_r than those possessed by saturated chain-structured compounds (paraffins). This is clear from the table below (p = 3 atm):

Type	ϕ_r	CO_{min} ppm	Remarks
Paraffins	0.675	320	Average value
Olefins	0.65	290	Average value
Naphthenes	0.7	450	
Aromatics	0.7	700	Average value

2) Within each fuel type both the critical equivalence ratio and the minimum CO level increase with an increase of the carbon number.

3) The influence of the H/C ratio is very complex; both ϕ_r and CO_{min} may increase or decrease with increased H/C, depending on the fuel type.

4) As the pressure increases, ϕ_r is slightly reduced while CO_{min} decreases sharply at first but at higher pressures CO_{min} varies with pressure in the same manner as the equilibrium value. The pressure effect varies from one fuel type to another.

5) Increasing the inlet temperature reduces the critical equivalence ratio and CO_{min} is reduced only by a modest extent.

8.2 INFLUENCE OF FUEL STRUCTURE ON CO PRODUCTION

As has been stated before, the observed influence of the chemical structure on ϕ_r and CO_{min} is a direct result of its effect on CO generation and oxidation rates. Attempts are made below to quantify this general statement by producing a simple kinetic mechanism which predicts the measured values.

8.2.1 CO Generation

Carbon monoxide generation relates closely to hydrocarbon oxidation reactions. For equivalence ratios near stoichiometric value, the fuel oxidation process is very fast, especially at high temperatures and pressures, hence fuel oxidation and CO generation can be considered to occur instantaneously. As the equivalence ratio

decreases, the fuel oxidation time increases and becomes comparable to the available combustion time in practical combustion systems such as gas turbine combustors (see Figure 8.12). Any effect of the fuel structure on its oxidation rate at these conditions will be important and must be considered.

To evaluate the fuel effect on fuel oxidation and CO generation, both CO and hydrocarbon profiles have been measured in flames operating under fixed conditions of pressure, temperature and equivalence ratios. Three fuels of three different types have been considered in these comparison tests. Typical results are as shown in Figure 8.13. CO is found to be generated faster in a propene flame than in a propane flame with the same equivalence ratio. The carbon monoxide reaches its peak concentration at a shorter time in the propene flame but the difference is not large. The fuel oxidation is also faster in propene flame as shown in Figure 8.14. The propene flame, however, has a higher flame temperature and one may attribute the observed differences in CO generation and fuel oxidation to differences in the flame temperature.

When a similar comparison is made between propane and o-xylene flames, a larger difference in both CO generation and fuel oxidation is observed (see Figures 8.15 and 8.16). This time the difference cannot be attributed to differences in flame temperatures as the flame temperature of o-xylene flame, which possesses a lower fuel oxidation rate, has the higher value. It is concluded that the difference in the chemical structure of fuels must be responsible for these variations and as a consequence that different global fuel oxidation rate equations are required for each fuel.

In an attempt to derive a global rate equation for propane and o-xylene oxidation, the measured oxygen, fuel and temperature profiles were used to evaluate the constants in the following rate equation (see Reference 22).

$$\frac{-d(C_nH_m)}{dt} = k\,(T/1111 - 0.5)\;\;(C_nH_m)^a\,(O_2)^b\;\;\;p^c\;\;\ldots\ldots\;\;\;(8.1)$$

where

$$k = A \cdot e^{-E/\bar{R}T}$$

and p is the pressure in atmospheres.

The values of a and b were chosen, and E and A determined. The choice of a is difficult as it is not a true constant and it changes from phase to phase during fuel oxidation. In the induction phase and slow reaction region, the value of a is negative while in the post-induction phase it is positive (Ref.15). It also varies with the temperature level in each phase (Ref.14). Moreover, the results of Reference 14 show a to depend on the equivalence ratio. The values of a and b accepted in this study are 0.7 and 0.8 respectively and follow that derived by Dryer et al (Ref.15) for their studies of the combustion of lean methane-air mixtures (ϕ < 0.5 and T = 1100-1400^{o}K).

The values of k have been calculated from the measured fuel oxidation rates in different flames (in the post induction region only), while the values of A and E were derived by plotting log k as a function of $\frac{1}{T}$ (see Figures 8.17 and 8.18). E is found to be equal to 26.5 and 27 kcal/mole for propane and o-xylene respectively, which are very close indeed. The value of A in the case of propane is found to be 2.5 times that of o-xylene and such large differences cannot be attributed to experimental errors.

However, although these derived values of A and E show clearly the effect of the chemical structure on fuel oxidation rate, they have been derived here under a very narrow range of conditions ($0.69 < \phi < 0.75$, $1600 < T < 2000^{o}K$ and $p = 1$ atm). The variations at higher pressures and temperatures cannot be measured with an acceptable accuracy because the fuel profiles are very steep. One way to check the applicability of these equations to the whole range of conditions investigated, however, is to compare the predicted and measured carbon monoxide profiles, as is carried later.

8.2.2 CO Oxidation

If CO oxidation is considered to take place via the reaction:

$$CO + OH \rightleftarrows CO_2 + H \qquad \ldots \quad (2)$$

then, neglecting the reverse reaction, the fractional conversion rate $d(CO)/dt/(CO)$, is a function only of OH concentration and flame temperature. The chemical structure of the fuel can then be expected to affect CO oxidation if it influences either the OH level or the flame temperature. If it is assumed that OH is equilibrated during CO oxidation, then OH levels will be nearly the same in different, adiabatic hydrocarbon-air flames of the same equivalence ratio and inlet temperature (see Section 3.3) and the CO conversion rate will depend on the flame temperature only. So, according to this assumption, higher CO conversion rates are expected to be found in flames burning aromatic compounds than those in flames burning hydrogen-rich paraffinic compounds due to their higher flame temperatures.

Experimental CO conversion rates were determined from the measured CO profiles in propane and o-xylene flames, using the one-dimensional flame equation formulated by Fristrom et al (Ref.37) and following the procedure of Ref.26. The diffusion coefficients used in the calculations are those given by Fenimore and Jones (Ref.27). These experimental conversion rates are compared in Figure 8.19. It is clear that CO conversion rates in the case of hydrogen-rich propane is about twice that in the case of o-xylene at the early stages of CO burnout, although the o-xylene flame has higher flame temperature and the equilibrium OH concentration is the same in both flames. Thus it is clear that the assumption of equilibrium OH levels during CO oxidation cannot explain the effect of fuel structure on CO oxidation.

It should also be mentioned here that the equilibrium OH concentration decreases with decreased equivalence ratio of adiabatic hydrocarbon-air flames, and according to the assumption of equilibrium OH level during CO oxidation, the CO conversion rate can be expected to be reduced as the equivalence ratio decreases. This however does not agree with the experimental results as shown in Figure 8.20 where the leaner flame possesses higher CO conversion rates.

These experimental results can be explained by use of the radical overshoot theory which has been explained before (see Section 4.3) and states that the actual concentration of radicals such as OH just downstream of the main reaction zone (Zone II, Figure 4.2) are much higher than their equilibrium values. The degree of overshoot ($(OH)_{max}/(OH)_e$) is higher for cooler and leaner flames (Refs. 26 and 48). When considering the two flames compared in Figure 8.19 the flame burning hydrogen rich fuel (propane) has a lower flame temperature than that burning the low hydrogen content o-xylene, and hence it possesses a higher degree of overshoot and as a consequence a higher OH level. This higher OH level is responsible for the observed higher CO conversion rates in the hydrogen rich fuel flames. The higher CO conversion rates in leaner flames can also be explained in the same way.

The super equilibrium concentration of OH cannot be calculated, however, with a high degree of precision by the use of approximate kinetic models (see Section 4.3). Account of this factor is usually provided by considering either a global CO oxidation rate equation or a partial equilibrium model for the CO burnout zone of the combustion process.

The experimental CO conversion rates have been compared with those calculated using a global CO oxidation equation, the assumption of OH total equilibrium, and also that of the OH partial equilibrium model. The results are shown in Figure 8.21. The global rate equation used was that derived by Howard et al (Ref.25) from data of several studies. The CO conversion rates calculated using the global rate equation are higher than the experimental values by a factor ranging from 4 at the early stages of CO burnout to more than 20 at the last stages. This large difference is another proof of the fact that the global rate equations are not universally applicable to conditions other than those to which they have been derived, or even to the whole region of CO burnout. It can be attributed to the fact that the method assumes the OH concentration to be related to O_2 and H_2O levels, but in fact it is a function of O_2 and H_2 concentrations (see Section 4.3). The reverse rate of reaction (2) is neglected and this may be very important, especially in the last stages of CO burnout. CO levels as calculated by the global rate equations are never equilibrated.

The CO conversion rates calculated from the equilibrium OH assumption and neglecting the reverse rate of reaction (2) are found to be much lower, and like the global results, not to agree with the experimental measurements. CO conversion rates calculated from the partial equilibrium model, however, are shown to be in good agreement with the experimental rates. Thus the influence of the fuel structure on CO burnout can be accounted for by using the partial equilibrium assumption. It should be noted however that the partial equilibrium assumption is not valid inside the main reaction zone. The conditions in this zone are calculated by the use of the carbon dioxide formation rate equation and the CO level is determined from a mass balance of the carbon atom as described in Chapter 4.4.

8.3 THEORETICAL PREDICTIONS AND COMPARISONS WITH EXPERIMENTAL DATA

So far only elements of the CO production model derived in Chapter 4 have been considered. In this section the full model is used to determine CO-time profiles and the position of the value of CO_{min}, and comparisons are made with the experimental data.

Most comparisons are made with the propane-air flames data as some degree of 'calibration' of the model is necessary in order to test the differing assumptions made and to determine the best values of the kinetic parameters. Further comparisons are made with the o-xylene flame data and, finally, the model is used to predict CO-time profiles for the many fuels tested. In all cases the following were applied to the model:

a) the measured flame temperature was used,

b) the temperature drop in the post-flame zone was accounted for by the following equation (Ref.41):

$$T = T_{max} - (T_{max} - T_f^{\wedge}) (1-e^{t})$$

where T_{max} is the maximum flame temperature, $T_f^{\wedge}$ is the temperature at the end of the main reaction zone and t is the time in milliseconds,

c) the equilibrium concentrations of different species at any temperature were calculated by minimizing the free energy of the system in a separate program and were given as input data to the main program.

8.3.1 Propane-Air Flame Data

The predicted rate of CO formation is controlled largely by the values assigned to A and E in the global fuel-oxidation rate equation, and the best fit values as determined from Figure 8.17 are found to be

1.5×10^9 and 26.5 kcal/mole respectively. Initially attempts were made to simulate the measured CO generation characteristics but it was found that satisfactory agreement could only be achieved with higher values of $A_{..}$ When A was taken to be equal to 4.5×10^9 then the level of agreement is as shown in Figure 8.22.

Further kinetic parameters must be set to determine the CO oxidation rate. In the model described in Chapter 4, it is assumed that the whole recombination proces is controlled by the following reactions:

$$H + O_2 + M \overset{k_{11}}{\rightleftarrows} HO_2 + M \quad .... \quad (11)$$

$$OH + HO_2 \overset{k_{12}}{\rightleftarrows} H_2O + O_2 \quad .... \quad (12)$$

and that $k_{-11}\,(M) \ll k_{12}\,(OH)$

This latter assumption tends to make the whole recombination process as a function of k_{11} only. k_{11} has to be defined and, unfortunately, neither its value at a point or its variation with temperature are known with any accuracy. Point values vary by a factor of 6 (Refs. 41 and 42) and many investigators have made the assumption that it is independent of temperature or that it has a very small and negative activation energy.

Many computer runs were made to determine the value of k_{11} that, combined with A and E values given above, gives the best agreement between predicted and measured CO-time profiles. The results, shown in Figure 8.22, indicate that a reasonable level of agreement can be obtained over the complete profile when:

$$A = 4.5 \times 10^9$$

$$E = 26.5 \text{ kcal/mole}$$

$$\text{and } k_{11} = 4 \times 10^{15}\ e^{500/T}\ \text{cm}^3\ \text{mole}^{-1}\ \text{sec}^{-1}$$

Many more calculations were made for the propane-air flames to determine values of ϕ_r and CO_{min} and the results were summarised in Figure 8.23. As before, Comparisons between predicted and measured results are shown to be acceptable. As in Figure 8.22, the predicted results are found to be significantly lower than measured values only at the final stages of CO burnout and this discrepancy is found to be more pronounced in lean flames. It can be attributed to the fact that in the last stage of burnout, the OH concentration approaches its equilibrium value and becomes very small, especially in the case of lean mixtures. This would make invalid the assumption that $k_{-11}(M) \ll k_{12}(OH)$ as is used by the model.

An alternative approach may be used by taking the results given in Reference 88. In this work equation 4.19 (see Section 4.4) is modified to include further rate constant, k_{12}, and like k_{11} its value is not precisely known. Variations exist in literature of between factors of 2 to 3. When k_{12} is taken equal to $5 \times 10^{13} e^{-500/T}$ (see Reference 48) the predicted CO levels show a lower degree of agreement than those obtained previously as shown in Figure 8.24. The conclusion from this work is that there is no advantage to be gained by the introduction of the second term, and it is better to use equation 4.19 (see Section 4.4) as it is.

Another assumption made in the present kinetic model is that partial equilibrium exists only after 95% of the fuel is consumed. If the partial equilibrium is assumed to be valid after 90% of the fuel is consumed, the predicted CO levels show a lower degree of agreement with experimental data specially for higher equivalence ratios, see Figure 8.25. This disagreement can be explained as follows. When the fuel concentration is high (i.e. in the main reaction zone), the O_2 concentration will be also high and the temperature is low, and this results in higher O atom concentration, as predicted from the partial equilibrium model (see Reference 51). As it has been shown in Chapter 4 that the relation between O, OH and H concentrations is

$$\frac{(O)}{(O)_e} = \frac{(OH)}{(OH)_e} = \left(\frac{(H)}{(H)_e}\right)^{\frac{2}{3}}$$

then the predicted H concentration will be very high which will cause the backward rate of the reaction:

$$CO + OH \rightleftarrows CO_2 + H \qquad \ldots\ldots \quad (2)$$

to be very high. This will result in the slower CO oxidation rate. It is concluded that the partial equilibrium model is only valid if at least 95% of the fuel is consumed, which is in agreement with the results of Reference 51.

Further calculations have been made for different propane-air flames for different stoichiometry and under different pressures using the kinetic parameters and assumptions as identified above. Good agreement is obtained between measured and predicted CO levels as shown in Figure 8.26. It is important to note that the model can satisfactorily predict the influence of both pressure and residence time on ϕ_r and CO_{min}. (c was found to be -0.4).

8.3.2 O-xylene/Air Flame Data

A similar model 'calibration' exercise has been carried out for the o-xylene data as described for propane data. A satisfactory comparison between predicted and measured results can be obtained by solely taking account of the change in fuel oxidation characteristics. As for propane, the best fit is obtained with an A value of equation 8.1 equal approximately four times that determined from the o-xylene profile measurements, see Figure 8.18. The best kinetic values found

to be given by

$$A = 2.8 \times 10^{9} \quad \text{(versus } 6 \times 10^{8}\text{)}$$

$$E = 27.0 \quad \text{kcal/mole}$$

$$k_{11} = 4 \times 10^{15} \; e^{500/T} \quad \text{(as for propane)}$$

The results, shown in Figure 8.27, are found to be in reasonable agreement for all ranges of equivalence ratios, residence times and pressures.

8.3.3 Application to Other Fuels

The model appears to offer a reasonable method of representing the CO kinetics for differing fuels with the major limitation that it may require individual global fuel oxidation rate equation for each fuel. It is possible, however, that the global oxidation rate equation derived for o-xylene can apply to all aromatic fuels and that for propane, to all aliphatic hydrocarbons. Figure 8.28 shows the CO levels predicted according to this assumption. The maximum flame temperature in each case is assumed to be equal to the calculated adiabatic flame temperature.

A very high oxidation rate is predicted for dodecane and dodecene (high carbon number fuels) which results in lower values of CO_{min} and ϕ_r when compared with other fuels. This contradicts the experimental results, see Figure 7.8. Moreover, the predicted ϕ_r for propene is shown to be nearly equal to that for propane, which also is in disagreement with the experimental results. Clearly such a simple approach cannot be adopted and it appears that changes must be made to the global rate equations.

A variation in the activation energy for each fuel can be calculated following the method of Chinitz (Ref.16). Consider the reaction:

$$C_nH_m + \tfrac{1}{2}(n + m/2)O_2 \rightarrow nCO + (m/2)H_2O$$

If it is assumed a true elementary reaction, the activation energy of the reaction can be given by:

$$E = \tilde{A} + B.\Delta H_r \qquad \ldots . \quad (8.6)$$

where $\tilde{A}$ and B are constants and ΔH_r is the heat of reaction (which is a function in the heat of formation of the fuel, $\Delta H_{f\ C_nH_m}$, as shown in Chapter 3) then it follows that:

$$E = \tilde{\tilde{A}} + \tilde{B} \; .\Delta H_{f\ C_nH_m} \quad \text{kcal/mole} \qquad \ldots . \quad (8.7)$$

The comparison between predictions and measurements showed that the values of $A^{``}$ and $B^{`}$ must vary with the fuel type, see table below:

Fuel Type	$A^{``}$	$B^{`}$
Paraffins	25.75	-0.03
Olefins	26.2	-0.04
Aromatics	27.2	-0.05

8.4 SUMMARY AND CONCLUSIONS

1. Fuel properties are shown to significantly influence the CO-time histories produced in flat flame burners operating under the following range of conditions:

   ϕ : 0.6 - 0.9

   T : $413^{o}K$

   p : 1 - 3 atm

   Fuels : Propane, dodecane, propene, dodecene, methylcyclohexane, benzene, o-xylene, tetralin and kerosine

2. The CO history can be characterised for a given combustion time by the lowest CO level obtained over the range of equivalence ratios tested, and the critical value of ϕ, termed as ϕ_r, at which it occurs. Aromatics and naphthenic fuels are shown to give higher values of both CO_{min} and ϕ_r than paraffins and olefins. The effect of increasing inlet pressure and temperature is to reduce both CO_{min} and ϕ_r and to reduce the differences between fuels.

3. The chemical structure of fuels is shown to affect ϕ_r mainly through its influence upon CO generation process (fuel oxidation process), rather than on CO burnout kinetics. The two generation equations derived for propane and o-xylene are:

$$d\,(C_3H_8)/dt = -4.5 \times 10^9\,(C_3H_8)^{0.7} \cdot (O_2)^{0.8} \cdot p^{-0.4} \left(\frac{T}{1111} - 0.5\right) \times e^{-26500/\bar{R}T}$$

$$d\,(C_8H_{10})/dt = -2.8 \times 10^9\,(C_8H_{10})^{0.7} \cdot (O_2)^{0.8}\; p^{-0.4} \left(\frac{T}{1111} - 0.5\right) \times e^{-27000/\bar{R}T}$$

4. The CO oxidation process is shown to be controlled by the radical recombination process. Global CO oxidation rate equations derived experimentally which relate CO oxidationsolely to the concentrations of stable species, are not generally applicable.

5. A reasonable agreement can be obtained between predicted CO histories and measurements for different fuels using the CO model developed in Chapter 4. Care has to be taken, however, in accurately defining and refining the global fuel oxidation model which is an integral part of the model.

CHAPTER 9

ANALYSIS AND DISCUSSION OF NO_x RESULTS

9. ANALYSIS AND DISCUSSION OF NO_x RESULTS

The experimental program on NO_x emissions involved the measurements of both nitrogen oxide, NO, and nitrogen dioxide, NO_2, (taken as the difference between total NO_x and NO). The results showed that higher than expected levels of NO_2 were measured in the main reaction zones of very lean flames and so the chapter begins with a discussion of this matter. It then goes on to present the data in such a way as to isolate the influence of fuel structure upon the NO_x emissions. An attempt is made to correlate these emissions to those fuel properties that can be measured in practical fuels by means of the predictive model presented in Chapter 5.

9.1 NO_x MEASUREMENTS

Although it was not amongst the objectives of the present study to deal with NO_2 formation kinetics, it is difficult to analyse the experimental results without referring to NO_2 as it was found to contribute a large percentage of the total NO_x measured in most flames investigated. Current kinetic mechanisms which describe NO_2 formation (see Section 5.5) suggest that high levels found in samples drawn from the main reaction zones result from NO oxidation in the flame front itself (or even in the sampling probe). Lower NO_2 levels in samples withdrawn from post-flame zone suggest that NO_2 may be partially re-converted into NO in the post-flame zone. This implies that measured NO profiles do not represent the actual formation in flames and hence all kinetic mechanisms and data derived from such profiles may need to be revised.

Figure 9.1 shows that in an atmospheric, lean, propane-air flame, NO_2 formation starts earlier than NO inside the main reaction zone and its concentration rapidly increases to reach a maximum value just outside the main reaction zone. In the post-flame zone, the NO_2 concentration level decreases slowly.

As it has been shown in Chapter 5, NO_2 is assumed to be formed from NO in the main reaction zone via the reaction

$$HO_2 + NO \rightleftarrows NO_2 + OH \qquad \ldots\ (23)$$

and that NO itself is formed in this zone via a non-Zeldovitch mechanism involving different intermediary compounds such as HCN, CN, NCO and NH, (Ref.89). The NO_2 reconversion to NO in the post-flame zone may

proceed via the reactions (Ref.88 and 89):

$$NO_2 + O \rightleftarrows NO + O_2 \quad \ldots\ldots (27)$$

$$NO_2 + M \rightleftarrows NO + O + M \quad \ldots\ldots (28)$$

As reaction (28) is expected to be equilibrated for temperatures higher than 1200°K (Ref.88),which is the case for all flames studied here, the ratio of NO_2/NO_x in Figure 9.1 should be found to be less than 1% in the post-flame zone where O atom concentration approaches its equilibrium value. This contradicts the experimental results where only a slight consumption of NO_2 is observed. This halt in NO_2 consumption in the post-flame zones of oxygen-rich flames, which was also reported in References 88 and 89 cannot be explained by considering the above kinetic mechanism. Further work is needed to derive a more reliable mechanism.

The ratio of NO_2 to NO_x that persists in the post-flame zone is measured to decrease as the equivalence ratio increases, see Figure 9.2, and it may tend to zero in rich flames (Ref.89). Figure 9.2 shows also that the ratio in relatively cool propane-air flames is higher than in propene and tetralin flames. The temperatures of these flames are higher than that of propane flame by about 70°C.

An increase in pressure is shown to increase the rate of formation of NO_2, see Figure 9.3, and it is found to reach its maximum concentration at the edge of the main reaction zone itself, before any concentration of NO is detected. After reaching the peak value, about 40% of the NO_2 is consumed very quickly in the post-flame zone but then its concentration is shown to remain constant. The region of high NO formation is shown to coincide with the NO_2 consumption zone. It appears necessary, therefore, that NO formation must consider both Zeldovitch type mechanism plus those that influence the NO_2 to NO conversion reactions. It is interesting to note that rapid quenching of NO_2 reconversion reactions will produce high NO_2/NO_x ratios as has been observed in some practical combustion system.

It has also been shown in Chapter 5 that the same conditions that favour NO_2 formation in the flame are, however, present in the sampling probe and hence NO_2 may be formed in the sampling system rather than in the flame. This subject is still not clear and its clarification may need the use of sampling techniques other than the conventional sampling probe techniques employed in the present study.

However, from the above discussion one can conclude that:

1) In lean flames, a fraction of the NO is generated inside the main reaction zone, probably via non-Zeldovitch mechanism. This NO is mostly converted to NO_2 in the flame front (or in the sampling probe) and a very small portion of it is reconverted into NO in the post-flame zone of atmospheric flames.

2) At elevated pressures, higher levels of NO_2 are formed in the flame front but also a large fraction is rapidly converted to NO just outside the main reaction zone causing the NO profiles in this zone to be very steep.

In the following analysis, however, the total oxides of nitrogen (NO_x) are considered to avoid these complications in NO/NO_2 kinetics.

9.2 INFLUENCE OF CHEMICAL STRUCTURE OF FUEL ON NO_x FORMATION

It has been shown in Chapter 5 that in the post equilibrium phase of combustion, NO_x formation in fuel-lean flames is dependant only on the flame temperature and the equivalence ratio. In adiabatic flames, fuel structure will affect NO_x formation through its effect on the adiabatic flame temperature. Quickly formed NO_x, or prompt NO_x as it will be referred to here, on the other hand, was shown to be dependant on the chemical structure of the fuel.

Prompt NO_x is usually determined by extrapolating the post flame NO_x profiles to the downstream edge of the primary reaction zone. These profiles are linear only when the flame temperature is constant (no heat loss) which is not possible in practical flames. So the extrapolation is somewhat arbitrary especially for higher temperature flames where the slopes of these profiles are large. This introduces a difficulty for this study as the errors in prompt NO_x determination can be higher than the effect of fuel structure itself. In low temperature flames, the slopes of the post equilibrium NO_x profiles are small and hence the errors are small. A comparison of the total NO_x formed after a fixed residence time in different hydrocarbon-air flames under the same pressure, equivalence ratio, and inlet temperature, is however a useful method of analysis as well as identification of the prompt NO_x fraction.

9.2.1 Fuel Type

The influence of the fuel type upon the level of NO_x formed after 6 milliseconds in different adiabatic hydrocarbon-air flames is shown in Figure 9.4. NO_x formed in aromatic-air flames are found to be more than twice that formed in paraffin-air flames at the same conditions. NO_x formed in olefin-air flames is only about 1.5 times that formed in paraffin-air flames while naphthenic flames produce NO_x levels which are only slightly higher than those of paraffinic flames. Thus the order of increasing NO_x is paraffins, naphthenes, olefins and aromatics.

The difference in NO_x levels can be due to differences in prompt NO_x and/or in post equilibrium NO_x (thermal NO_x). In the Figure, prompt NO_x values are shown to be influenced by fuel type to a lesser extent than total NO_x, with prompt NO_x for the aromatics being less than twice that of paraffins.

As the equivalence ratio is decreased, the flame temperature decreases and the importance of thermal NO_x decreases. Total NO_x levels will then approach prompt NO_x levels (see NO_x levels at $\phi = 0.65$ in Figure 9.4). Conversely, as the equivalence ratio increases, post equilibrium NO_x makes the major contribution and prompt NO_x will represent a declining fraction of the total, as shown in Figure 9.5

Calculations show that the variations in prompt NO_x levels that exist between the fuels cannot be explained only in terms of the influence of fuel type upon flame temperature. As an example, for $\phi = 0.7$ the adiabatic flame temperature of propene-air flame is only $10^{o}C$ less than that of benzene-air flames, whereas a significant difference in prompt NO_x between those two flames is shown in Figure 9.4, and this can only be attributed to the influence of their chemical structure. These measurements support the findings of Ref.83 where higher prompt NO_x is reported for the flames burning cyclic compounds.

9.2.2 Carbon Number

Although only two or three members of each hydrocarbon type are investigated, one can conclude from the data collected that, at fixed operating conditions, the NO_x level varies with the carbon number of the fuel burnt, see Figure 9.6. For both aromatics and olefins the flame temperature decreases as the carbon number increases, so perhaps it is not surprising to find that NO_x production decreases with increased carbon number. For paraffins the flame temperature increases with the increase of the carbon number and, consistently, higher NO_x levels are produced in higher paraffin flames. For the same carbon number, aromatic compounds produce more NO_x in their flames than paraffins and olefins but differences between types decrease as the carbon number increases.

9.2.3 Hydrogen-Carbon Ratio (H/C)

A plot of measured total NO_x versus the fuel hydrogen-to-carbon ratio (H/C) for fixed combustion conditions is shown in Figure 9.7. Although the NO_x levels are shown to decrease with an increase in H/C, the scatter of data points is large. It is interesting to note that this parameter, which is usually used to correlate the practical fuel

emission performance to the fuel composition, also fails to correlate the flame temperature or the equilibrium NO for different fuels. The scatter, however, is a maximum for the olefins and naphthenes which have the common H/C value of 2.0.

9.2.4 Adiabatic Flame Temperature

The difference in the chemical structure of fuel which includes variations in fuel type, carbon number and H/C, causes variations in both flame temperature and equilibrium concentrations and hence in thermal NO_x formation. Thermal NO_x formation, however, has been shown in Chapter 5 to depend on the flame temperature only irrespective of the fuel composition. This is confirmed in Figure 9.8.

The chemical structure of fuel may be expected to influence the kinetics and species levels within the main reaction zone, and may, therefore, influence prompt NO_x formation. If this is the case, then prompt NO_x formation is not a function in temperature only and some evidence of this is also given in Figure 9.8.

9.2.5 Correlation of Prompt NO_x with Practical Fuel Properties

All commercial hydrocarbon fuels are a complex mixture of different hydrocarbon compounds, and are not normally specified in terms of percentage type, carbon number, etc. Although the H/C value is a property which can be readily determined for such fuels, it is not a unique property for olefins and naphthenes as is shown above. The heat of formation per unit mass of fuel is another property which can be calculated easily from the heat of combustion of fuel and the H/C ratio. This property does provide a better differentiation between the fuels; it does, for example, separate the olefins and naphthenes.

A plot of NO_x levels versus the standard heat of formation per unit mass of fuel (Δh_f) is shown in Figures 9.9 and 9.10. A very satisfactory level of correlation is shown for all fuels at different pressures and different equivalence ratios. A similar plot of prompt NO_x versus heat of formation produces a higher degree of scatter as shwon in Figure 9.11. This is to be expected as prompt NO_x depends on both the fuel structure as well as flame temperature. It is shown, therefore, that to correlate prompt NO_x it is necessary to take into account both the heat of formation and H/C ratio. These two properties together do provide a better description of the thermal-chemical properties of the fuel and it is to be expected that a better correlation can be obtained if both are used. As the flame temperature varies directly with the heat of formation and inversely with H/C ratio (see Chapter 3), then useful correlation may be obtained with the parameter $\Delta h_f/(H/C)$. Figure 9.12 shows the level of agreement obtainable.

It should be noted that this Figure only gives prompt NO_x values for different fuels assuming adiabatic combustion at constnat equivalence ratio. For flame temperatures other than the adiabatic temperature, according to References 81 and 82 prompt NO_x can be calculated from that at adiabatic conditions using the relation:

$$\text{prompt } NO_x = B\, e^{-E/T_f}$$

where E is about 35 kcal/mole as experimentally determined for lean flames and T_f is the flame temperature.

9.3 INFLUENCE OF PRESSURE

It has been shown in Chapter 5 that thermal NO_x formed after a fixed residence time in adiabatic flames is proportional to $\sqrt{p}$. The influence of pressure upon prompt NO_x is not so clearly defined at present. Fenimore (Ref.74) and Bowman (Ref.57) have suggested that prompt NO_x formed in adiabatic, fuel lean flames, is proportional to $\sqrt{p}$ while investigations carried out by Heberling (Ref.81) suggest that for $\phi < 0.8$, prompt NO_x is independant of pressure. Although the common range of equivalence ratios investigated at different pressures in the present study is very small, the data in Figure 9.13 indicates that for equivalence ratios around 0.7 a small difference in total NO_x is measured when the pressure is increased from 1.0 to 3.0 atm. This small difference may, however, be due to differences in thermal NO_x rather than in prompt NO_x. Although the fraction of prompt NO_x formed in the flame front increases with pressure (see Figures 9.1 and 9.3), the prompt NO_x formed just outside the main reaction zone via an accelerated Zeldovitch mechanism may decrease due to an increased radical recombination rate. The influence of pressure on prompt NO_x is clearly shown in Figure 9.14 where $\dot{N}O_x$ profiles of two similar propane-air flames are compared. In the high pressure flame, NO_x is formed at high rate but the C-H-O equilibrium is attained faster and the prompt NO_x level is observed to be essentially the same for both flames. It is concluded that in lean flames and for $\phi < 0.8$ the measured prompt NO_x levels formed in adiabatic hydrocarbon-air flames are independant of pressure, which supports the results reported in Reference 81.

9.4 COMPARISON OF THEORETICAL PREDICTIONS WITH EXPERIMENTAL DATA

As fully described in Chapter 5, it is convenient to consider that there are three main mechanisms by which NO (NO_2 is formed from NO) can be formed:

a) thermal NO which is produced by oxidation of atmospheric nitrogen via the Zeldovitch mechanism assuming that C-H-O system is in equilibrium,

and there are two forms of "prompt" NO,

b) that due to overshoot of the oxygen atom above the equilibrium level. This occurs in the region just downstream the main reaction zone,

c) that formed within the flame front by a mechanism which is not fully understood but which is thought to include the intermediary hydrocarbon species (most of the NO formed by this step is oxidised to NO_2).

The model presented in Chapter 5 is able to take only the first two mechanisms into account as the fuel oxidation is represented by a global rate equation which cannot predict the intermediary hydrocarbon species. Only limited comparison between experimental and theoretical results can be made, therefore, and that at these conditions where the contribution made by the third mechanism is limited. All results are used, however, to attempt to isolate the contribution made by this mechanism.

Calculation of NO emissions, therefore, involve a determination of the contribution made by the Zeldovitch mechanism only. The determination of the O atoms levels required for computations is based upon the use of a partial equilibrium model described in Chapter 4 and refined in Chapter 8. Temperature profiles are determined and heat losses are allowed for as explained in Section 8.4.

A comparison for propane-air flames between measured and predicted values is shown in Figure 9.15. Calculations are made using the knowledge gained from the CO study. The value of k_{11} of the reaction

$$O_2 + H + M \xrightarrow{k_{11}} HO_2 + M \quad \ldots \quad (11)$$

was taken to be $4 \times 10^{15} e^{500/T}$ which is the relationship found to give good CO agreement, and partial equilibrium assumption was assumed to be applicable after 95 percent of the fuel had been oxidised. Calculations were also made for the 90 percent level but as the Figure shows, the level of agreement is decreased.

The same level of agreement between measured and predicted NO profiles is obtained for other fuels as shown in Figures 9.16 and 9.17. This however tends to justify the assumption that, at atmospheric pressure, the NO profiles measured experimentally are those formed outside the main reaction zone via the Zeldovitch mechanism, while most prompt NO formed in the main reaction zone (i.e. see c above) is converted into NO_2 and as it has been shown in Section 9.1, a very small fraction of which is reconverted into NO in the post-flame zone.

The method is extended to compute total NO levels for all the fuels tested in the present study and results are shown in Figure 9.18. They follow the same trends as those measured experimentally. Calculated prompt NO due to O atom overshoot is found to increase with the equivalence ratio in the same manner as total NO, but with a reduced rate of increase, see Figure 9.19.

For nonadiabatic flames, prompt NO is found to decrease with an increase in the equivalence ratio if the flame temperature is kept constant, see Figure 9.20. This, however, contradicts the experimental results of Fenimore (Ref.74) where the converse was found. These contradictions can be explained if it is assumed that prompt "c" NO, i.e. that is formed by intermediary hydrocarbon species, in the flame front, increases with equivalence ratio at constant flame temperature. It is then possible for both sets of information to be correct as the trend will depend upon the relative contribution of the two differing mechanisms of prompt NO.

The total NO levels predicted at higher pressure are found to be less than those predicted at atmospheric pressure, as shown in Figure 9.21. The slopes of NO profiles in the post-flame zone are, however, higher for the high pressure conditions, which suggests that the lower NO concentration at high pressure is due to the decrease of predicted prompt NO with pressure. A comparison between predicted and measured prompt NO levels are made difficult due to the inherent difficulties in determining the measured prompt NO. Slight error in measurement of the thermal NO slope can produce a significant change in the extracted prompt NO particualrly at high pressure and temperature. When the predicted total NO profiles at high pressure are compared with those measured experimentally, they are found to be much smaller, see Figure 9.22. The discrepancy found can be attributed mainly to the reduction in the predicted prompt NO at high pressure (note that the slopes of the measured and predicted NO profiles are nearly the same in the post-flame zone, which means equal predicted and measured thermal NO).

In fact, the variation of prompt NO with inlet pressure will depend again upon the relative significance of the two prompt NO mechanisms. As the inlet pressure increases, prompt 'b' NO, i.e.that formed due to O atom overshoot, decreases due to the increased recombination rate. On the other hand, prompt 'c' NO, formed in the flame front by interaction with the C-O-H intermediary species may increase with increased pressure. Although this flame front NO is instantaneously oxidised into NO_2 in the flame front, a large percentage is reconverted into NO in the post-flame zone and causes the measured NO levels to be higher than that predicted theoretically, as shown in Figure 9.22. This, however, can also explain the results of Heberling (Ref.81) who found that, although the measured prompt NO remains constant as the pressure increases (for $\phi < 0.8$), the predicted prompt NO was found to be proportional to $p^{-0.8}$, even if the O atom overshoot is taken into account. Clearly, further improvements are needed to the NO model for more reliable predictions at different combustion conditions.

9.5 SUMMARY AND CONCLUSIONS

1) Appreciable amounts of NO_x were measured in the relatively low temperature lean flames investigated in the present study, and most of it was found to be formed within, and very near, the primary reaction zone. NO_2 represented a large percentage of the total NO_x measured and it was found to be formed in the early stages of the flame, most likely from NO (there is a possibility that the NO_2 was formed in the sampling system).

2) The influence of the chemical structure of the fuel upon thermal NO_x and prompt NO_x was found to differ. In the case of thermal NO_x the influence could be explained solely in terms of the influence that the fuel had upon flame temperature, whereas prompt NO_x levels were influenced more strongly than might be expected for temperature considerations alone.

3) Prompt NO_x was found not to increase with pressure (for $\phi < 0.8$), but the relative significance of the two different formation mechanisms did exhibit a change. As the pressure increased, the contribution made by O atom overshoot coupled with Zeldovitch formation kinetic scheme was found to decrease, whereas the prompt NO_x formed in the main reaction zone increased and became more important.

4) The partial equilibrium kinetic model developed here which assumes NO formation via Zeldovitch mechanism was found to be satisfactory for all fuels only at low pressure (1 atm) conditions. This supports the assumption that in atmospheric pressure burners the NO measured is formed mostly in the post flame zone, while that formed in the flame front appears as NO_2.

5) Predicted NO profiles at high pressure do not agree with those measured experimentally. This can be attributed to the fact that a proper account is not taken of the NO and NO_2 formation mechanisms in the main reaction-zone.

CHAPTER 10

CONCLUSIONS AND RECOMMENDATIONS FOR FURTHER WORK

10. CONCLUSIONS AND RECOMMENDATIONS FOR FURTHER WORK

In this chapter, attempts are made to summarise the main conclusions of the work and to isolate factors that can be useful in the design of combustion systems. Recommendations for further work in areas relevant to the present study are then presented.

10.1 SUMMARY AND CONCLUSIONS

An investigation of the influence of the fuel structure on both CO and NO_x formation in lean, premixed, flat flames has been carried out under the following operating conditions:

ϕ = 0.6 - 0.9

p = 1-3 atm

T_i = 413^oK

fuels : propane, dodecane, propene, dodecene, benzene, o-xylene, tetralin and kerosine.

The conclusions drawn from this work may be stated as follows:

(A) Experimental measurements and results confirm the following points:

1. Fuel structure influences the CO-time history significantly. This time history can be characterised by the minimum CO level, CO_{min}, that can be obtained for a given combustion time and the equivalence ratio at which it occurs, ϕ_r. Aromatics and naphthenes give higher values of both ϕ_r and CO_{min} than paraffins and olefins. Among each hydrocarbon type both ϕ_r and CO_{min} increase with increased carbon number but the dependence on H/C mole ratio is very complicated.

2. Increasing the inlet temperature and pressure reduces both ϕ_r and CO_{min} and also reduces the differences among fuels.

3. The fuel structure affects ϕ_r mainly through its influence on CO generation process rather than on its burnout; CO generation times are very important especially at weak mixtures and low temperature conditions.

4. Experimentally derived global fuel oxidation rate equations proved to be dependent on the fuel structure, and different equations are obtained for different fuels.

5. The CO oxidation process is controlled by the radical recombination rate; the experimentally derived global CO oxidation rate equations are not generally applicable for different flames or even within the whole oxidation range in the same flame.

6. Fuel structure affects CO burnout within, and very near, the main reaction zone by influencing the super-equilibrium radical concentrations.

7. NO_x formation starts in the main reaction zone even in very lean flames at relatively low temperature; NO_2 constitutes a large percentage of the total NO_x under these conditions but this percentage decreases as both the equivalence ratio and the flame temperature increase.

8. NO_2 is formed in the early stages of combustion, probably from NO, and it is reconverted into NO in the post-flame zone with the reconversion rate increasing with increased pressure and equivalence ratio.

9. The fuel structure does not affect NO_x formation in the post equilibrium phase of combustion (thermal NO_x) if account is taken of the flame temperature differences, but it strongly influences quickly formed "prompt" NO_x within, and very near, the main reaction zone. Aromatics produce more prompt NO_x than paraffins.

10. Increasing the pressure does not affect prompt NO_x in lean flames ($\phi < 0.8$), but the relative significance of the two formation mechanisms does change. While prompt NO_x formation in the flame via the non-Zeldovitch mechanism increases, the contribution made by the O atom overshoot coupled with the Zeldovitch formation mechanism becomes less significant.

(B) A kinetic model based on the partial equilibrium assumption has been developed to predict both CO and NO time-histories. The fuel oxidation is allowed for by using a global fuel oxidation rate equation while NO is assumed to form entirely via the extended Zeldovitch mechanism and its formation to start at the end of the main reaction zone. Based on the comparison between theoretical predictions and experimental data, the following can be concluded:

1. The model can predict the measured CO-time histories satisfactorily for different fuels and under different conditions if the global fuel oxidation equation is accurately defined for each fuel.

2. NO profiles for different fuels can be accurately predicted only at atmospheric pressure; at high pressures the predicted NO concentrations are much lower than those measured experimentally. This is attributed to the fact that proper account is not taken

of the NO and NO_2 formation mechanisms that involve the hydrocarbon radicals. It is not clear at present whether a more detailed fuel oxidation mechanism can resolve the differences or whether additional reactions for the formation of NO are required.

10.2 RECOMMENDATIONS FOR FURTHER WORK

1. The presence of aromatic compounds are shown to be very important when considering both CO and NO_x emissions with a wide variation among its members. It is suggested that more members of this type be investigated; polycyclic aromatics may also be investigated.

2. Influence of the fuel structure on soot formation is an important aspect to be taken into account when considering the fuel effects on the combustion process. The ability of global fuel oxidation models to predict the influence of the fuel structure on soot formation should be studied.

3. From practical considerations it is important that the fuel effects on combustion should be investigated over a wider range of conditions. The same fuels as used here can be investigated in laminar, premixed turbulent, and turbulent diffusion flames. The interaction between the differing fluid mechanics, the fuel chemical and physical properties may reduce or magnify the differences between the fuels.

4. NO_2 was shown to be a very important component in total NO_x emissions in very weak mixture combustion. The kinetics of its formation and decomposition must be explored so that it can be fully taken into account in any future investigation of NO_x formation.

REFERENCES

1. Goodger, E.M. — Hydrocarbon Fuels. The Macmillan Press Ltd., London and Basingstoke, 1975

2. Obert, E.F. — Internal Combustion Engines, 3rd Ed. International Text Book Company, Scranton, Pennsylvania, 1970. pp 222-290

3. Harrington, J.A. & Shishu, R.C. — A single cylinder engine study of the effects of fuel type, fuel stoichiometry, and hydrogen-to-carbon ratio on CO, NO, HC exhaust emissions. SAE Paper 730476, 1973

4. Butze, H.F. & Ehlers, R.C. — Effect of fuel properties on performance of a single aircraft turbo-jet combustor. NASA TMX-71789, October 1975

5. Harting, R.G.T. & Wanger, H.G. — Thermal decomposition of methane behind reflected shock waves. Thirteenth Symposium "International" on Combustion, The Combustion Institute, Pittsburgh, 1971, pp.147

6. Asaba, T. & Fujii, N. — Shock-tube study of high-temperature pyrolysis of benzene. Thirteenth Symposium "International" on Combustion, The Combustion Institute, Pittsburgh, 1971, pp.155

7. Gardner, W.C., Owen, J.H., Clark, T.C., Dave, J.E., Bauer, S.H., Miller, J.A. and McLean, W.J. — Rate and mechanism of methane pyrolysis from 2000° to 2700°K. Fifteenth Symposium "International" on Combustions, The Combustion Institute, Pittsburgh, 1974, pp.857

8. Bradley, J.N. — Flames and Combustion Phenomena. Chapman and Hall, 1969

9. Baldwin, R.R. & Walker, R.W. — Problems and progress in hydrocarbon oxidation. Fourteenth Symposium "International" on Combustion, The Combustion Institute, Pittsburgh, 1973, pp.241

10. Fristrom, R.M., Avery, W.H. & Grunfelder, C.
Reaction of simple hydrocarbons in flame fronts. Micro structure of C_2 hydrocarbon-oxygen flames.
Seventh Symposium "International" on Combustion, Butterworth Scientific Publications, London 1959, pp.304

11. Porter, R.P. & Clark, A.H.
A study of hydrocarbon flames.
Eleventh Symposium "International" on Combustion, The Combustion Institute, Pittsburgh, 1967, pp.907

12. Westenberg, A.A. &Fristrom, R.M.
H and O atom profiles measured by ESR in C_2 hydrocarbon - O_2 flames
Tenth Symposium "International" on Combustion, The Combustion Institute, Pittsburgh, 1965, pp.473

13. Williams, G.C. & Hottle, H.C.
The combustion of methane in jet stirred reactor.
Twelvth Symposium "International" on Combustion, The Combustion Institute, Pittsburgh, 1969, pp.913

14. Koslov, G.I.
On high temperature oxidation of methane.
Seventh Symposium "International" on Combustion, Butterworth Scientific Publications, London, 1959, pp.142

15. Drayer, F.L. & Glassman, I.
High-temperature oxidation of CO and CH_4.
Fourteenth Symposium "International" on Combustion, The Combustion Institute, Pittsburgh, 1973, pp.987

16. Chinitz, W.
Theoretical analysis of non-equilibrium methane-air combustion.
AIAA Paper No. 64-524, May, 1964

17. Bowman, C.T., & Seery, D.J.
An experimental and analytical study of methane oxidation behind shock wave.
Combustion and Flame, Vol.14, 1970, pp.37

18. Soreson, S.C., Myers, P.S. & Uyehara , O.A.
Ethane kinetics in spark ignition engine exhaust gases.
Thirteenth Symposion "International" on Combustion, The Combustion Institute, Pittsburgh, 1971, pp.451

19. Chinitz, W. & Baurer, T.
An analysis of non-equilibrium hydrocarbon-air combustion.
Paper WSCI 65-19, Western State Section, The Combustion Institute, 1965

20. Kollrack, R. & Aceto, L.D. — Nitric oxide formation in gas turbine combustors. AIAA Journal, Vol.11 No.5, May 1973 pp.664.

21. Mosier, S.A., Roberts, R. & Henderson, R.E. — Development and verification of an analytical model for predicting emission from gas turbine engine combustion during low power operation. AGARD Conference Proceedings No.125, Paper 25, 1973.

22. Edelman, R.B., & Fortune, O.F. — A quasi-global chemical kinetic model for the finite rate combustion of hydrocarbon fuels with application to turbulent burning and mixing in hypersonic engines and nozzles. AIAA Paper No. 69-86, 1969.

23. Edelman, R.B. & Economos, C. — A mathematical model for the jet engine combustor pollutant emissions. AIAA Paper No. 71-714, 1971.

24. Schefer,R.W. & Sawyer, R.F. — Lean premixed recirculating flow combustion for control of oxides of nitrogen. Sixteenth Symposium "International" on Combustion, The Combustion Institute, Pittsburgh, 1976, pp.191-137.

25. Howard, J.B. Williams, G.C., & Fine D.H. — Kinetics of carbon monoxide oxidation. Fourteenth Symppsium "International" on Combustion. The Combustion Institute, Pittsburgh, 1973, pp.975.

26. Singh, T. and Sawyer, R.F. — CO Reaction in the After Flame Region of Ethylene/Oxygen and Ethane/Oxygen Flames. Thirteenth Symposium "International" on Combustion, The Combustion Institute, Pittsburgh, 1971, pp.403

27. Fenimore,C.P. & Jones, G.W. — The high temperature oxidation of carbon monoxide. J.Phys.Chem., Vol.61, 1957, pp.651-654

28. Sobelev, G.K. — High temperature oxidation and burning of carbon monoxide. Seventh Symposium "International" on Combustion, Butterworth Scientific Publications, London, 1959, pp.385.

29. Fine, B. — Chemical sampling downstream of lean flat hydrogen and propane flames. NASA TN 0198, 1959, pp.15-18

30. Hottle, H.C., Williams, G.C., Nerheim, N.M. & Schneider, G.R.
Kinetic studies in stirred reactors: combustion of carbon monoxide and propane. Tenth Symposium "International" on Combustion, The Combustion Institute, Pittsburgh, 1965, pp.111-121

31. Kaskan, W.E.
The decay of the carbon monoxide in the flame gases of some lean flames. Combustion and Flame, Vol.3, 1959, pp.49

32. Baulch, D.L., Drysdale, D.D. & Lloyd, A.C.
High Temperature Reaction Rate Data. Dept. of Phy.Chem. Report No.1, University of Leeds, England, 1968

33. Dryer, F.L., Naegli, D.W. & Glassman, I.
Temperature dependence of the reaction $CO + OH \rightarrow CO_2 + H$. Combustion and Flame, Vol.17, 1970, pp.270

34. Vandooren, J., Peeters, J. and Tiggelen, V.P.J.
Rate constant of the elementary reaction of carbon monoxide with Hydroxyl radical. Fifteenth Symposium "International" on Combustion, The Combustion Institute, Pittsburgh, 1975, pp.745.

35. Baulch, D.L. & Drysdale, D.D.
An evaluation of the rate data for the reaction $OH + CO \rightarrow CO_2 + H$. Combustion and Flame, Vol.23, 1974, pp.215.

36. Waldman, C.H., Wilson, R.D. & Engleman, V.S.
Analysis of the kinetic mechanism of methane-air combustion with air pollutant formation. Paper WSS/CI 74-2, Western States Section, The Combustion Institute, 1974.

37. Fristrom, R.M. & Westenberg, A.A.
Flame Structure. McGraw-Hill, New York, 1965.

38. Leonard, P.A., Plee, S.L. & Mellor, A.M.
Hydrocarbon combustion kinetics, I : Burner studies. Technical Report No. 11916, U.S.Army Tank Automotive Command, Warren, Mich. 1974.

39. Westenberg, A.A. & de Haas, N.J.
Steady state intermediate concentrations and rate constants, Some HO_2 results. J.Phy.Chem., Vol.176, 1972, pp.1589.

40. Homer, J.B. & Sutton, M.M.
Nitric oxide formation and radical overshoot in premixed hydrogen flames.
Combustion and Flame, Vol.20, 1973, pp.71-76

41. Fenimore, C.P. & Moore, J.
Quenched carbon monoxide in fuel lean flame gases.
Combustion and Flame, Vol.22, 1974, pp.343-351

42. Biordi, J.C., Lazzara, C.P. & Papp, J.E.
An examination of the partial equilibrium, hypothesis and radical recombination in 1/20 atm methane flames.
Sixteenth Symposium "International" on Combustion, The Combustion Institute, Pittsburgh, 1976,pp.1097

43. Westenberg, A.A.
Kinetics of NO and CO in lean,premixed hydrocarbon-air flames.
Comb.Sci.Technol., Vol.4, 1971, pp.59-64.

44. Sheppard, C.
A simple model for carbon monoxide oxidation in gas turbine combustors.
Comb.Sci.Technol., Vol.11, 1975, pp.49.

45. Bulewicz, E.M., James, E.G., &
Photometric investigations of alkali metals in hydrogen flames.
II : Study of excess concentration of hydrogen atom in burnt gas mixtures.
Proc.Roy.Soc. A.235, 1958, pp.89

46. Kaskan, W.E.
Hydroxyl concentrations in rich hydrogen-air flames held on porous burner.
Combustion and Flame, Vol.2, 1958, pp.229

47. Kaskan, W.E. & Scott, G.L.
Requirements imposed by stoichiometry in dissociation-recombination reactions.
Combustion and Flame, Vol.6, 1962, pp.73

48. Ay, J.H. & Sichel, M.
Theoretical analysis of NO formation near the primary reaction zone in methane combustion.
Combustion and Flame, Vol.26, No.1, Feb.1976, pp.1-7

49. Keck, J.C. & Gillespie, D.
Rate-controlled partial-equilibrium method for treating reacting gas mixtures.
Combustion and Flame, Vol.17, 1971, pp.737-741

50. Morr, A.R. & Heywood, J.B.
Partial equilibrium model for predicting concentration of CO in combustion.
ACTA Astronautica, Vol.1, 1974, pp.949-966

51. Thompson, D., Brown, T.D. & Beer, J.M.
Formation of NO in a methane-air flame.
Fourteenth Symposium "International" on Combustion, The Combustion Institute, Pittsburgh, 1973, pp.787

52. Sarofirm, A.F. & Pohl, J.H.
Kinetics of nitric oxide formation in premixed laminar flames.
Fourteenth Symposium "International" on Combustion, The Combustion Institute, Pittsburgh, 1973,, pp.739

53. Iverach, D., Basden, K.S. & Kirov, N.Y.
Formation of nitrog oxide in fuel-lean and fuel-rich flames.
Fourteenth Symposium "International" on Combustion, The Combustion Institute, Pittsburgh, 1973, pp.767

54. Friedman, R.
Measurement of the temperature profile in a laminar flame.
Fourth Symposium "International" on Combustion, Mass.Inst.Tech., 1952, Wilkins & Co, Baltimore, 1953, pp.259.

55. Gaydon, A.G. & Wolford, H.G.
Flames, Their Structure, Radiation and Temperature.
3rd ed. Chapman & Hall Lt.d, 1976, pp.85

56. Brown, N.J., Fristrom, R.M. & Sawyer, R.F.
A simple premixed flame model including an application to H_2 Air Flames.
Combustion and Flame, Vol.23, 1974, pp.269

57. Bowman, C.T.
Kinetics of nitric oxide formation in combustion process.
Fourteenth Symposium "International' on Combustion, The Combustion Institute, Pittsburgh, 1973, pp.724-737

58. Bowman, C.T.
Kinetics of pollutants formation and destruction in combustion.
Progress in Energy and Combustion Science. "An International Journal", Vol.1, No.1, 1975, pp.33

59. Zeldovitch, Ya.B., Sandovnikov, P.Ya. & Frank-Kamenetskii,D.A. — Oxidation of nitrogen in combustion. Academy of Science of USSR, Institute of Chem.Phys., MOSCO, Leningrad, 1947

60. Fenimore, C.P. & Jones, G.W. — Nitric oxide decomposition at 2200-2400^{o}K. J.Phys.Chem., Vol.61, 1957, pp.654

61 Singer, J.M., Cook, E.B., Harris, M.E., Powe, V.R. & Grumer, J. — Flame characteristics causing air pollution, I : Production of oxides of nitrogen and carbon monoxide. US Dept. of Int.Bureau of Mines, Report No. 6958, presented at Symp.Comb.Reaction of Fossil Fuels, Div.Fuel Chem., American Chemical Society, Sept.1966.

62. Boulch, D.L., Drysdale, D.D., Horne, D.G. & Lloyd, A.C. — Evaluated Kinetic Data for High Temperature Reactions. Vol.2, CRC Press, 1973.

63. Lavoie, A.G., Heywood, J.B. & Keck, J.C. — Experimental and theoretical study of nitric oxide formation in internal combustion engines. Combustion Science Technology, Vol.1, 1970, pp.313

64. Campbell, I.M.& Thrust, B.A. — Reactivity of hydrogen to atomic nitrogen and atomic oxygen. Trans.Faraday Soc., Vol.64, 1968, pp.1265

65. Baulch, D.I., Drysdale, D.D., Horne, D.G. & Lloyd, A.C. — Evaluated Kinetic Data for High Temperature Reactions. Vol.1, CRC Press 1972.

66. Flower, W.L., Hanson, R.K. & Kruger, C.H. — Kinetics of the reaction of nitric oxides with hydrogen. Fifteenth Symposium "International" on Combustion, The Combustion Institute, Pittsburgh, 1975, pp.823

67. Duxbury, J. & Pratt, N.H. — A shock tube study of NO kinetics in the presence of H_2 and Fuel-N. Fifteenth Symposium "International" on Combustion, The Combustion Institute, Pittsburgh, 1975, pp.843

68. Bradley, J.N. & Graggs, P. — The reaction of hydrogen with nitric oxide at high temperature. Fifteenth Symposium "International" on Combustion, The Combustion Institute, Pittsburgh, 1975, pp.833

69. Benson, S.W., Golden, D.M., Lawrence, R.W.& Shaw, R. — Estimated combustion and nitric oxide kinetics. Quarterly Progress Report 2, EPA Grant R-800 - 798, February, 1973.

70. Bowman, B.R., Pratt, D.T. & Crowe, C.T. — Effect of turbulent mixing and chemical kinetics on nitric oxide production in a jet-stirred reactor. Fourteenth Symposium "Internaitonal" on Combustion, The Combustion Institute, Pittsbury, 1973, pp.819

71. Malte, P.C. & Pratt, D.T. — The role of energy releasing kinetics in NO_x formation : fuel-lean, jet stirred, CO-air combustion. Comb.Sci.Technol. Vol.9, 1974, pp.221

72. Fletcher, R.S. & Heywood, J.B. — A model for nitric oxide emissions from aircraft gas turbines. Paper 71.123 Presented at AIAA 9th Aerospace Science Meeting, N.Y. 1971

73. Semerjian, H. & Vranos, A. — NO_x formation in premixed turbulent flames. Sixteenth Symposium "International" on Combustion, The Combustion Institute, Pittsburgh, 1976, pp.167

74. Fenimore, C.P. — Formation of nitric oxide in premixed hydro-carbon flames. Thirteenth Symposium "International" on Combustion, The Combustion Institute, Pittsburgh, 1971, pp.373

75. Newhall, H.K. & Shahed, S.M. — Kinetics of nitric oxide formation in high pressure flames. Thirteenth Symposium "International" on Combustion, The Combustion Institute, Pittsburgh, 1971, pp.381

76. Fletcher, R.S., Siegel, R.D. & Bastress, E.K. — The control of oxides of nitrogen emissions from aircraft gas turbine engines. NREC Report No.1162, Vol.1, Northern Research and Eng.Corp., Cambridge, Mass., 1971

77. Haynes, B.S., Iverach, D. & Kirov, N.W.
The behaviour of nitrogen species in fuel-rich hydrocarbon flames.
Fifteenth Symposium "International" on Combustion, The Combustion Institute, Pittsburgh, 1975, pp.1103-1111

78. Leonard, P.A., Plee, S.L. & Miller, A.M.
Nitric oxide formation from fuel and atmospheric nitrogen.
Combus.Sci.Technol. Vol.14, 1976, pp.183-193

79. Blauwen, J., Smets, B. & Peeters, J.
Mechanism of "prompt" NO formation in hydrocarbon flames.
Sixteenth Symposium "International" on Combustion, The Combustion Institute, Pittsburgh, 1976, pp.1055

80. de Soete, G.G.
Overall reactions rates of NO and N_2 formation from fuel nitrogen.
Fifteenth Symposium "International" on Combustion, The Combustion Institute, Pittsburgh, 1975, pp.1093

81. Heberling, P.W.
Prompt NO measurements at high pressure.
Sixteenth Symposium "Internaional" on Combustion, The Combustion Institute, Pittsburgh, 1976, pp.154-166.

82. Eberius K.H. & Just, Th.
NO formation in rich flames: a study on the influence of hydrocarbon structure.
AGARD Conference on Air Pollution, Polleten 125, 1973, paper 16.

83. Bachmaier, F, Eberius K.H. & Just, T.
The formation of nitric oxide and the detection of HCN in premixed hydrocarbon-air flames at 1 atmosphere.
Combustion Sci.Technol, Vol.7, 1973, pp.77-84

84. Fenimore,C.P.
Formation of nitric oxide from fuel nitrogen in ethylene flames
Combustion and Flame Vol.19, 1972 pp.289-296

85. Flagan, R.C., Serge, G. & Appleton, J.
Rate constrained partial equilibrium models for the formation of nitric oxide from organic fuel nitrogen.
Combustion and Flame, Vol.22, 1974, pp.299-311

86. Schefer, R.W., Mathews, R.D., Gernansky, N.P. & Sawyer, R.F.
Measurements of NO and NO_2 in combustion systems.
Paper WSCI 73-31, Western State Sect., The Combustion Institute, El Segundo, California, 1973.

87. Anon.
Exhaust emission test, AiResearch aircraft propulsion and auxiliary power gas turbine engine.
AiResearch Corp., Rep.No. GT 8747-R-10, September, 1971.

88. Fenimore, C.P.
The ratio of NO_2/NO in fuel-lean flames.
Combustion and Flame, Vol.25, 1975, pp.85.

89. Herryman, E.L. & Levy, A.
Nitrogen oxide formation in lean flames: the role of NO_2 and fuel nitrogen.
Fifteenth Symposium "International" on Combustion, The Combustion Institute, Pittsburgh, 1975, pp.1073

90. Allen, J.D.
Probe sampling of oxides of nitrogen from flames.
Combustion and Flame, Vol.24, 1975, pp.193

91. Tottle, J.H., Shister, R.A., & Mellor, A.M.
Nitrogen dioxide formation in gas turbine engine, measurements and measurement method.
Combustion Sci.Technol., Vol.9, 1974, pp.261-271

92. Calcote, H.F.
Accurate control and vaporising system for small liquid flows.
Analytical Chem., Vol.20, 1950, pp.1058

93. Sawyer, R.F., Teixeira, D.P. & Starkman, E.S.
Air pollution characteristics of gas turbine.
ASME Trans., Oct.1969, pp.29.

94. Kaskan, W.E.
The dependence of flame temperature on mass burning velocity.
Sixth Symposium "International" on Combustion, The Combustion Institute, Pittsburgh, 1957, pp.134

95. Starkman, E.S., Mizutani, Y., Sawyer, R.F. & Teixeira, D.P.
The role of chemistry in gas turbine emissions.
ASME Paper 70-GT-81, 1970

APPENDIX A : FUEL CHARACTERISTICS AND PROPERTIES

Table A.1 : Chemical and Physical Properties of Investigated Pure Hydrocarbons

Fuel	Formula	Molecular weight	H/C mole ratio	Heat of* formation kcal/mole	Heat of combustion kcal/mole	Stoichio-metric fuel-to-air ratio $(F/A)_s$	Boiling point ^oC	Freezing point ^oC	Relative density at 20^oC
Propane	C_3H_8	44.094	2.667	-24.82	530.6	0.064	-41.92	-187.54	gas
Dodecane	$C_{12}H_{26}$	170.328	2.167	-69.52	1947.84	0.0667	216.43	-9.44	0.748
Propene	C_3H_6	42.078	2.00	4.88	491.8	0.0678	-47.57	-185.1	gas
Dodecene	$C_{12}H_{24}$	168.312	2.00	-39.52	1908.96	0.0678	213.5	-1.0	0.76
Methyl-cyclo-hexane	C_7H_{14}	98.182	2.00	-36.99	1044.3	0.0678	101.08	-126.44	0.771
Benzene	C_6H_6	78.108	1.00	19.82	788.99	0.0755	80.25	-5.68	0.878
O-xylene	C_8H_{10}	106.106	1.25	4.54	1098.1	0.0733	144.56	-25.3	0.879
Tetralin	$C_{10}H_{12}$	132.196	1.20	6.6	1347.5	0.0738	206	-	0.968

* To convert to SI units multiply kcal/mole by 4.1868 to get kJ/mole

Table A.2 : D.Eng.R.D. Specifications for Kerosines (Ref.1)

Type	Aviation gas turbine kerosine AVTUR	High flash kerosine AVCAT
Designation	JET A - JET A1	JP5
Relative density	0.775 to 0.83 (0.794)	0.788 t 0.845
Net calorific value (kcal/kg)	10222.2 (10338.8)	10166.7
Distillation (% vol)	IBP (150°C)	-
	10 at (174°C)	10 at 204°C
	20 at 200 (180°C)	-
	50 at (198°C)	-
	90 at (226°C)	-
	FBP 288 (243°C)	288°C
Residue (% vol)	1.5	1.5
Loss (% vol)	1.5	1.5
Flash point (°C)	38 (47.2)	60
Viscosity (cSt at 20°C)	2.0	-
Freezing point (°C)	-50 (-52)	-46
Smoke point (mm)	20 (26.3)	20
Sulphur (% wt)	max. 0.2 (0.015)	max. 0.3
Olefins (% vol)	max. 5 (0.3)	max. 5
Paraffins (% vol)	(56.5)	-
Naphthenes	(25.5)	-
H/C (mole ratio)	(1.96)	
Stoichiometric fuel-to-air ratio (F/A)s	0.068	0.068

Note: Values between brackets are specified by the supplier for type of kerosine investigated in the present study.

APPENDIX B. A COMPUTER PROGRAM TO CALCULATE CO AND NO_x IN PREMIXED FLAMES.

B.1. FLOW CHART

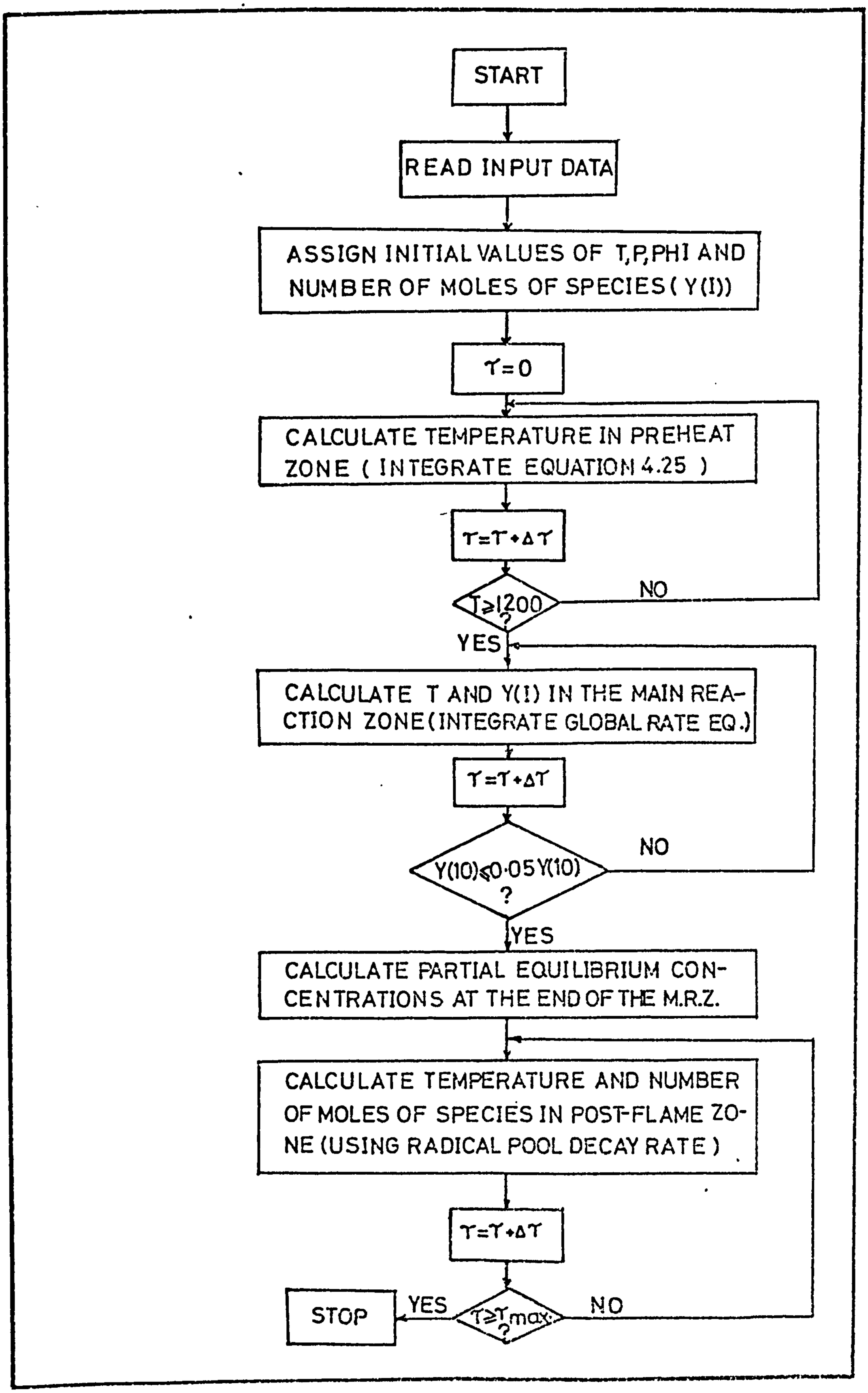

B.2 COMPUTER PROGRAM

```
DOC SOURCE-R62B
      LIBRARY(SUBGROUPNAGF)
      PROGRAM(R62B)
      COMPACT DATA
      INPUT 1=CR0
      OUTPUT 2=LP0
      END
      MASTER AHAD
      DIMENSION EP(3),H(10), X(4),F(4),AJINV(4,4),W(52),AML(10)
     U,V(4) ,S(10),D(4),PHI(10),ATI(10),ACO(10),AMS(10),AOE(6),
     1AHE(6),AH2(6),AAN(6),AAM(6) ,AFE(8) ,AOH(6),A(10,10)
      EXTERNAL FUNCT,MONIT,LSQ
      COMMON  G(10),Y(11),AJA(20,20)
      COMMON C1,C2,AA1,AA2,AA3,AB,X3 ,AMMM
C
C       Y(I)=NUMBER OF MOLES OF SPECIE I
C      Y(1)   H
C      Y(2)   O
C      Y(3)   H2O
C      Y(4)   OH
C      Y(5)   H2
C      Y(6)   O2
C      Y(7)   CO2
C      Y(8)   CO
C      Y(9)   N2
C      Y(10) FUEL
C      Y(11) NO
C
C
C      READ INPUT DATA  (THERMOCHEMICAL DATA,FUEL PROPERTIES ,
C      MIXTURE STRENGTH,MASS FLOW AND EQUILIBRIUM DATA )
C
      DO 5 I=1,9
      READ(1,4)(A(I,J),J=1,7)
4     FORMAT(7E11.4)
5     CONTINUE
      K=4
      READ(1,44)(AFE(I),I=1,K)
      READ(1,44)(AAN(I),I=1,K)
      READ(1,44)(AAM(I),I=1,K)
      READ(1,44)(AMS(I),I=1,K)
      READ(1,44)(PHI(I),I=1,K)
      READ(1,44)(ATI(I),I=1,K)
      READ(1,44)(ACO(I),I=1,K)
      READ(1,44)(AOE(I),I=1,K)
      READ(1,44)(AOH(I),I=1,K)
      READ(1,44)(AHE(I),I=1,K)
      READ(1,44)(AH2(I),I=1,K)
44    FORMAT(6F0.0)
      DO 333 KK =1,2
      DO 555 KI=1,K
```

```
C
C       ASSIGN INITIAL VALUES
C
        PH=PHI(KI)
        ANNN=AAN(KI)
        AMMN=AAM(KI)
        C1=2.*ANNN+AMMM/2.
        C3=ANNN*PH
        C2=AMMM*PH
        C4=C1*79/21
        PP=1.0
        TI=400.
        TF=ATI(KI)
        TTO=1200.+.95*(TF-1200.)
        TO=650.
        DTM=0.000005
        RATCOS=4.5E9
        IF(KK.GT.1) RATCOS=1.5E9
        EEEE=25,755
        EEE=.03
        E=EEEE-EEE*(AFE(KK))
        TM=0.0
        ATM =0.0
        CCOE=ACO(KI)
        OE=AOE(KI)*PP/(84.8*TF)
        OHE=AOH(KI)*PP/(84.8QTF)
        H2E=AH2(KI)*PP/(84.8*TF)
        HE=AHE(KI)*PP/(84.8*TF)
        DO 444 I=1,11
        Y(I)=0.
444     CONTINUE
        Y(10)=PH
        Y(11)=0.
        Y(6)=C1/2.
        YY=Y(10)
        Y(9)=C4/2.
        Y(6)=(C1-1.*Y(3)-2.*Y(7)-Y(8))/2.
        DTIME=.0005
C
C       CALCULATE TEMPERATURE PROFILE IN PREHEAT ZONE
C
        AMASS=AMS(KI)*(PH/15.7+1.)* 1./60.
        AREA=3.14*(2.54*2.125)*2.54*2.125/4.
        T=TI
        CPA=.3200*AMASS*T*29.3/(10.*AREA)
        CON =10,98*.49*.19/(.765*,237*36000.)
8       T=TO+(TO-TI)*(AMASS/AREA)*(CPA/CON)*DTM*(TO/TI)**.25
        TM=TM+DTM
        IF(TM.LT.ATM) GO TO 122
        URITE(2,500)TM,T
        ATM =ATM+DTIME
122     TO=T
        IF(T.LT.1200.) GO TO 8
C
C       CALCULATE SPECIES AND TEMPERATURE PROFILES IN THE MAIN REACTION
C       ZONE
C
```

```
      X3=Y(1)+Y(2)+Y(3)+Y(4)+Y(5)+Y(6)+Y(7)+Y(8)+Y(9)+Y(10)
777   Y(9)=C4/2-Y(11)/2
      IF(Y(10).LT..05*PH) GO TO 111
      VL=(X 3 *84.8*T)/PP
      BX=(Y(10)/VL)**.3
      F1=((RATCOS )*(T/1111.0-0.5)/ PP**0.4)*1.*EXP(-E/(0.002*T))
      B11    =-F1*Y(6)**.8/((VL**.8)*BX)
      A0=Y(10)
      A1=Y(10)*EXP(B11*DTM/2.0)
      A2=Y(10)*EXP(B11*DTM)
      FFF=(2.6E10)*EXP(-15000./(2.*T))
      AB11=FFF*(Y(3)**.4)*(Y(6)**.35)*DTM/VL**.75
      AB11=-AB11
      Y(7)=(C3-ANNN*A1)-(C3-ANNN*A1-Y(7))*EXP(AB11)
      Y(10)=A2
      Y(8)=C3-ANNN*Y(10)-Y(7)
      Y(3)=C2/2.-AMMM*Y(10)/2.
    Y(6)=(C1-Y(8)-2.*Y(7)-Y(3))/2.
      TM=TM+DTM
      T=T0+(TT0-T0)*(YY-Y(10))/YY
      TT=T
      X3=Y(1)+Y(2)+Y(3)+Y(4)+Y(5)+Y(6)+Y(7)+Y(8)+Y(9)+Y(10) +Y(11)
      IF(TM.LT.ATM) GO TO 777
      DO 77 I=1,11
      AML(I)=Y(I)/X 3
77    CONTINUE
      WRITE(2,500) TM, T , AML (10) ,AML(11)
      WRITE(2,500)(AML(I),I=1,9)
      ATM =ATM+DTIME
      GO TO 777
C
C     CALCULATE PARTIAL EQUILIBRIUM CONCENTRATIONS AT THE END OF THE
C     MAIN REACTION ZONE
C
111   X(2)=Y(3)
      X(1)=Y(6)
      AA2=(Y(8)/Y(7))*10**(1180./T-.9)
       AA1=6.852*(EXP(-4881./T))*(AA2/T**.1825)**.5
      AA3=(AA1*Y(8)/Y(7))*10**(-1.965+4590./T)
      IW=52
      N=2
      EP(1)=.000001
      EP(2)=.000001
      EP(3)=.000001
      MODE=1
      IR=1
      CALL COSPAF(N,X,F,SS,EP,MODE,D,W,IW,FUNCT,LSQ,MONIT,9,
     U100,IR)
      Y(1)=AA3*(X(1)*X(2))**.5
      Y(2)=AA2*X(1)
      Y(3)=X(2)
      Y(4)=AA1*(X(1)*X(2))**.5
      Y(6)=X(1)
      Y(5)=C2-Y(1)-2.*(Y(3))-Y(4)-    Y(10)*AMMM
      Y(5)=Y(5)/2.
      X(2)=Y(3)
      Y(9)=C4/2.-Y(11)/2.
      X3=Y(1)+Y(2)+Y(3)+Y(4)+Y(5)+Y(6)+Y(7)+Y(8)+Y(9)+Y(10) +Y(11)
      ATM =ATM-DTIME
```

```
565     Y(9)=C4/2.-Y(11)/2.
        DO 99 I=1,11
        AML(I)=Y(I)/X 3
99      CONTINUE
        XXX=Y(1)+Y(4)+2.*(Y(3)+Y(5)) +10*Y(10)
        WRITE(2,500) TM, T , AML (10) ,AML(11)
878     WRITE(2,500)(AML(I),I=1,9)
00      FORMAT(/9E15.4)
        ATM =ATM+DTIME
        IF(TM.GT.0.005) GO TO 555
        GO TO 877
C
C       POST FLAME  ZONE CALCULATIONS
C       1- FUEL,CO  AND CO2 CONCENTRATIONS
C
877     PP=PP
        VL=(X 3 *84.8*T)/PP
        F2=(6.76E10)*EXP(T/1102.)
        AAAK=(10)**(-1.965+4590./T)
        B2=F2/AAAK
        IF(Y(10).LE.(1.0E-14))       Y(10)=1.0E-14
        BX=(Y(10)/VL)**.3
        F1=((RATCUS )*(T/1111.0-0.5)/ PP**0.4)*1.*EXP(-E/(0.002*T))
        B11    =-F1*Y(6)**.8/((VL**.8)*BX)
        A0=Y(10)
        A1=Y(10)*EXP(B11*DTM/2.0)
        A2=Y(10)*EXP(B11*DTM)
        A3=ANNN
         AAAAK=Y(6)
         Y(6)=((Y(6)/VL)**.8)*VL
         AK1=(A3*F1*Y(6)Q(A0)/BX    +B2*Y(1)*(C3-A3*A0-Y(8))-F2*Y(8)*Y(4)
       U*DTM/VL
         AK2=(A3*F1*Y(6)*(A1)/BX+B2*Y(1)*(C3-A3*A1-Y(8)-AK1/2.)-F2*(Y(8)
       U+AK1/2.)*Y(4))*DTM/VL
         AK3=(A3*F1*Y(6)*(A1)/BX +B2*Y(1)*(C3-A3*A1-Y(8)-AK2/2.)-F2*(Y(8
       U)+AK2/2.)*Y(4))*DTM/VL
         AK4=(A3*F1*Y(6)*(A2)/BX+B2*Y(1)*(C3-A3*A2-Y(8)-AK3/1.)-F2*(Y(8
       U)+AK3)*Y(4))*DTM/VL
         Y(10)=A2
         Y(8)=Y(8)+(AK1 +2.*(AK2+AK3)+AK4)/6.
         Y(7)=C3-Y(10)*ANNN-Y( 8)
         Y(6)=AAAAK
C
C          2- NO   CONCENTRATION
C
        RA=(14.E13)*EXP(-37900./T)
        RB=(6.4E9)*EXP(-3140./T)
        RC=4.E13
        RD=RA/(1.6629*(T**0.11865)*EXP(-37600./T))
        FF=19.001985*(T**0.01266)*EXP(-21736./T)
        AN1=2.*RA*Y(2)*Y(9)/(X3*X3)
        AN2=FF*Y(9)*Y(6)/(X3*X3)
        AN3=(RB*Y(6)+RC*Y(4))/X3
        AN4=PP/(84.8*T)
        Z=Y(11)/X3
        BTM=DTM*AN4
        AD0=AN1*(1.-Z   *Z   /AN2)*BTM/(1.+RD*Z   /AN3)
        ZZ=Z+AD0/2.
        AD1=AN1*(1.-ZZ  *ZZ  /AN2)*BTM/(1.+RD*ZZ  /AN3)
```

```
      ZZZ=Z  +AD1/2.
      AD2=AN1*(1.-ZZZ*ZZZ/AN2)*BTM/(1.+RD*ZZZ/AN3)
      ZZY=Z   +AD2
      AD3=AN1*(1.-ZZY*ZZY/AN2)*BTM/(1.+RD*ZZY/AN3)
      Y(11)=Y(11)+(AD0+2.*(AD1+AD2)+AD3)*X3/6.
      DTM=0.000001
C
C     3-     RADICAL RECOMBINATION RATE AND CONCENTRATIONS
C
      PA=(3.2E16)*(EXP(+500./T))*X3*OE/(VL*10**(-3410./T+1.065))
      PB=4.*(OE/OHE+H2E/OHE)
      PC=9.*HE/OHE
      AP =1.
      ROA=Y(2)/(VL*OE)
      RR   =ROA
      S1=PA*(RR**2.-1.)/(AP+PB*RR**.5+PC*RR)
      S1=S1*DTM
      RR=RR-S1/2.
      S2=PA*(RR**2.-1.)/(AP+PB*RR**.5+PC*RR)
      S2=S2*DTM
      RR=ROA-S2/2.
      S3=PA*(RR**2.-1.)/(AP+PB*RR**.5+PC*RR)
      S3=S3*DTM
      RR=ROA-S3
      S4=PA*(RR**2.-1.)/(AP+PB*RR**.5+PC*RR)
      S4=S4*DTM
      ROA=ROA-(S1+2.*(S2+S3)+S4)/6.
      Y(2)=ROA*OE*VL
      Y(1)=HE*VL*ROA**1.5
      Y(4)=OHE*VL*ROA**.5
      Y(5)=ROA*VL*H2E
      Y(3)=(C2-2.*Y(5)-Y(4)-Y(1)-AMMM*Y(10))/2.
      Y(6)=(C1-Y(4)-Y(3)-Y(2)-Y(8)-2.*Y(7))/2.
      X3=Y(1)+Y(2)+Y(3)+Y(4)+Y(5)+Y(6)+Y(7)+Y(8)+Y(9)+Y(10)  +Y(11)
      X3=Y(1)+Y(2)+Y(3)+Y(4)+Y(5)+Y(6)+Y(7)+Y(8)+Y(9)+Y(10)  +Y(11)
C
C     4-    CALCULATION OF TEMPERATURE AT THE END OF THE TIME STEP
C
      IF(Y(10).LT.0.0010) GO TO 778
8     T=T0+(TT0-TU)*(YY-Y(10))/YY
      TM=TM+DTM
      COI=Y(8)/X 3
      ATTIM=TM
      TT=T
      IF(TM.LT.ATM) GO TO 877
      GO TO 565
778   CU=Y(8)/X 3
      T=TF -(TF-TT )   *(CO-CCOE)/(COI-CCOE)
      TM=TM+DTM
      IF(TM.LT.ATM) GO TO 877
      GO TO 565
555   CONTINUE
333   CONTINUE
      STOP
      END
      SUBROUTINE FUNCT(ID,N,X,F,IFL)
      LOGICAL IFL
      DIMENSION X(4),F(4)
      COMMON  G(10),Y(11),AJA(20,20)
```

```
      COMMON C1,C2,AA1,AA2,AA3,AB,X3 ,AMMM
      IF(X(2).LT.0.00002) X(2)=0.00002
      AB=X(1)*X(2)
      AB1=AB**.5
      AB2=X(1)
      AB3=AB1
      F(1)=C1-2.*X(1)-AA1*AB1-AA2*AB2-X(2)-2.*Y(7)-Y(8) -Y(11)
      F(2)=C2-2.*X(2)-AA1*AB1-AA3*AB3-AMMM*Y(10)
      RETURN
      END
      SUBROUTINE MONIT(M,N,X,F,SS,V,NUM)
      DIMENSION X(4),F(4),V(4)
      IF(NUM)10,310,310
10    WRITE(2,300)
      GO TO 12
11    WRITE(2,301)NUM
12    WRITE(2,302)SS
      WRITE(2,304)(X(I),I=1,N)
      WRITE(2,305)
      WRITE(2,304)(F(I),I=1,N)
      IF(NUM.LT.0)GO TO 310
      WRITE(2,306)
      WRITE(2,304)(V(I),I=1,N)
310   RETURN
300   FORMAT(15HOSOLUTION FOUND)
301    FORMAT(6HOAFTER,I4,5HCALLS)
302   FORMAT(14H SUM OF SQARS=,E16.8)
305   FORMAT(10H RESIDUALS)
306   FORMAT(9H GRADIENT)
304   FORMAT(1H ,6X,3E12.4)
      RETURN
      END
      SUBROUTINE LSQ(ID,N,X,F,AJINV,V)
      DIMENSION X(N),F(N),AJINV(N,N),V(N)
      COMMON  G(10),Y(11),AJA(20,20)
      COMMON C1,C2,AA1,AA2,AA3,AB,X3 ,AMMM
      IF(X(2).LT.0.00002) X(2)=0.00002
      AJA(1,1)=-2.-AA1*AB1/(2.*X(1)) -AA2
      AJA(1,2)=-1.-AA1*AB1/(2.*X(2))
      AJA(2,1)=  -(AA1+AA3)*AB1/(2.*X(1))
        AJA(2,2)=-(AA1+AA3)*AB1/(2.*X(2))-2.
      DO 200 I=1,N
      SM=0.
      DO 201 K=1,N
201   SM=SM+AJA(K,I)*F(K)
      V(I)=SM
      DO 200 J=I,N
      SM=0.
      DO 202 K=1,N
202   SM=SM+AJA(K,I)*AJA(K,J)
      AJINV(I,J)=SM
200   CONTINUE
      RETURN
      END
      FINISH
```

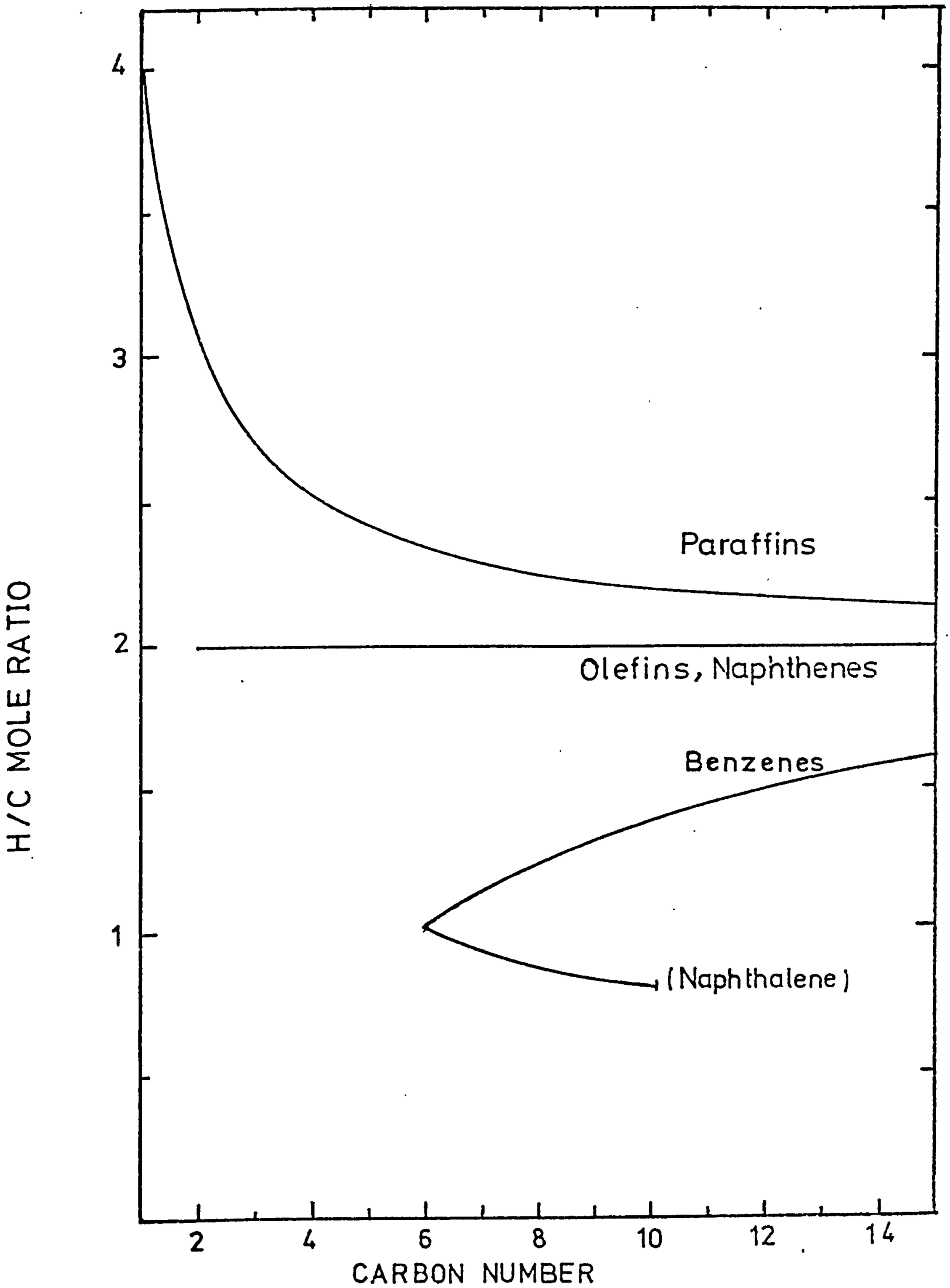

FIGURE 3.1 Variation of the hydrogen-carbon ratio with carbon number for different hydrocarbon types

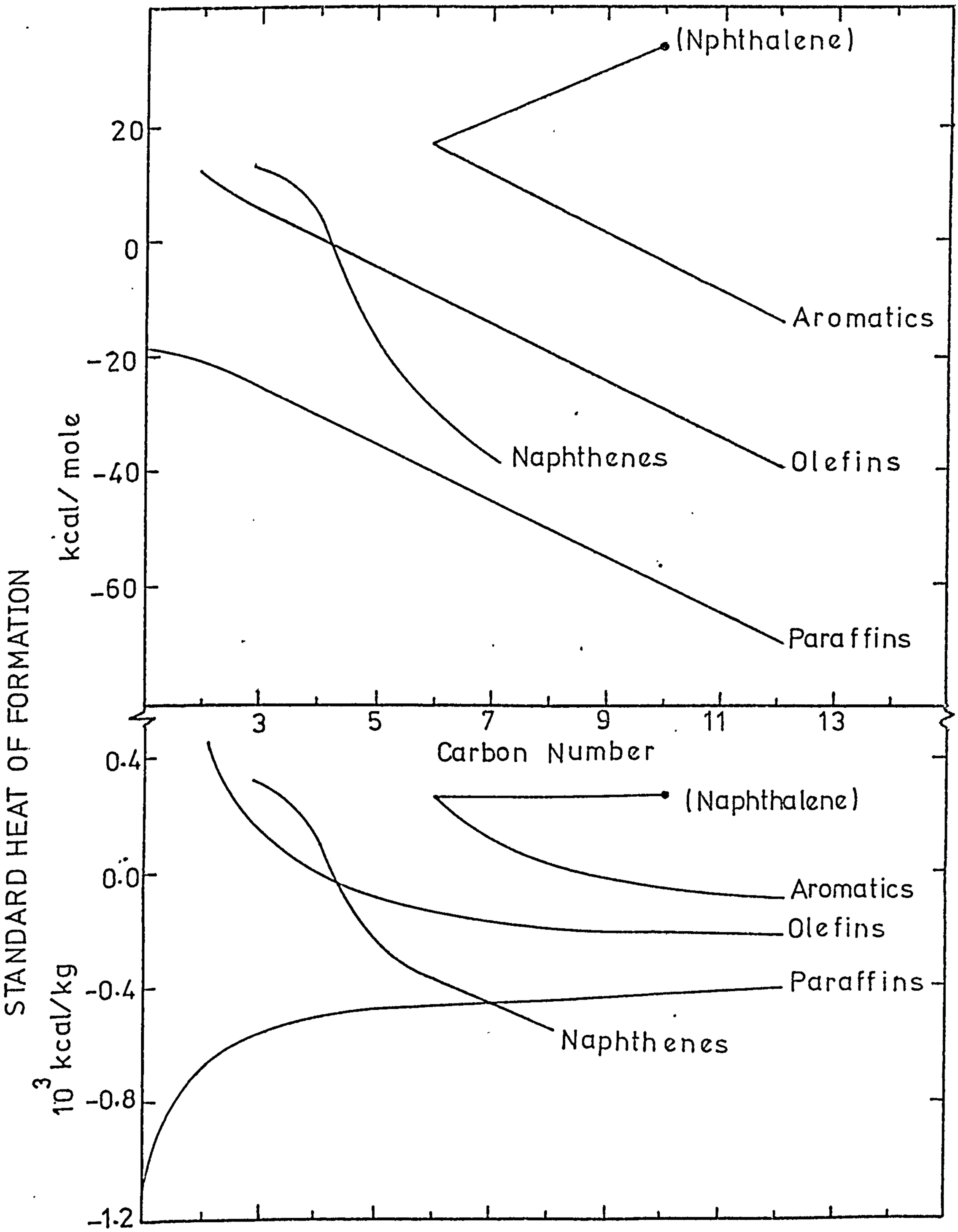

FIGURE 3.2 Variation of the standard heat of formation with carbon number for different hydrocarbon types (gaseous phase)

(Ref.1)

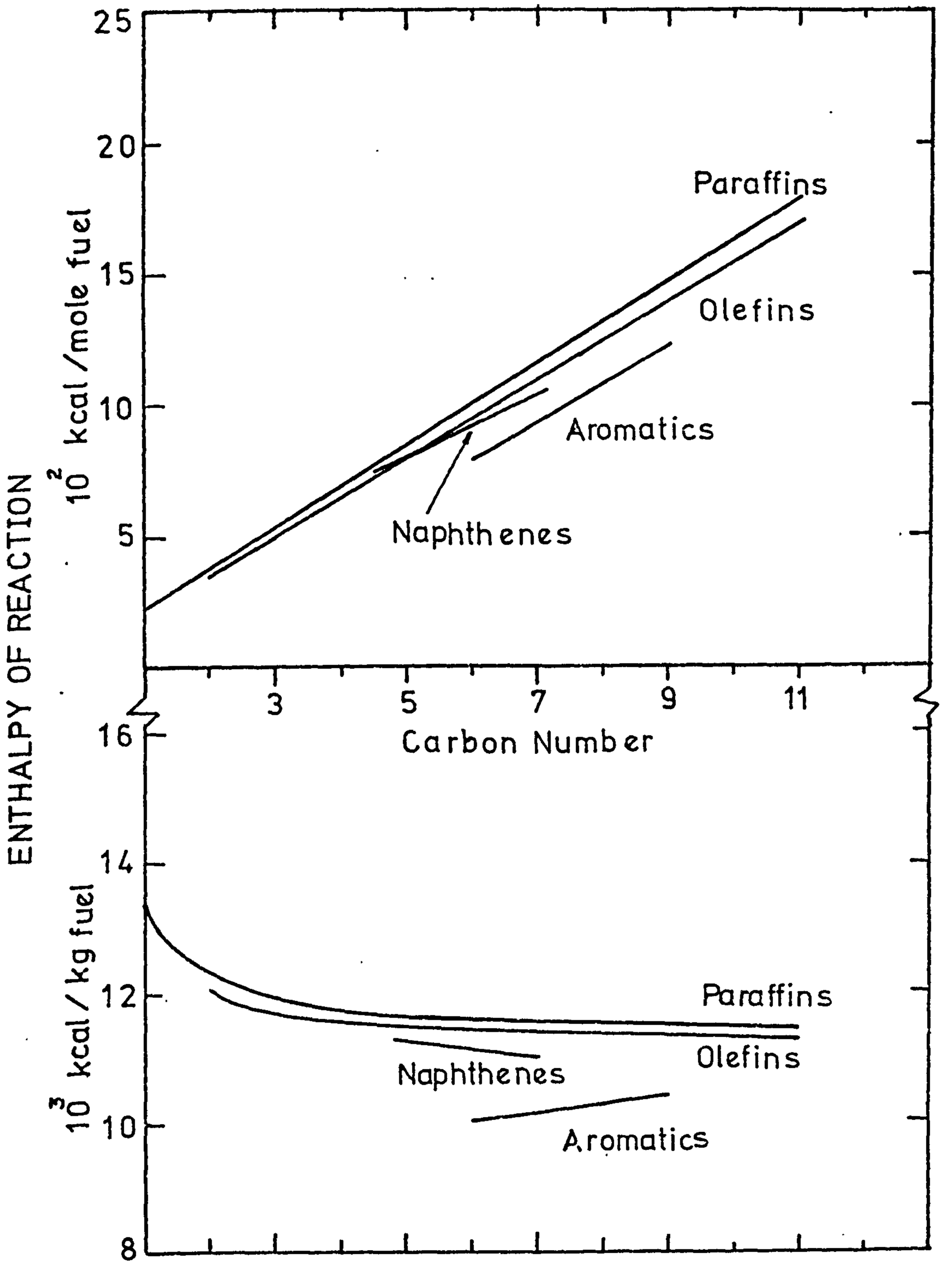

FIGURE 3.3 Enthalpies of reaction of hydrocarbons; reactants and products in gaseous phase.

(Ref.1)

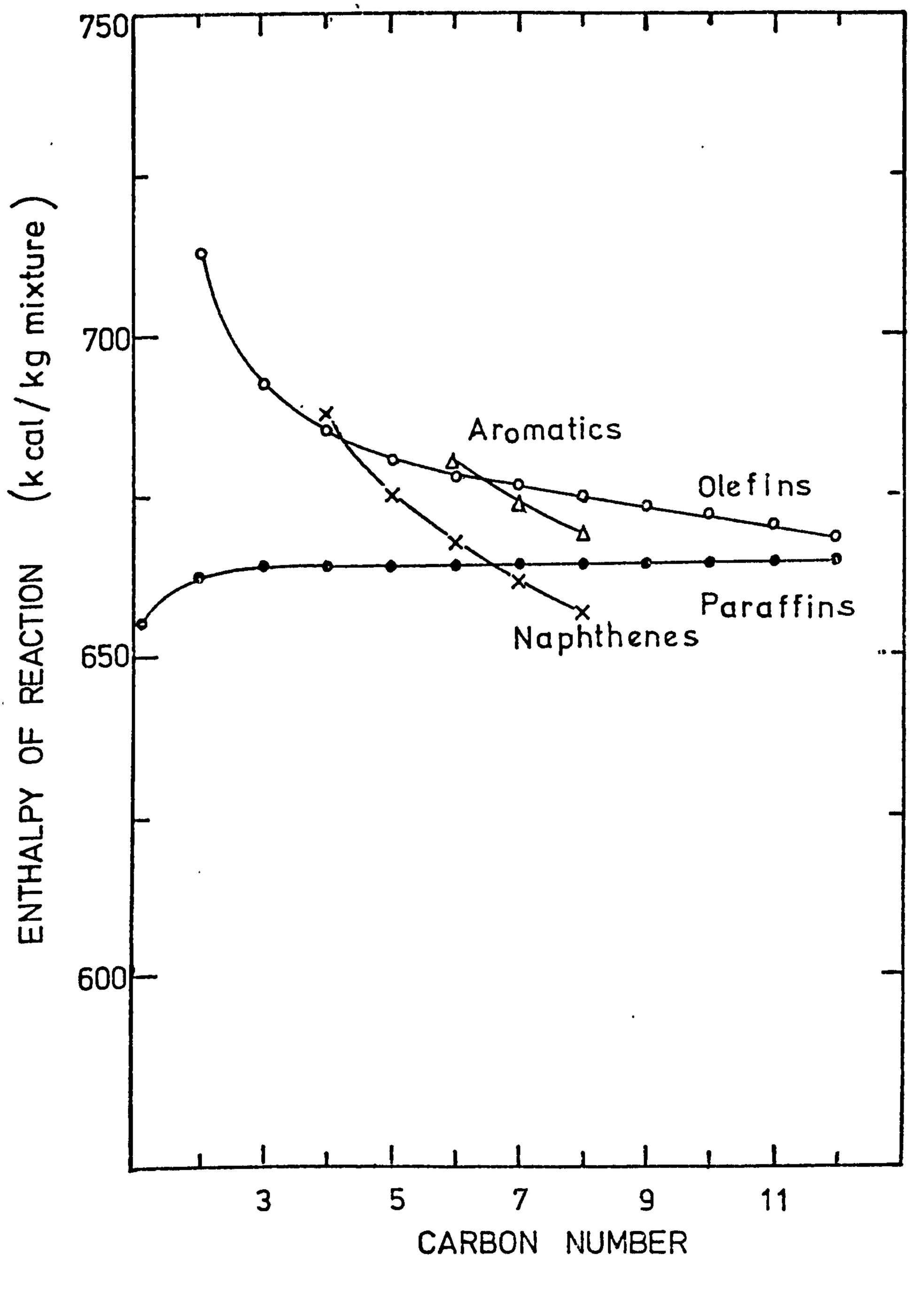

FIGURE 3.4 Enthalpies of reaction of stoichiometric hydrocarbon – air mixtures ; reactants and products in gaseous phase. (Ref. 1)

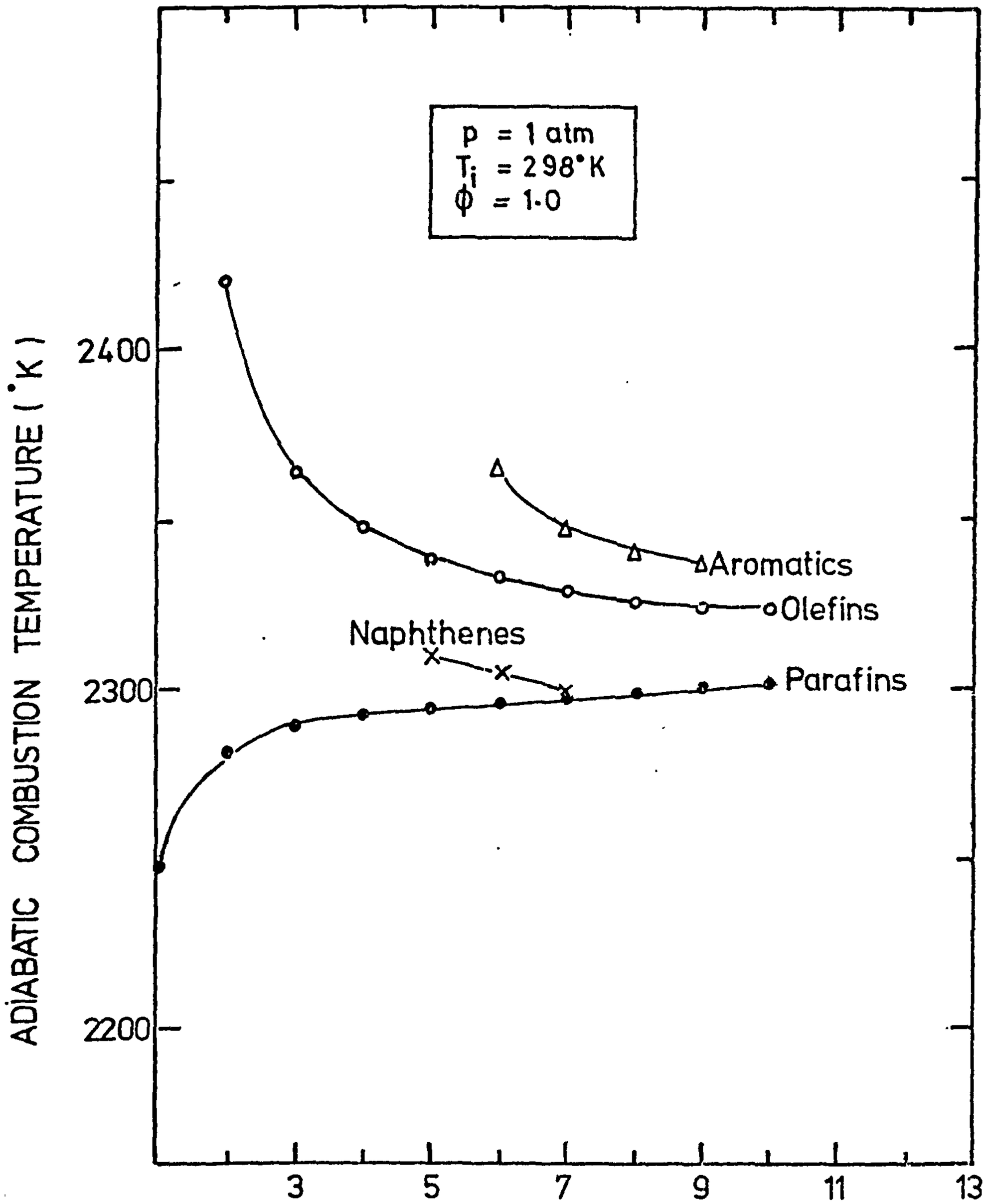

FIGURE 3.5 Adiabatic combustion temperatures for stoichiometric hydrocarbon – air mixture; reactants and products in gaseous phase

(Ref. 1)

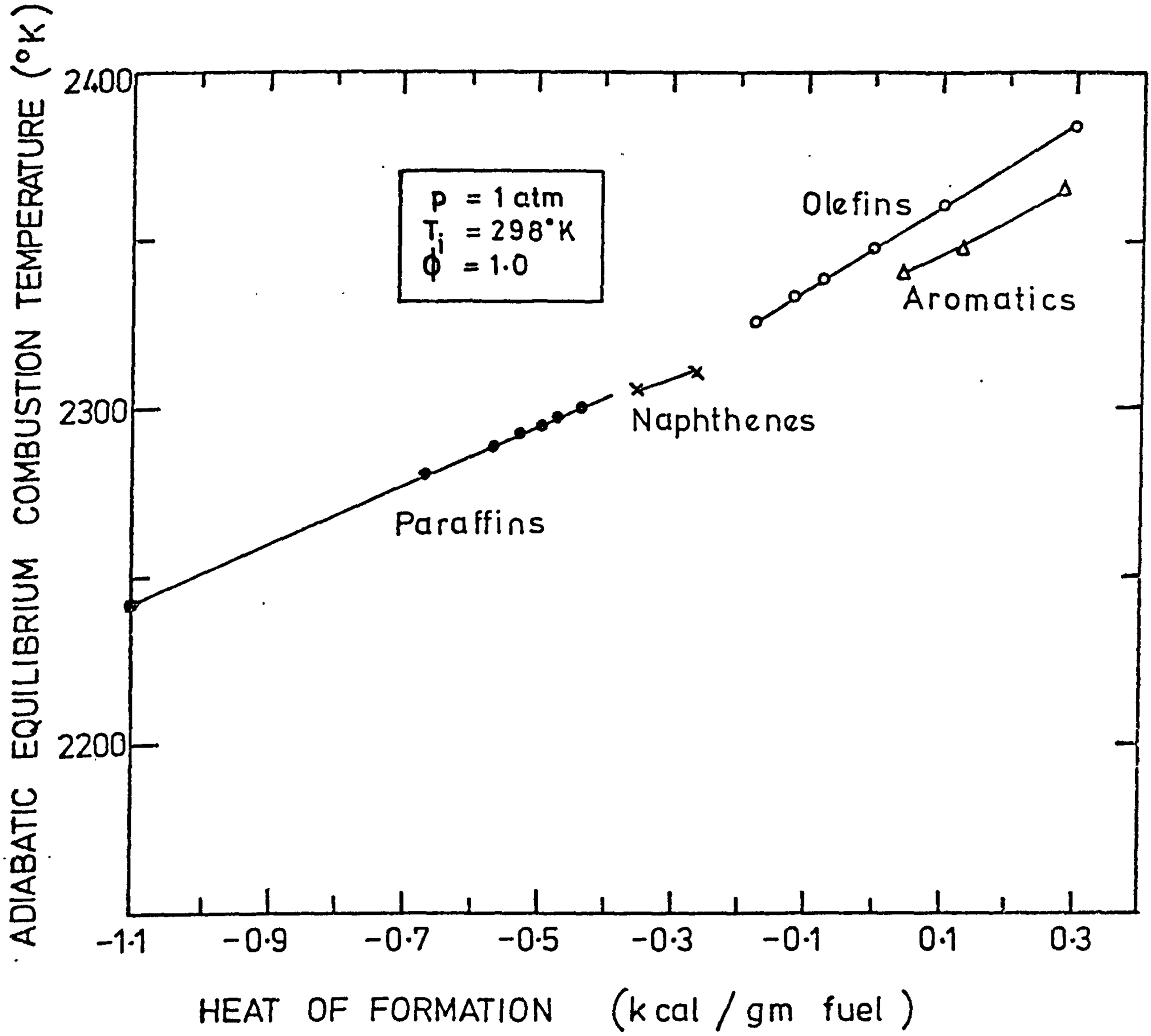

FIGURE 3.6 Variation of the adiabatic combustion temperature with the standard enthalpy of formation of fuel.

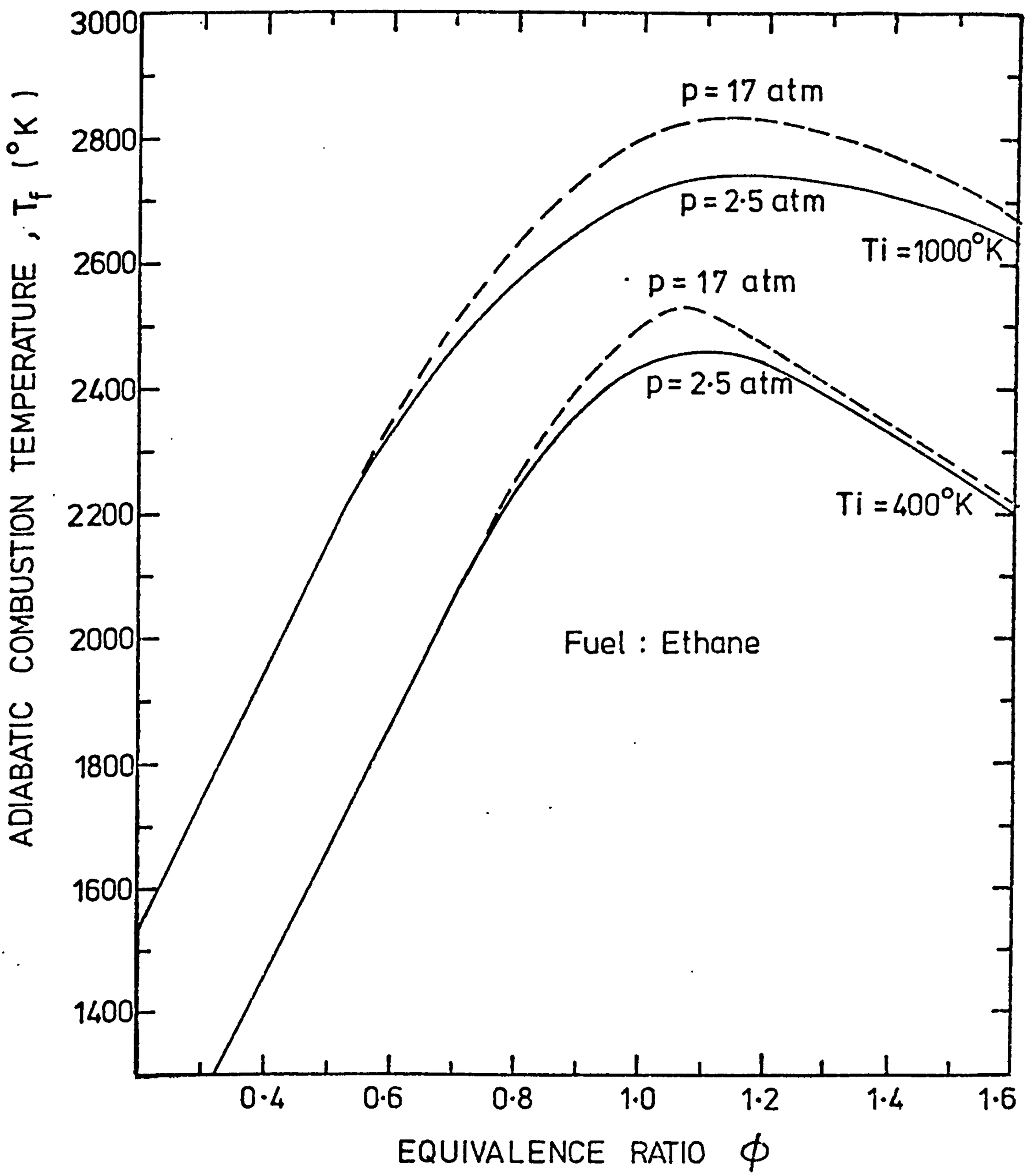

FIGURE 3.7 Variation of the adiabatic combustion temperature with equivalence ratio at different pressures and initial temperatures.

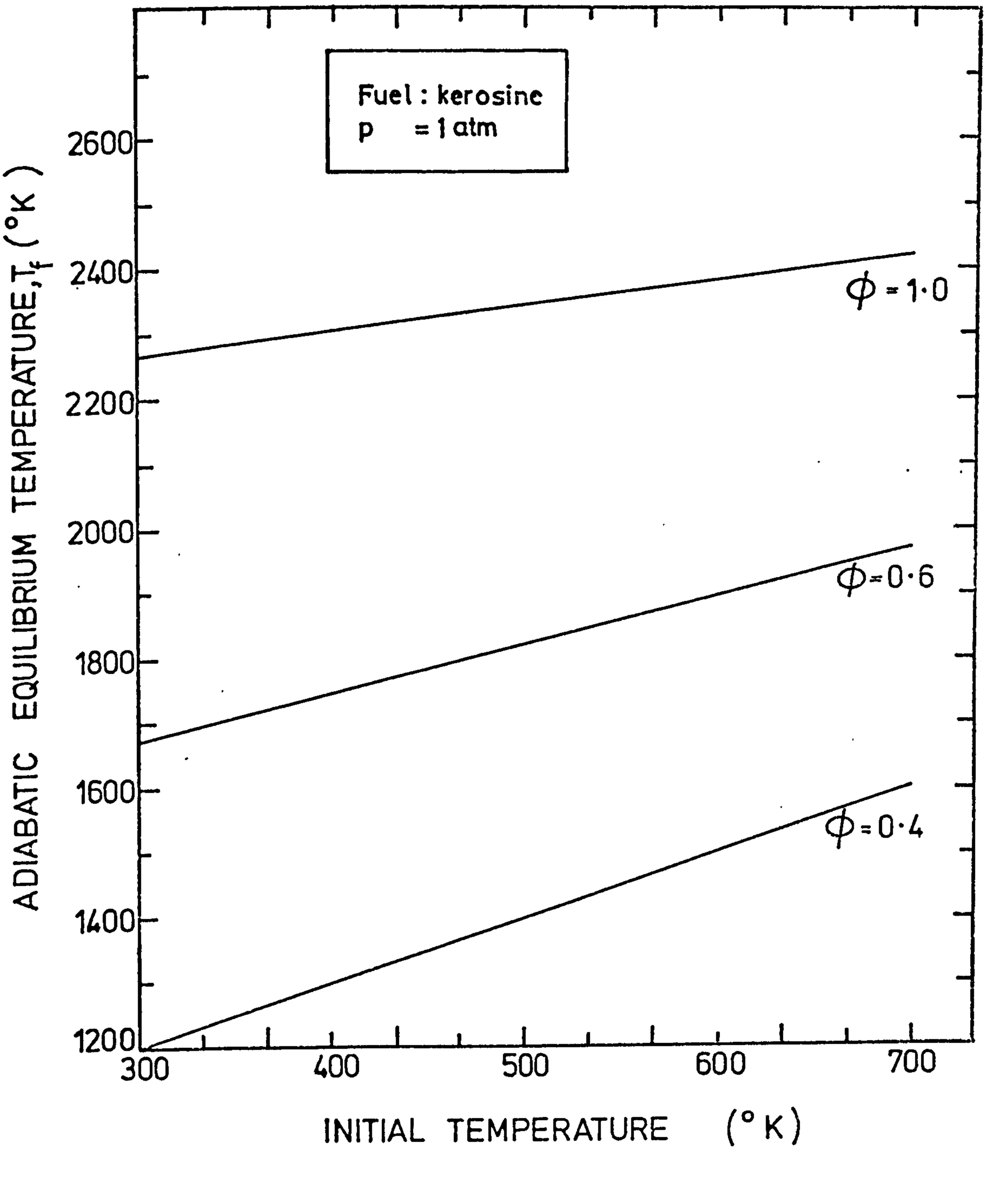

FIGURE 3.8 Influence of initial temperature on adiabatic combustion temperature.

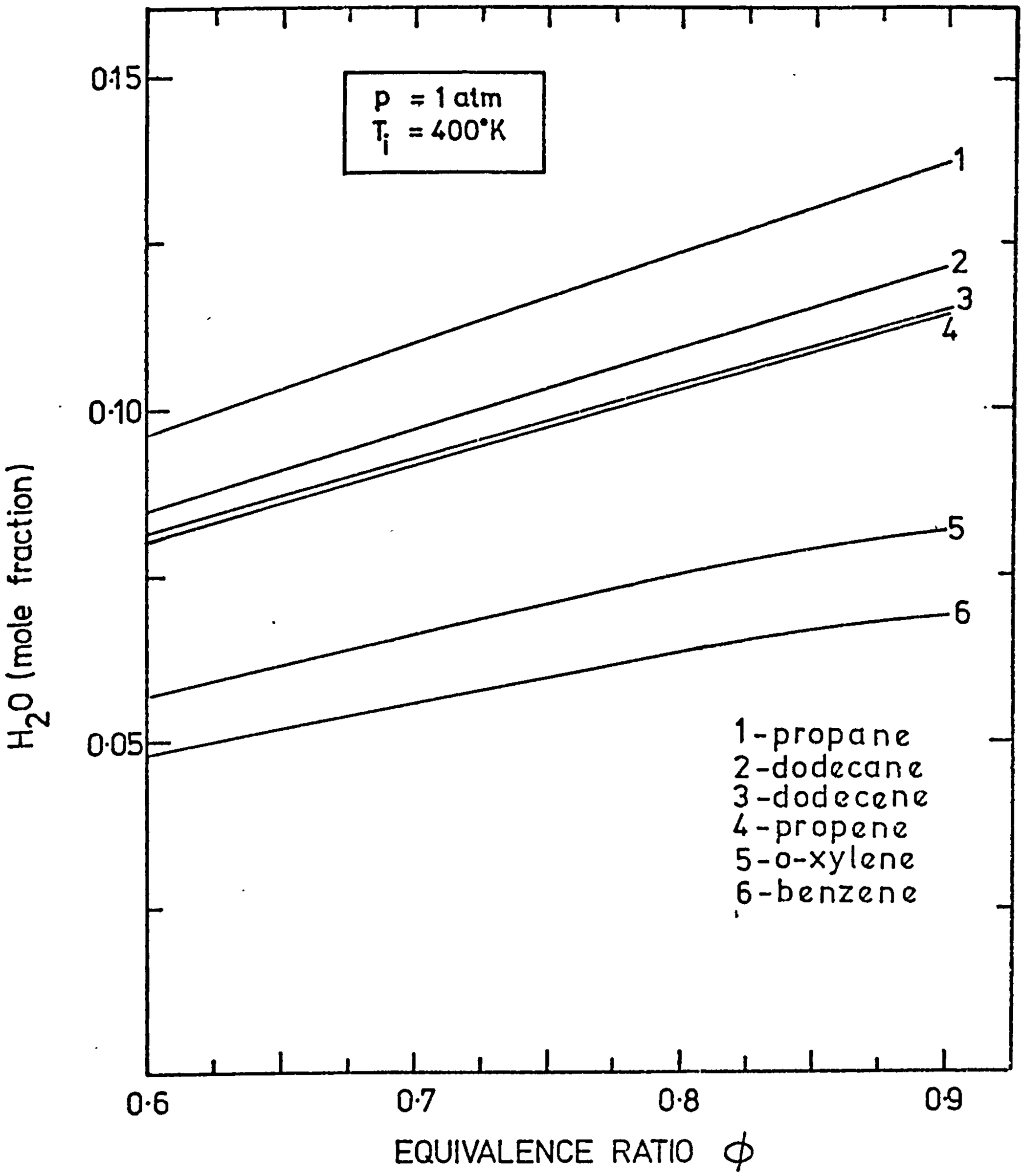

FIGURE 3.9 H_2O concentration in the combustion products of different hydrocarbon – air mixtures

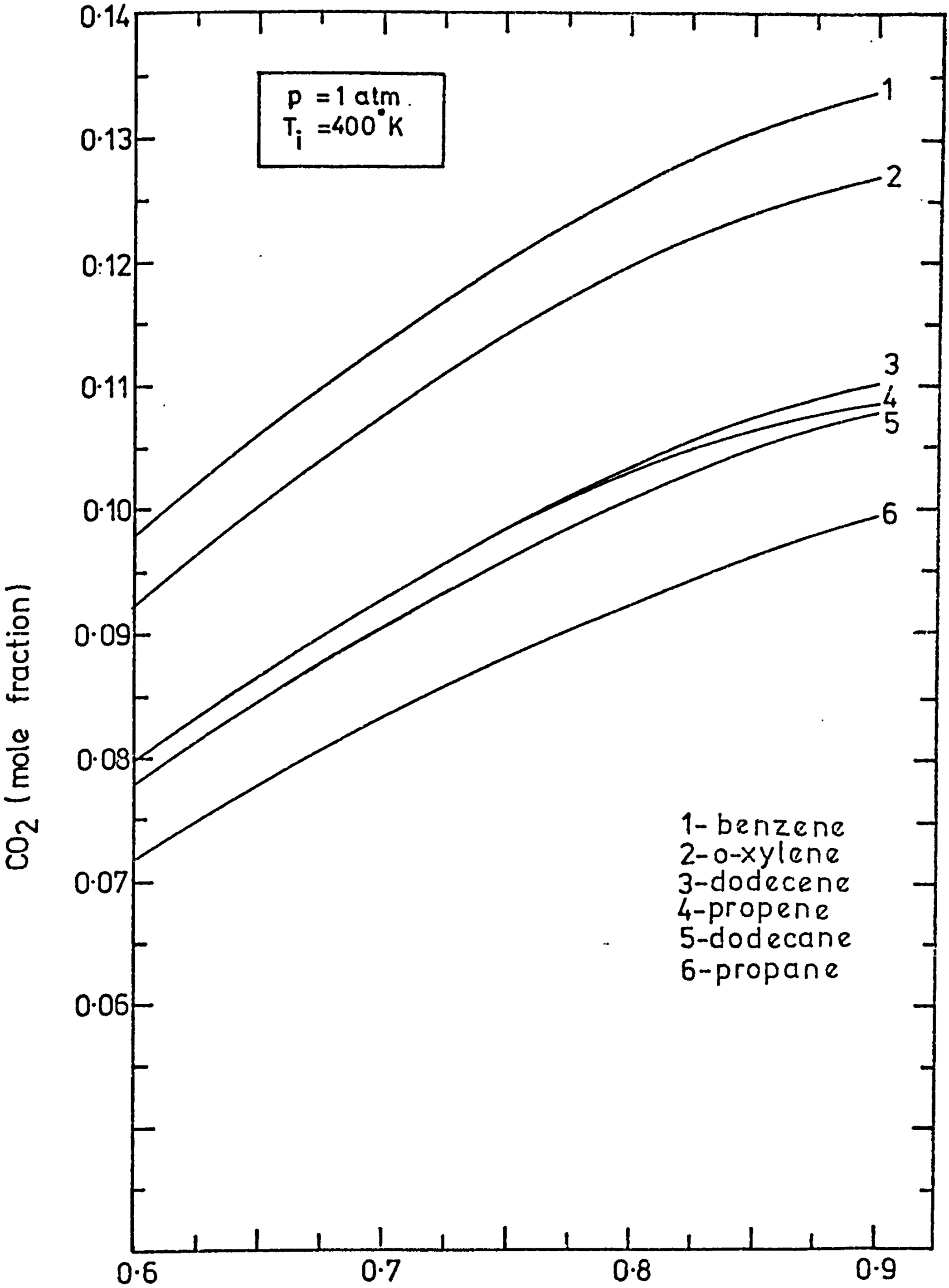

FIGURE 3.10. CO_2 concentration in the combustion products of different hydrocarbon - air mixtures

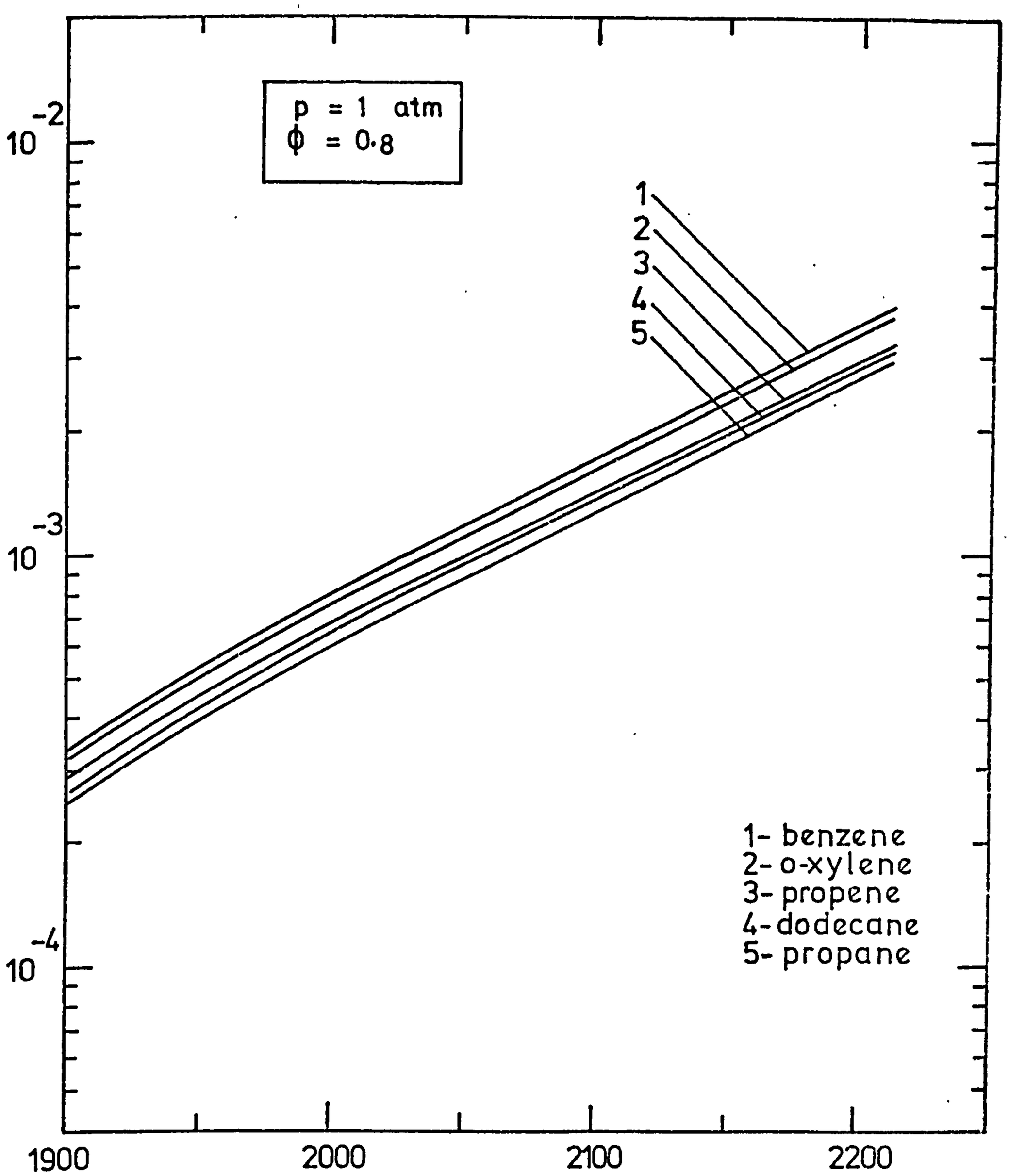

FIGURE 3.11 Influence of the flame temperature on equilibrium CO concentration in the products of combustion of different hydrocarbons

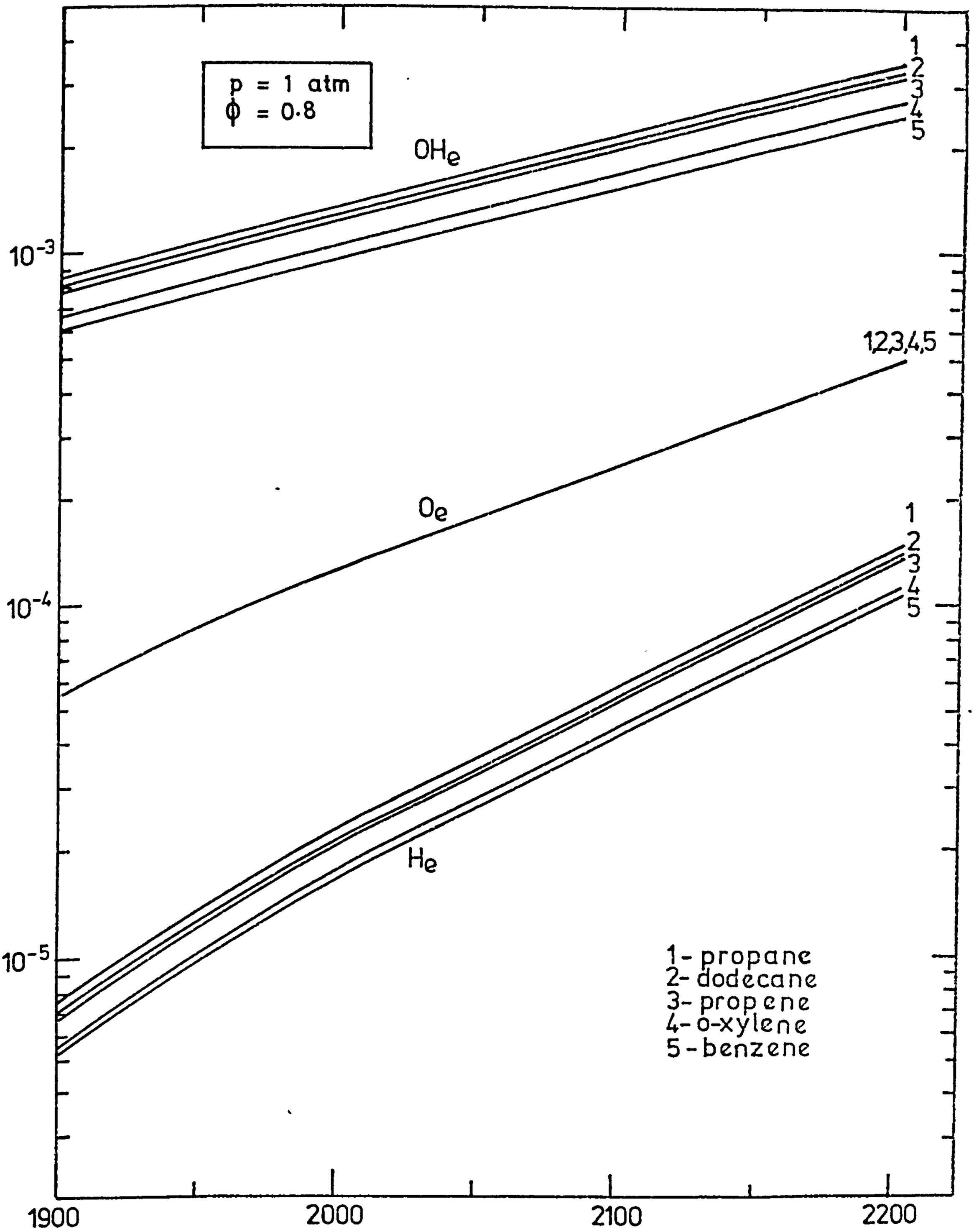

FIGURE 3.12. Influence of the flame temperature on the equilibrium concentrations of OH , O and H in the products of combustion of different hydrocarbons

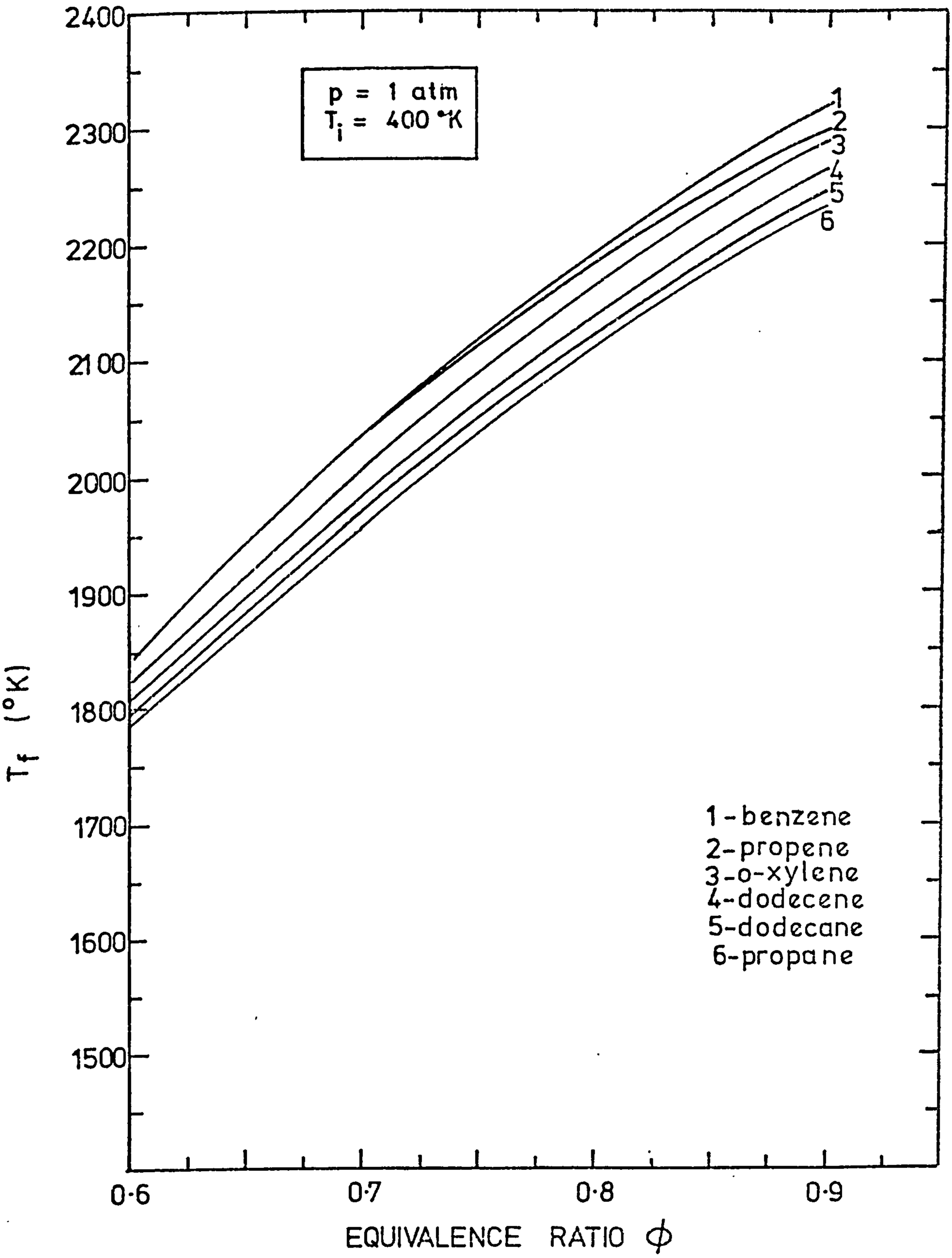

FIGURE 3.13 Variation of the adiabatic flame "combustion" temperature with the equivalence ratio for different hydrocarbons

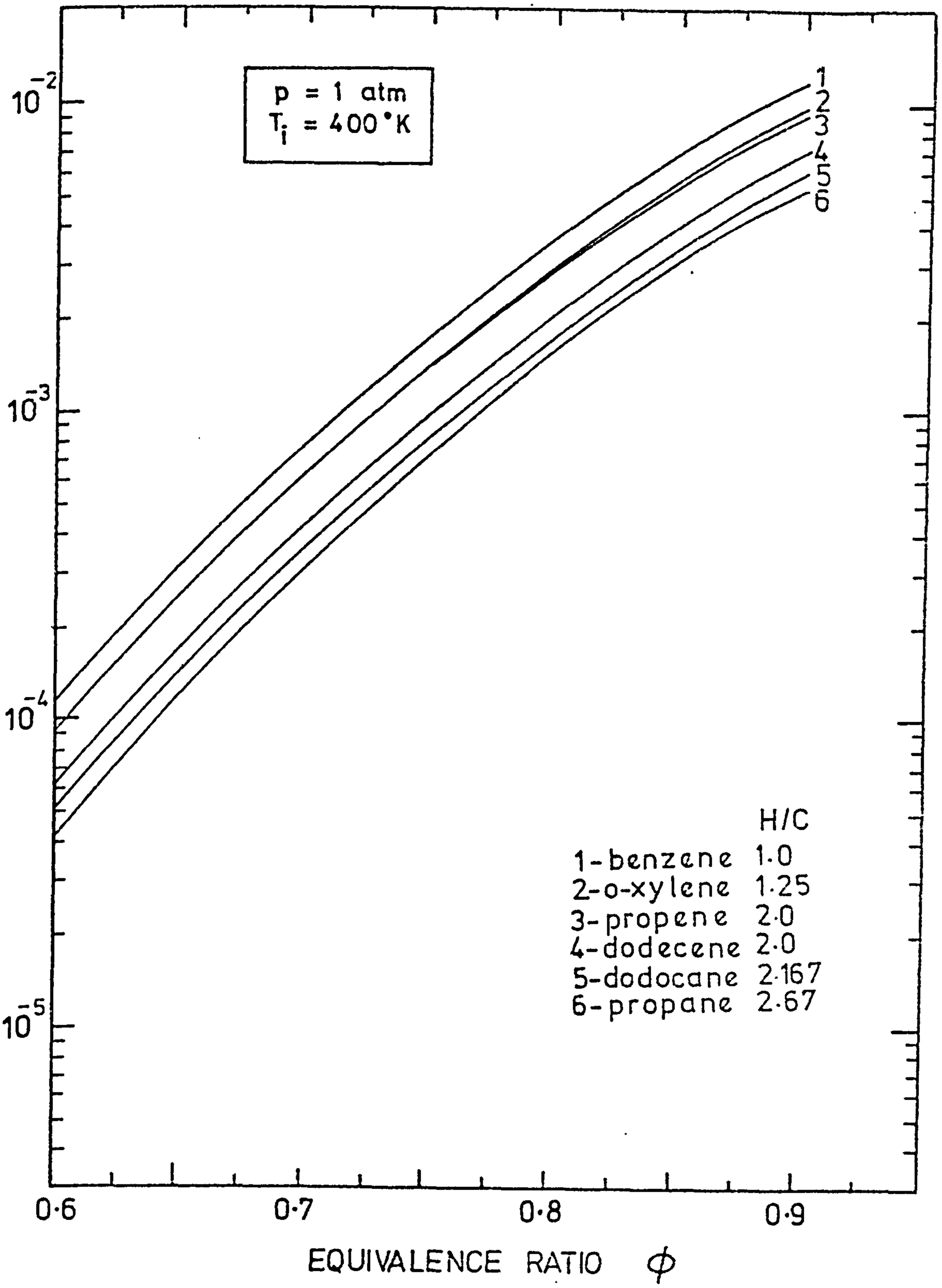

FIGURE 3.14 Equilibrium CO concentrations in the product of adiabatic combustion of different hydro-carbon-air mixtures.

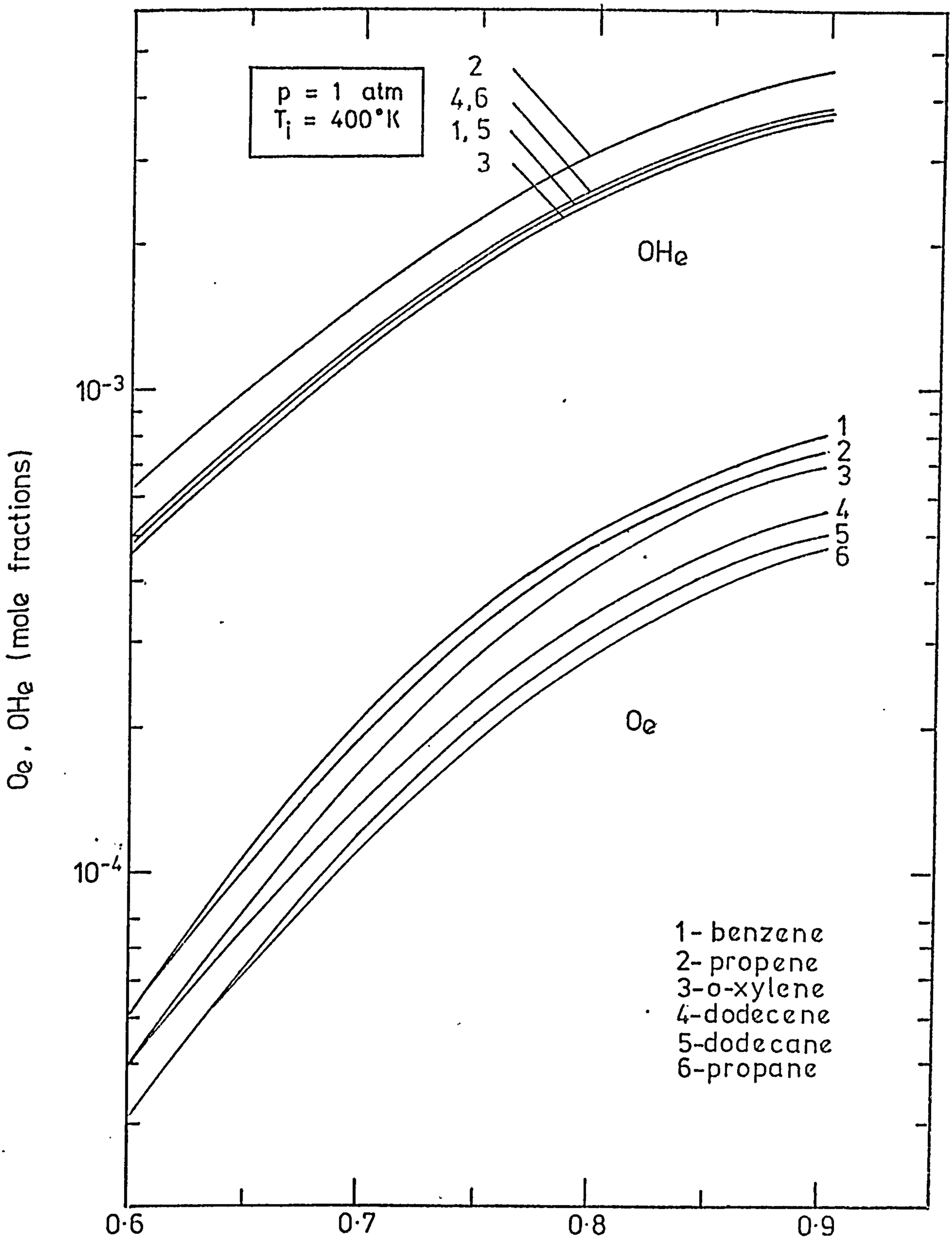

FIGURE 3.15. Equilibrium concentrations of OH and O in the products of adiabatic combustion of different hydrocarbon-air mixtures

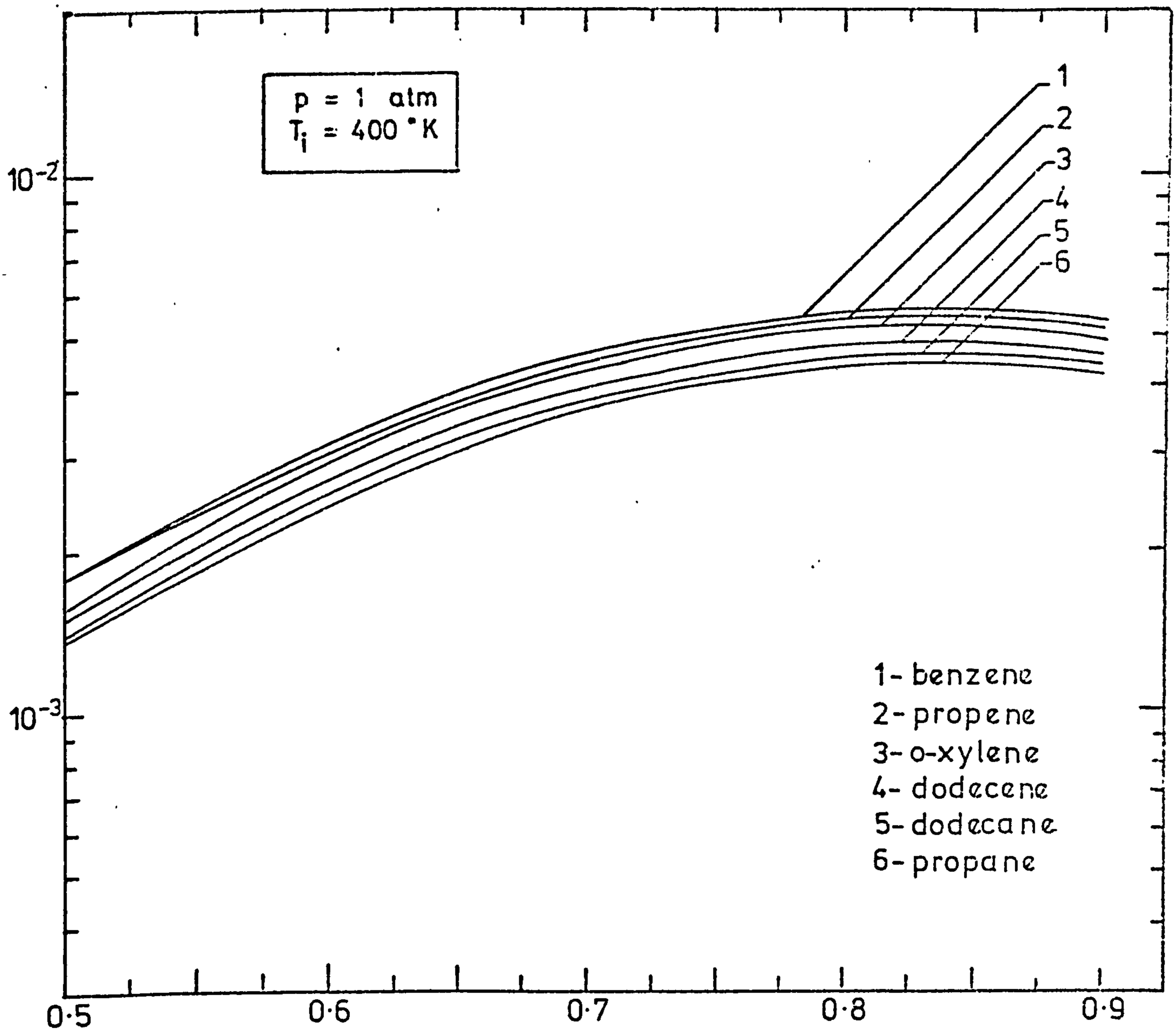

FIGURE 3.16. Equilibrium NO concentration in the products of the adiabatic combustion of different hydrocarbon-air mixtures

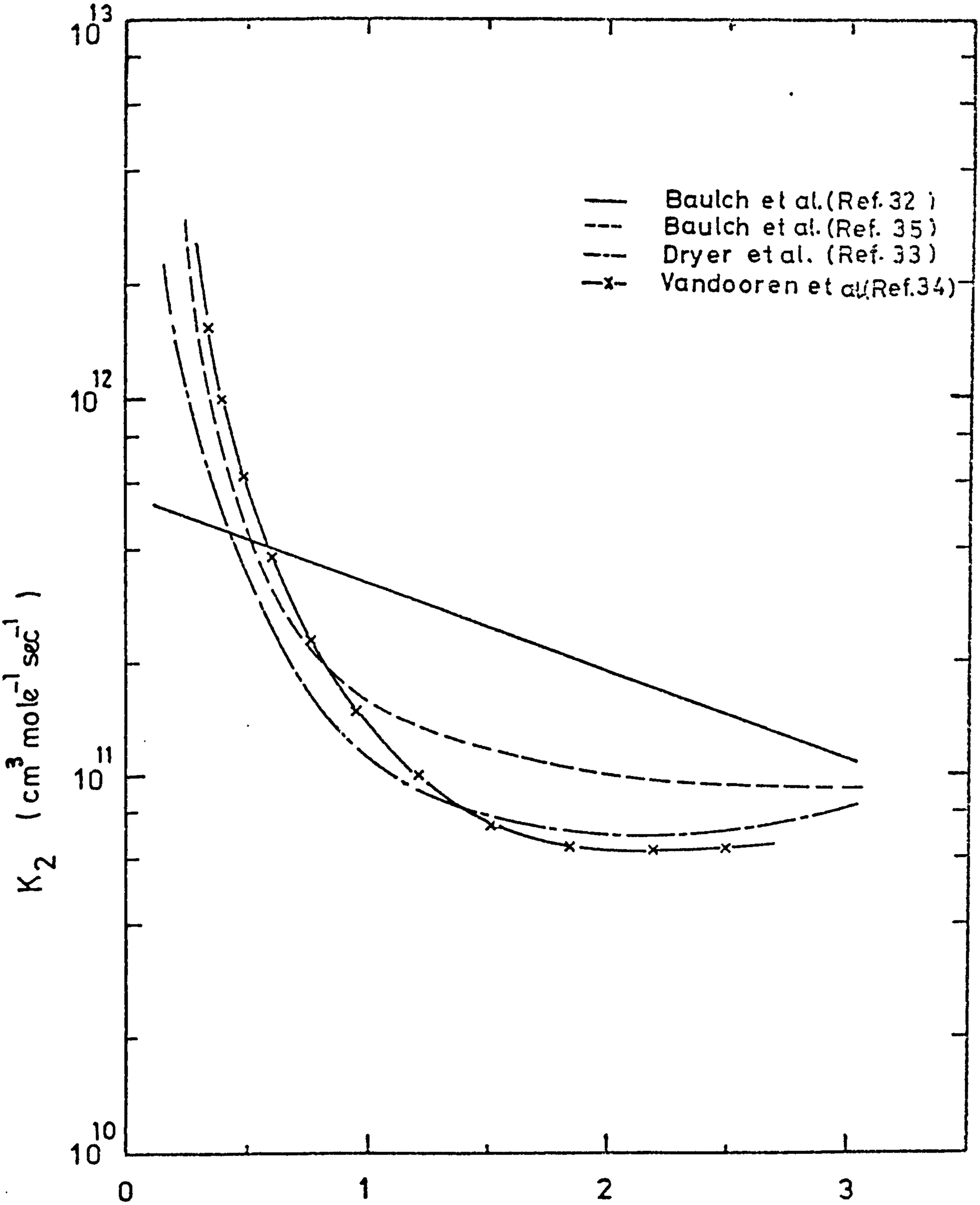

FIGURE 4.1 Comparison of different expressions for the rate constant of the reaction:

$$CO + OH \xrightarrow{k_2} CO_2 + H$$

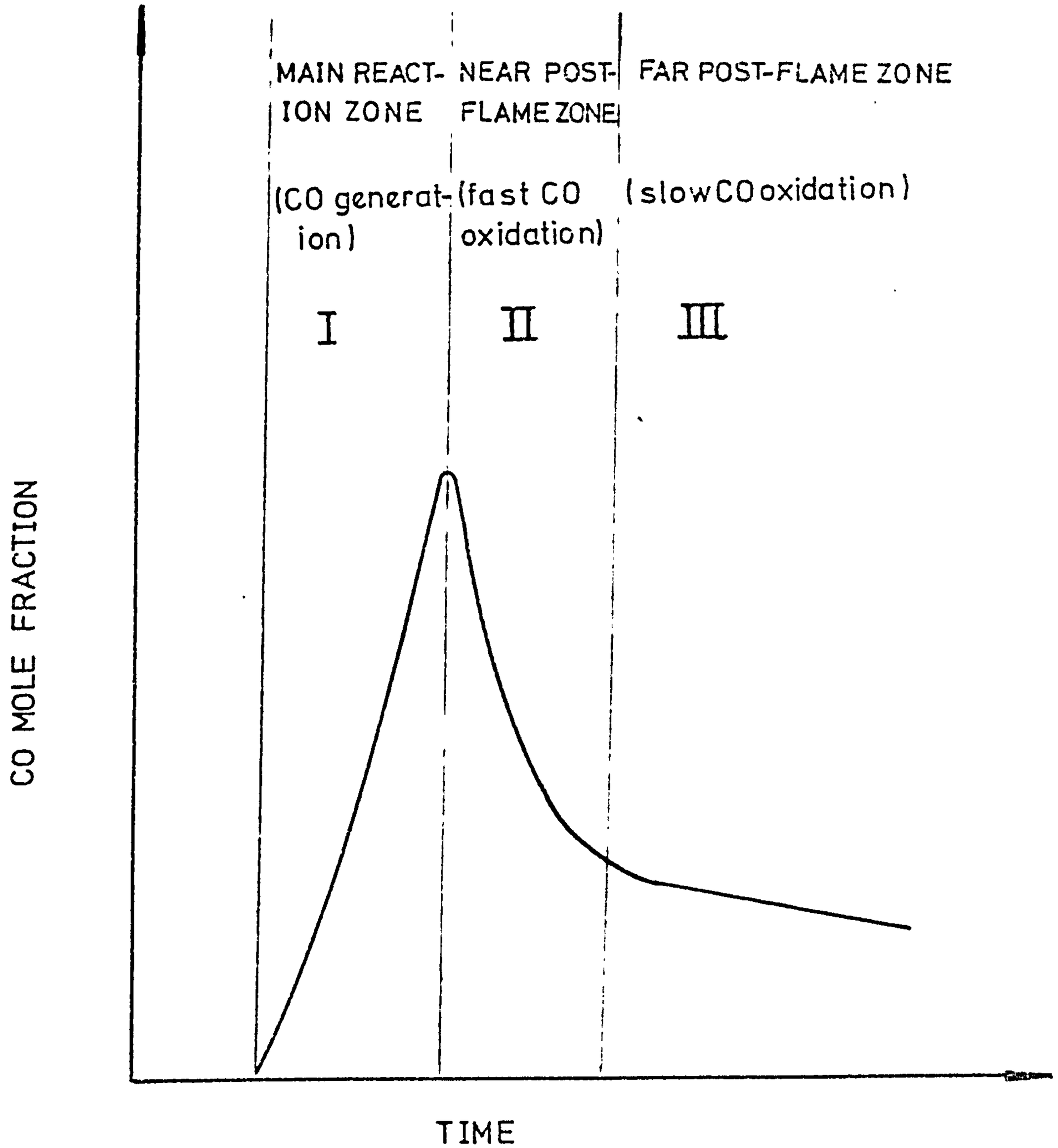

FIGURE 4.2 Different CO reation zones considered in kinetic modeling

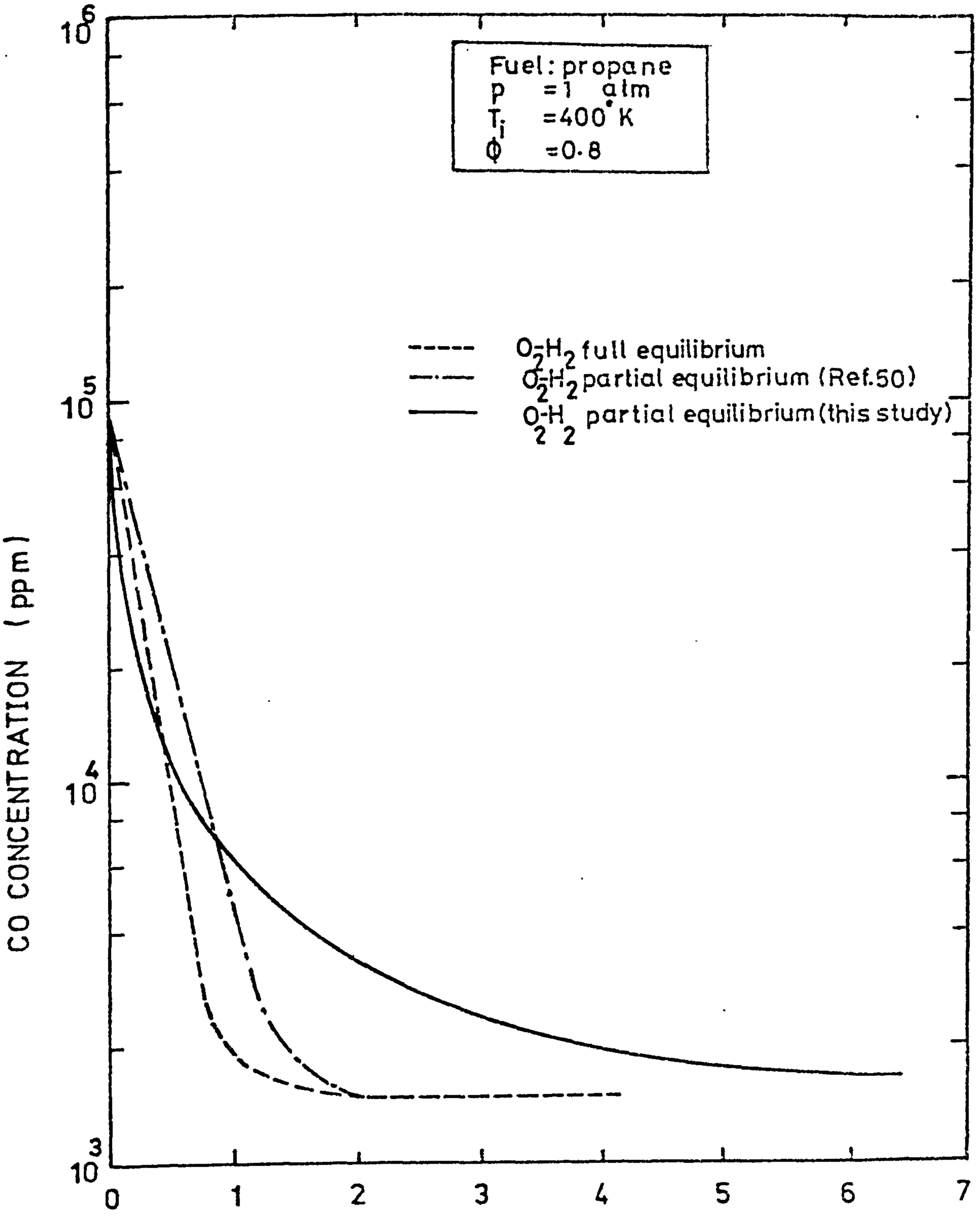

FIGURE 4.3 Comparison of CO profiles predited by different kinetic models in a lean, premixed propane-air flame

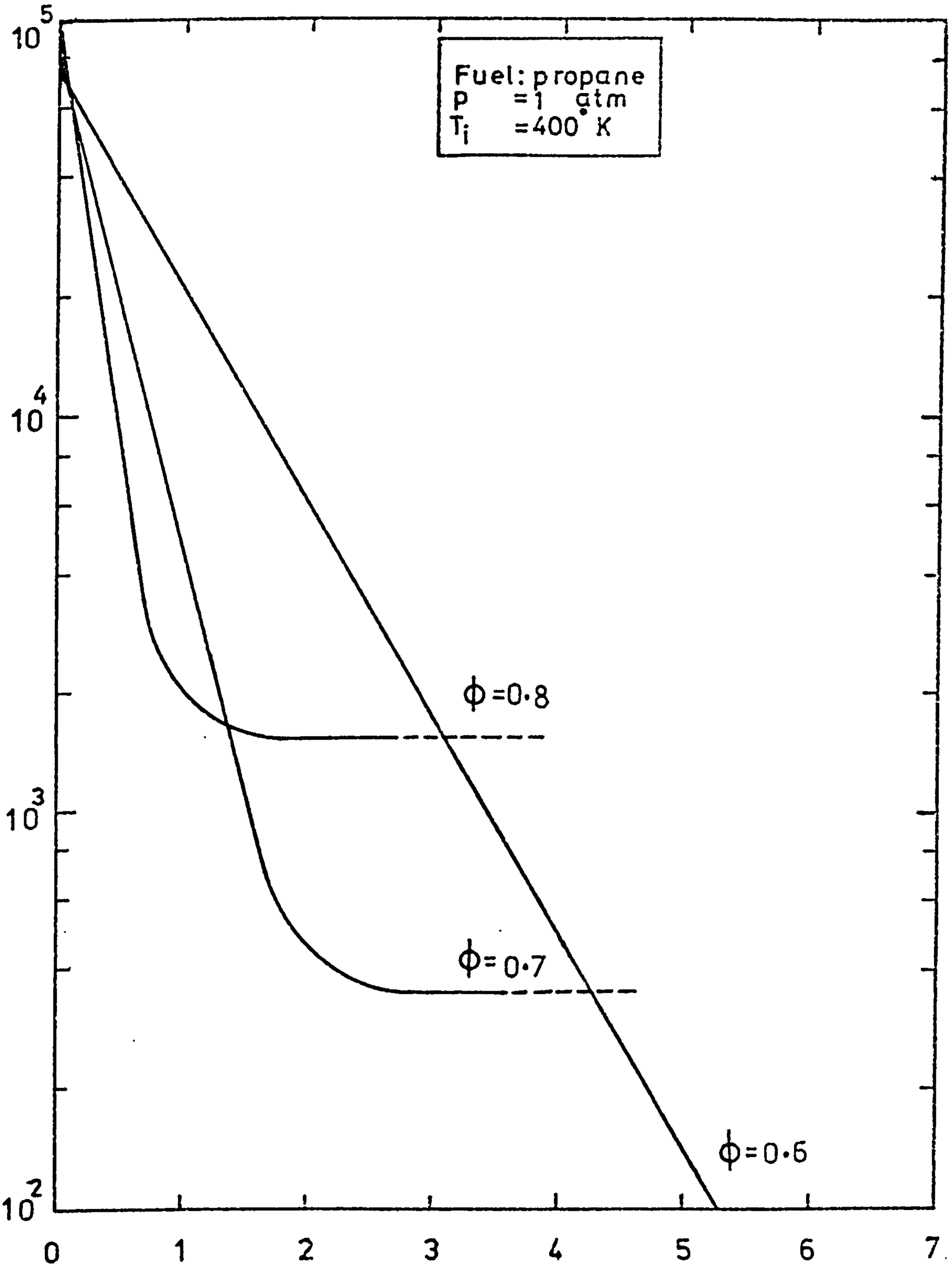

FIGURE 4.4 Effect of the equivalence ratio on CO profiles predicted by full O_2-H_2 equilibrium model in lean, premixed propane-air flames

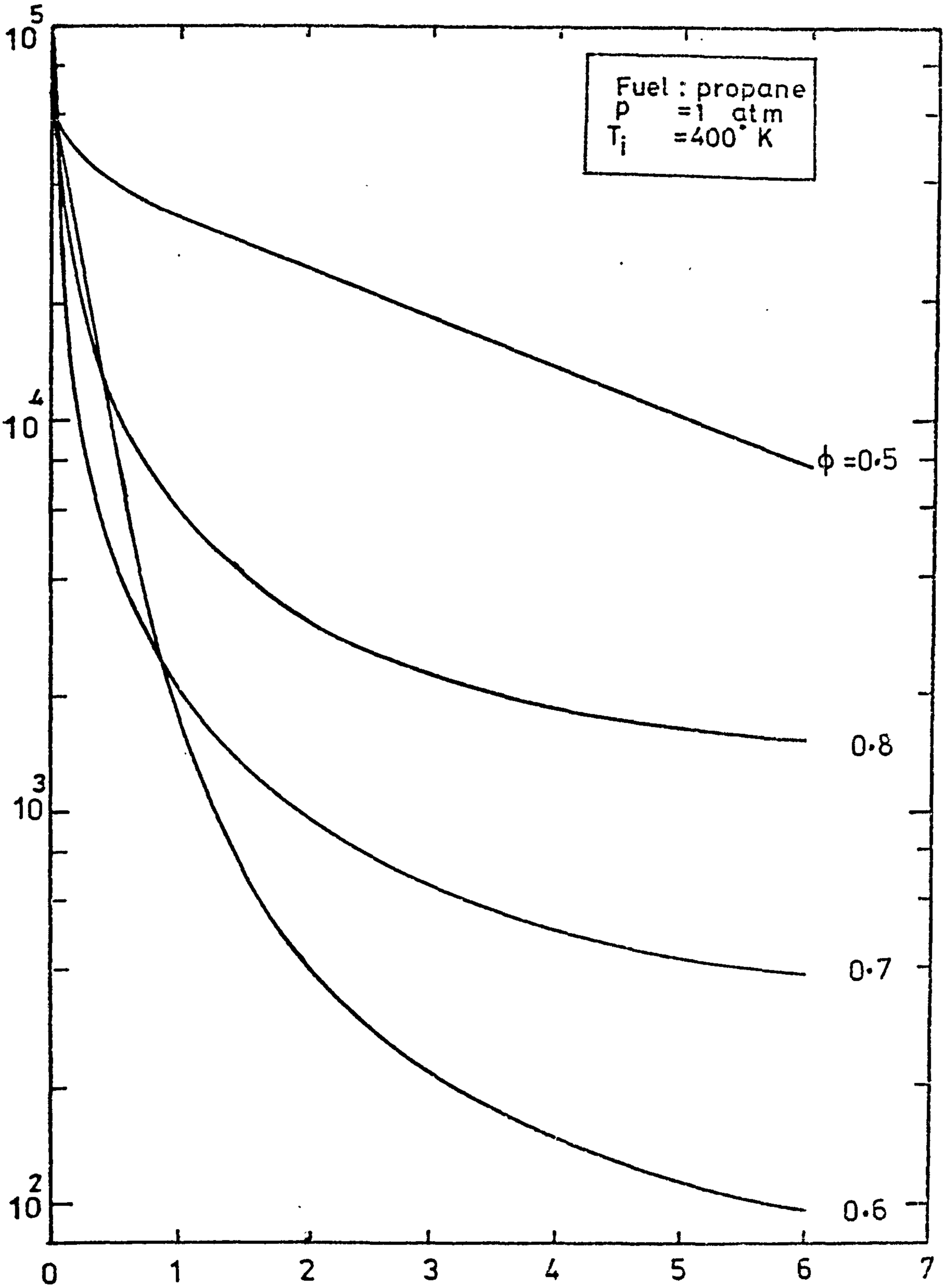

FIGURE 4.5 Effect of equivalence ratio on CO profiles Predicted by O_2-H_2 partial equilibrium model in lean, premixed propane-air flames

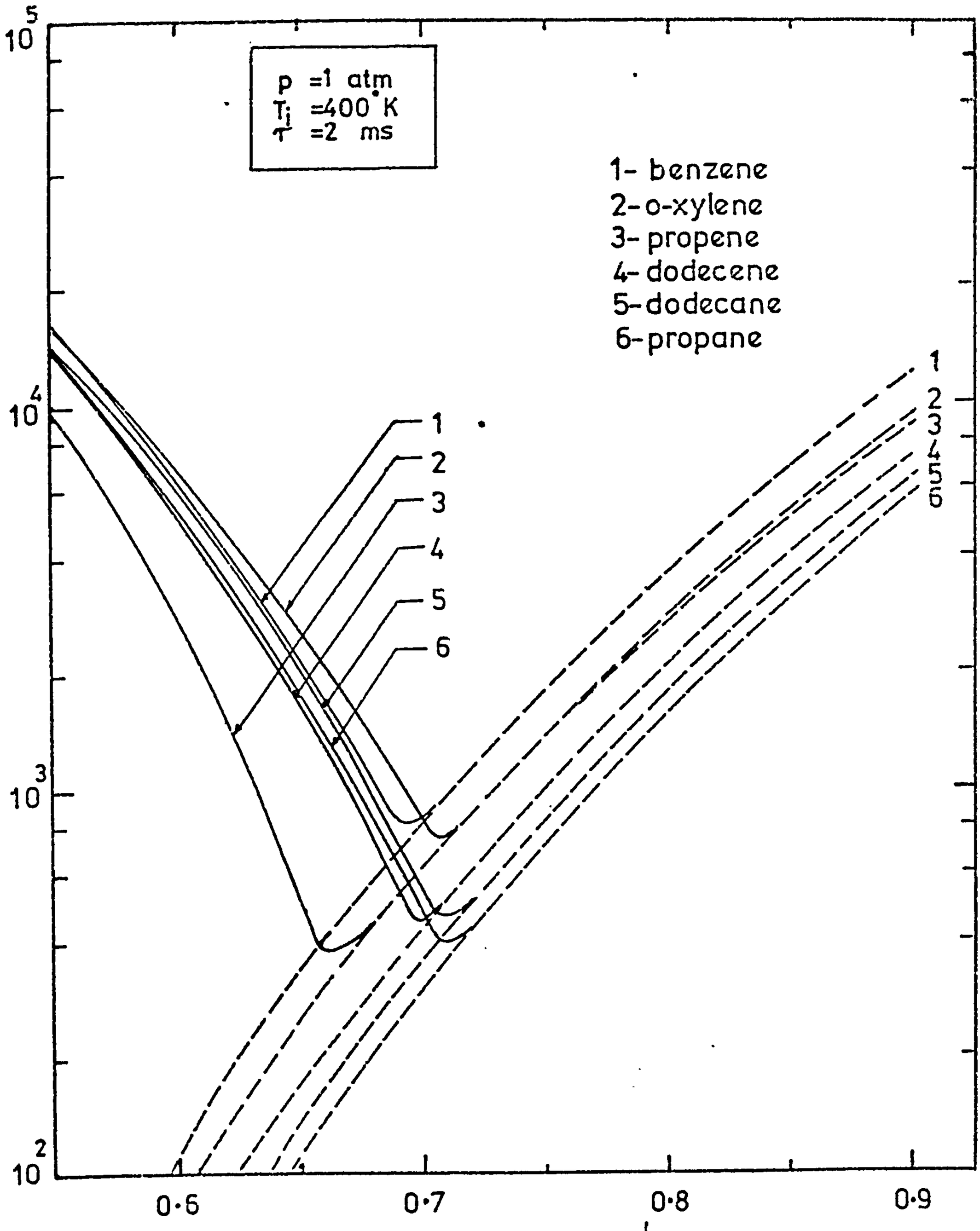

FIGURE 4.6 Effect of fuel kind on CO levels as predicted by full O_2-H_2 equilibrium model in different, lean, premixed hydrocarbon-air flames.

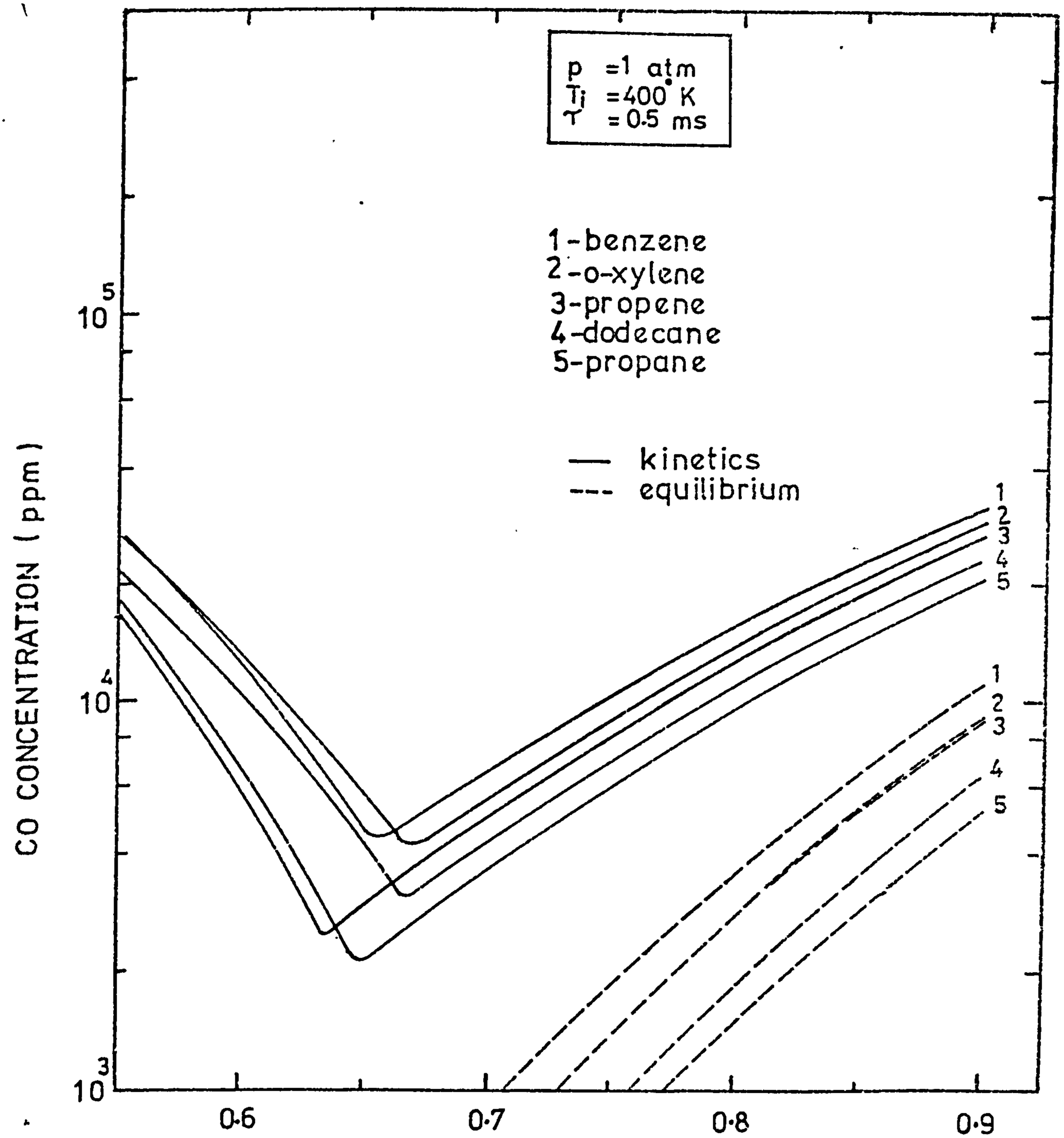

FIGURE 4.7 Effect of fuel kind on CO levels predicted by O_2-H_2 partial equilibrium model in different, lean, premixed hydrocarbon-air flames

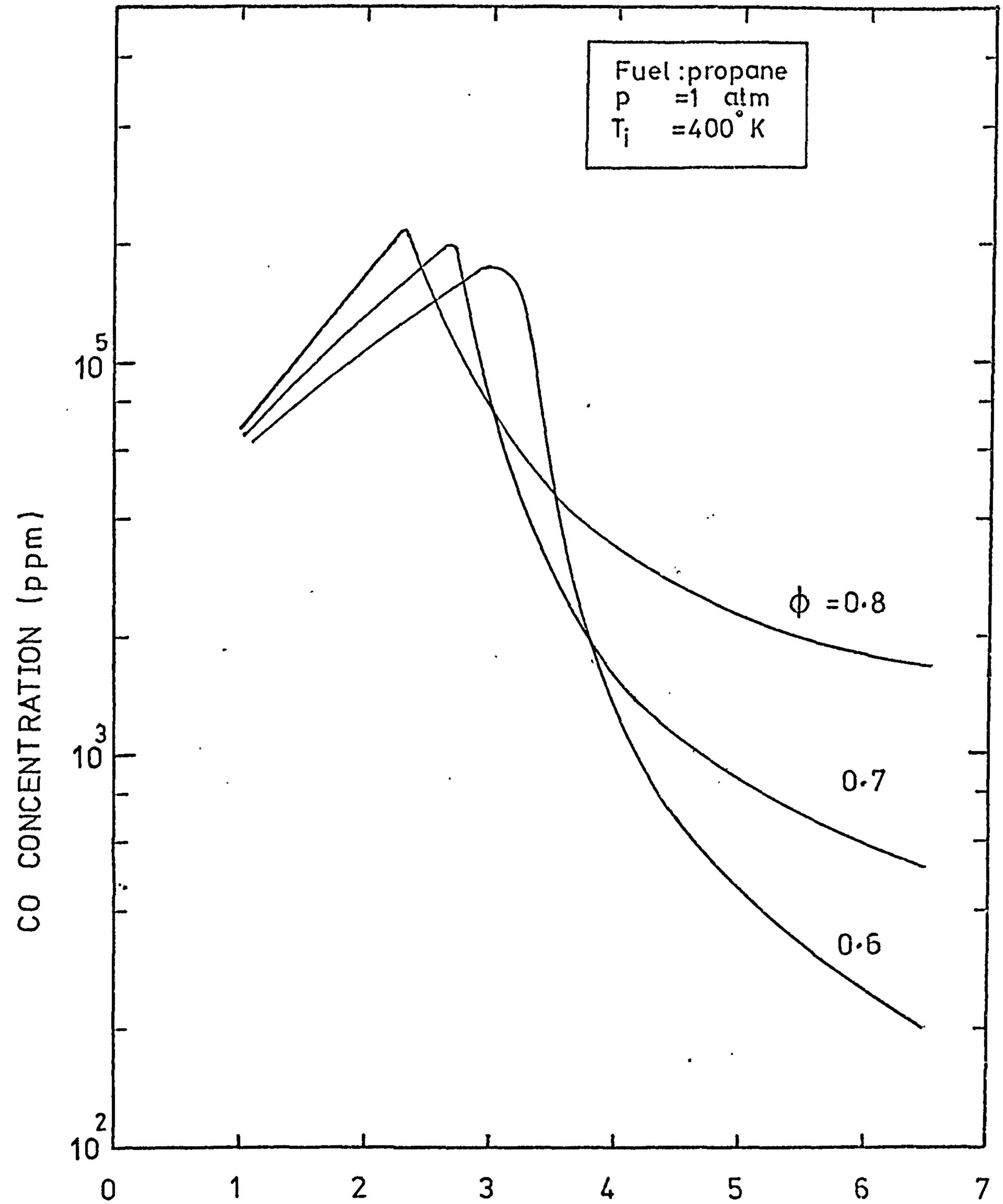

FIGURE4.8 Effect of the equivalence ratio on CO profiles as predicted by O_2-H_2 partial equilibrium model, assuming a finite fuel pyrolysis rate in lean, premixed propane-air flames

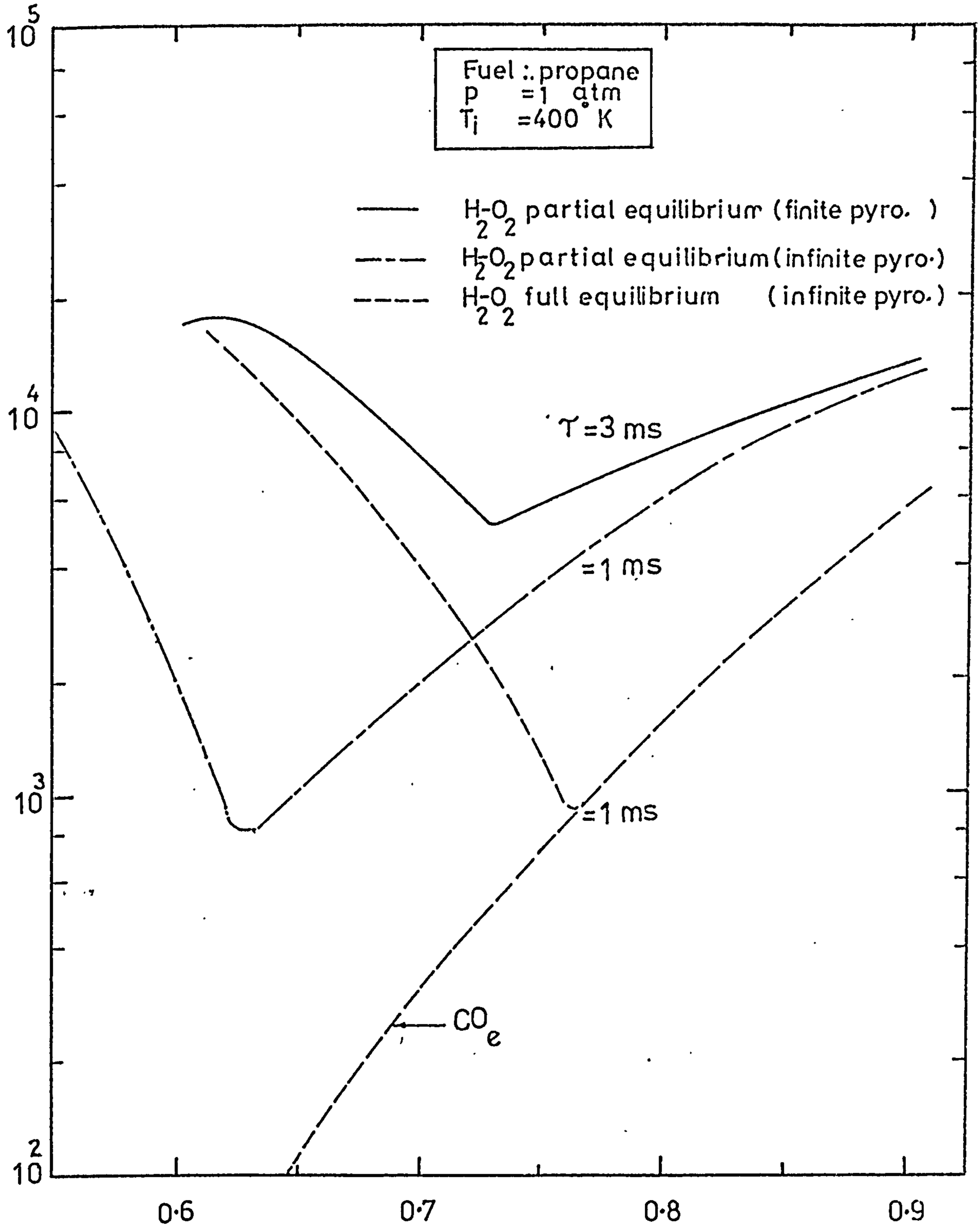

FIGURE 4.9 Comparison of CO levels predicted by different models in lean, premixed propane-air flames

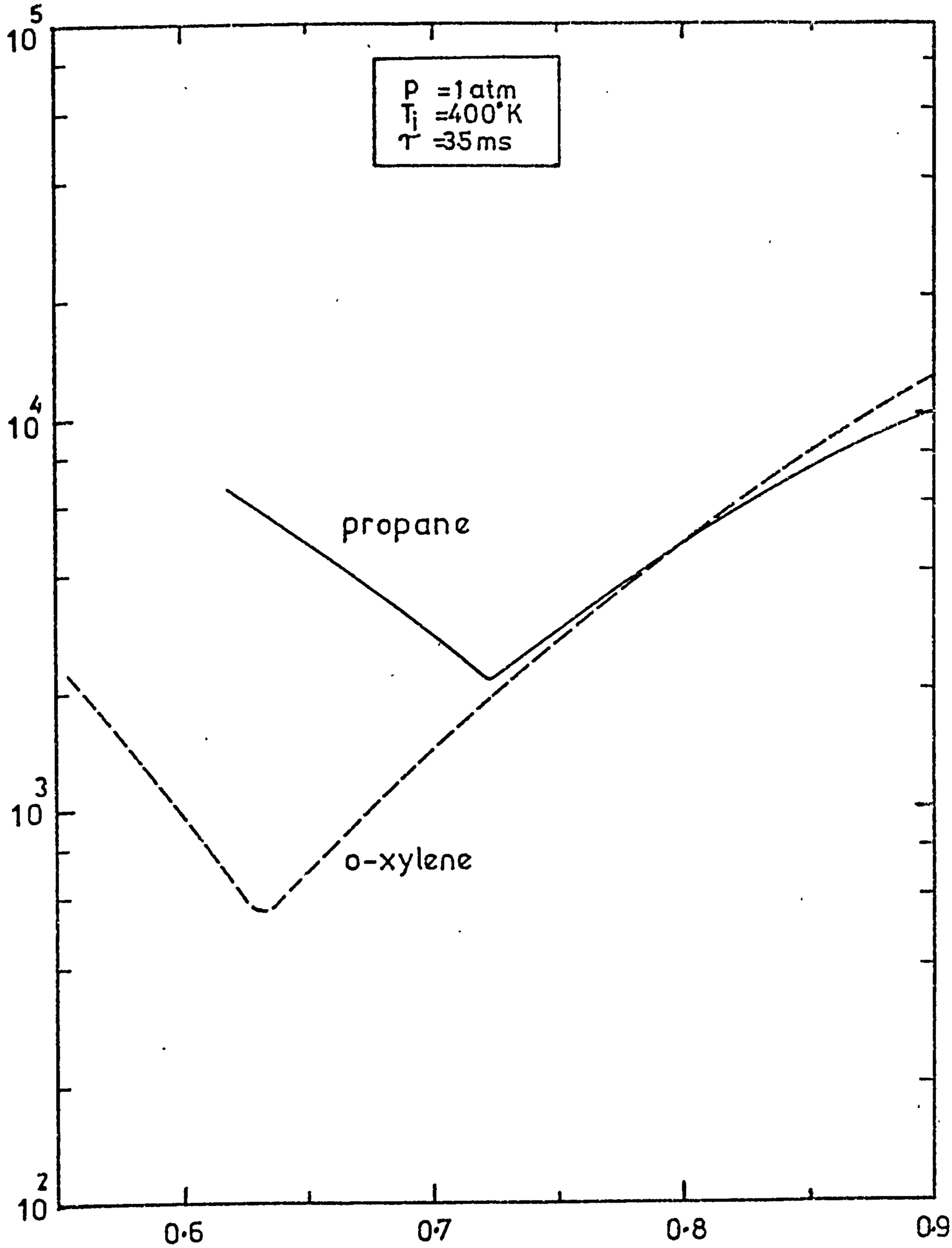

FIGURE 4·10 Comparison of CO levels predicted by O_2–H_2 partial equilibrium models in propane and o-xylene/air flames when using the same fuel oxidation rate equation

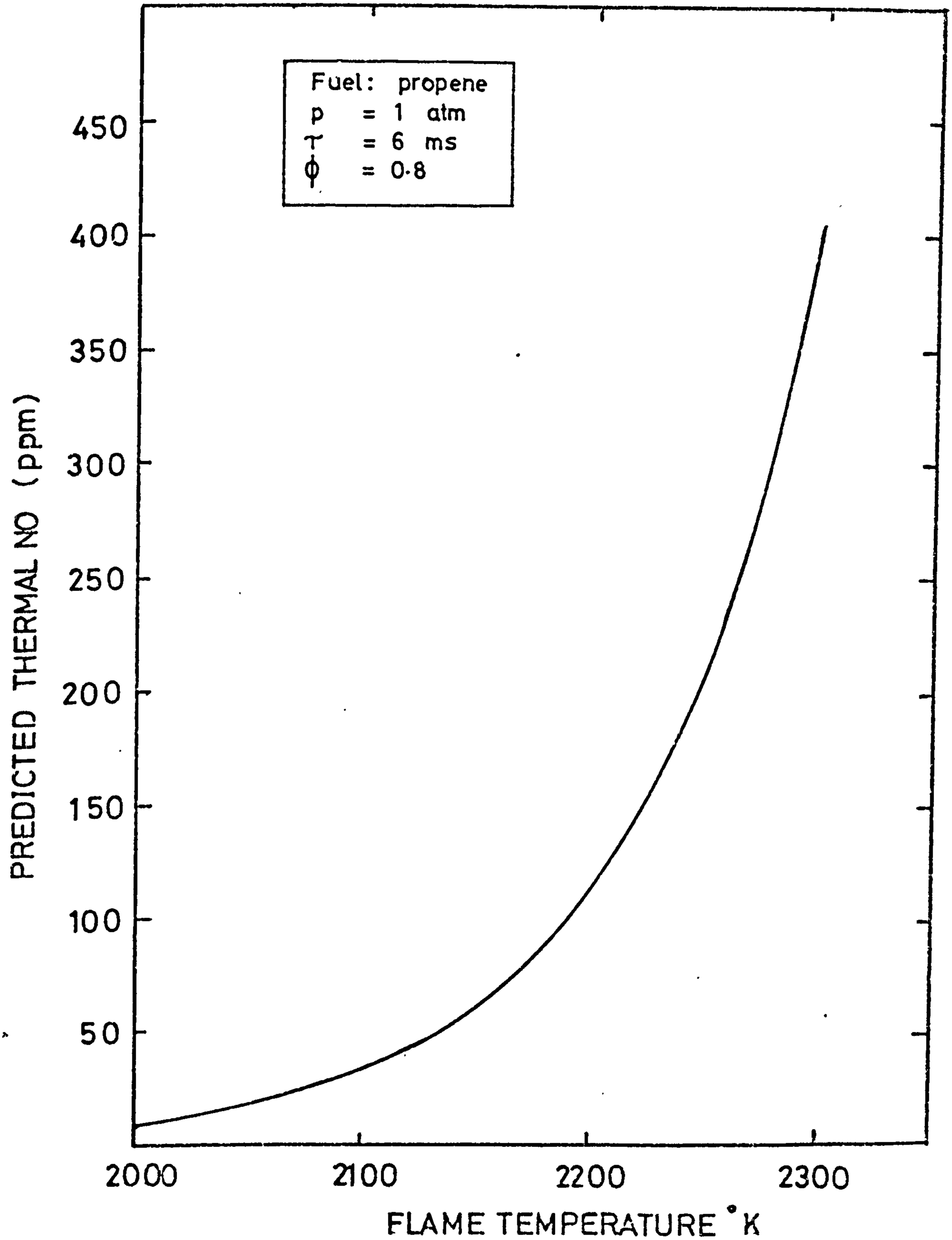

FIGURE 5.1 Variations of predicted thermal NO with flame temperature in lean hydrocarbon-air flames

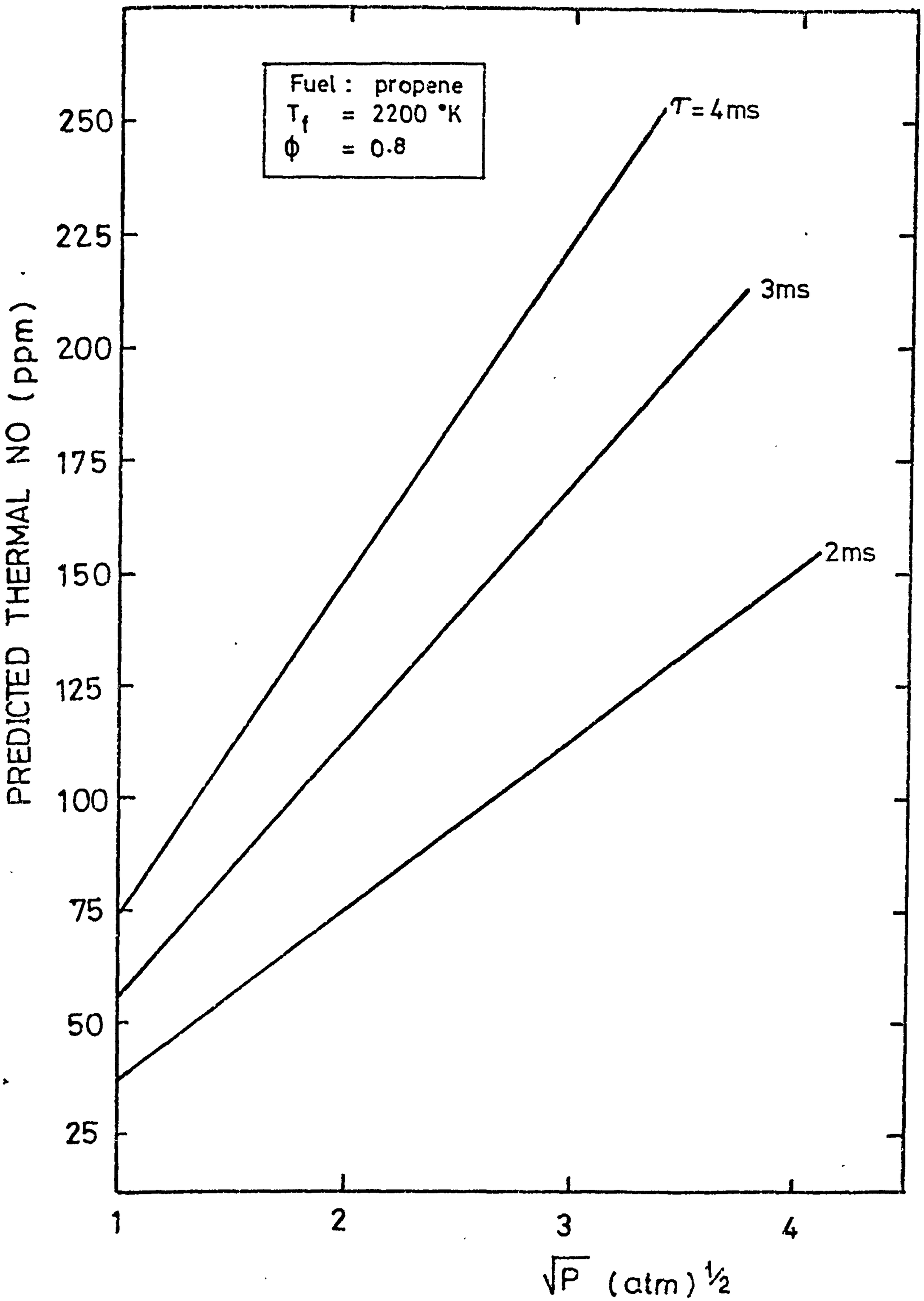

FIGURE 5.2 Effect of pressure on predicted thermal NO in lean flames

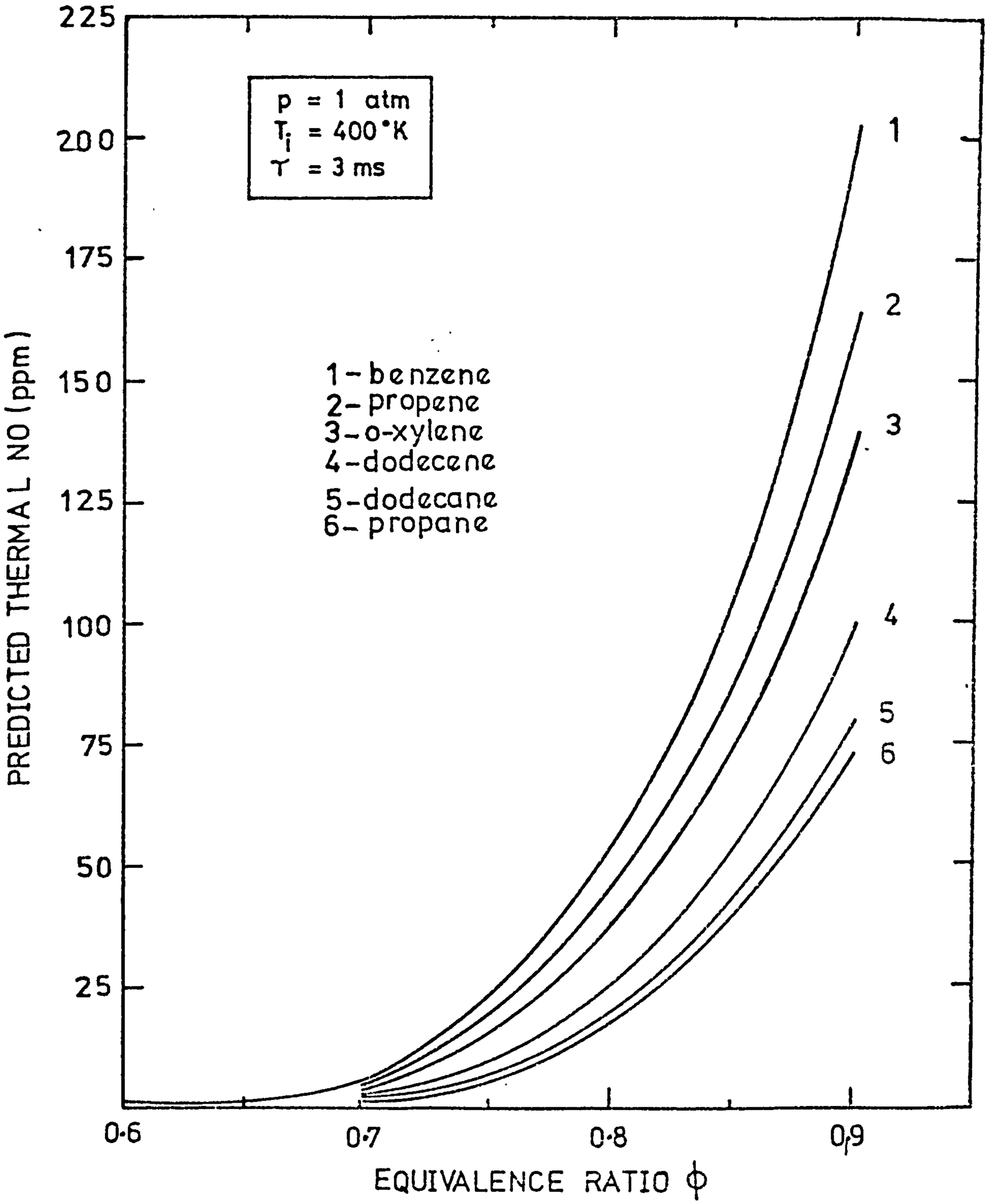

FIGURE 5.3 Predicted thermal NO in different lean, premixed hydrocarbon-air flames.

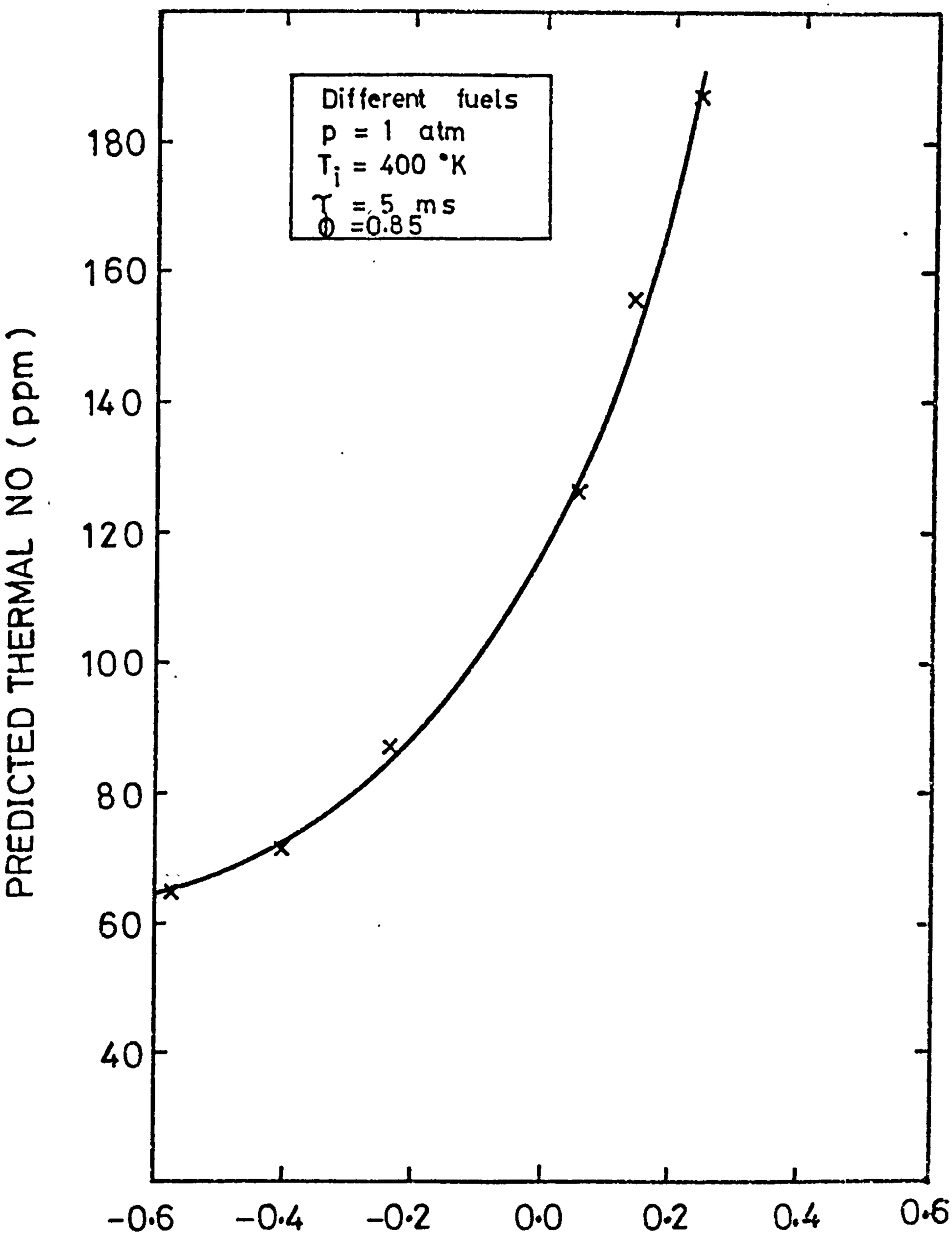

FIGURE 5.4 Variation of predicted thermal NO in lean hydrocarbon -air flames with the heat of formation of the fuel

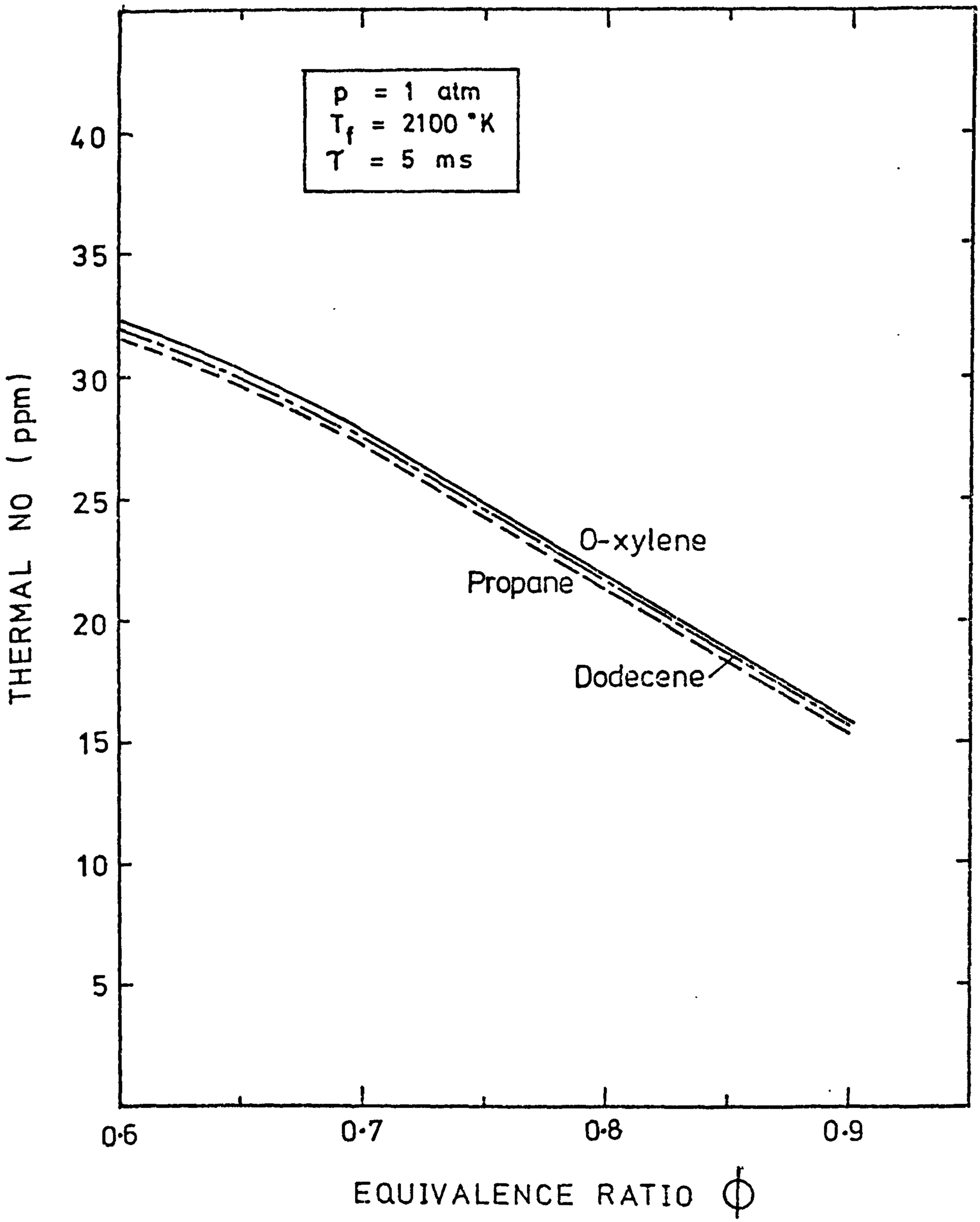

FIGURE 5.5 Predicted thermal NO in different hydrocarbon-air flames of the same T_f and equivalence ratio

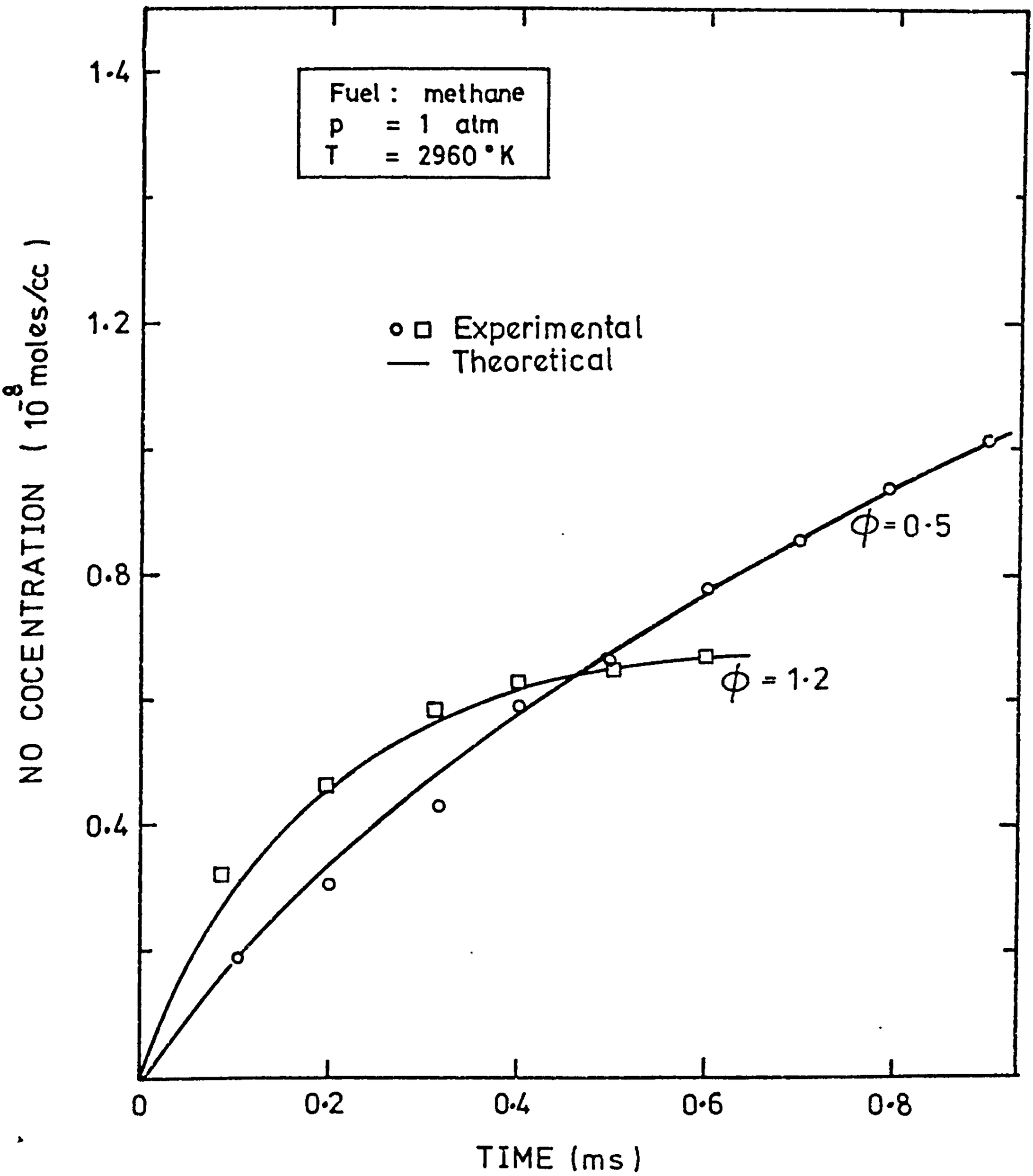

FIGURE 5.6 Predicted and measured NO levels in shock tube experiments. (Ref.57)

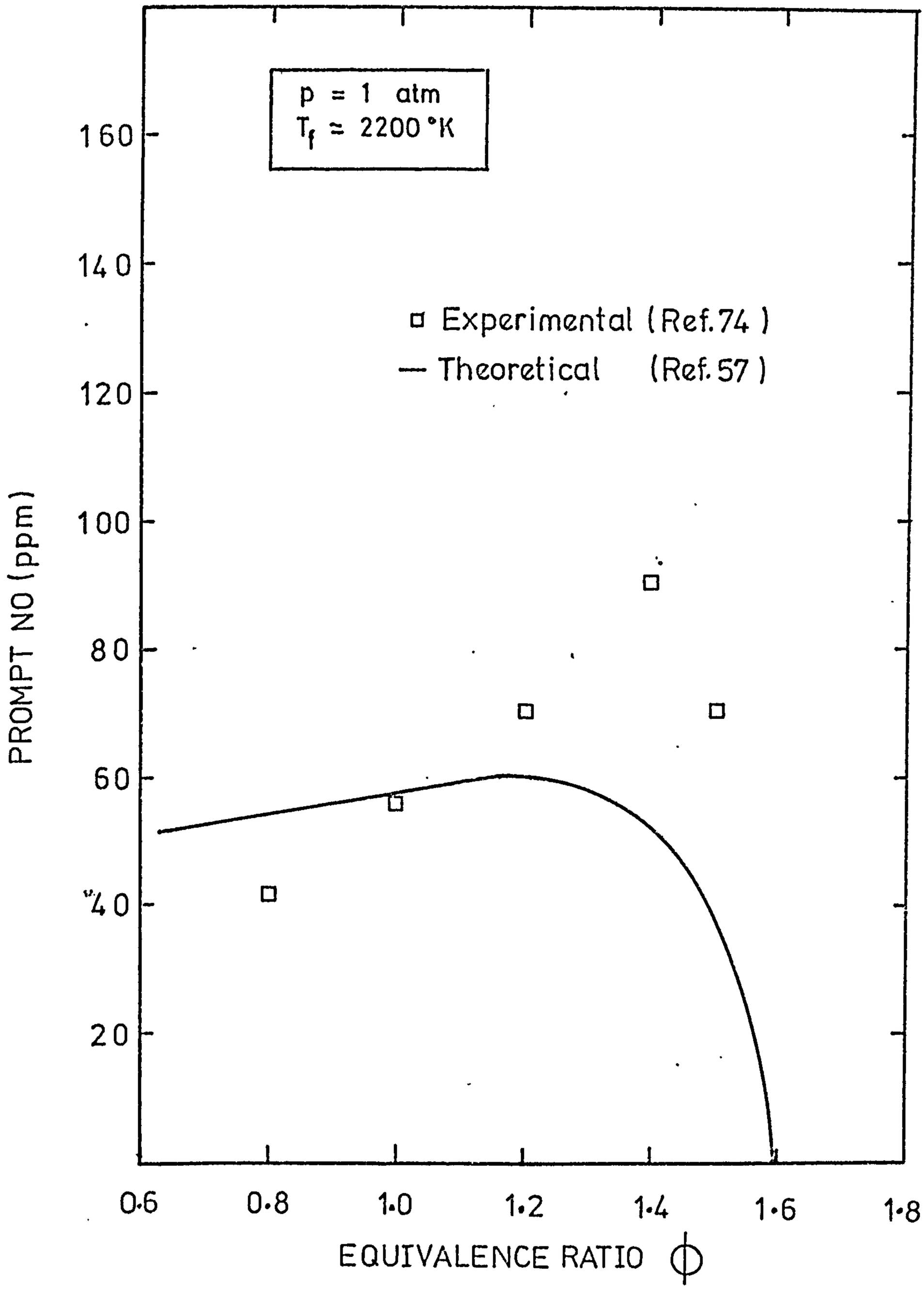

FIGURE 5.7 Comparison of predicted and measured prompt NO levels

(Ref. 57)

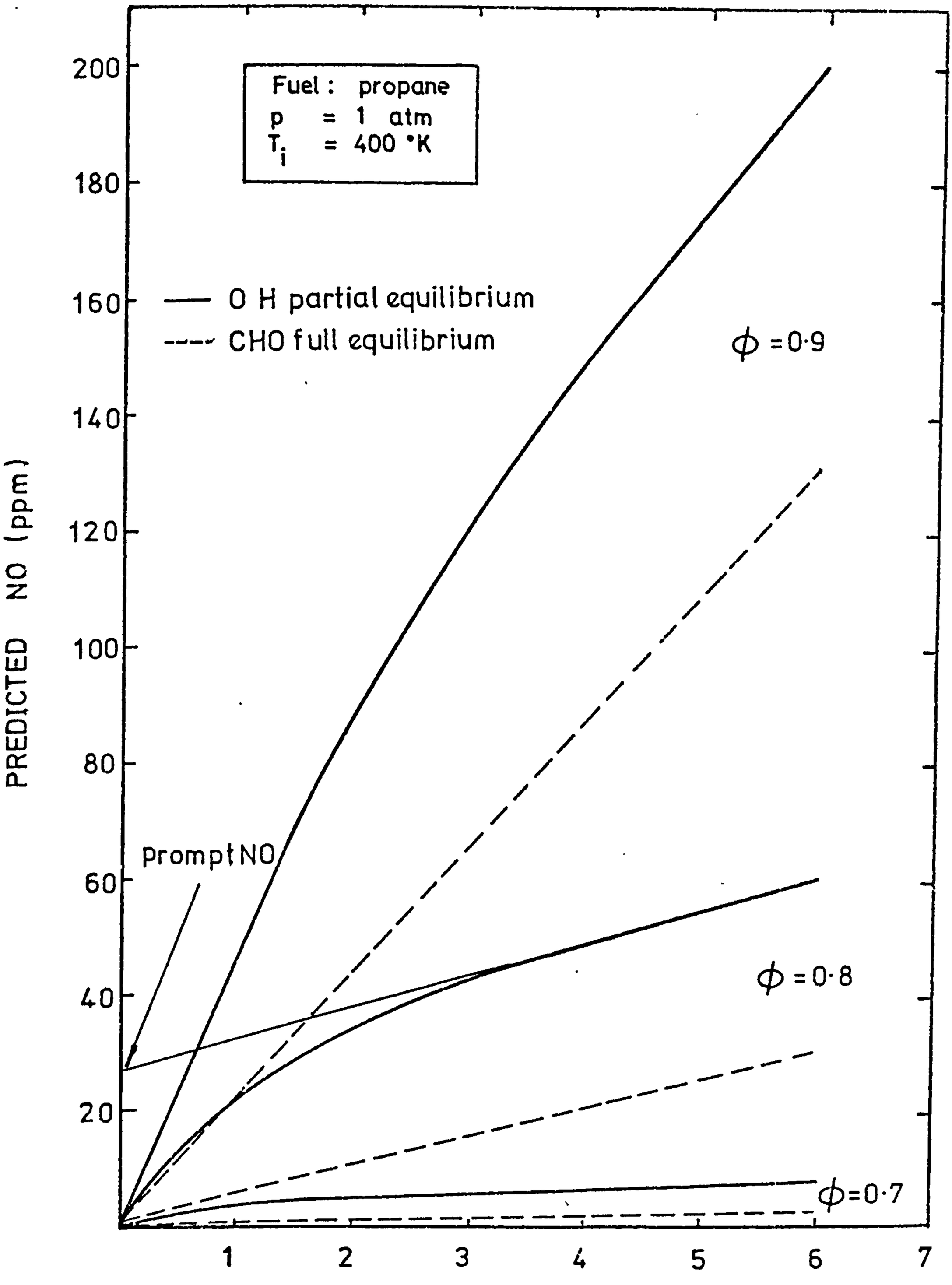

FIGURE 5.8 Predicted NO profiles in premixed, propane-air flat flames.

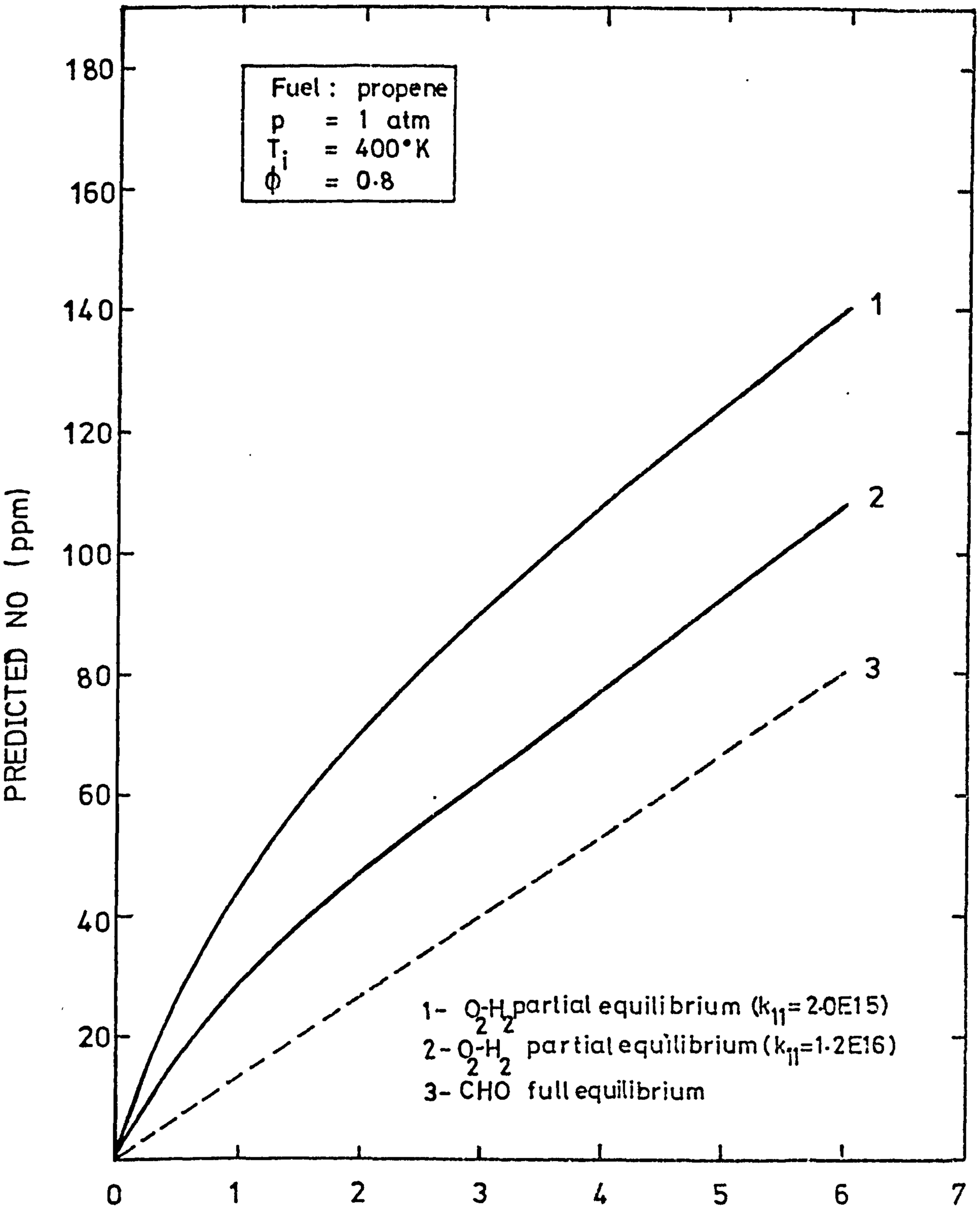

FIGURE 5.9 Effect of recombination rate on predicted NO profiles in lean, propane-air flat flames.

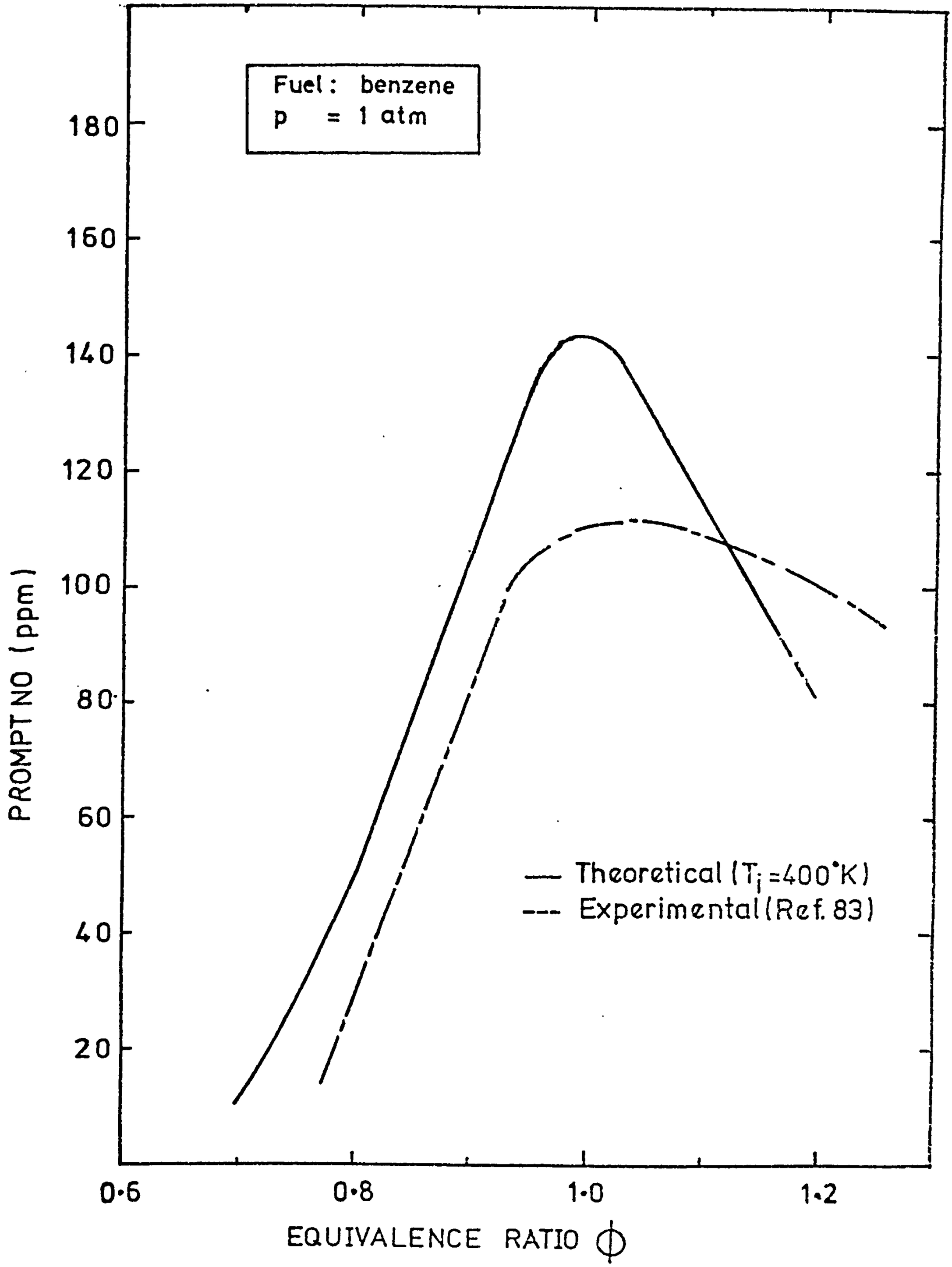

FIGURE 5.10 Variation of predicted prompt NO with equivalence ratio in adiabatic benzene-air flames.

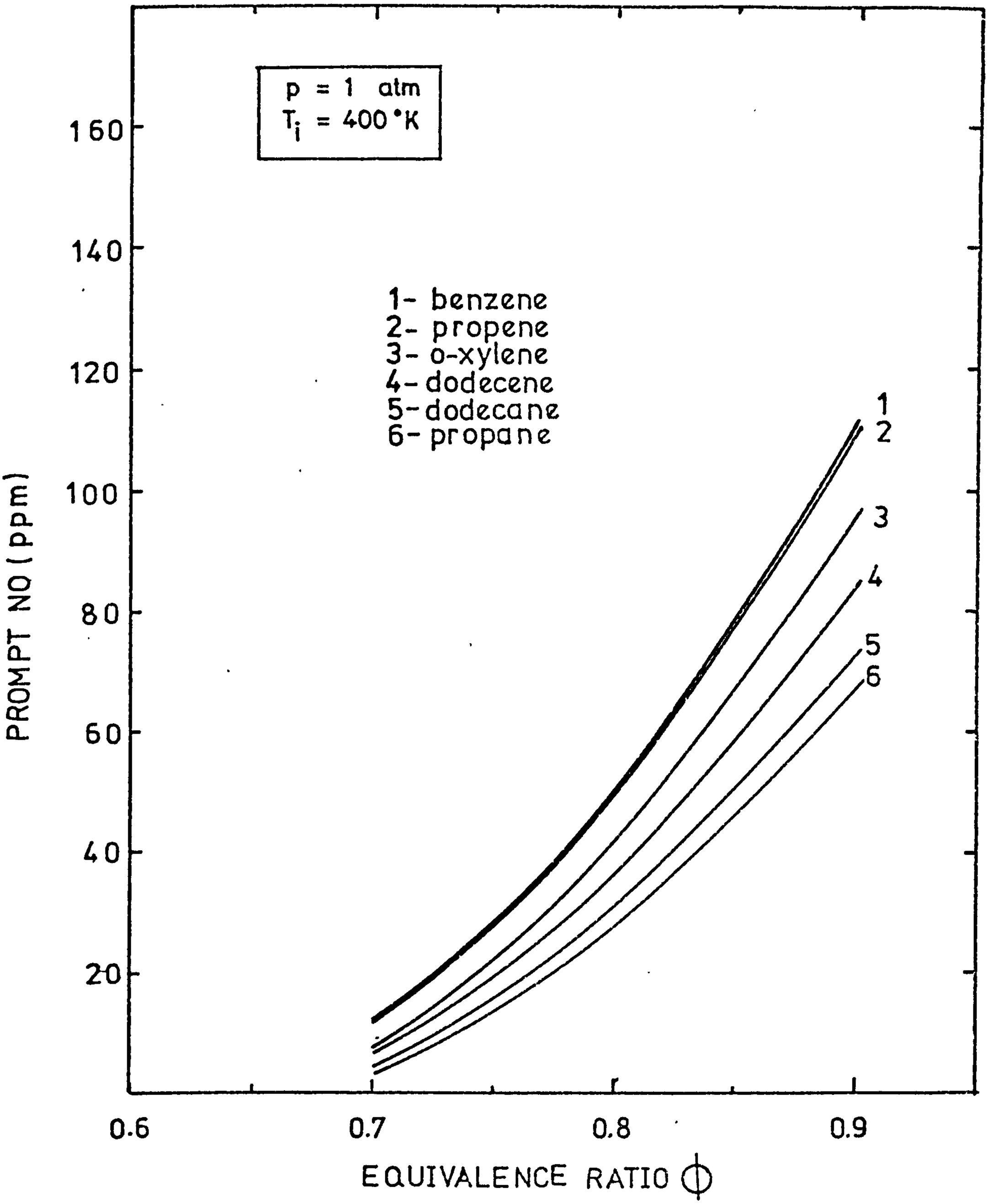

FIGURE 5.11 Predicted prompt NO levels in different, adiabatic, lean hydrocarbon - air flames.

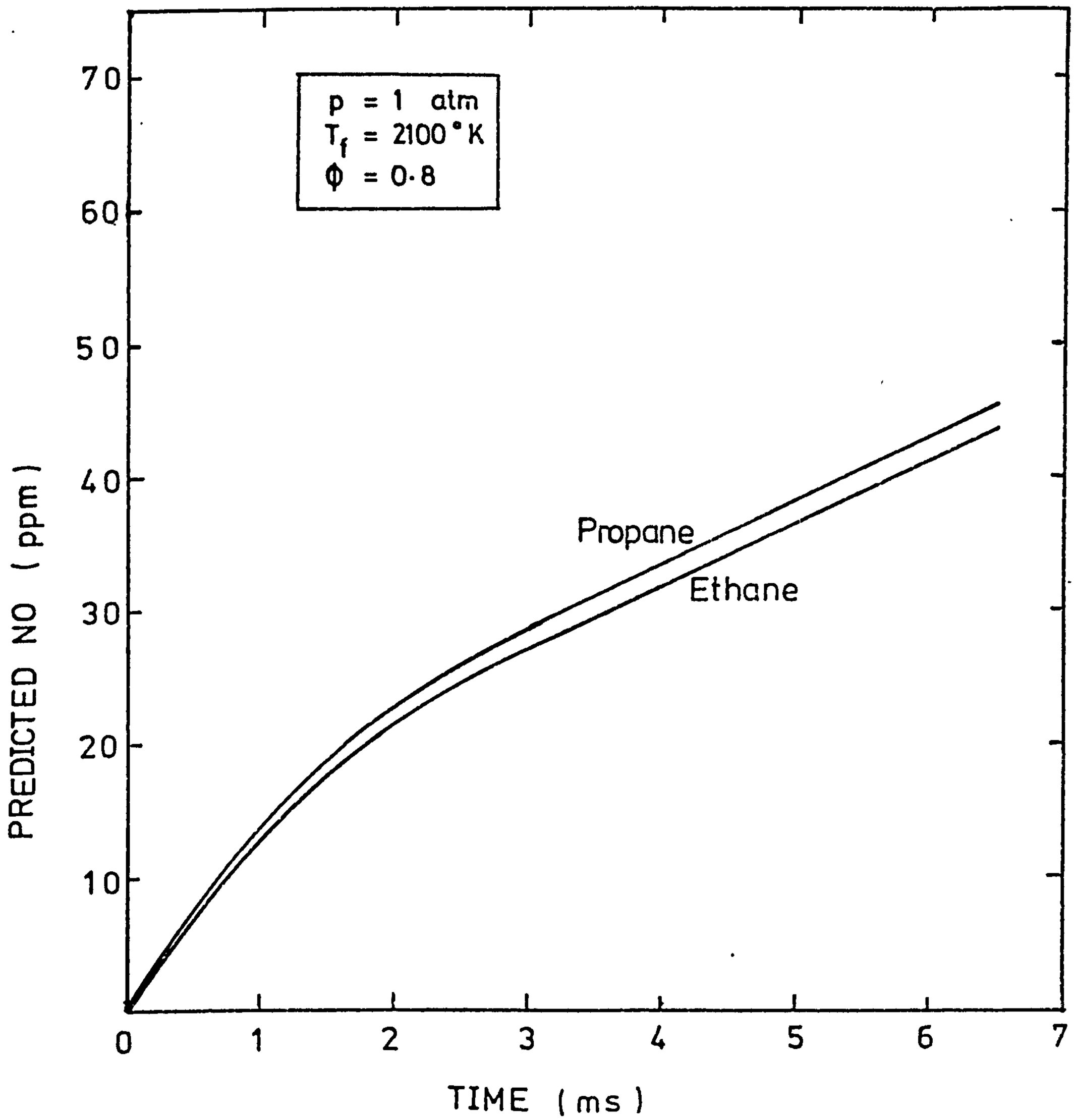

FIGURE 5.12 Effect of fuel structure on NO profiles in lean hydrocarbon flames of the same flame temperature and equivalence ratios.

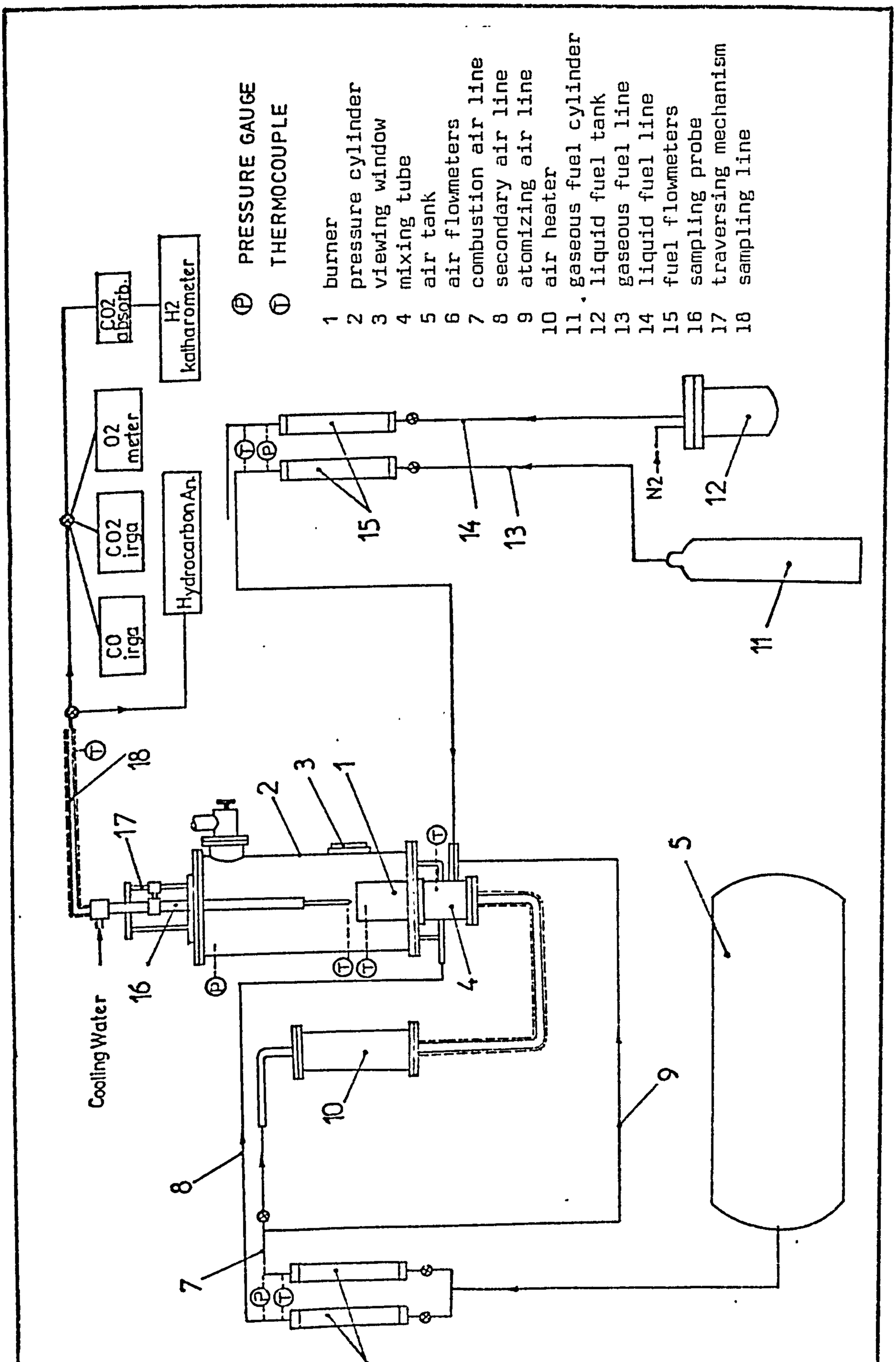

FIGURE 6.1 Layout of test facility

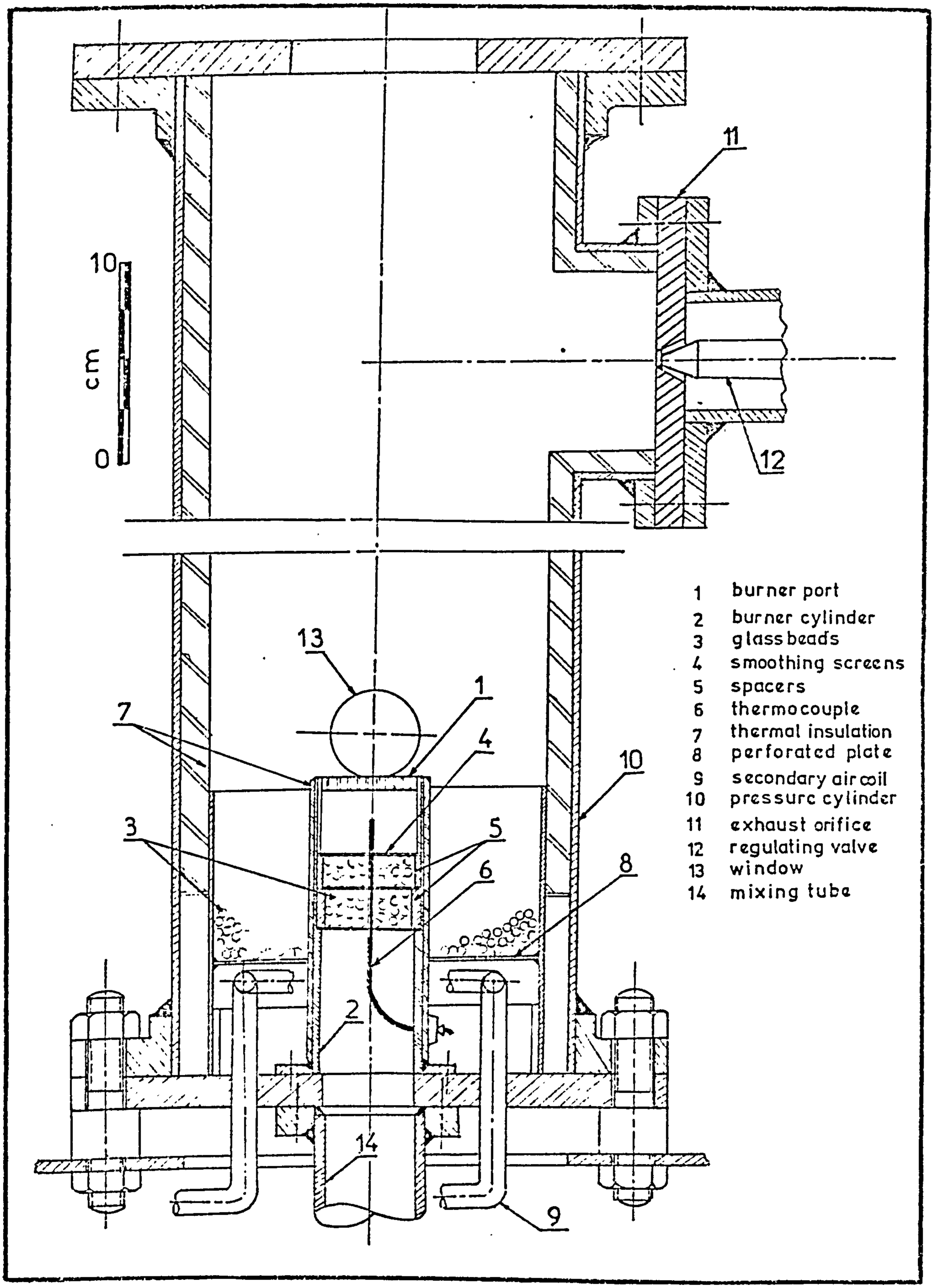

FIGURE 6.2 Burner assembly

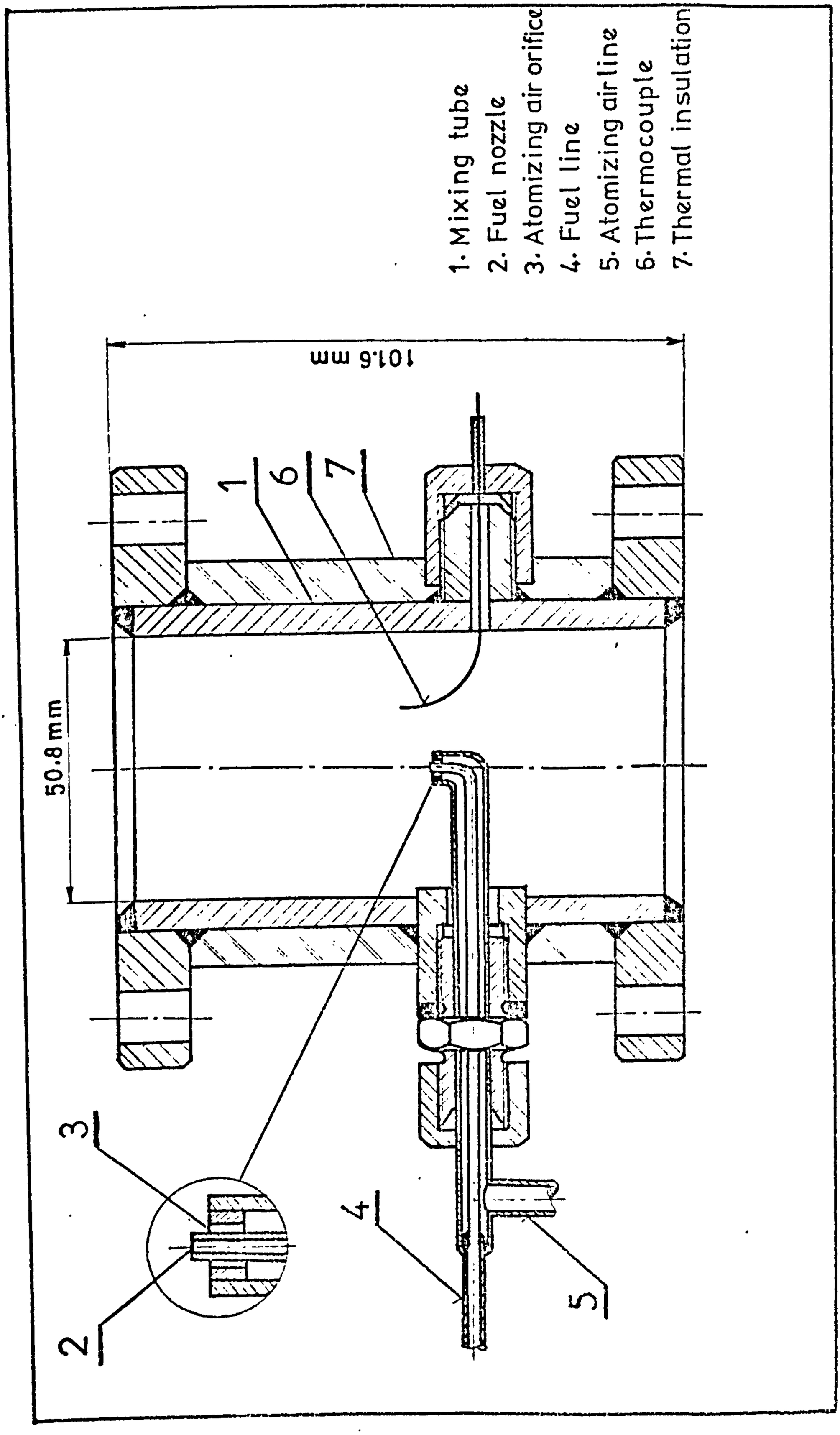

FIGURE 6.3 Mixing tube assembly

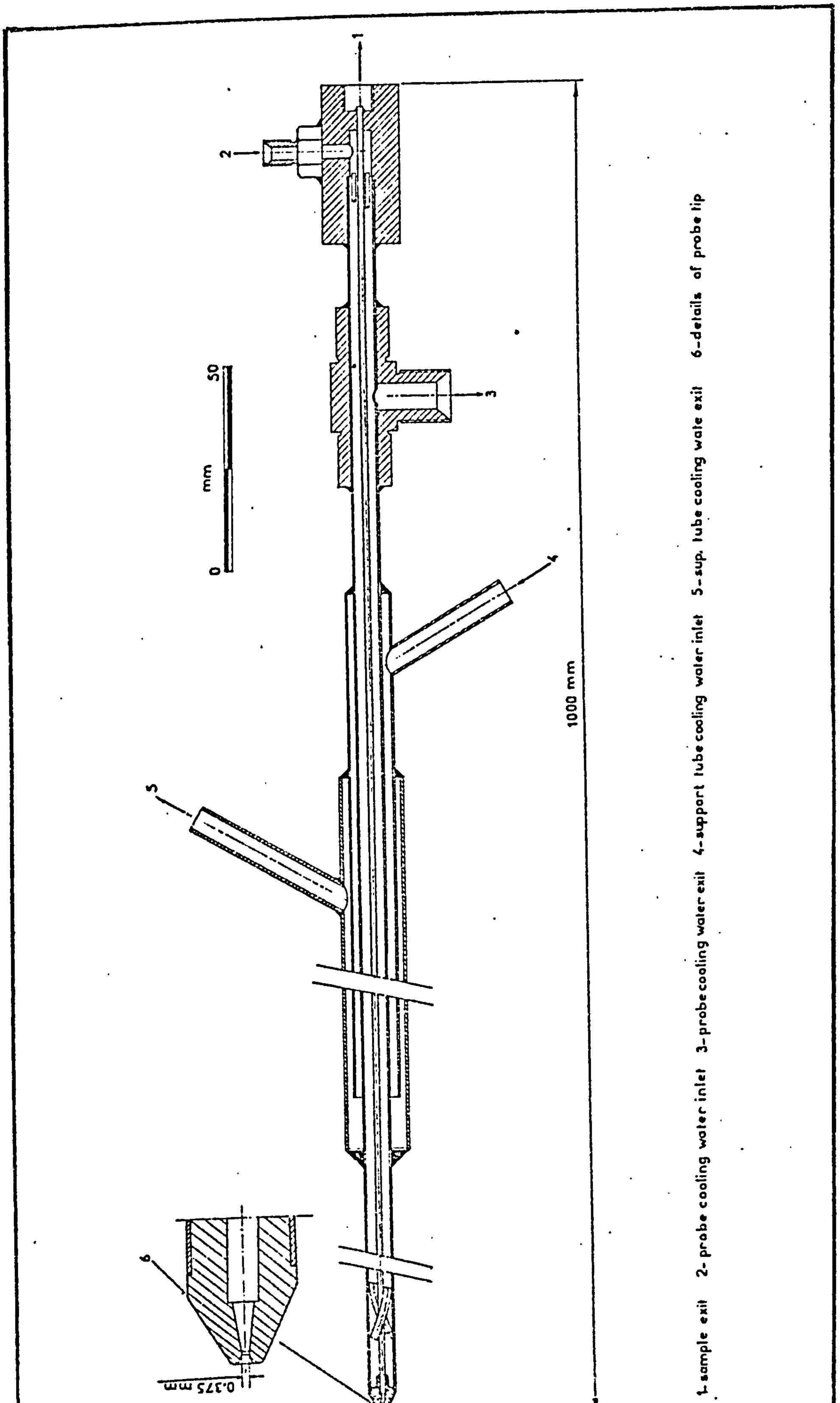

FIGURE 6.4 Sampling probe

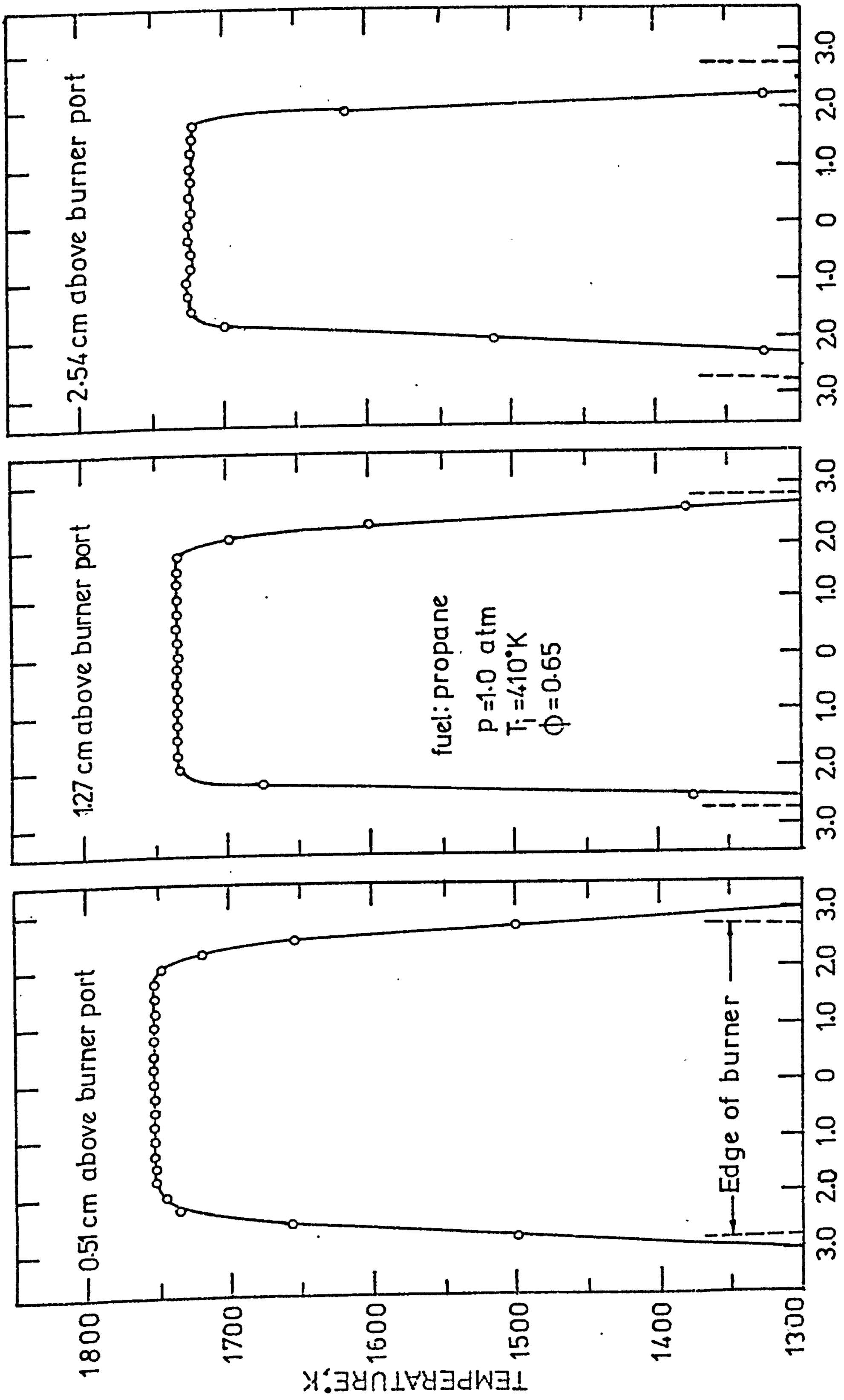

FIGURE 7.1 Temperature profiles across a flat, atmospheric propane–air flame.

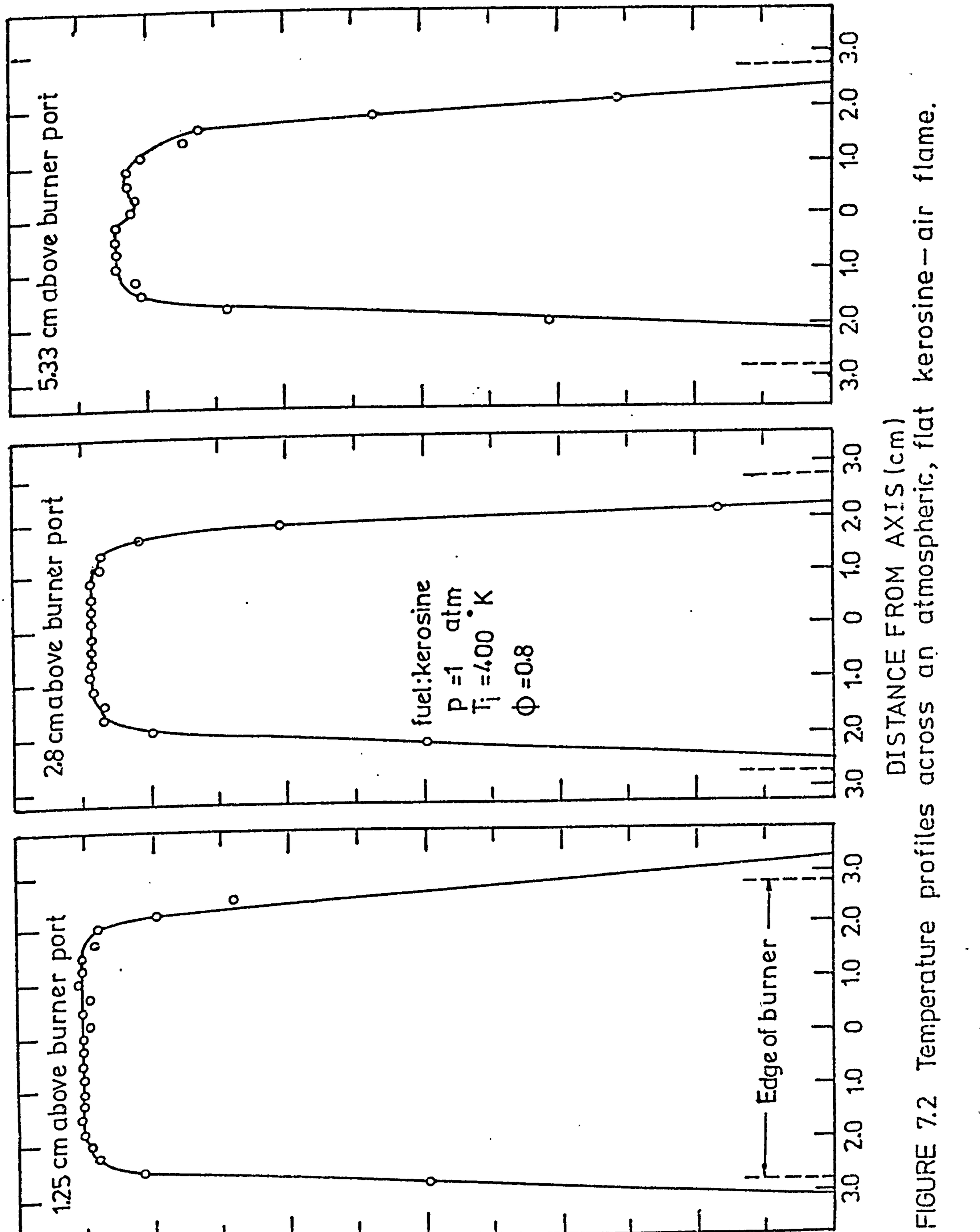

FIGURE 7.2 Temperature profiles across an atmospheric, flat kerosine–air flame.

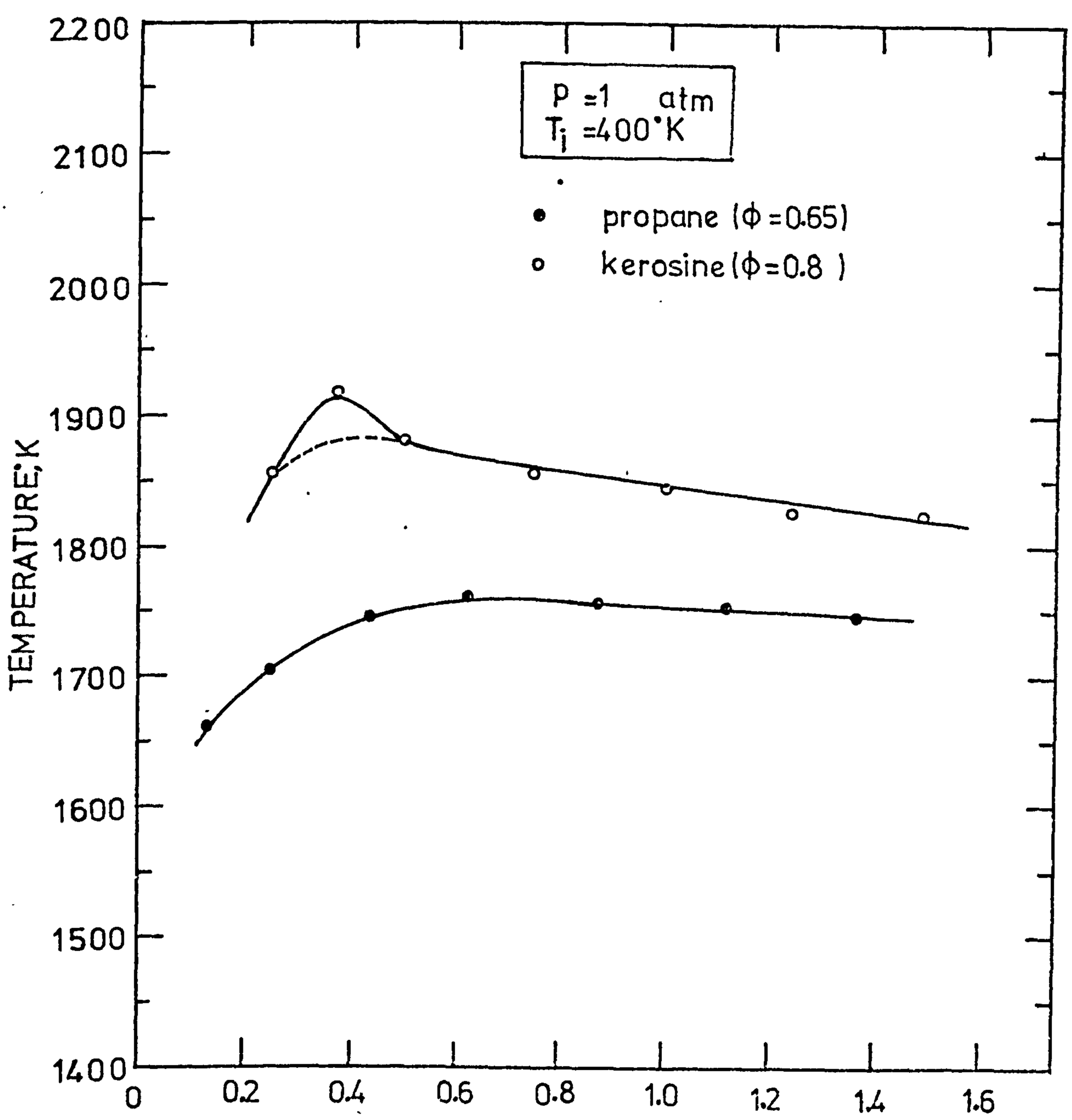

FIGURE 7.3 Temperature profiles along the axis of flat propane and kerosine-air flames.

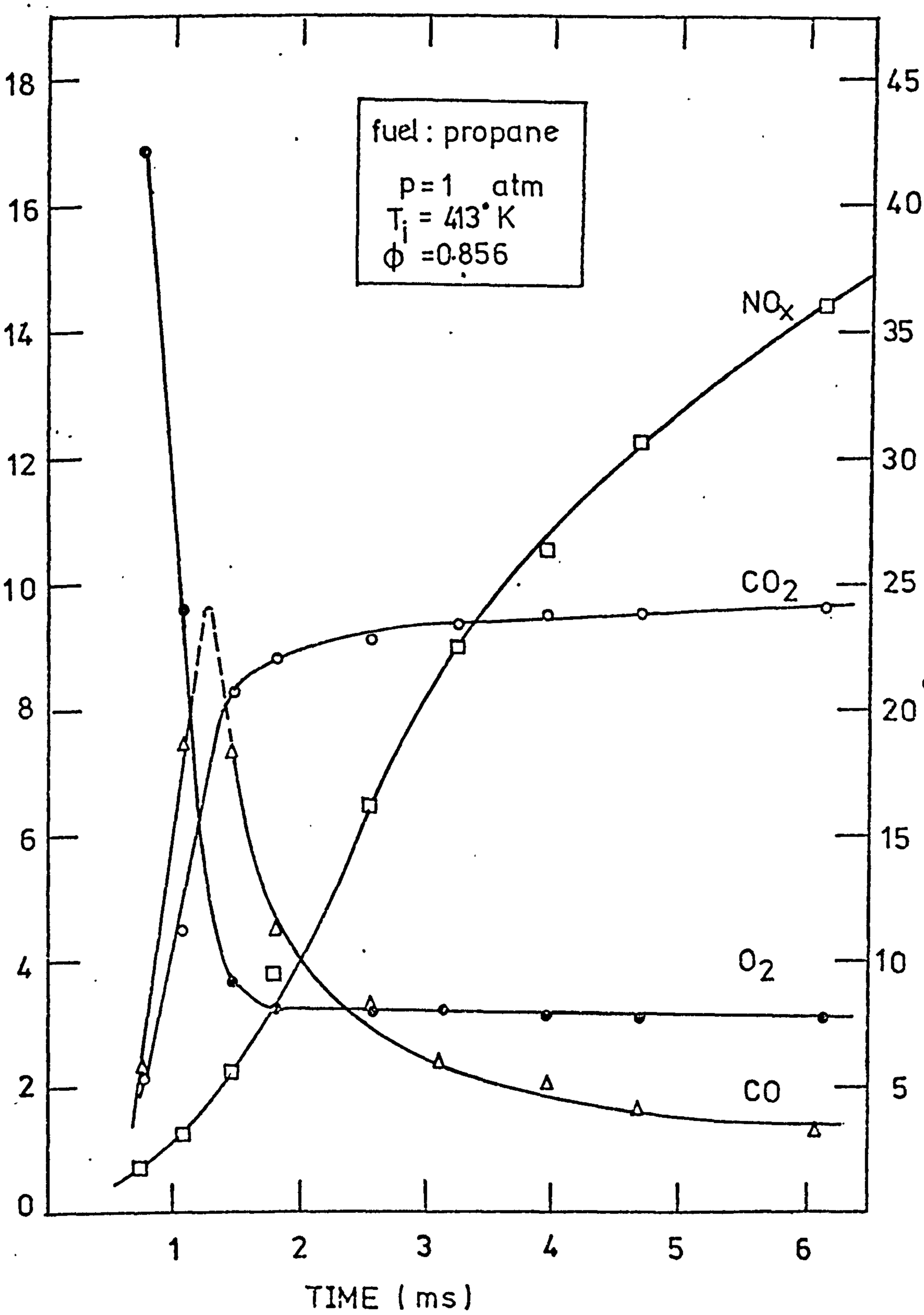

FIGURE 7.4 Concentration profiles in an atmospheric, flat propane-air flame.

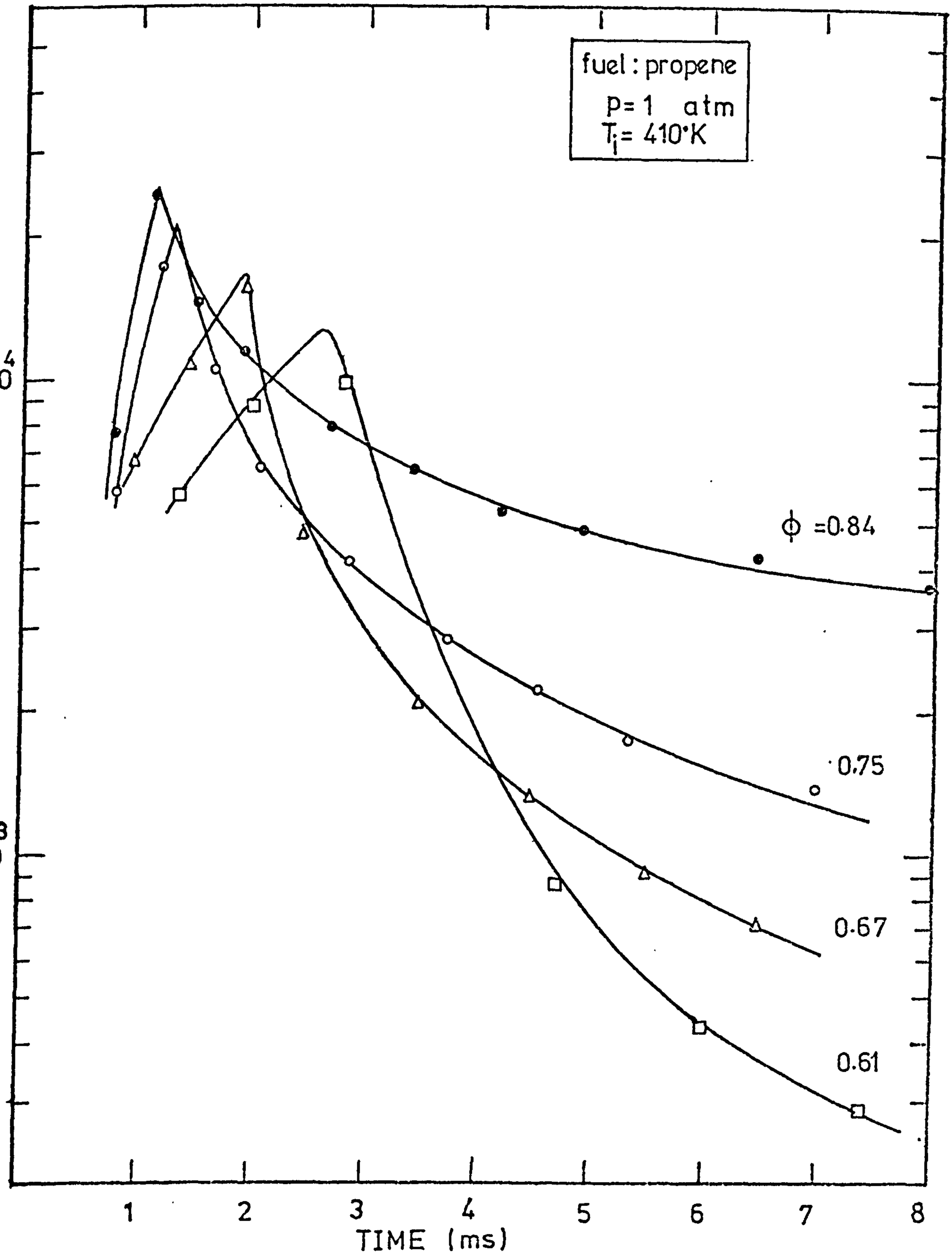

EIGURE 7.5 CO profiles in different atmospheric, flat propene-air flames.

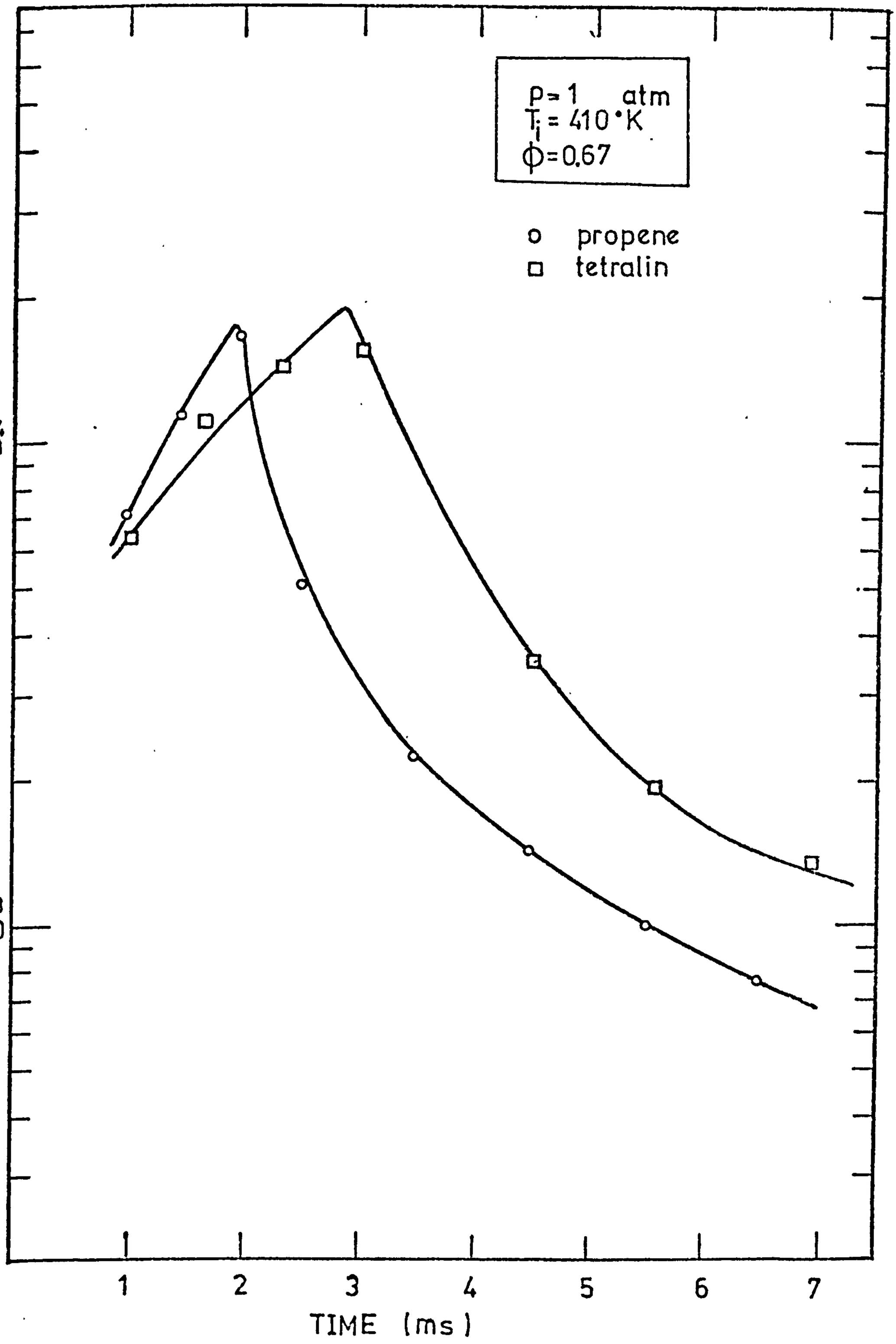

FIGURE 7.6 Dependance of CO profiles on the fuel structure

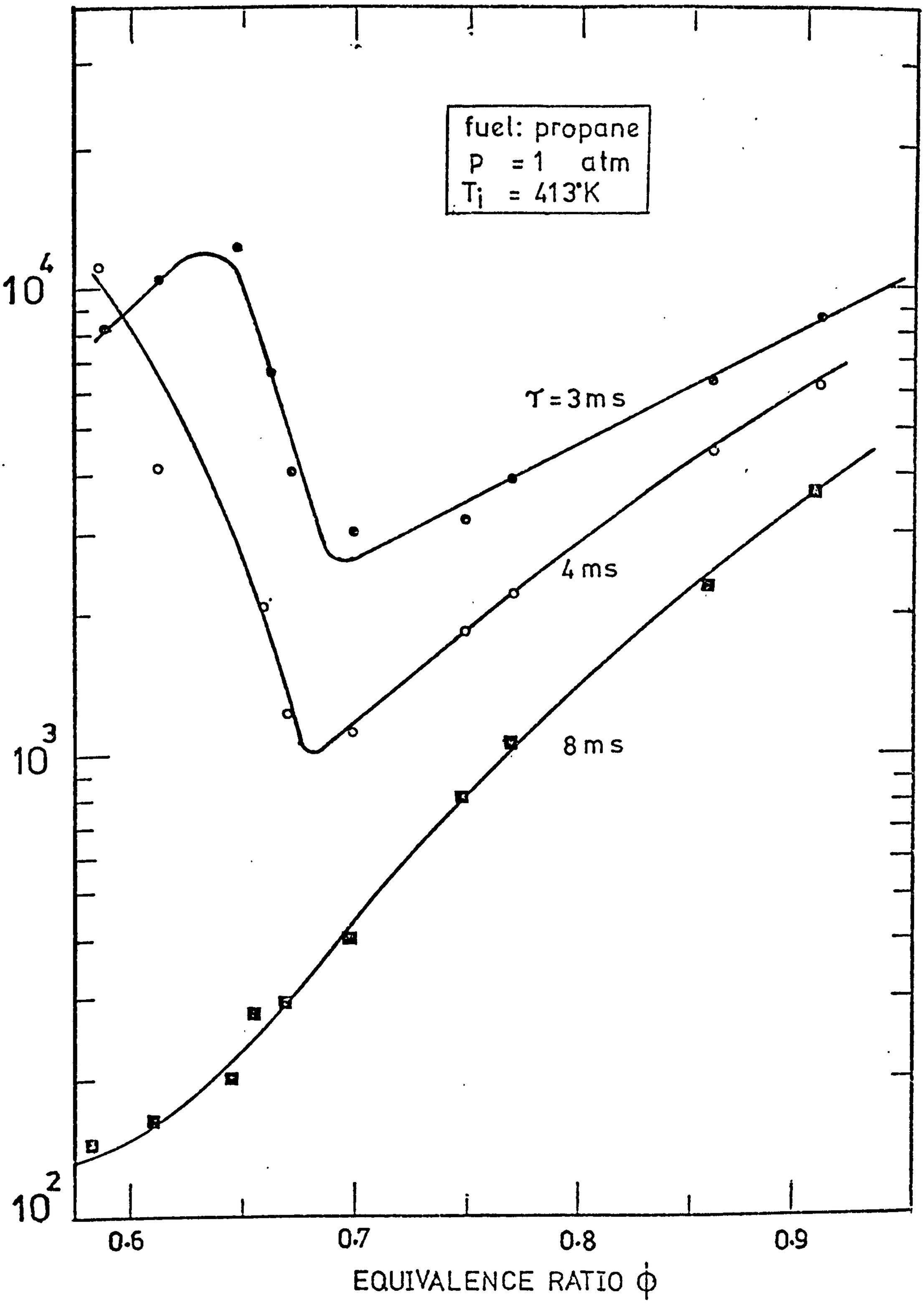

FIGURE 7.7 CO levels at different residence times in atmospheric, flat propane-air flames

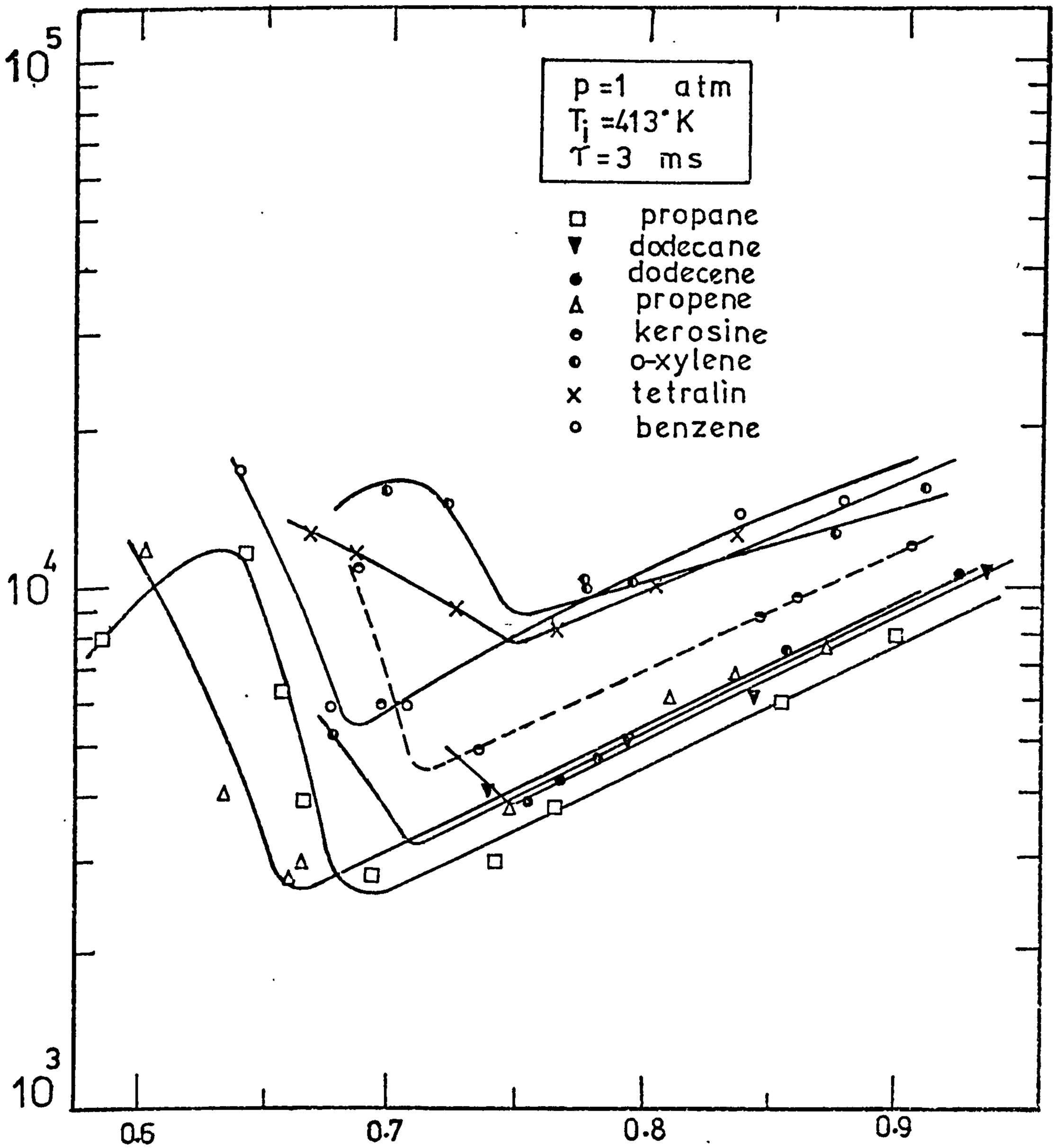

FIGURE 7.8 Carbon monoxide levels in different hydrocarbon-air flames under atmospheric pressure and after three milliseconds

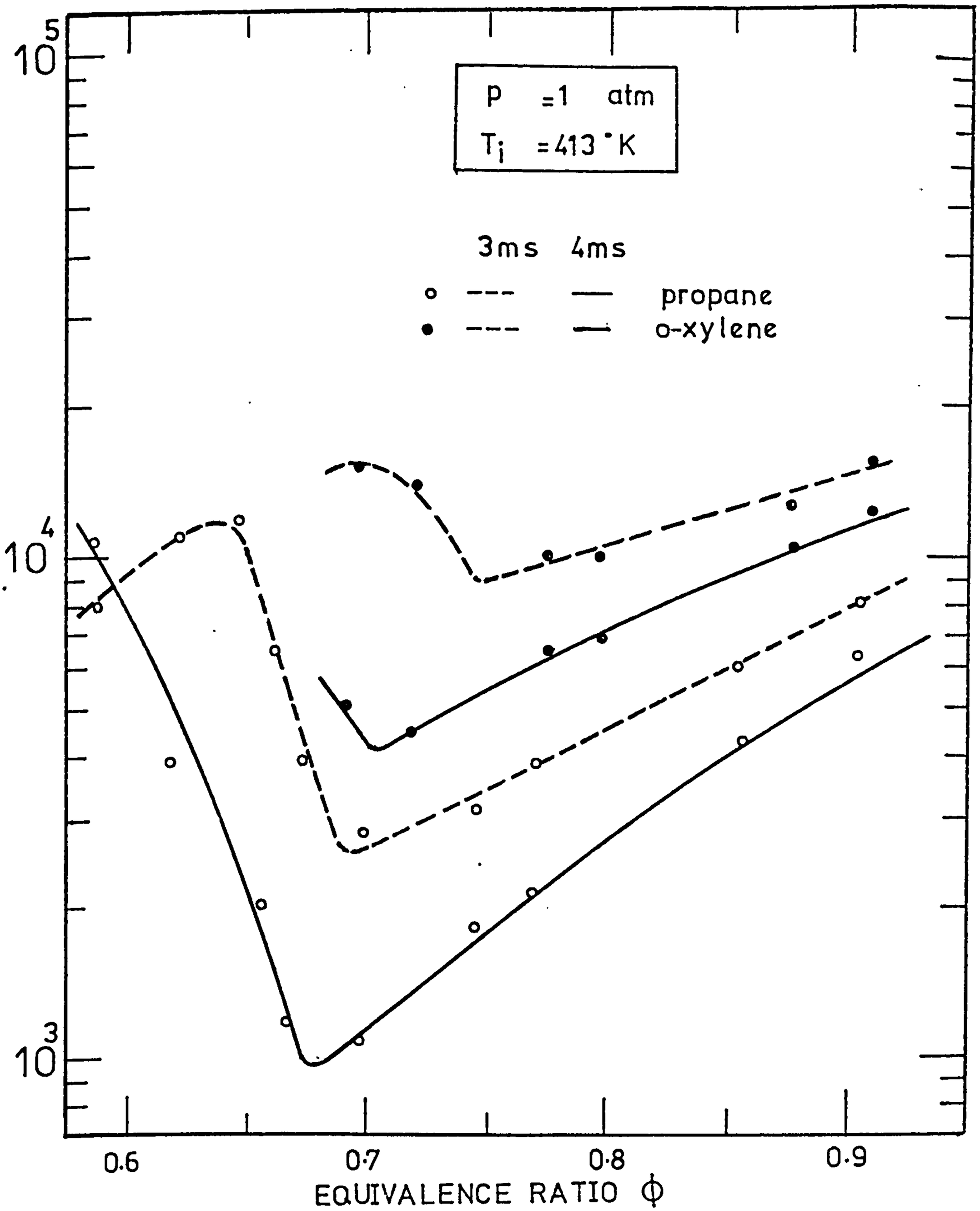

FIGURE 7.9 Comparison of CO levels in atmospheric propane and o-xylene/air flames at different equivalence ratios and residence times

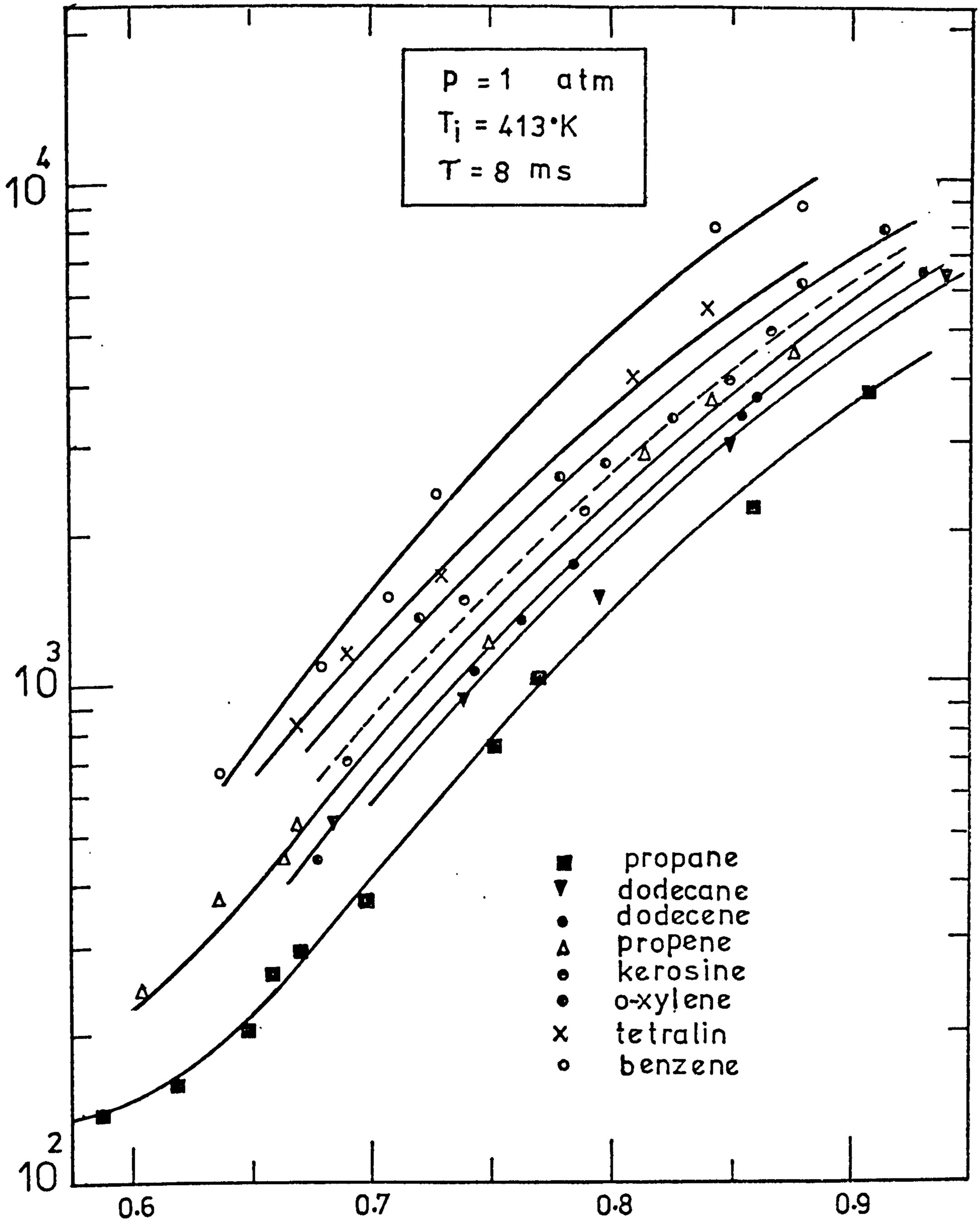

FIGURE 7.10 Carbon monoxide levels in different hydrocarbon-air flames under atmospheric pressure and after eight milliseconds

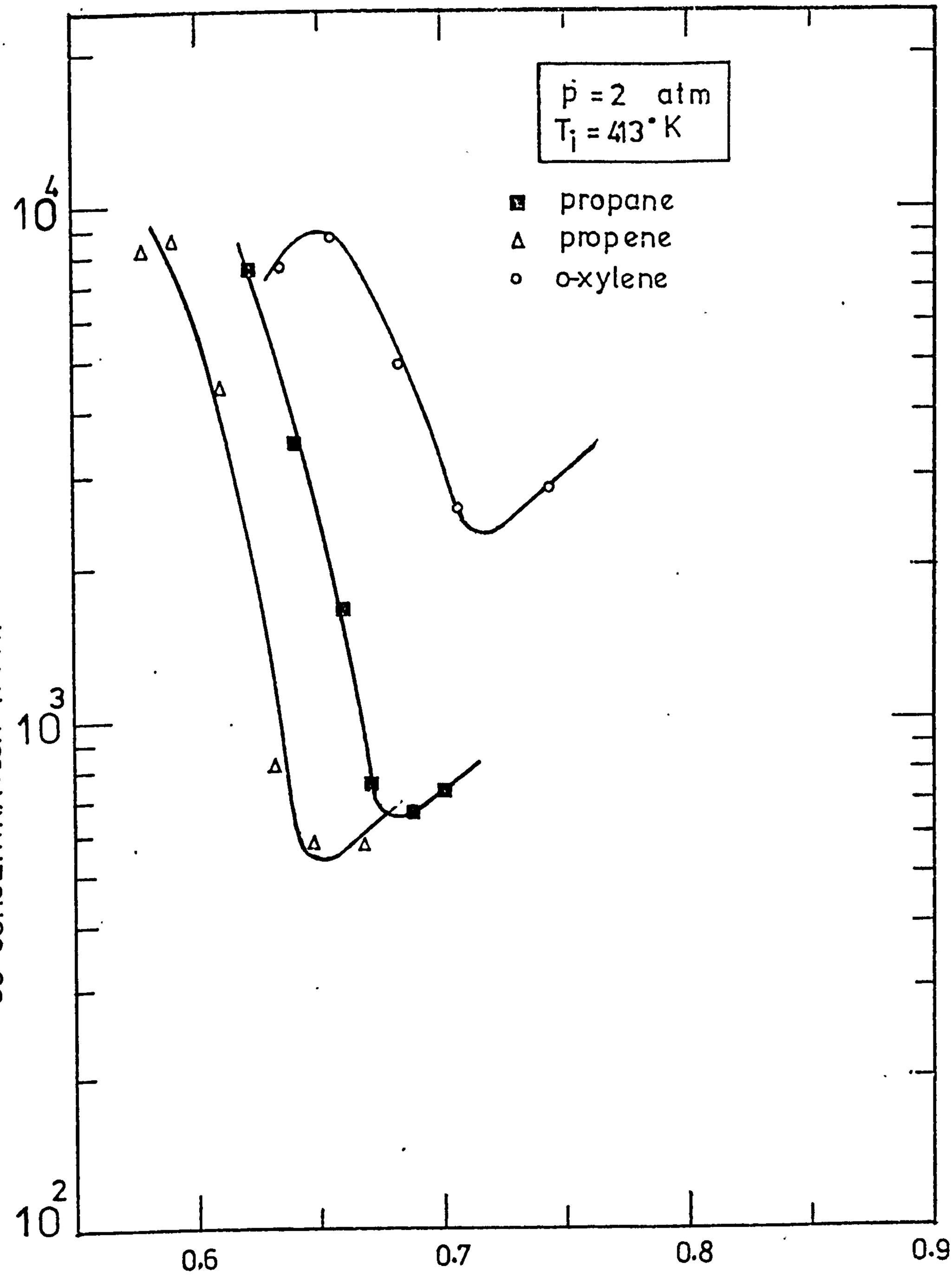

FIGURE 7.11 CO levels in different hydrocarbon-air flames at 2 atm pressure and after three milliseconds

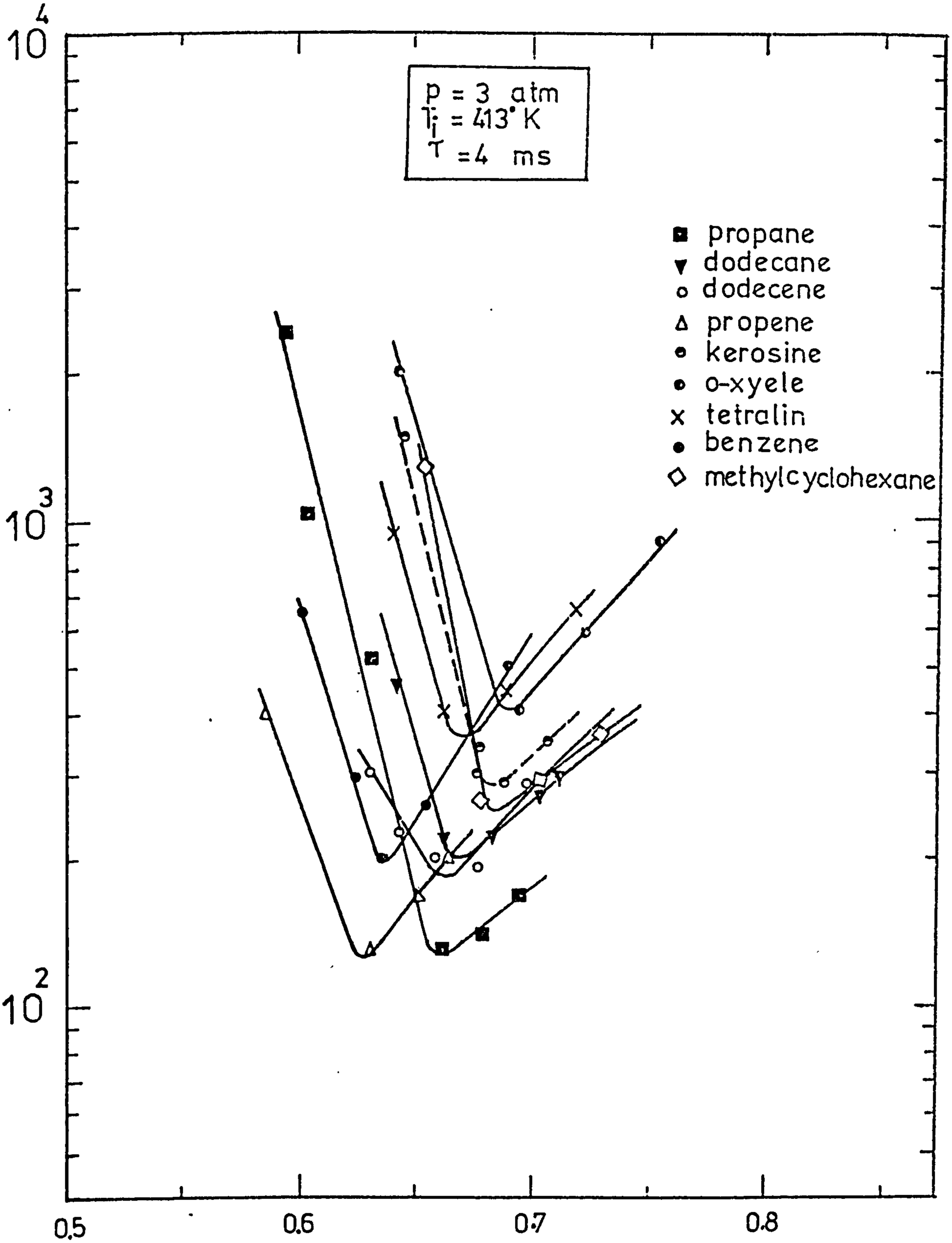

FIGURE 7.12 CO levels in different hydrocarbon-air flames at 3atm pressure and after four milliseconds

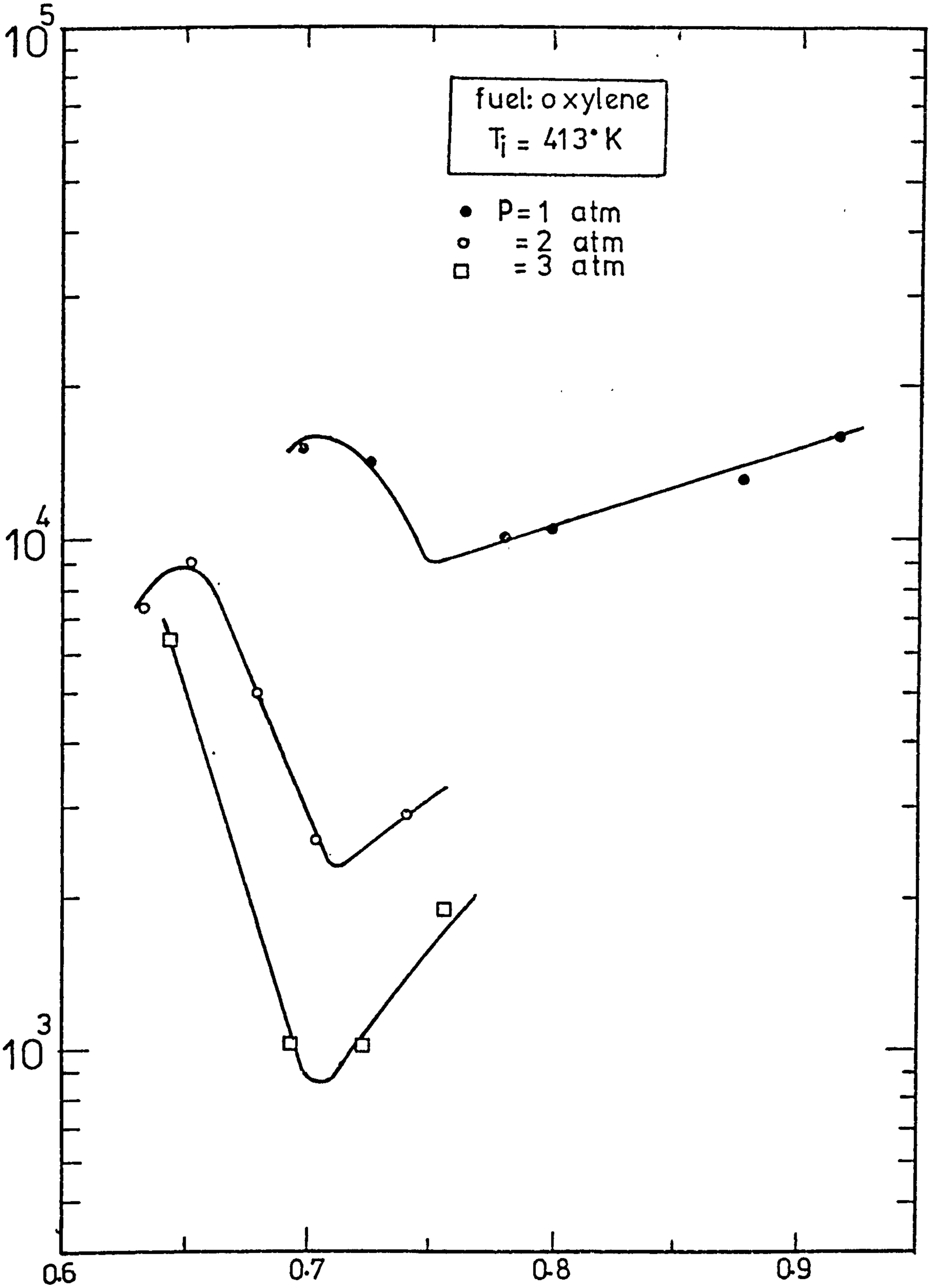

FIGURE 7.13 CO levels at different pressures in o-xylene/air flames after three milliseconds

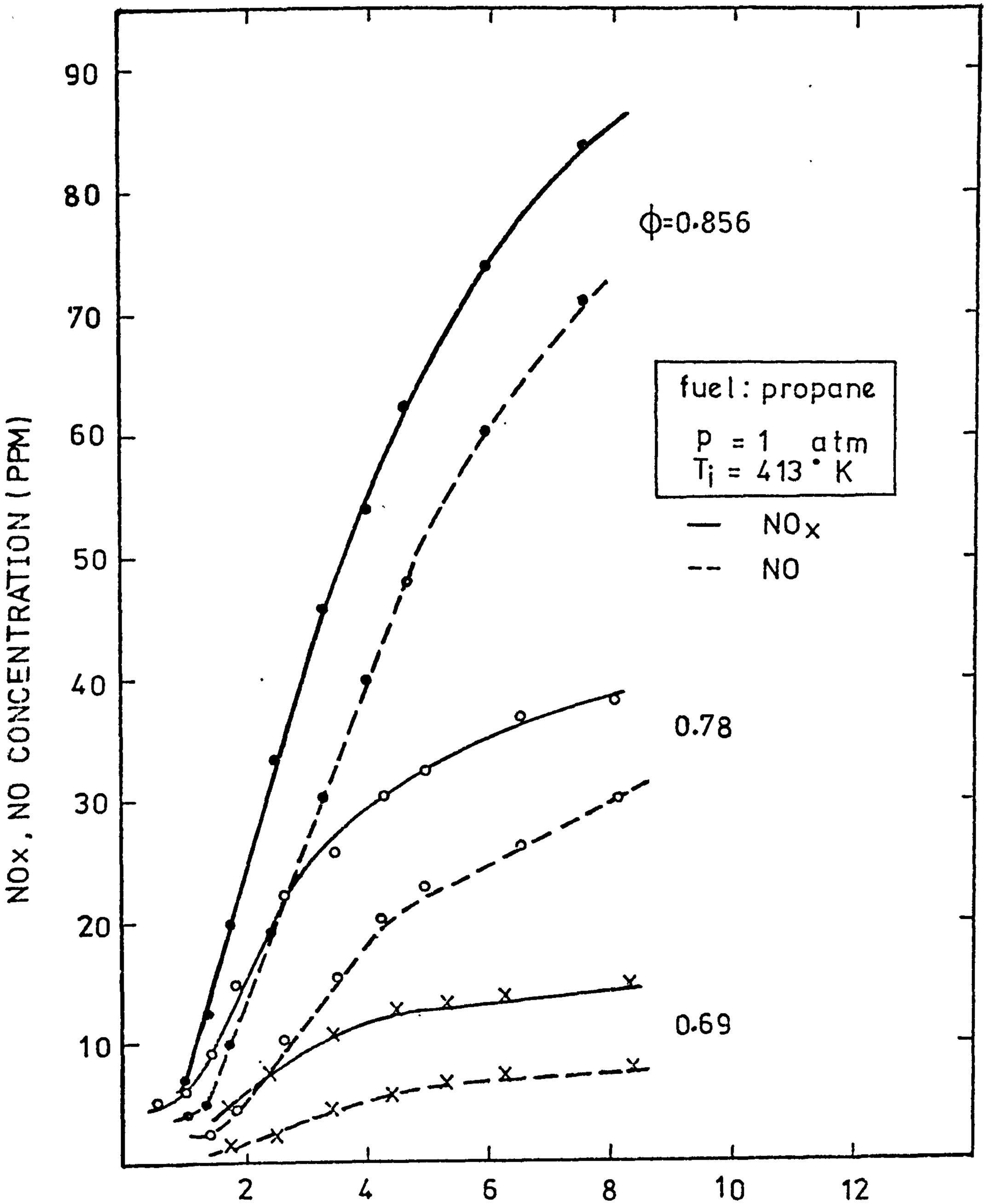

FIGURE7.14 Profiles of the oxides of nitrogen in different atmospheric propane-air flames

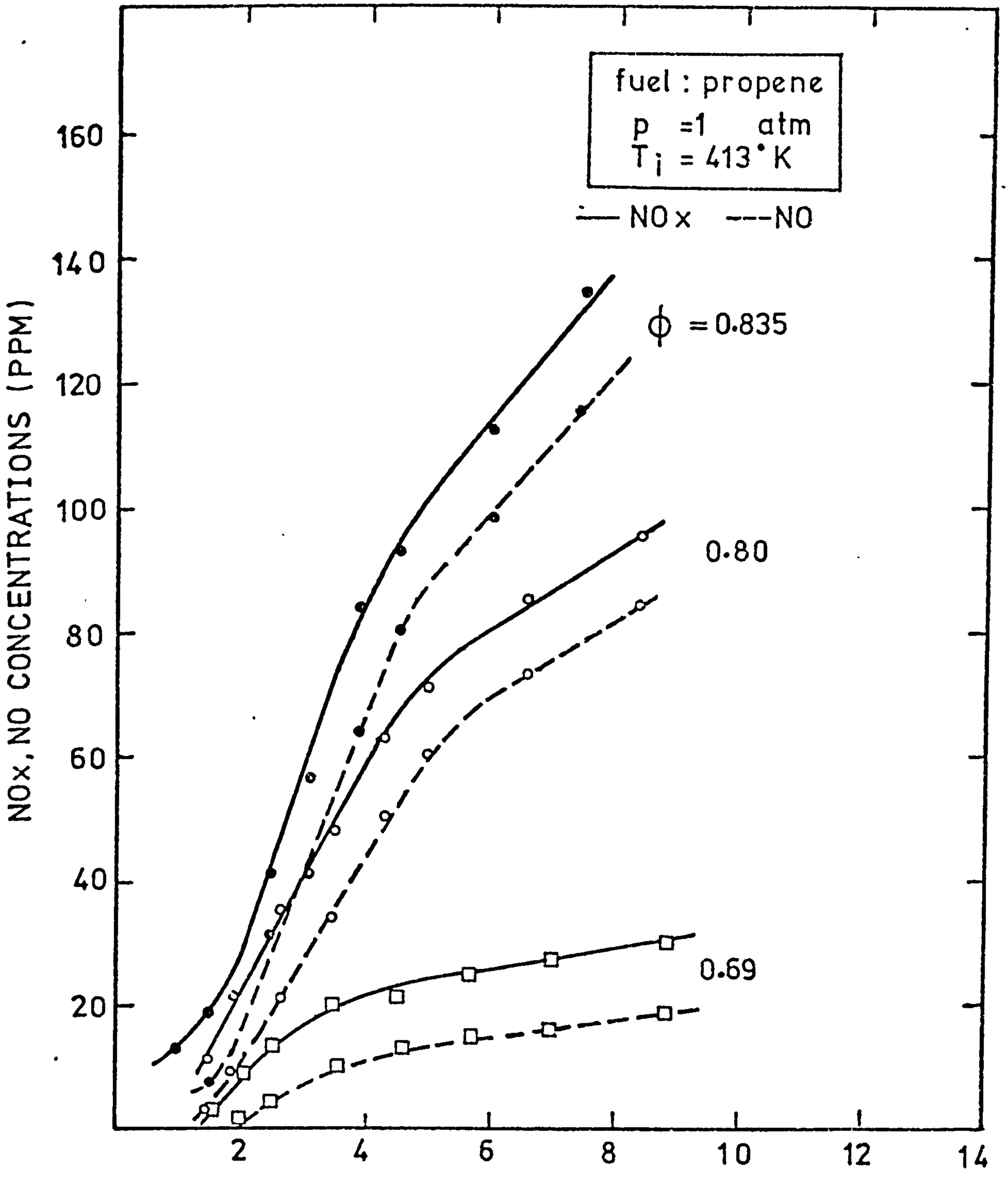

FIGURE7.15 Profiles of the oxides of nitogen in different atmospheric propene-air flames

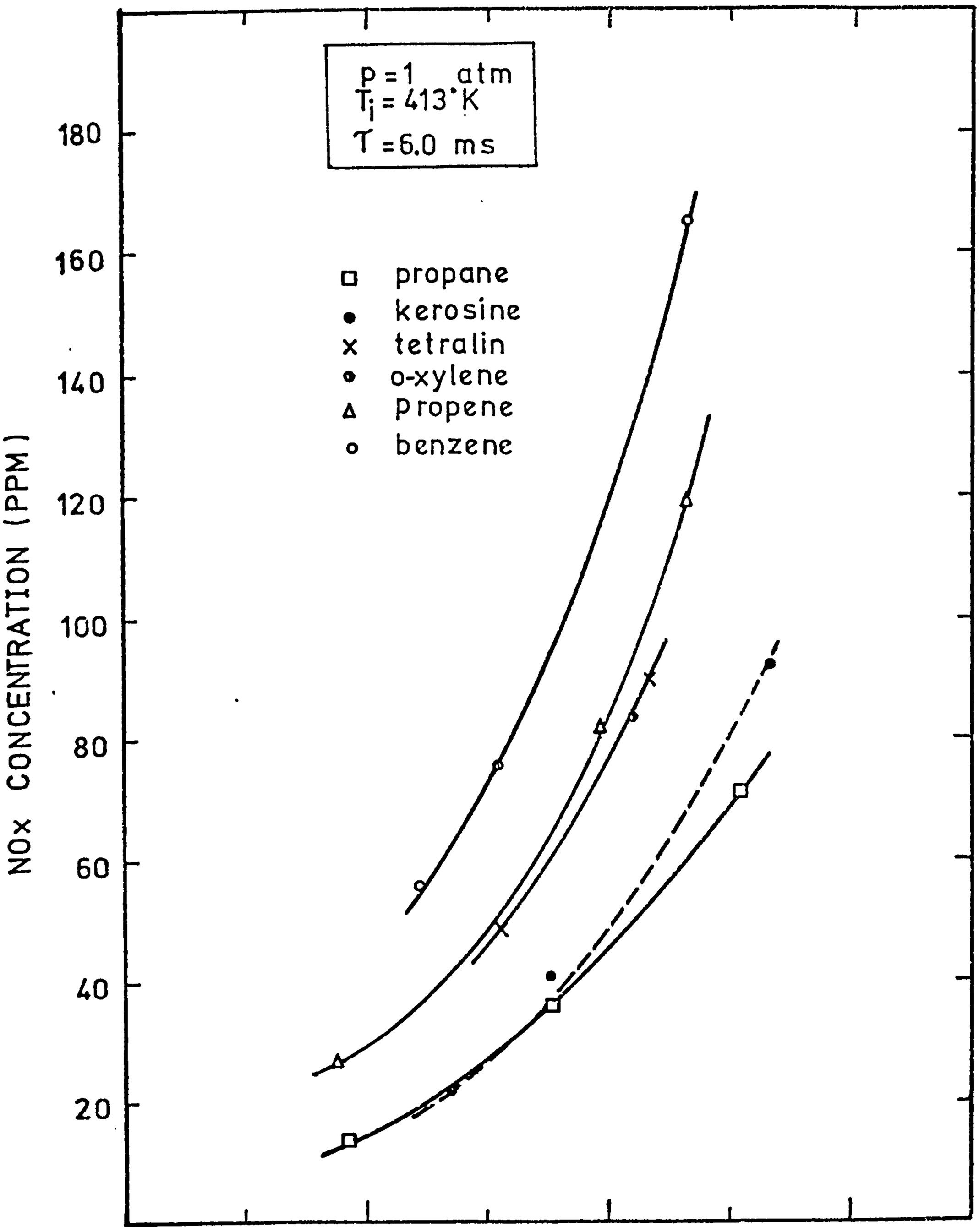

FIGURE 7.16. NO_x levels in different atmospheric hydrocarbon-air flames after six milliseconds.

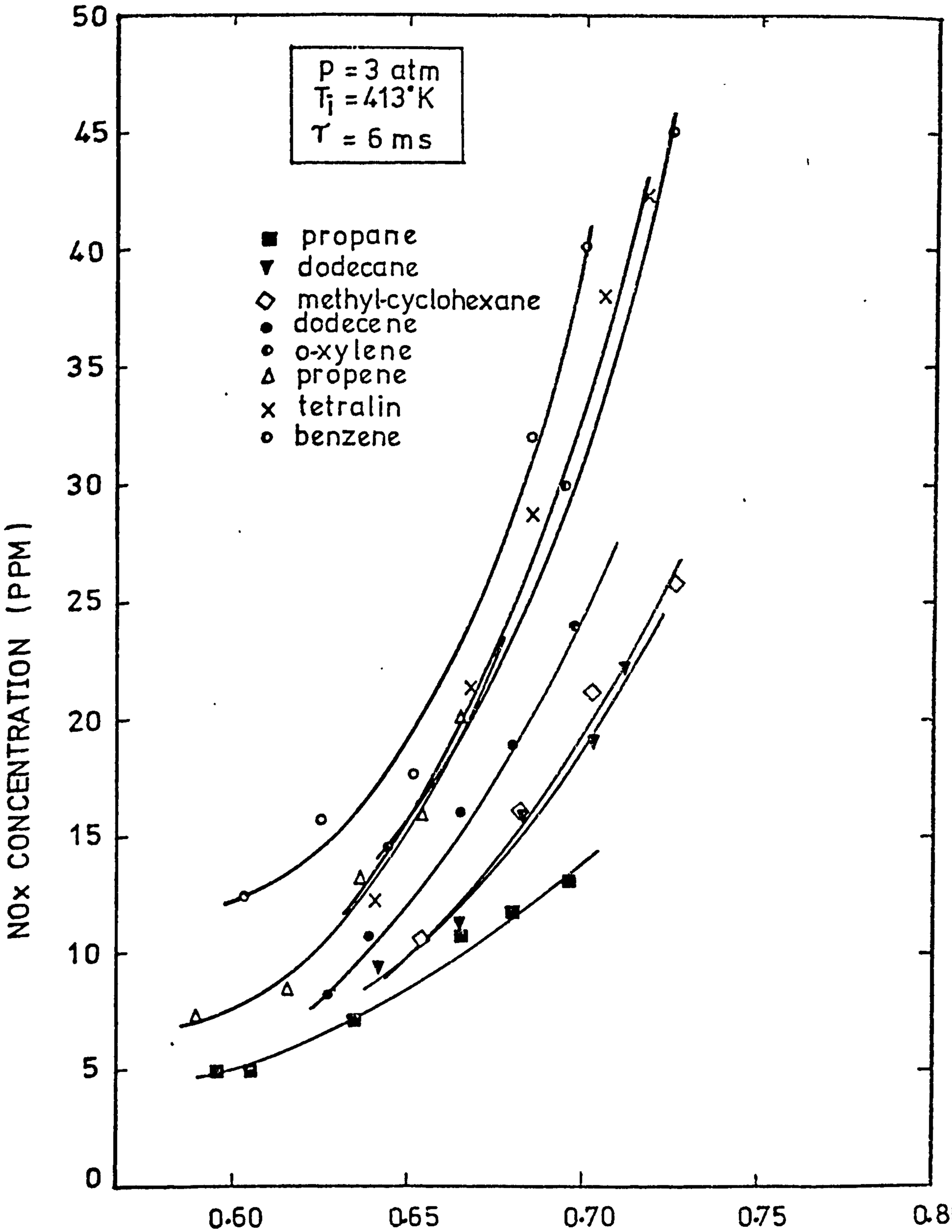

FIGURE 7.17 Total NO_x levels in different hydrocarbon - air flames at 3 atm pressure and after six milliseconds.

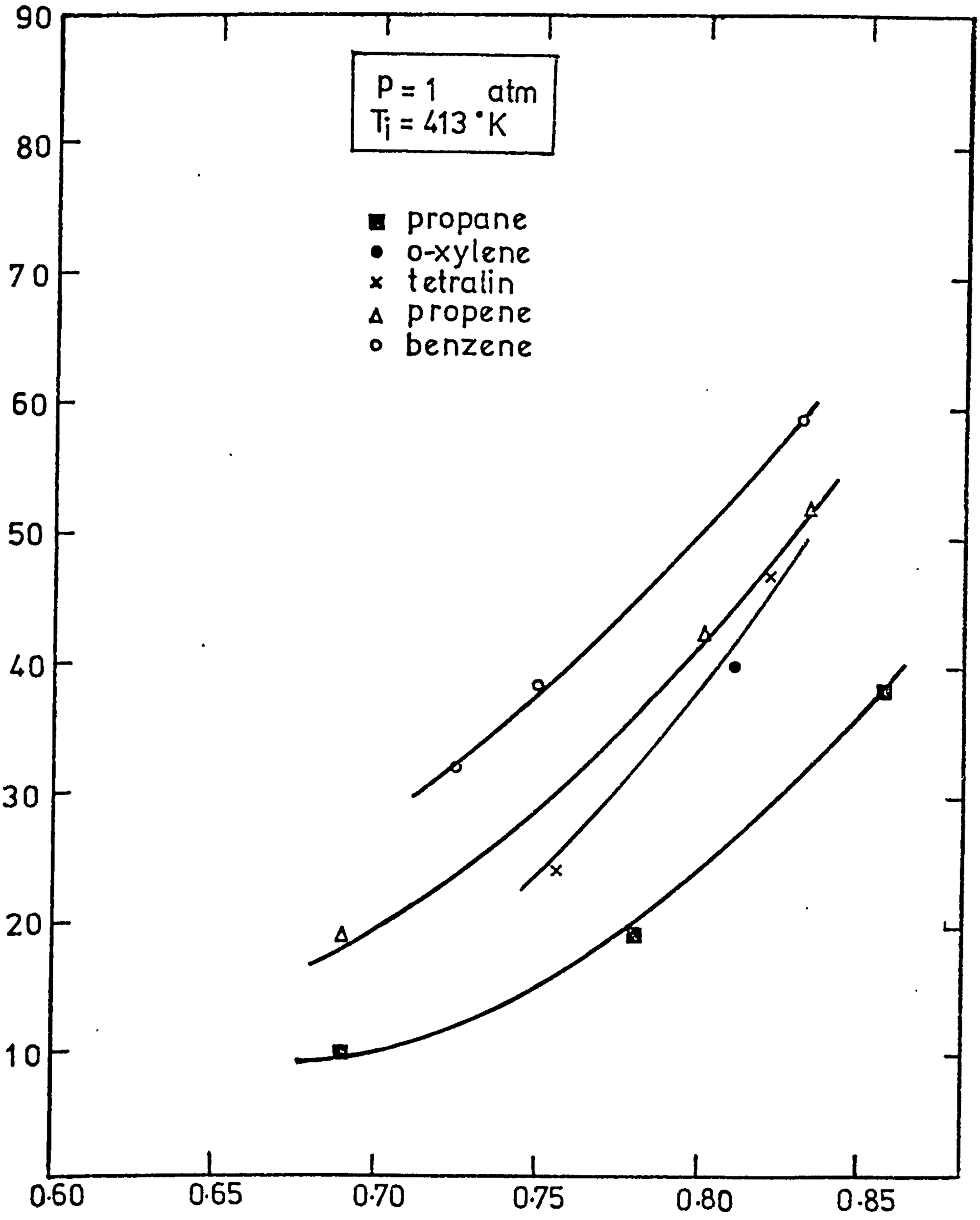

FIGURE 7.18. Prompt NO_x levels in different atmospheric hydrocarbon - air flames.

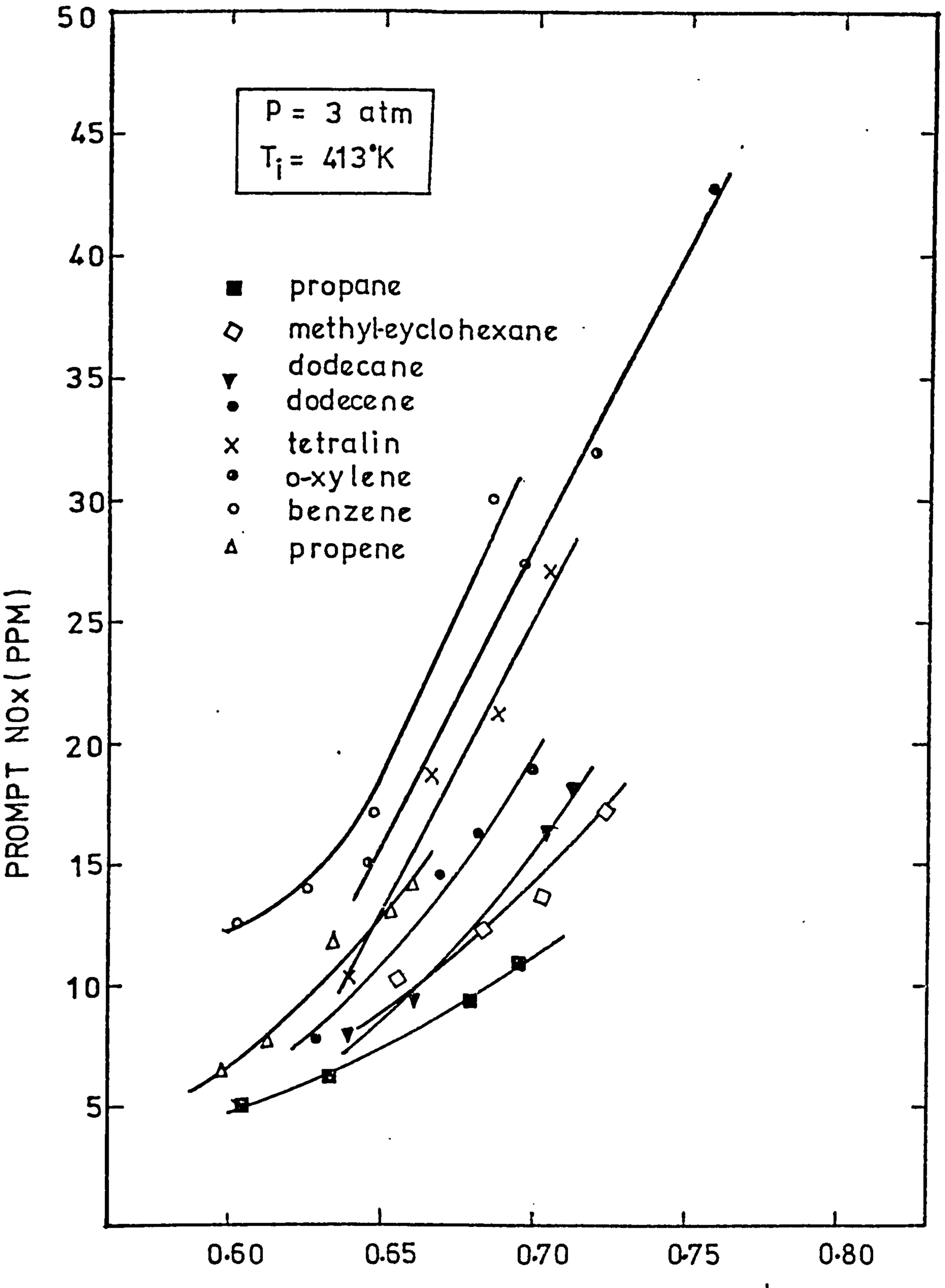

FIGURE 7.19 Prompt NO_x levels in different hydrocarbon-air flames at high pressure.

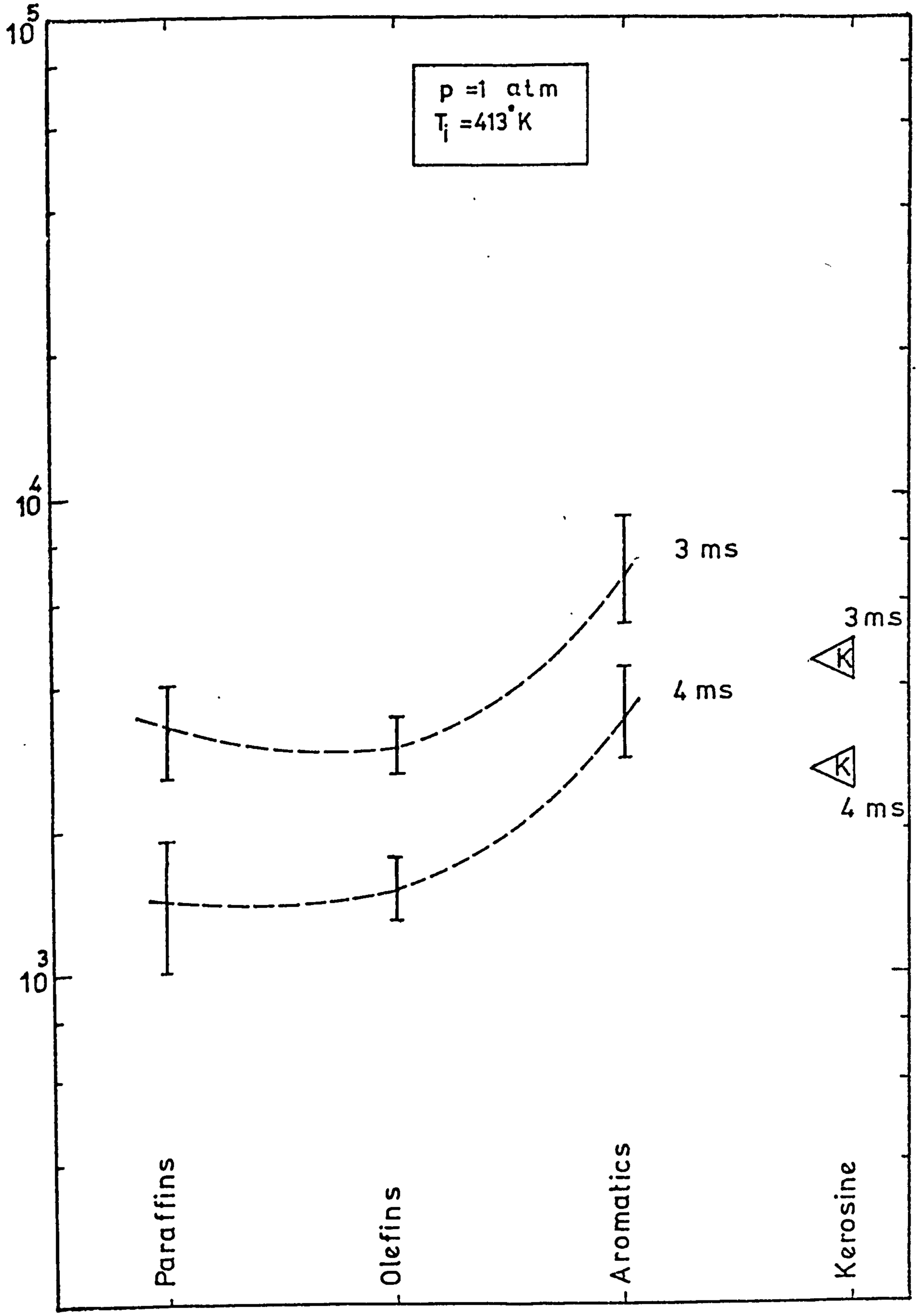

FIGURE 8.1 Minimum CO levels for different hydrocarbons at atmospheric pressure

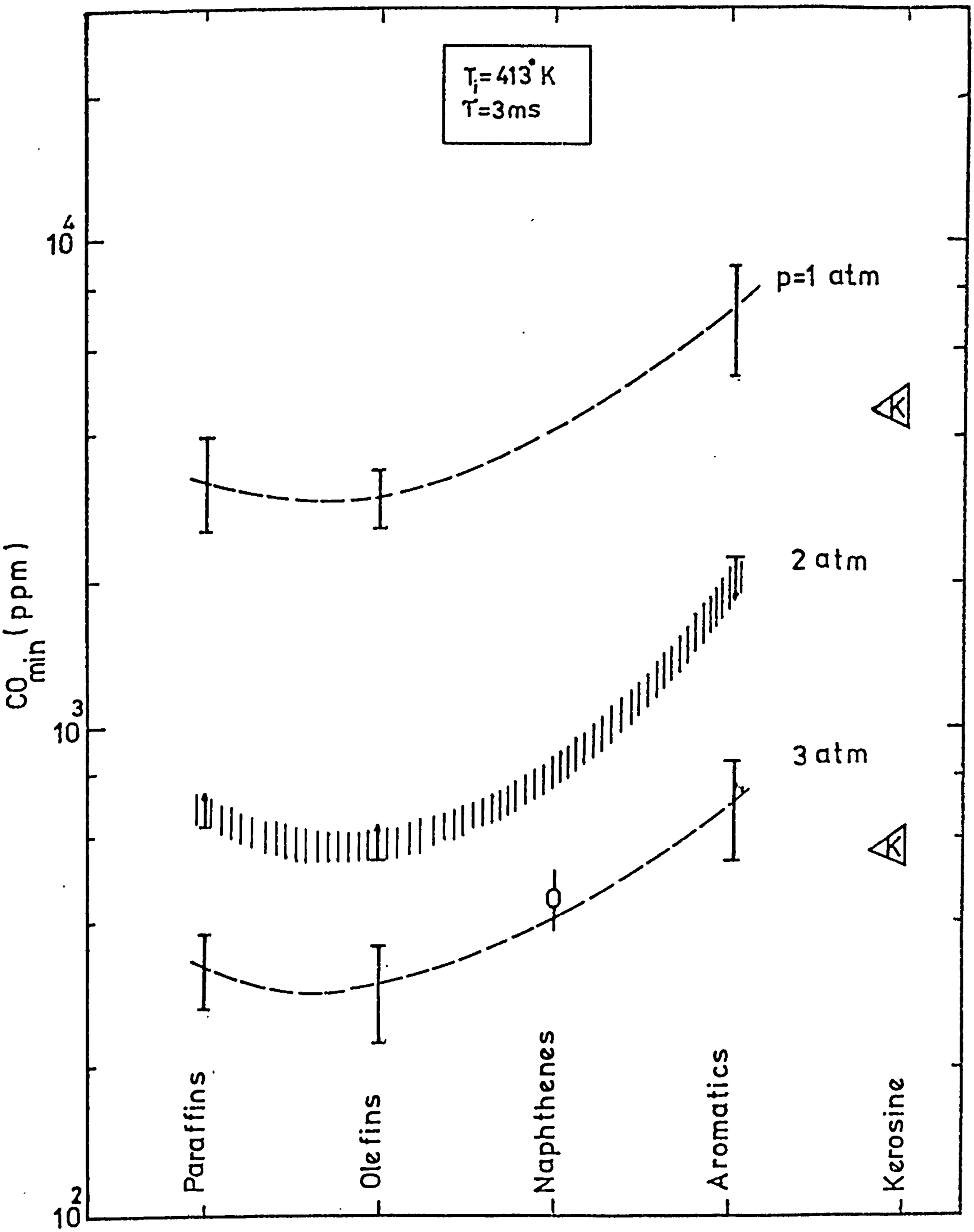

FIGURE 8.2 Minimum CO levels for different hydrocarbon types at different pressures

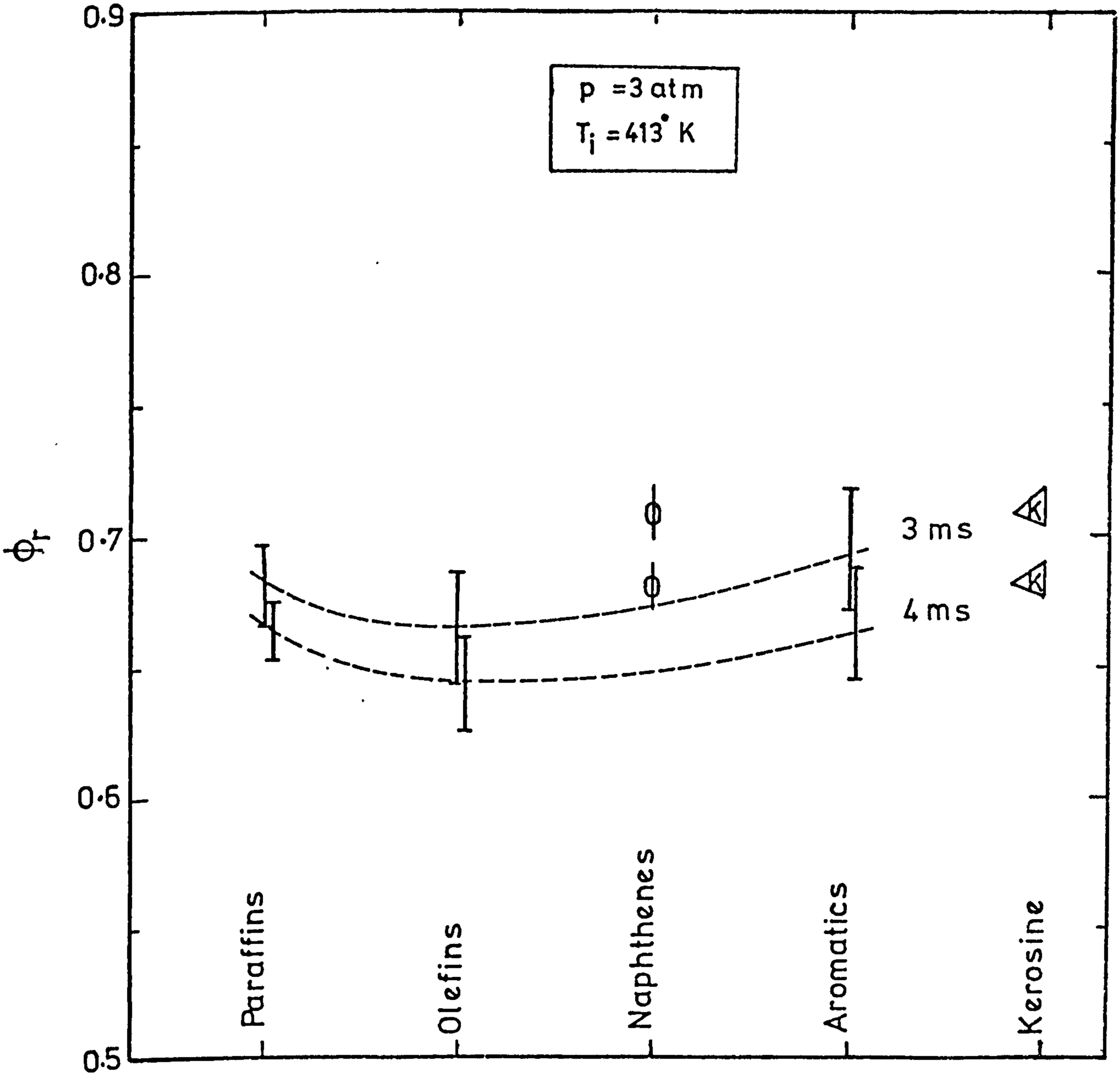

FIGURE 8.3 Critical equivalence ratios for different hydrocarbon types at high pressure

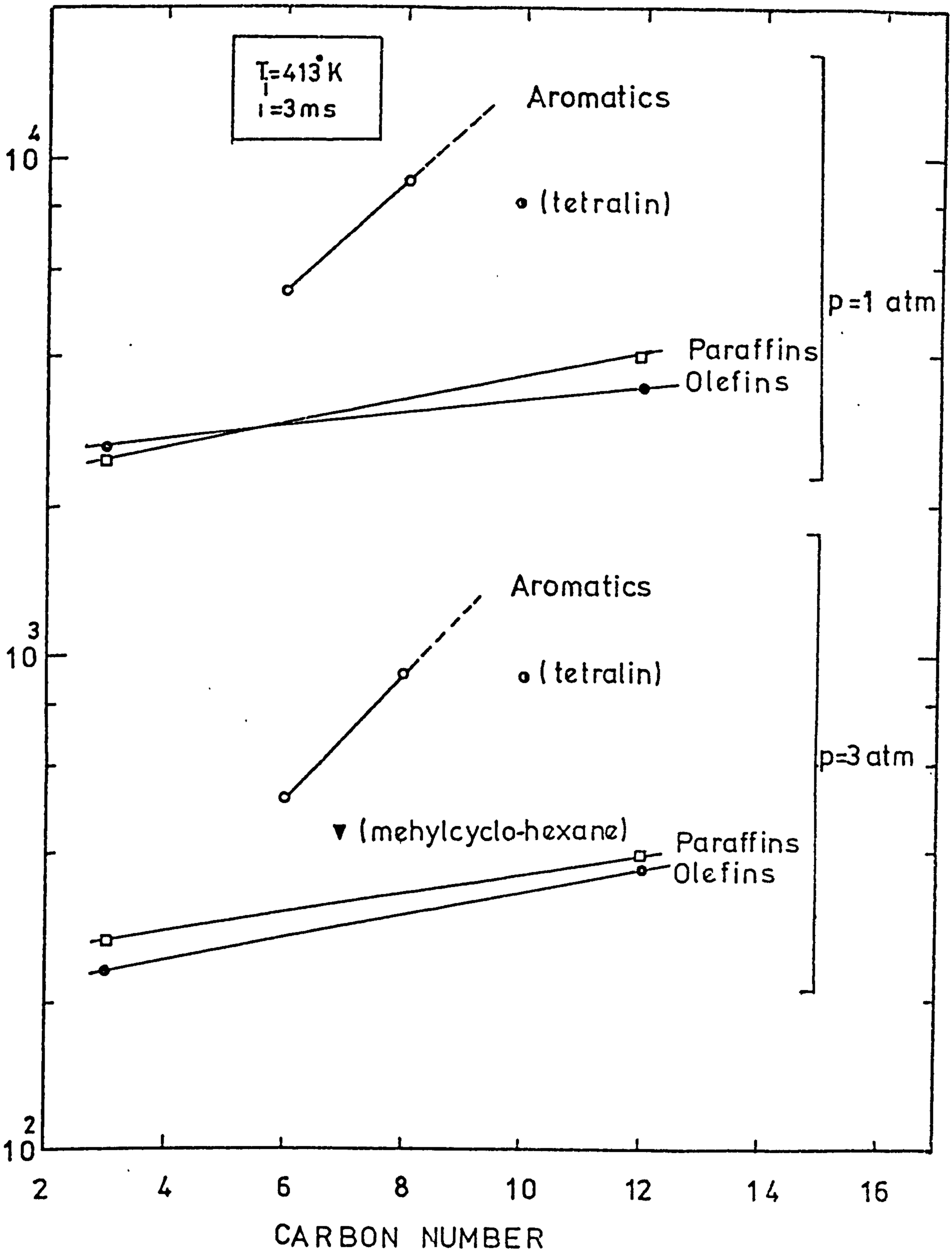

FIGURE 8.4 Influence of the carbon number on minimum CO levels

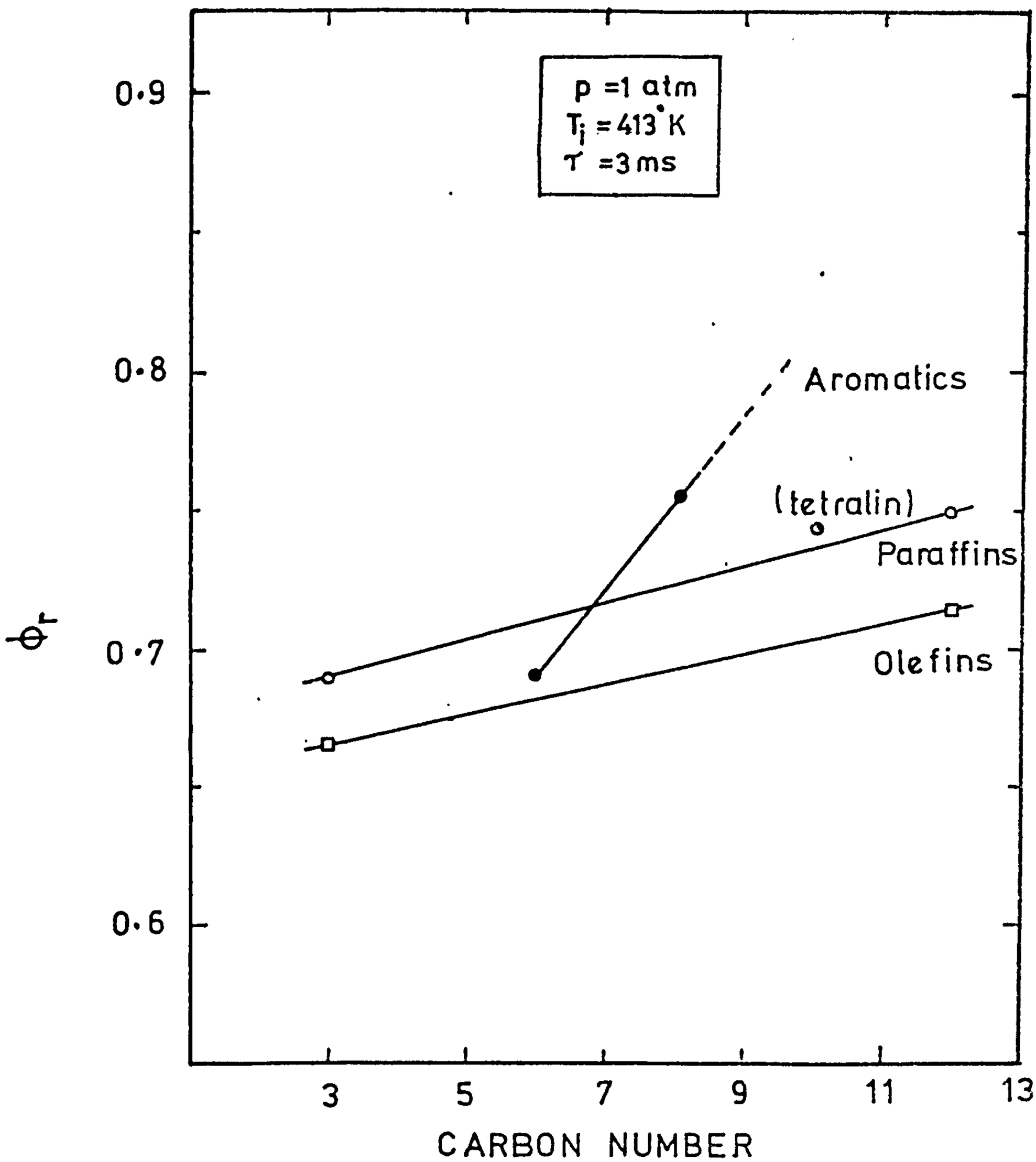

FIGURE 8·5 Influence of the carbon number on the critical equivalence ratio

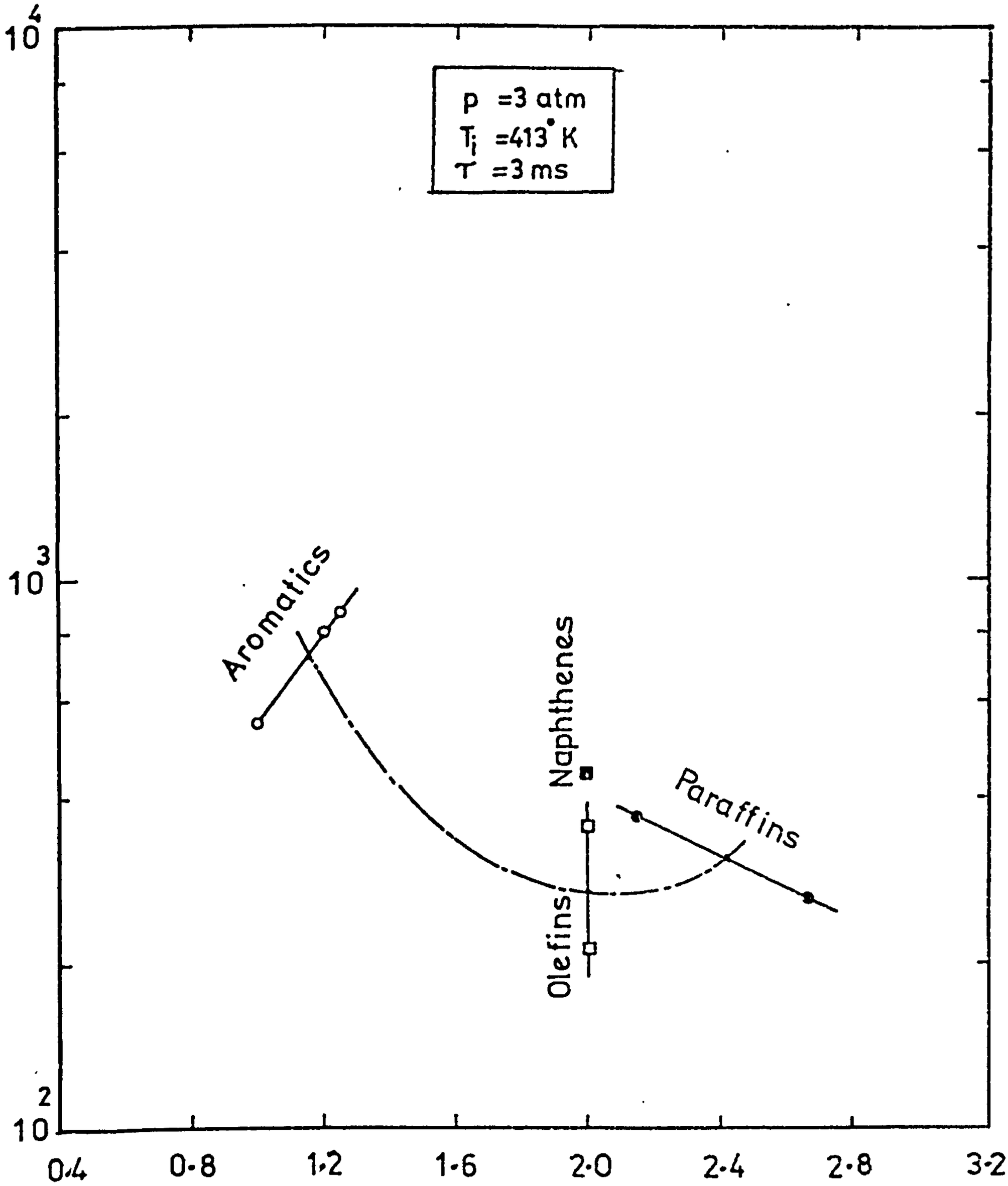

FIGURE 8.6 Influence of H/C ratio on minimum CO levels for different hydrocarbons

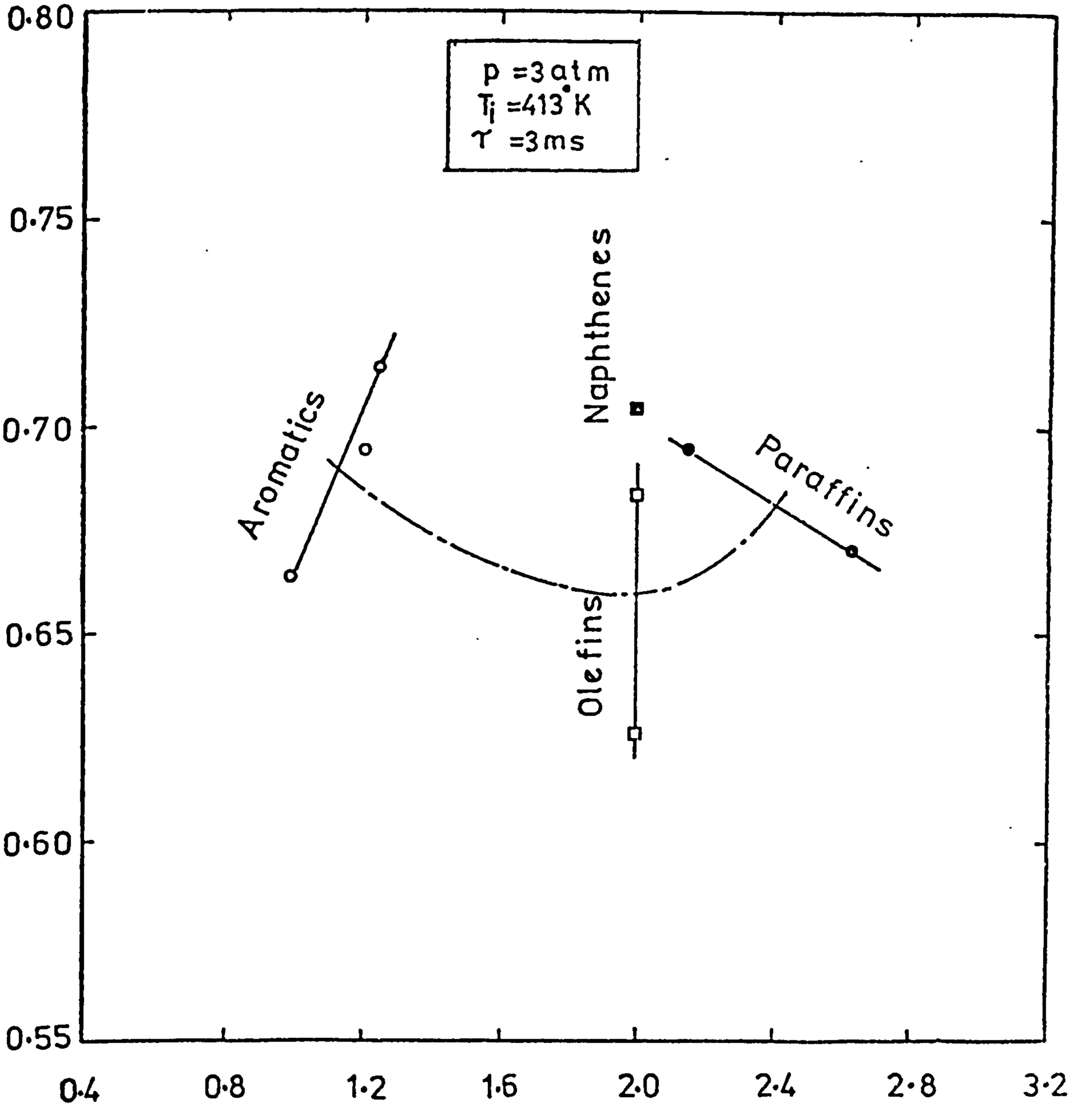

FIGURE 8.7 Influence of H/C ratio on the critical equivalence ratio

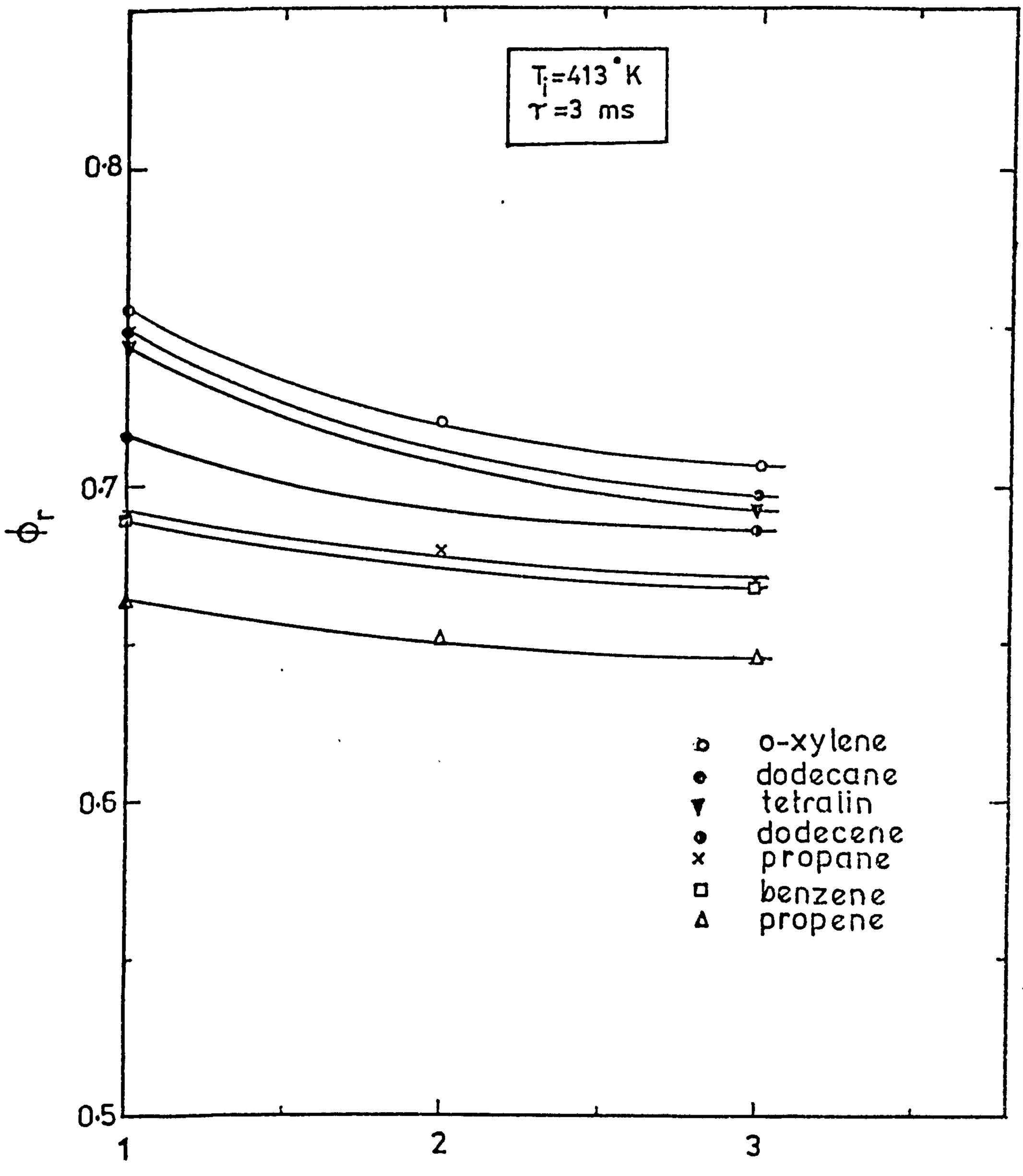

FIGURE 8.8 Influence of pressure on the critical equivalence ratio for different hydrocarbons

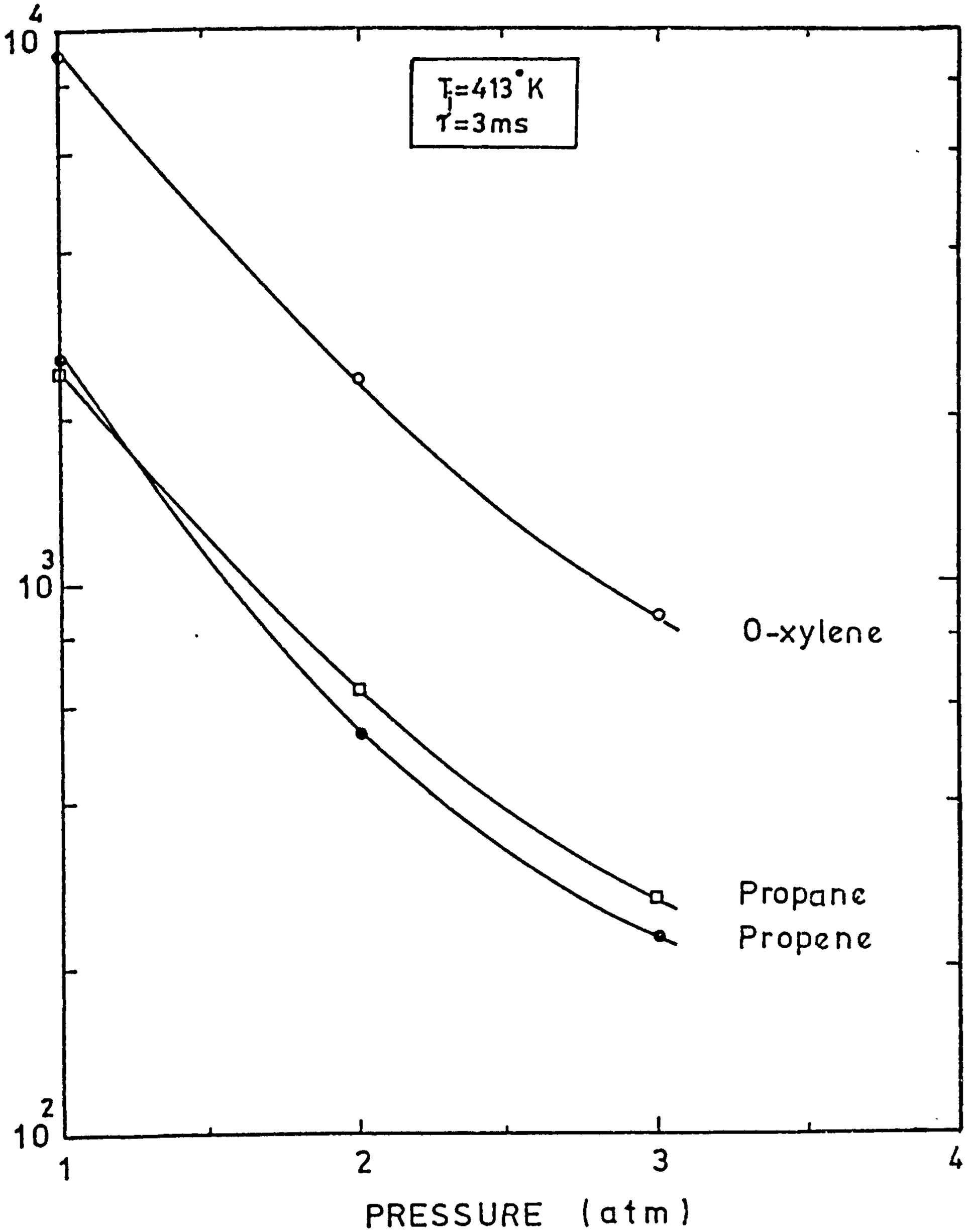

FIGURE 8.9 Influence of pressure on minimum CO levels for different hydrocarbons

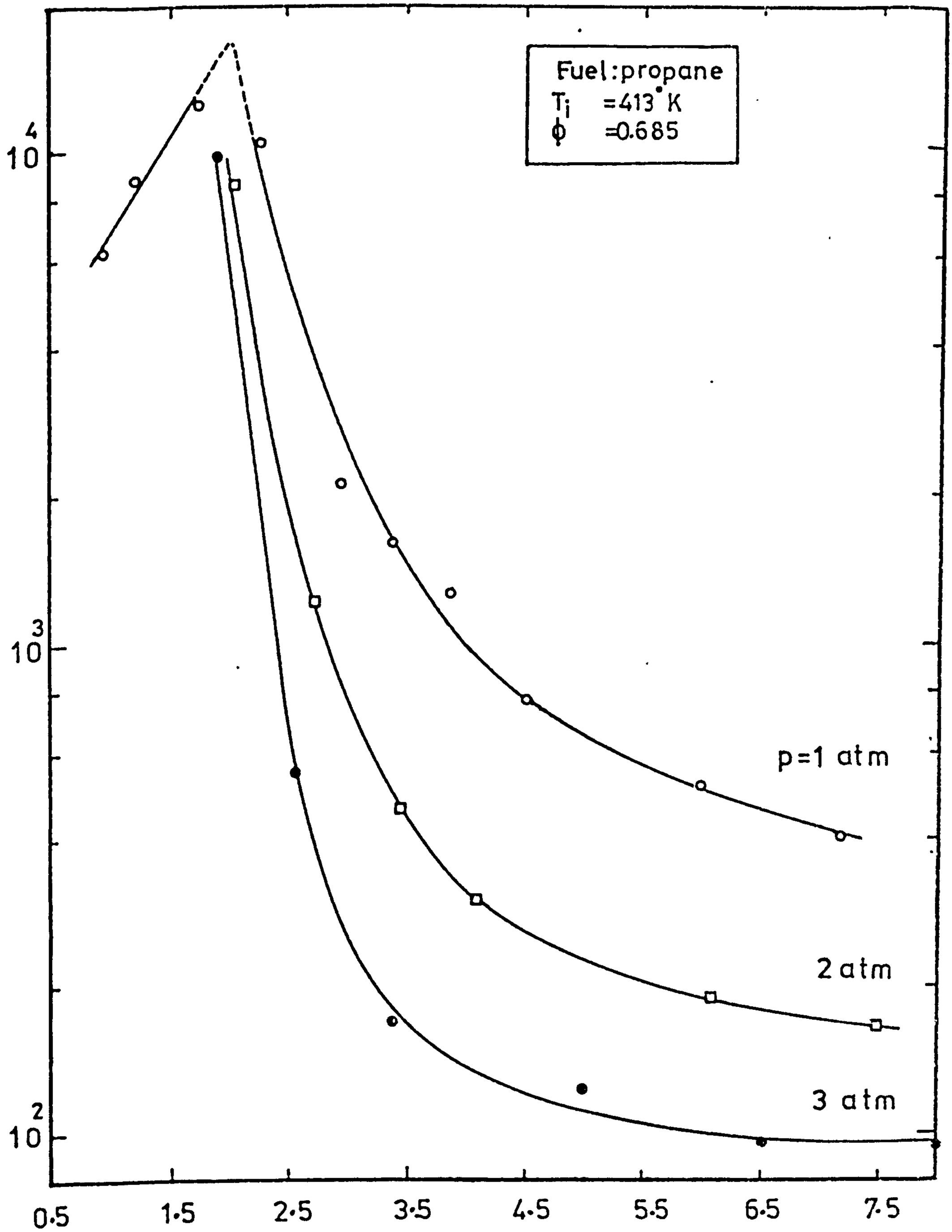

FIGURE 8.10 Influene of pressure on measured CO profiles in propane-air flames

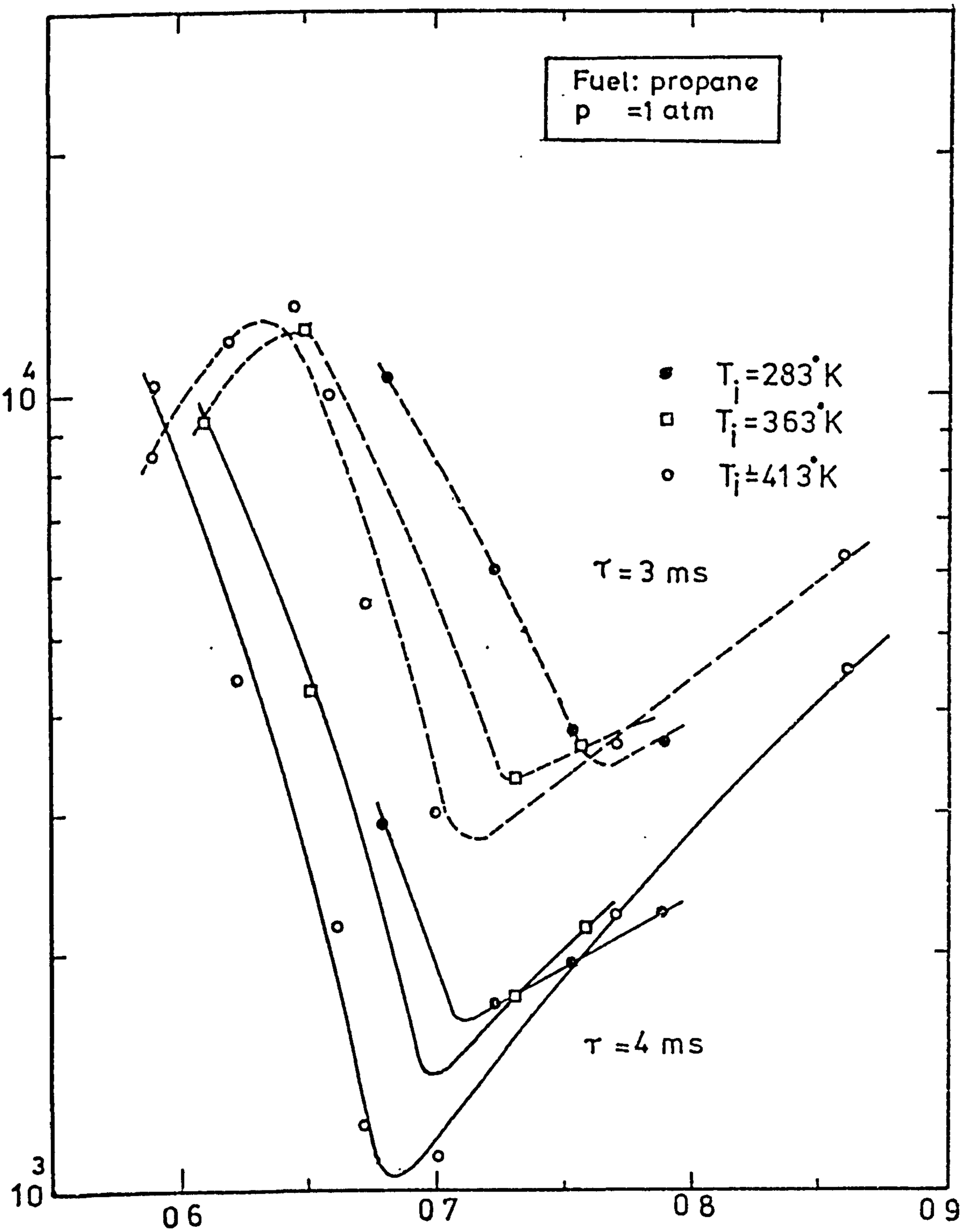

FIGURE 8.11 Influene of the inlet temperature on measured CO levels in propane-air flames

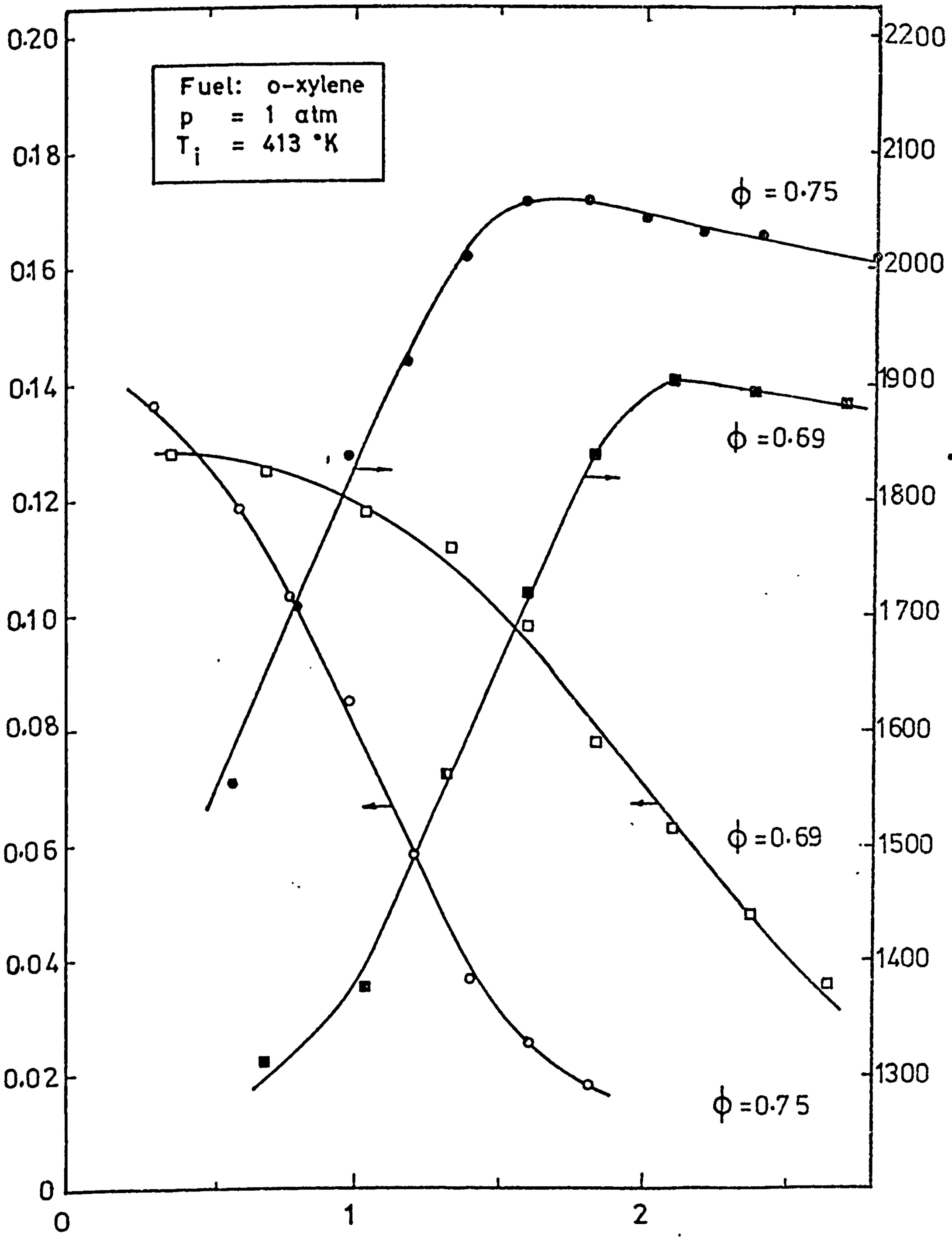

FIGURE 8.12 Measured fuel and temperature profiles in o-xylene/air flames

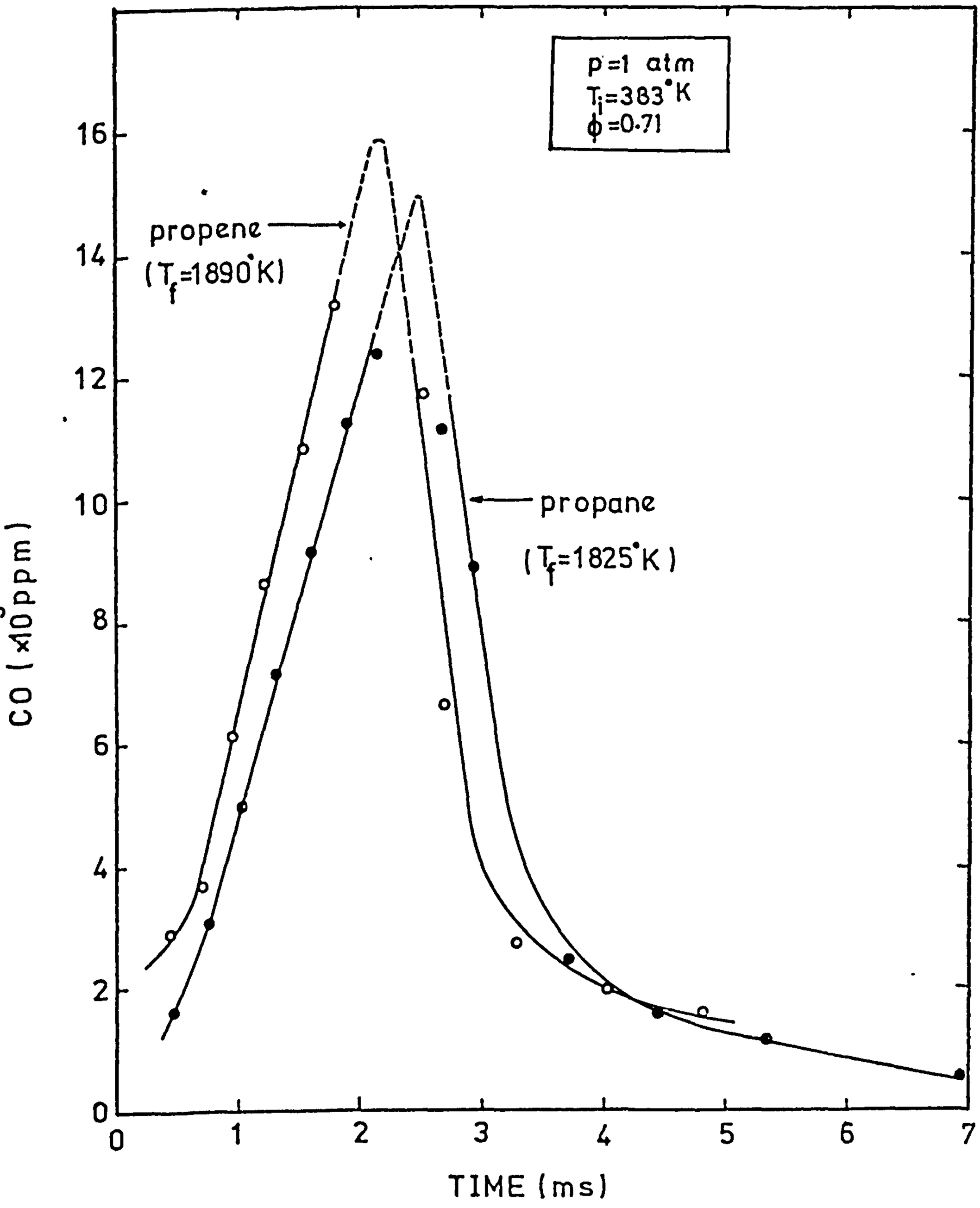

FIGURE 8.13 Measured CO profiles in propane-air and propene-air flames

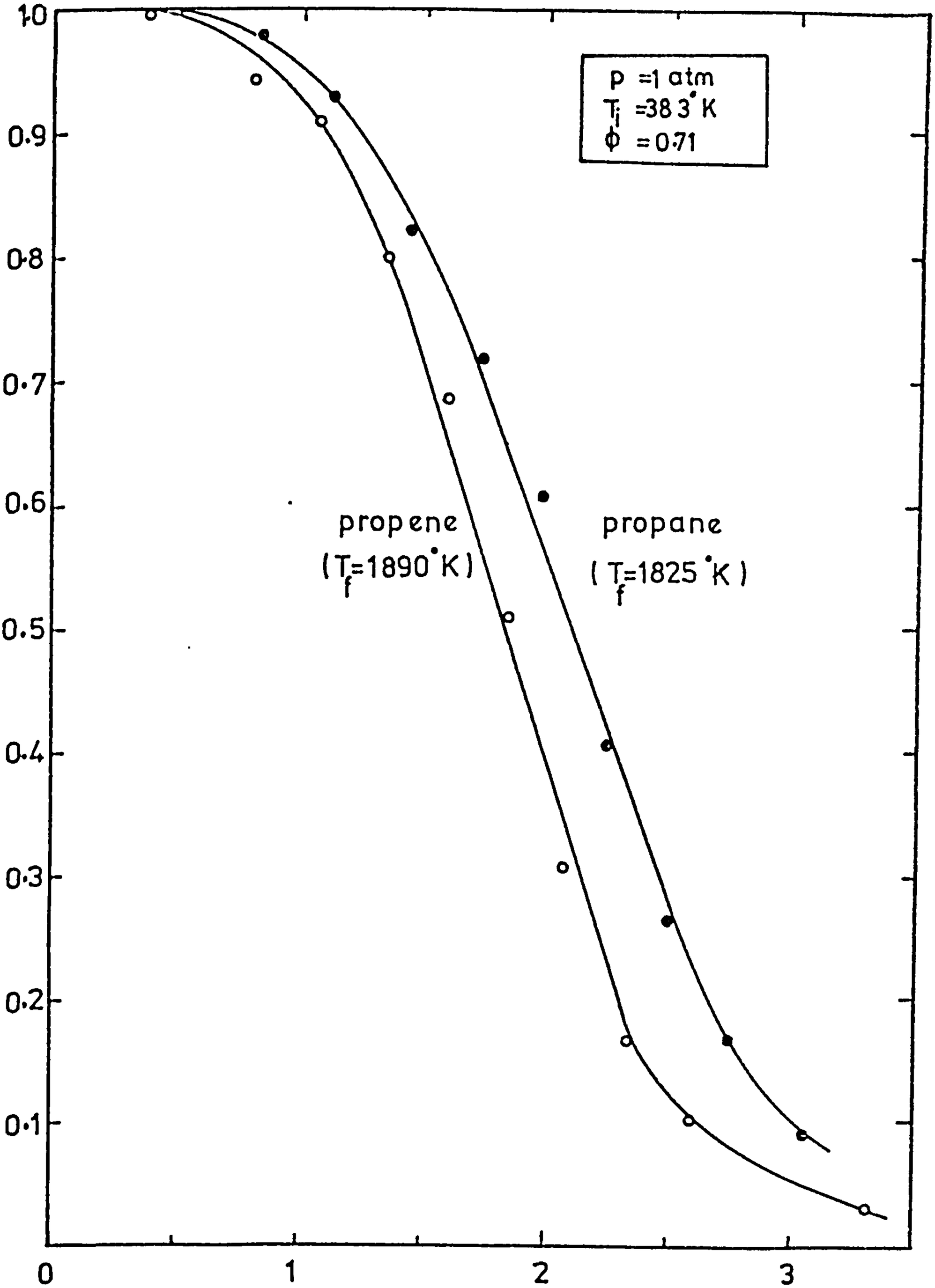

FIGURE 8.14 Comparion of normalized fuel concentration profiles in propane-air and propene-air flames

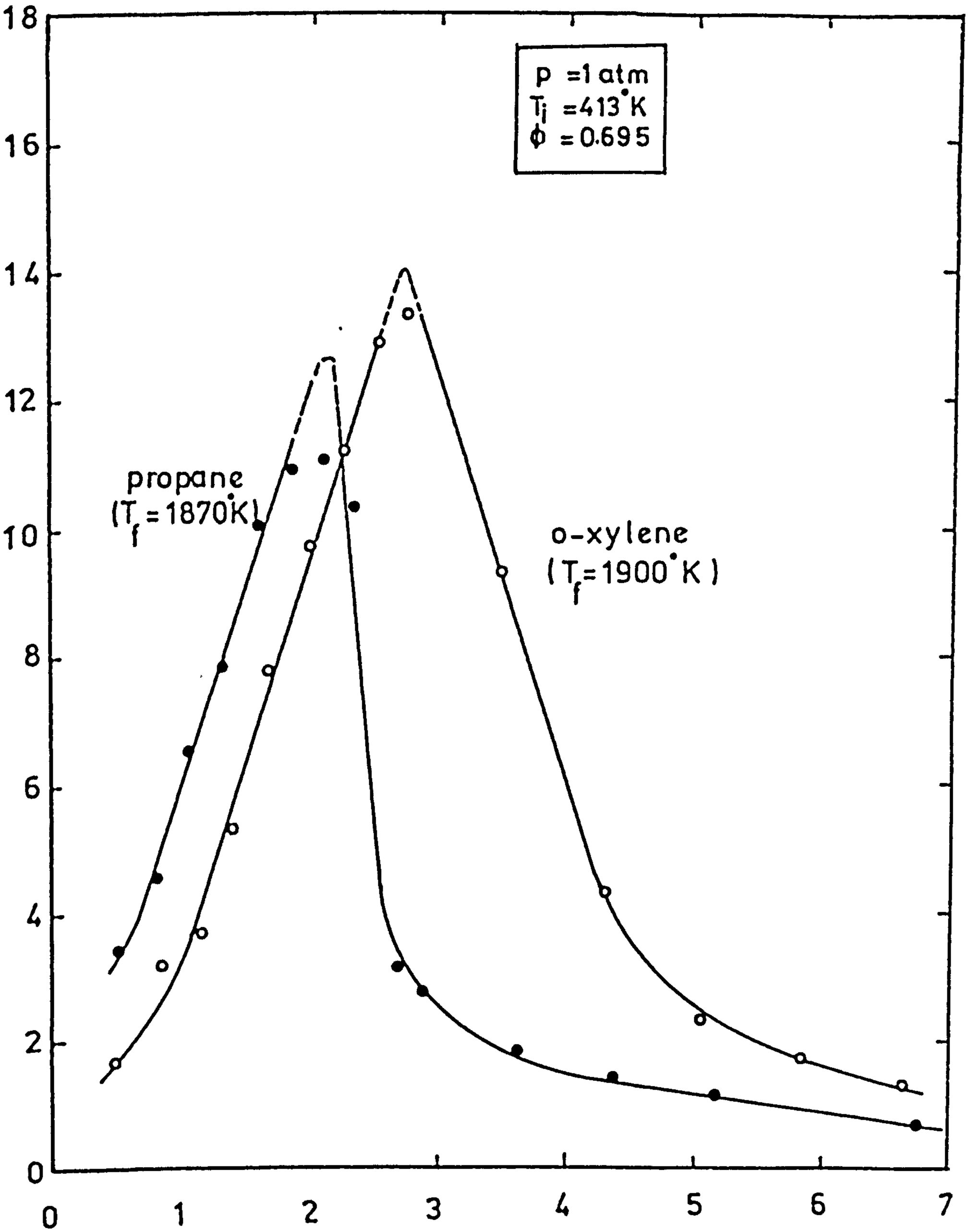

FIGURE 8.15 Measured CO profiles in propane-air and o-xylene-air flames

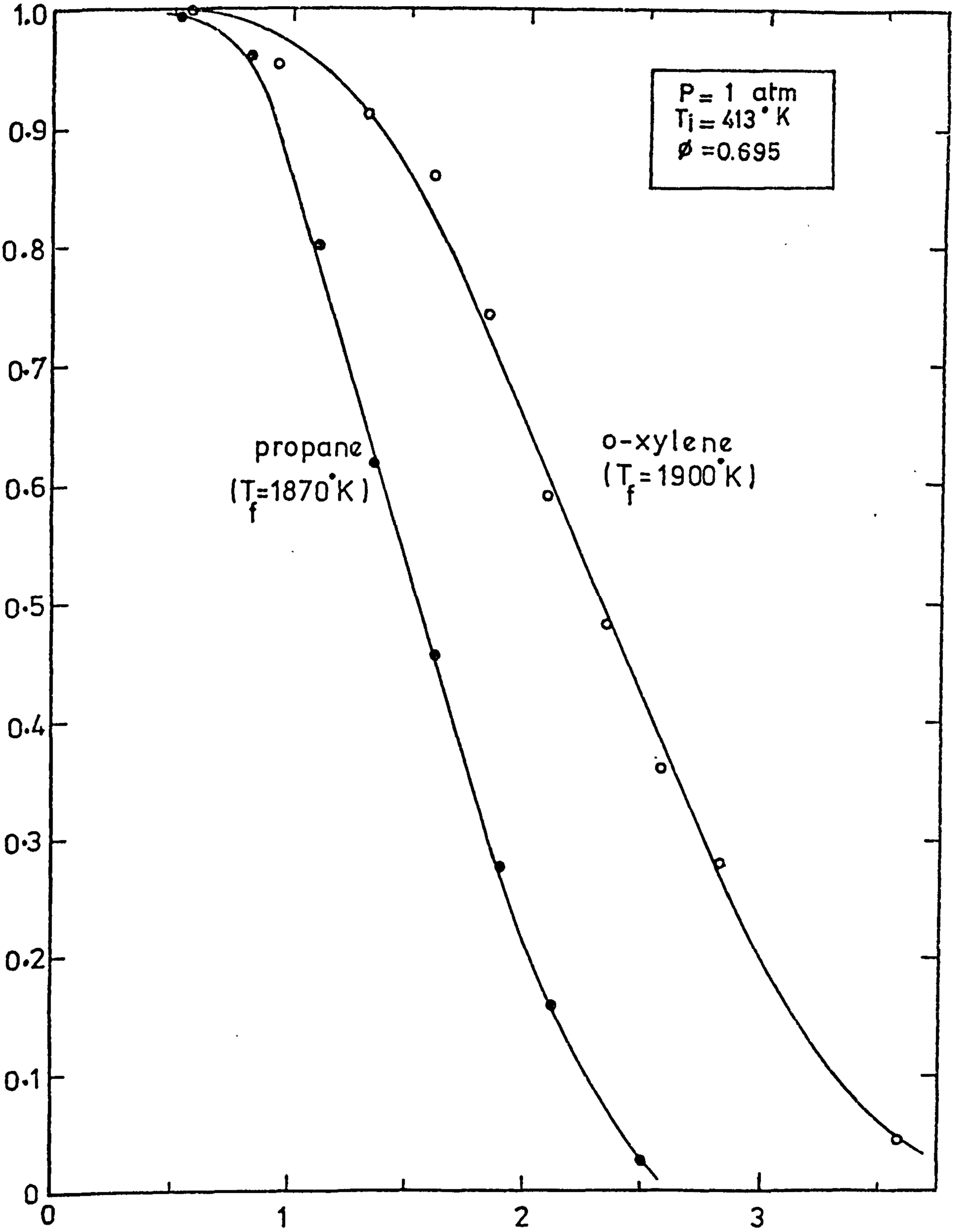

FIGURE 8.16 Comparison of normalized fuel concentration profiles in propane-air and o-xylene/air flames

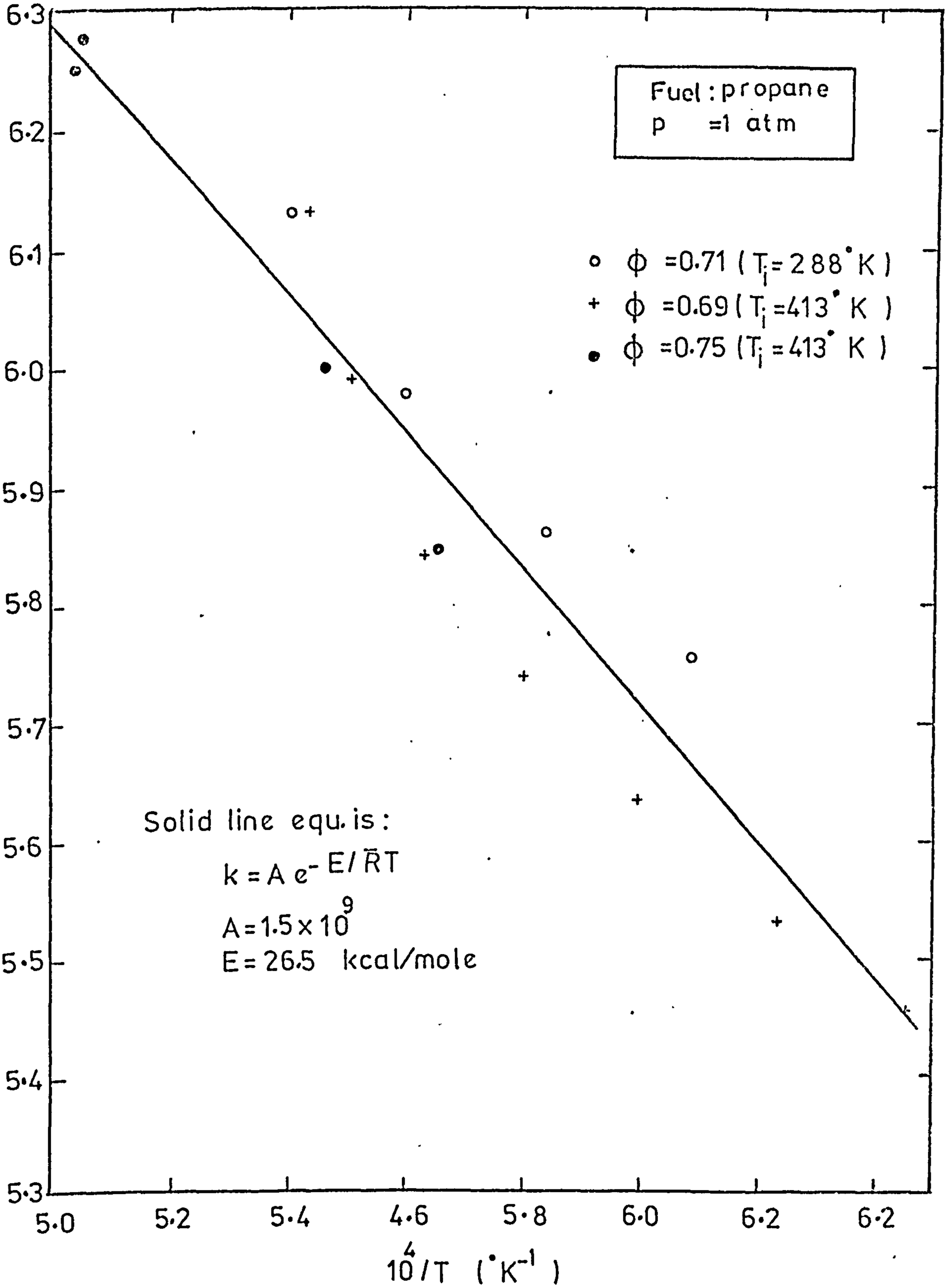

FIGURE 8.17 Overal rate correlation of propane disappearance rate in the post induction phase

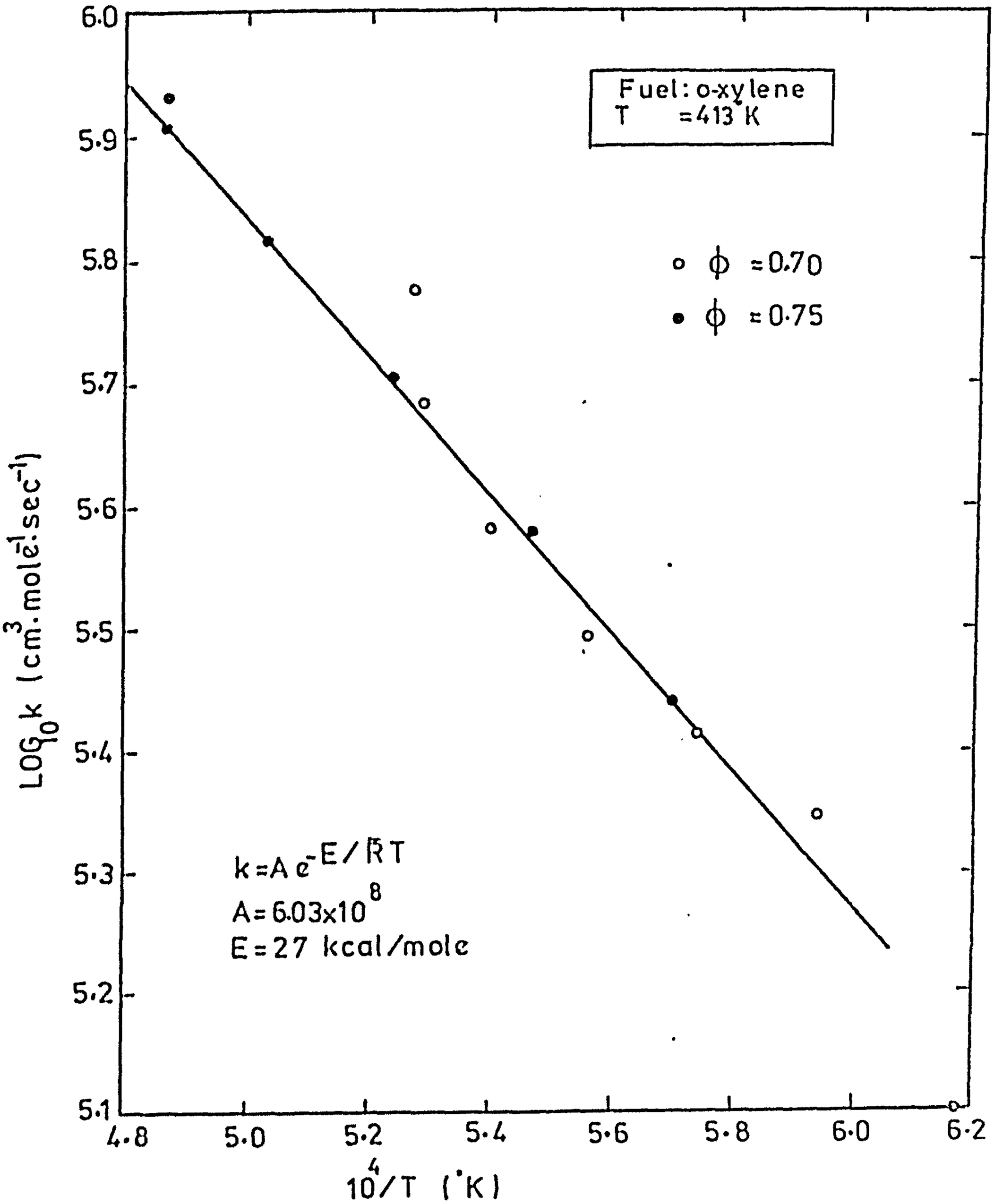

FIGURE 8.18 Overall rate correlation of o-xylene disappearance rate in the post induction phase

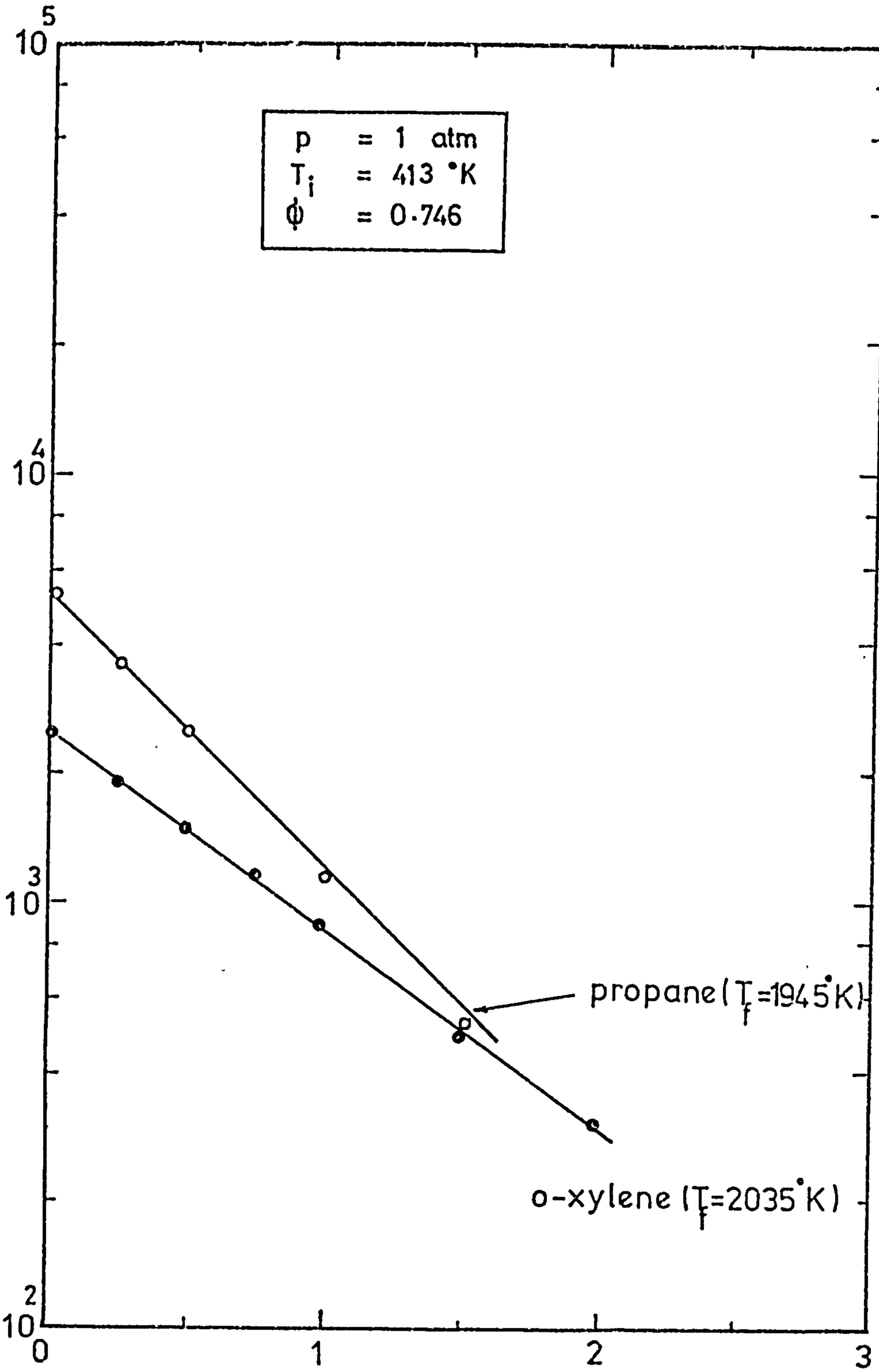

FIGURE 8.19 Measured CO fractional conversion rates in different hydrocarbon-air flames

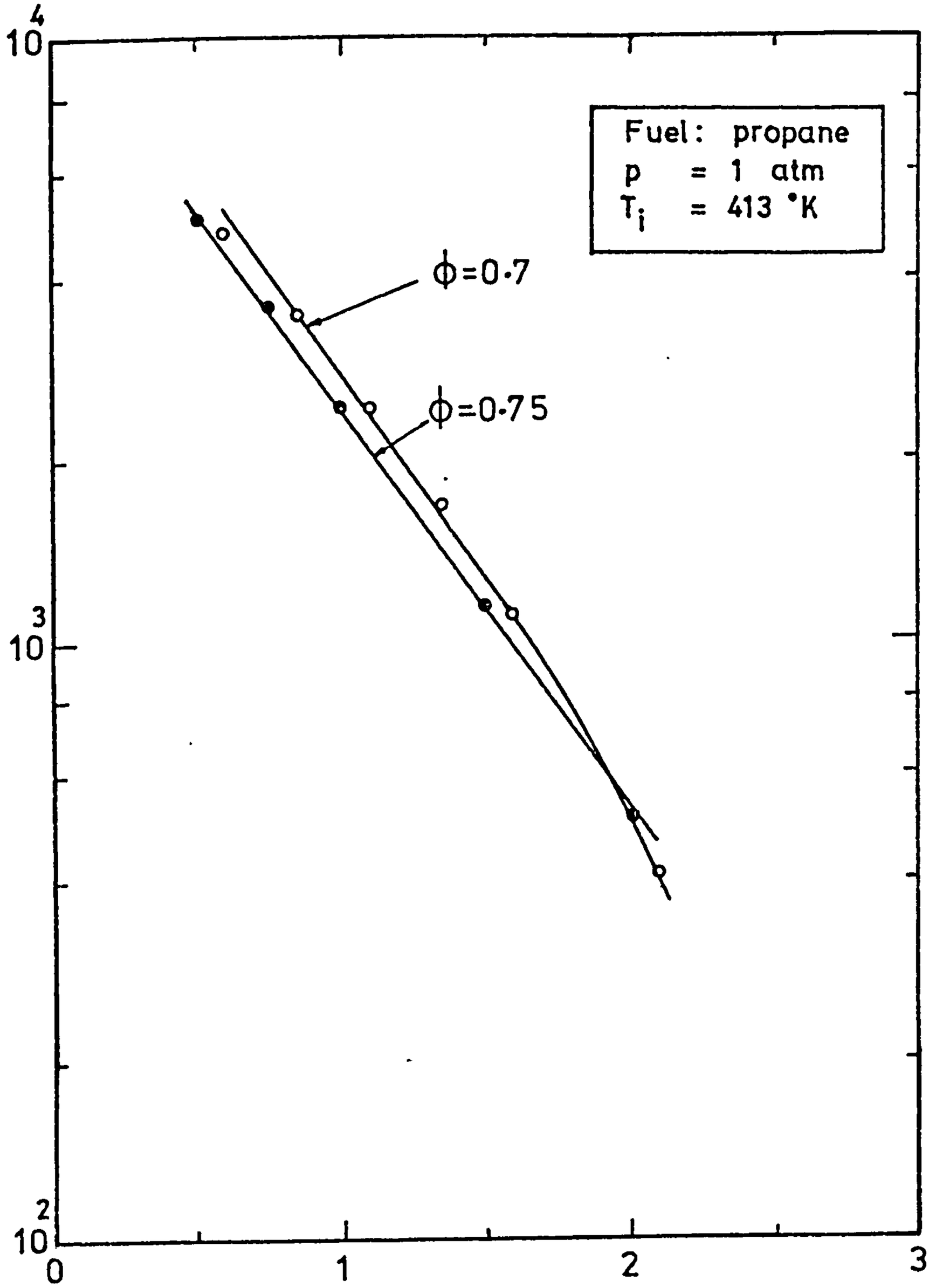

FIGURE 8·20 Measured CO fractional conversion rates in different propane-air flames

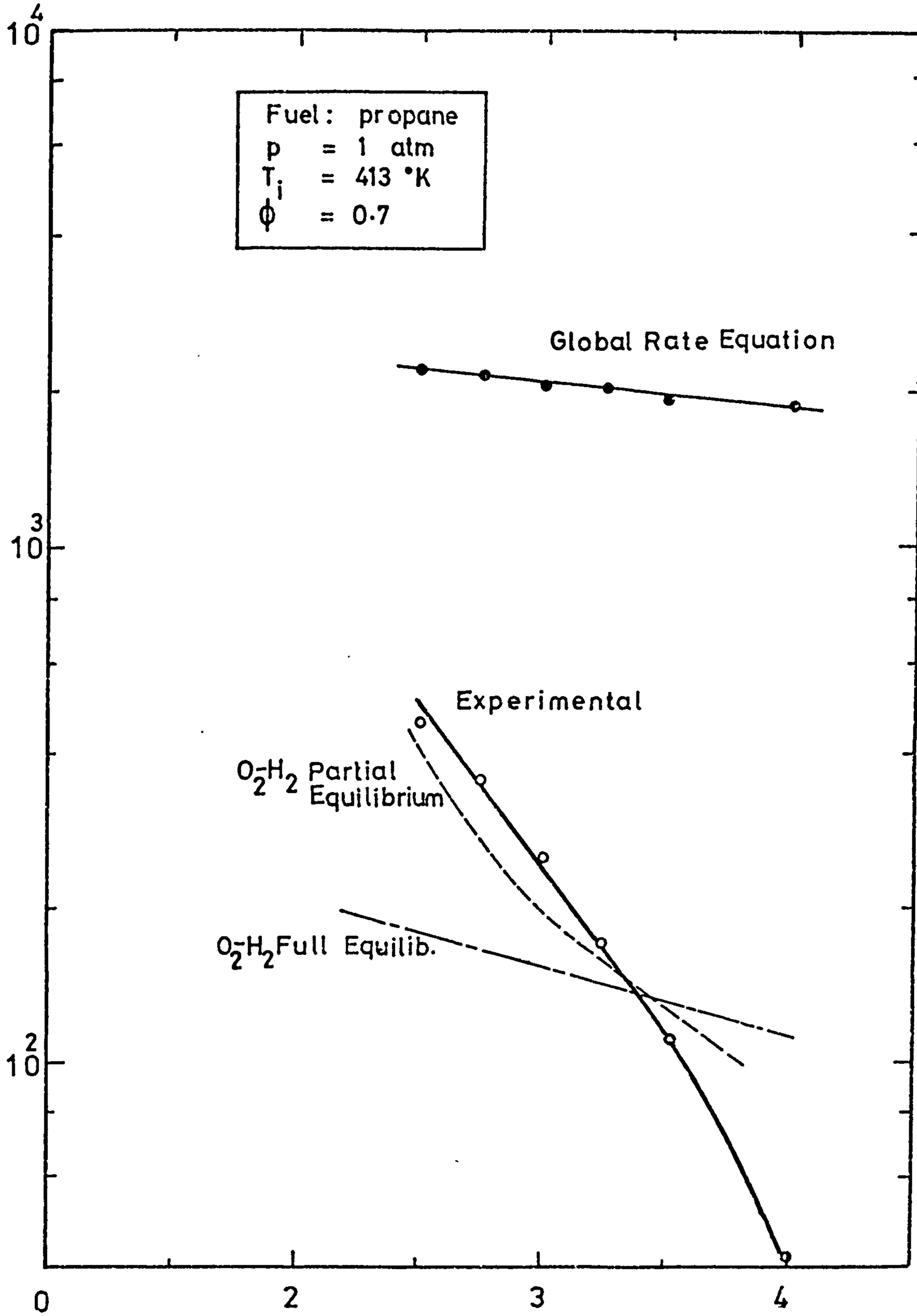

FIGURE 8.21 Calculated and measured CO fractional conversion rates in a propane-air flame

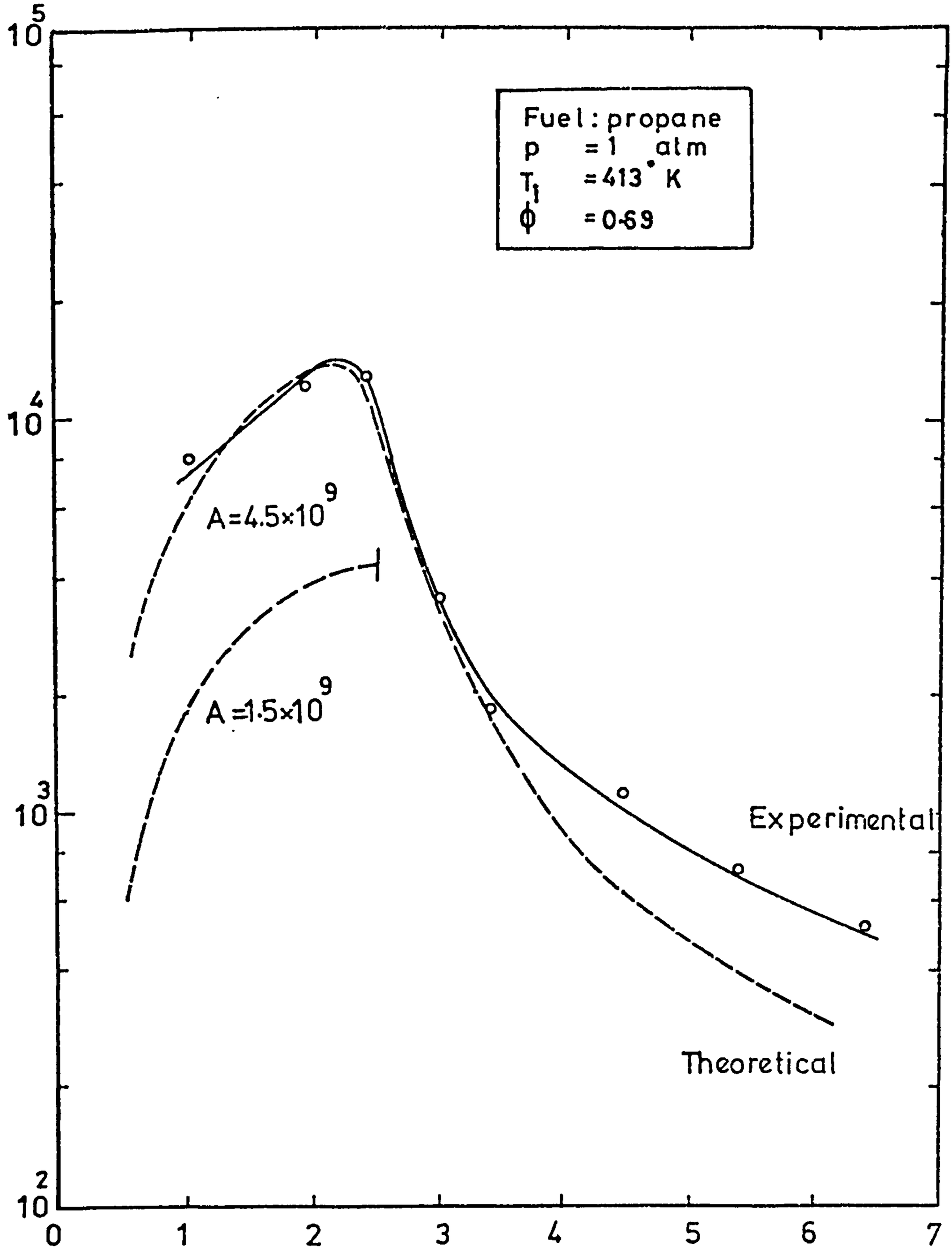

FIGURE 8·22 Comparison between predicted and measured CO profiles in a propane-air flame

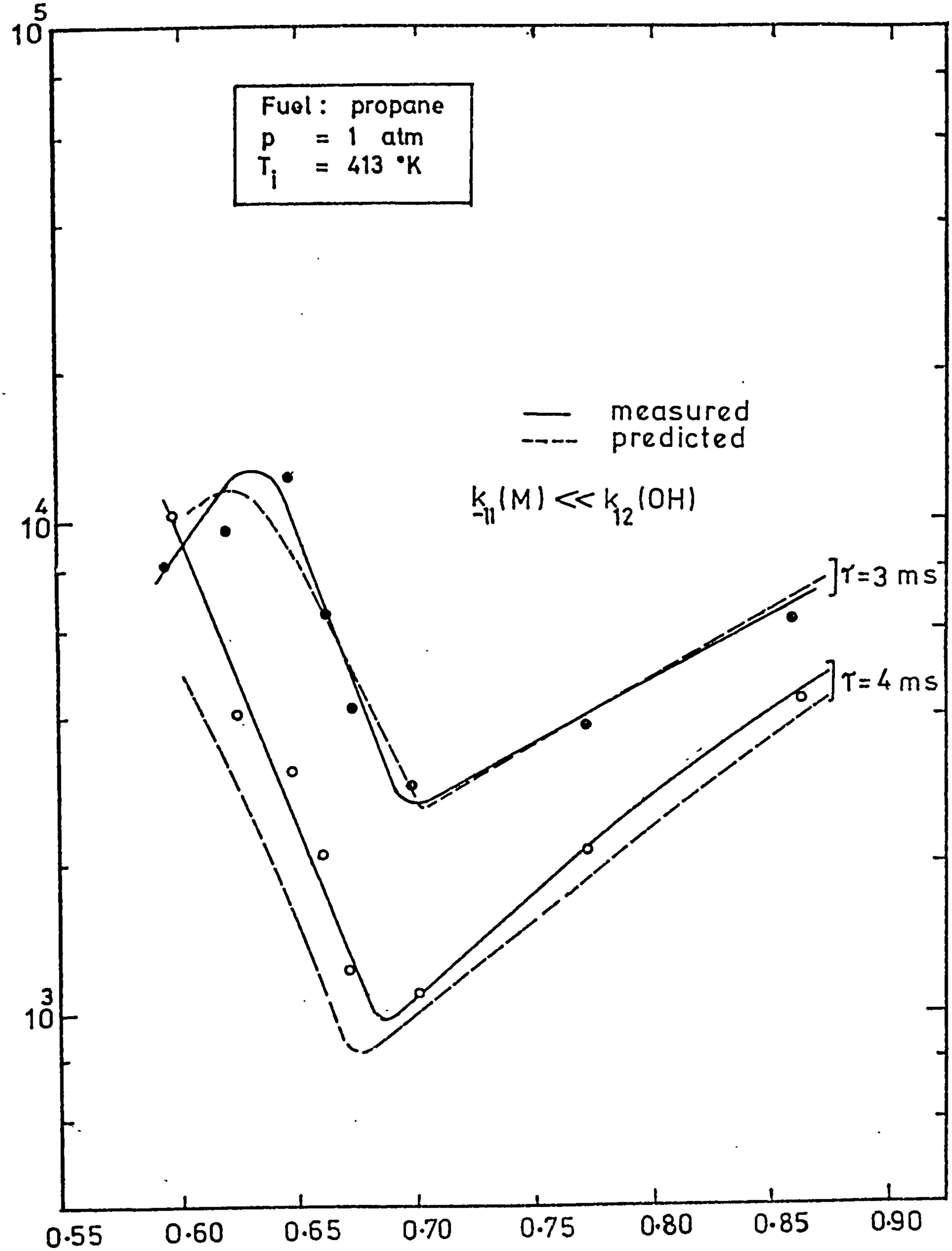

FIGURE 8·23 Comparison between measured and predicted CO levels in propane-air flames

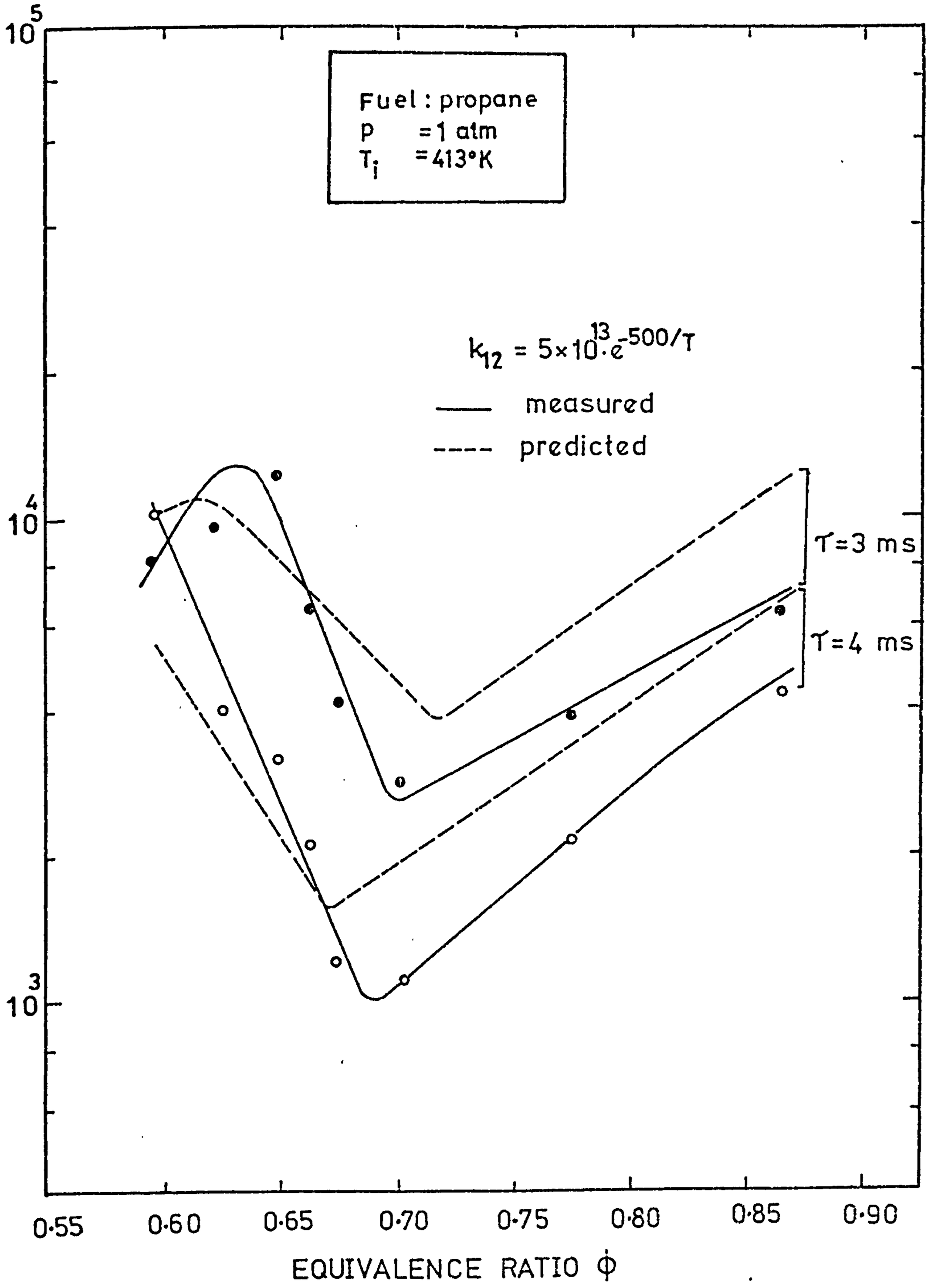

FIGURE 8.24 Comparison between predicted and measured CO levels in propane-air flames

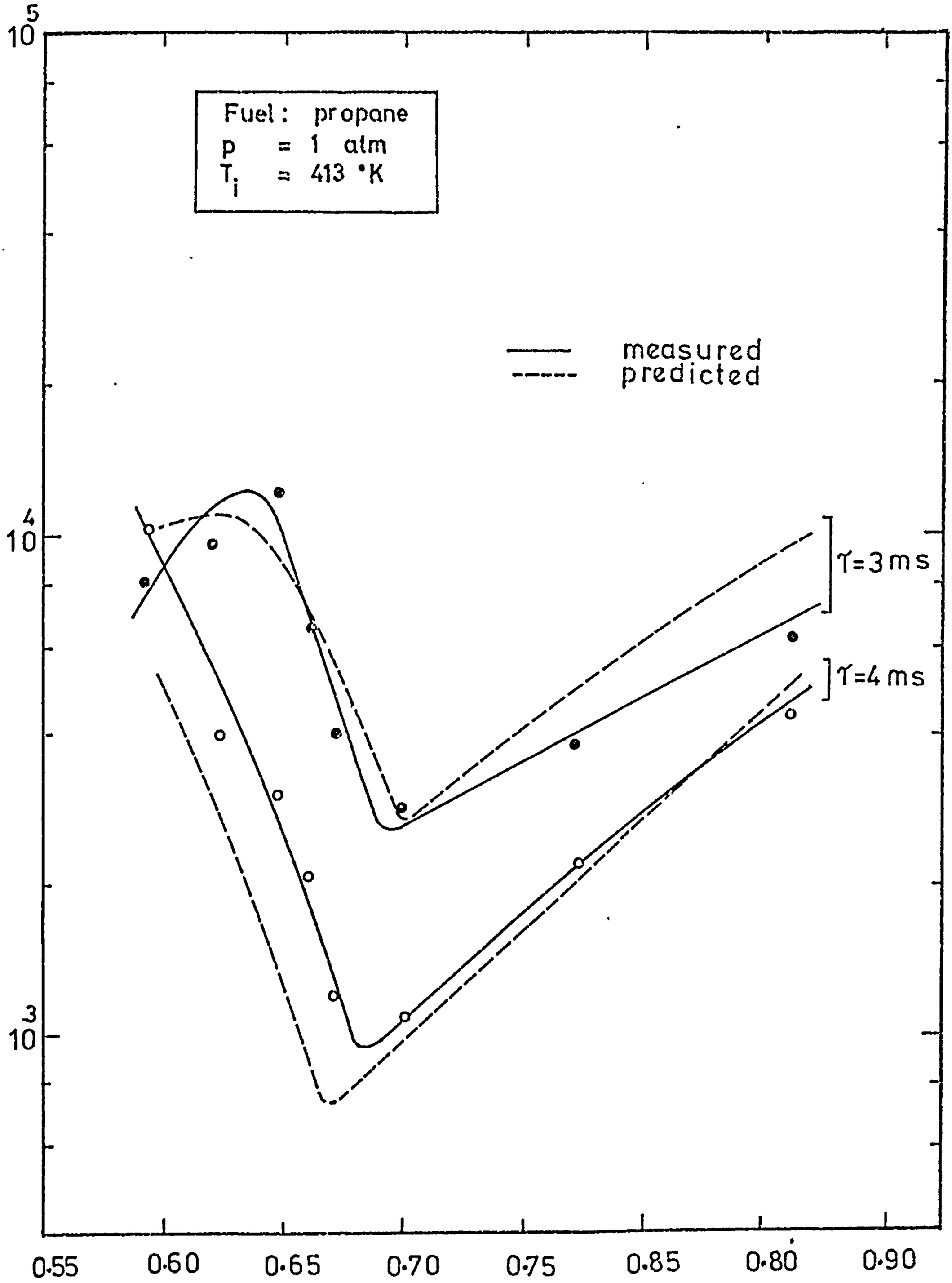

FIGURE8·25 Comparison between predicted and measured CO levels in propane-air flames (PE after 90 pecent of fuel consumed)

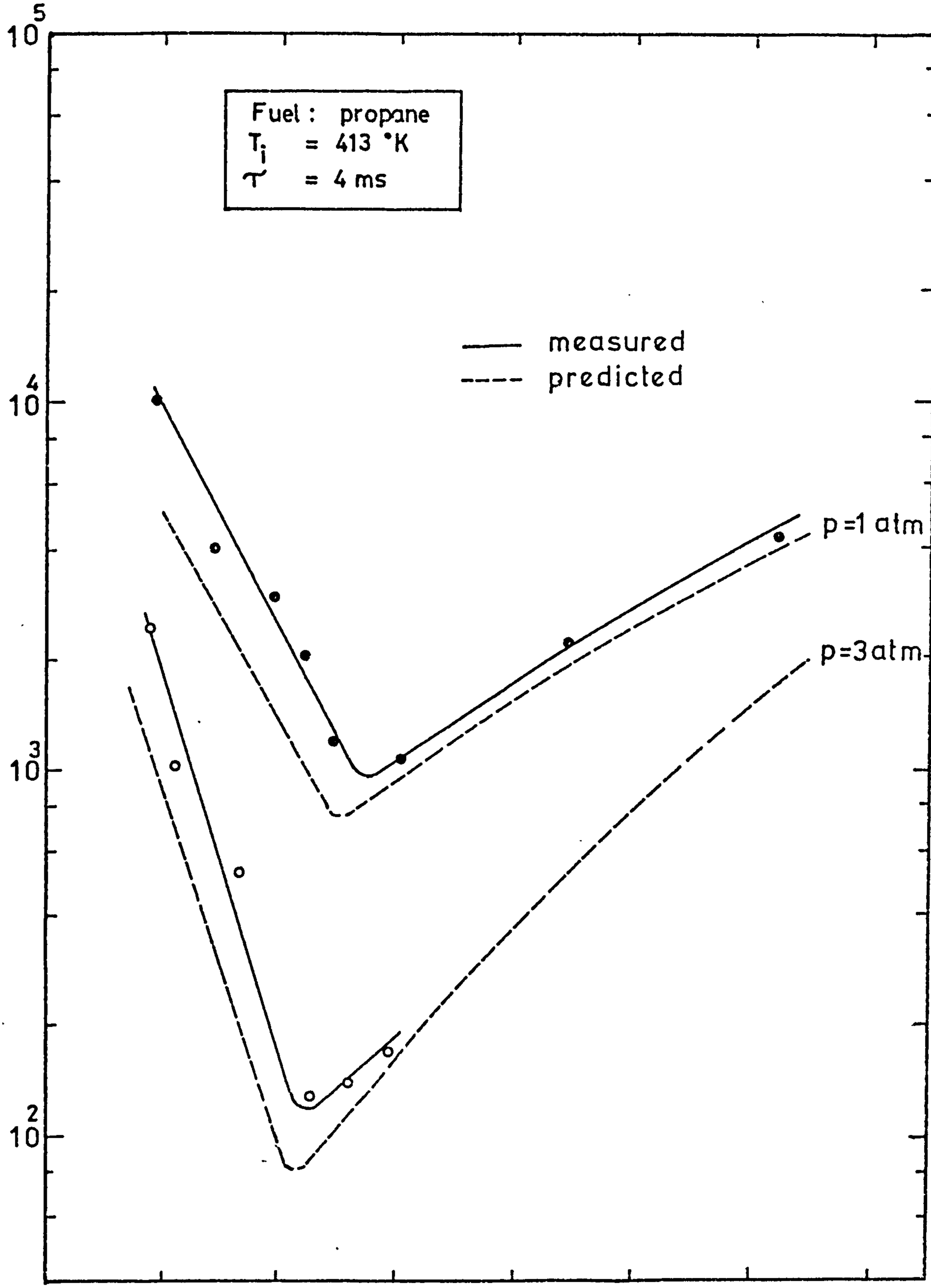

FIGURE 8·26 Comparison between predicted and measured CO levels in propane-air flames

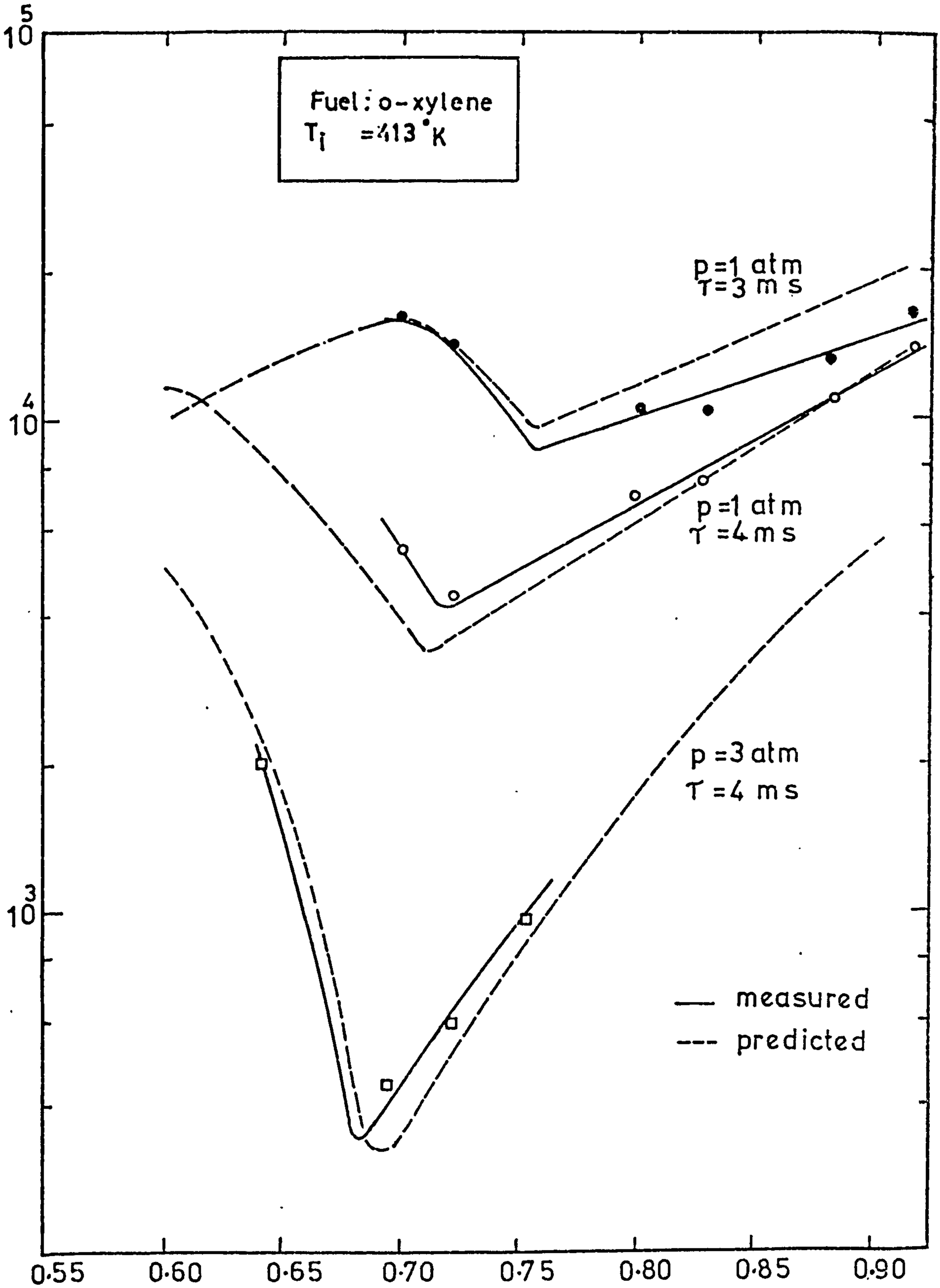

EIGURE 8·27 Comparison of predicted and measured CO levels in o-xylene/air flames

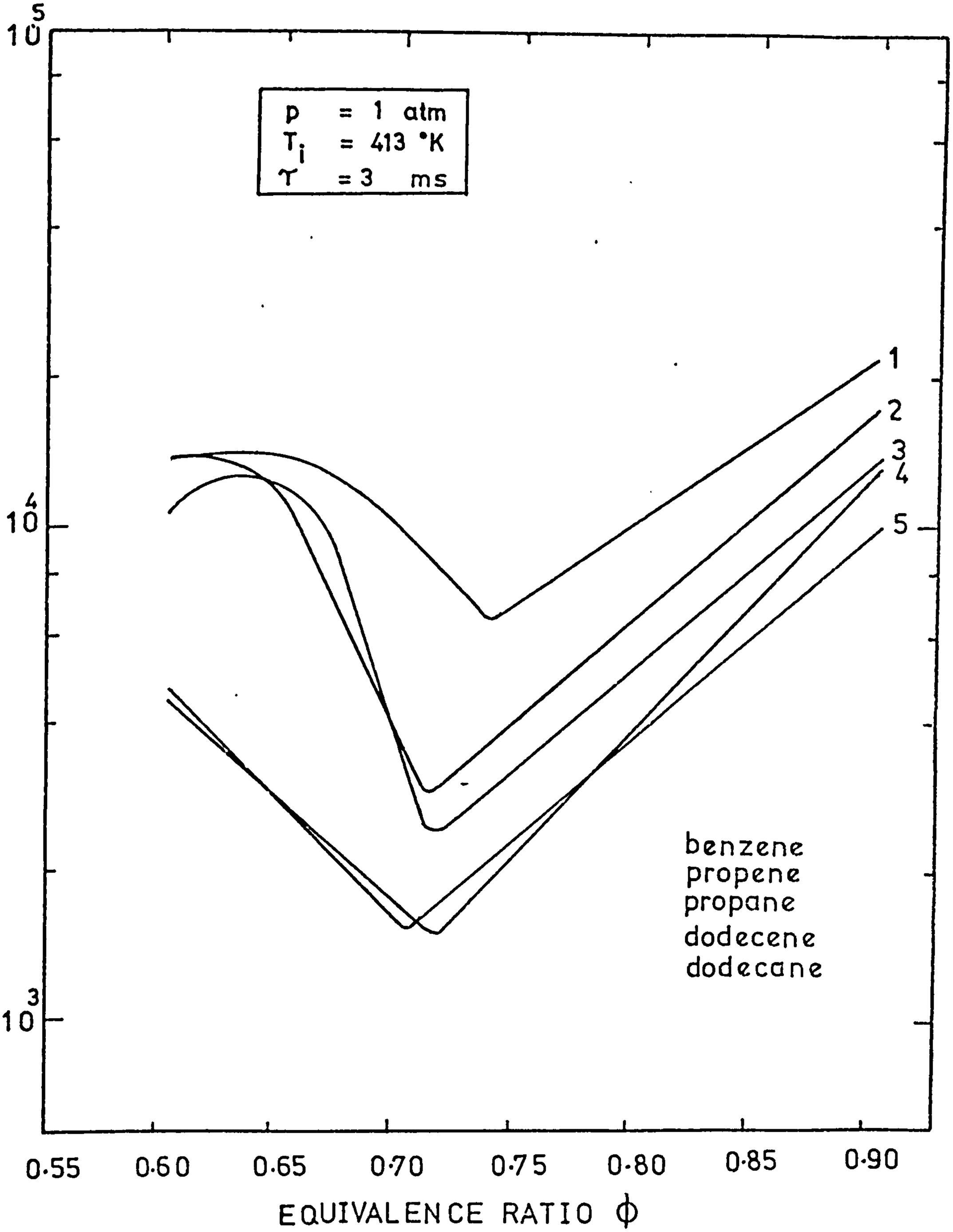

FIGURE 8·28 Predicted CO levels for different hydrocarbons assuming one fuel oxidation rate equation for aromatics and another for aliphatics

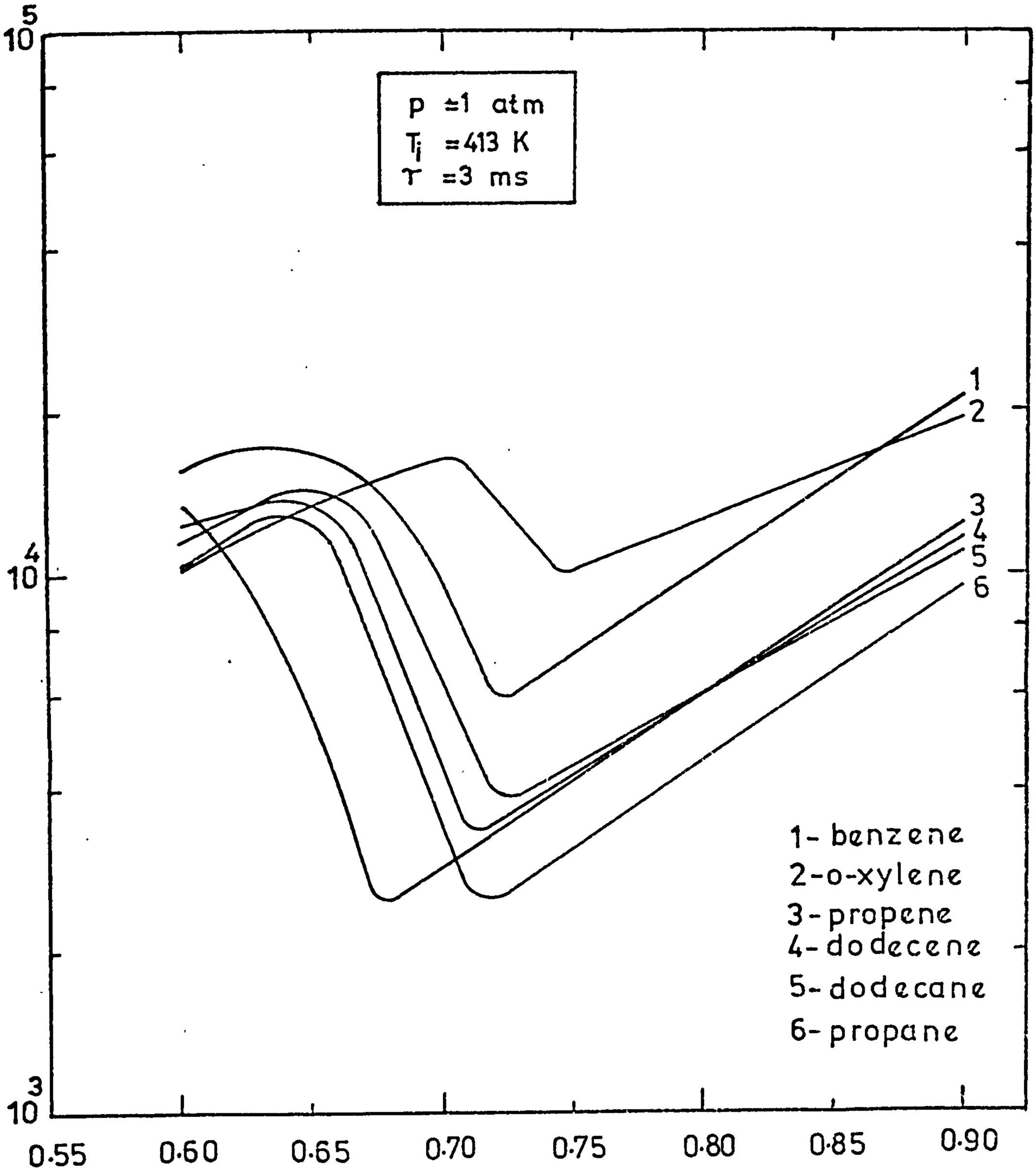

FIGURE 8·29 Predicted CO levels in different hydrocarbon-air flames using different global rate equations for different fuels

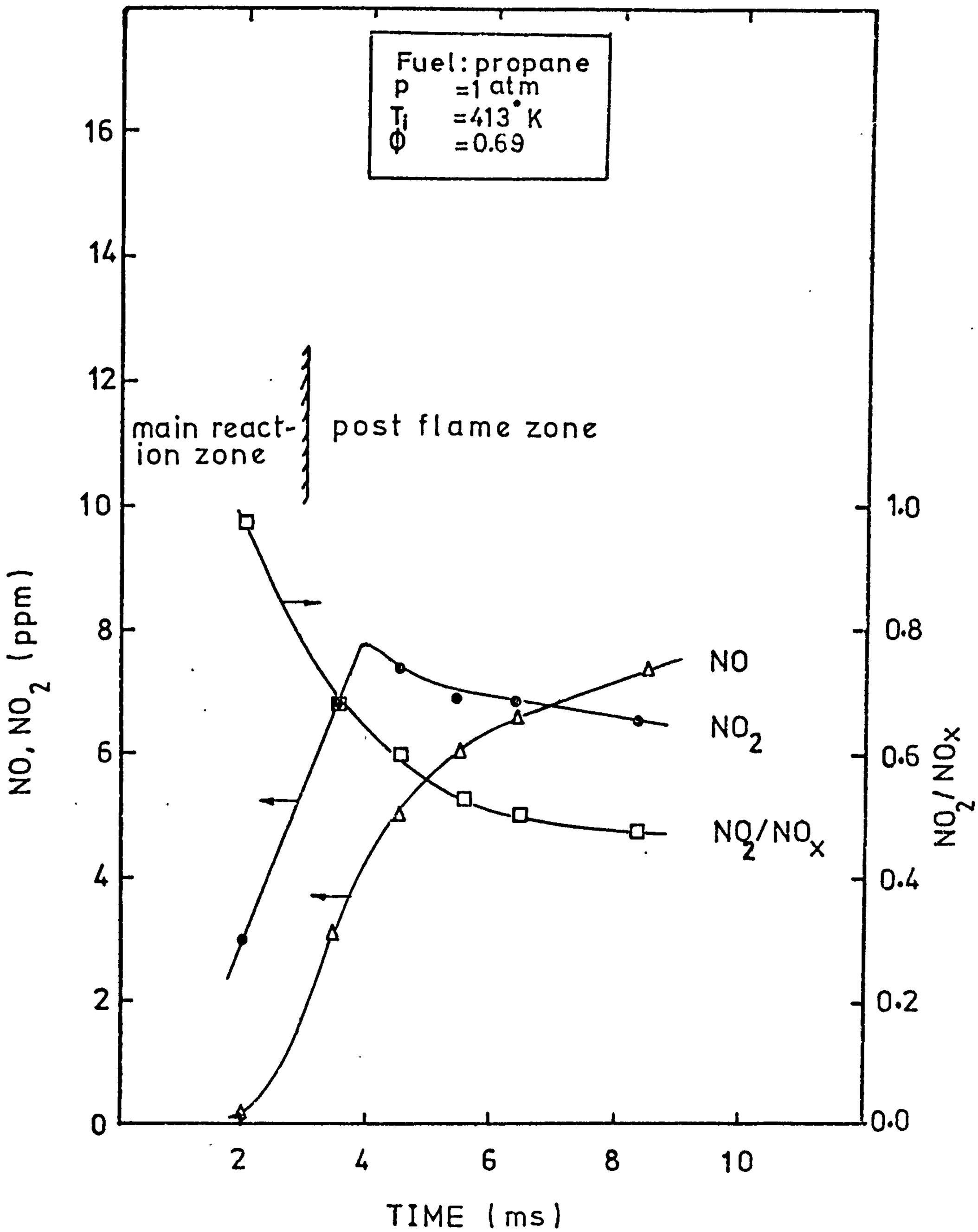

FIGURE 9.1 NO_2 and NO levels in an atmospheric propane-air flame

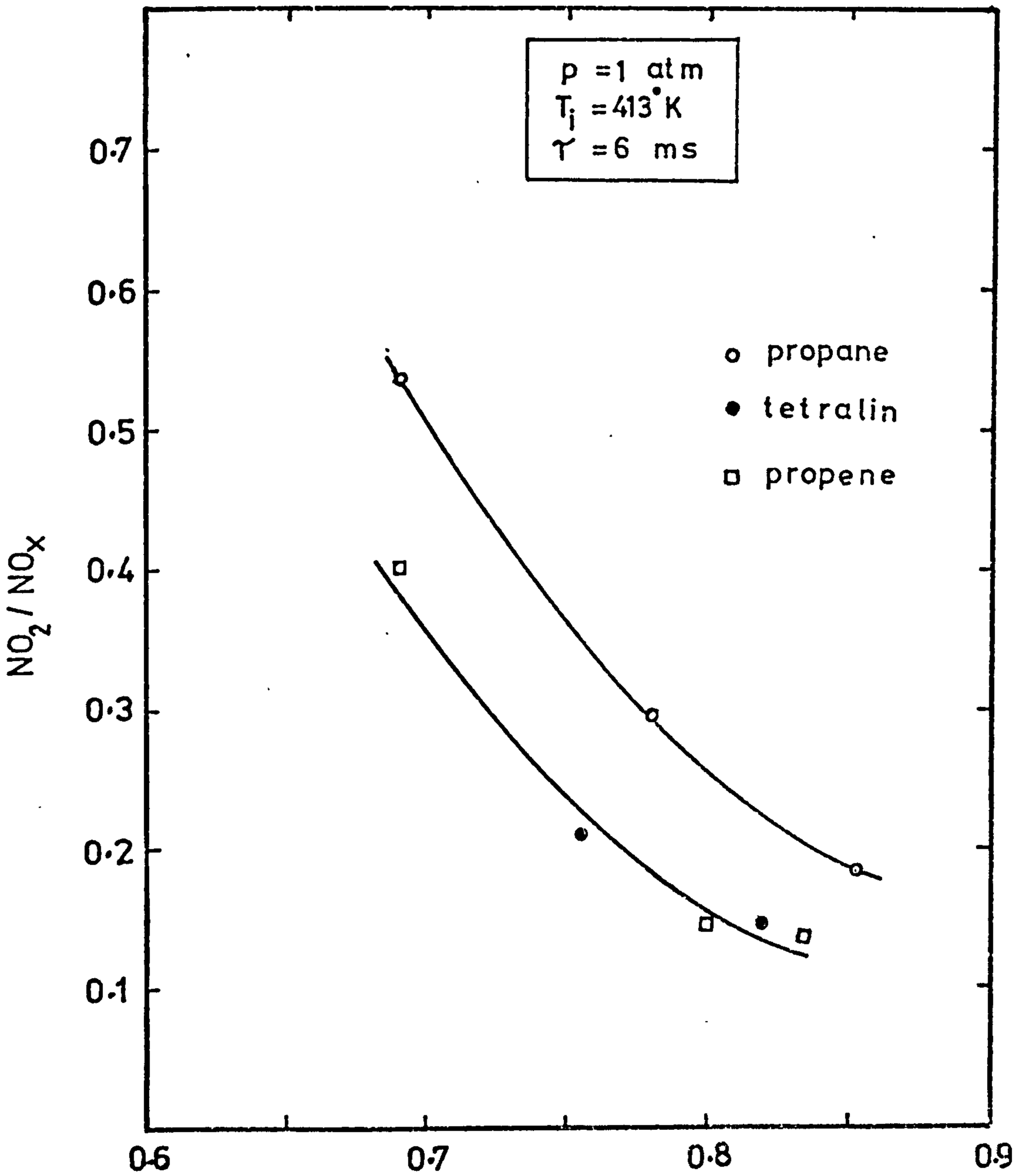

FIGURE 9.2 Variation of NO_2/NO_X ratio with the equivalence ratio in different hydrocarbon-air flames

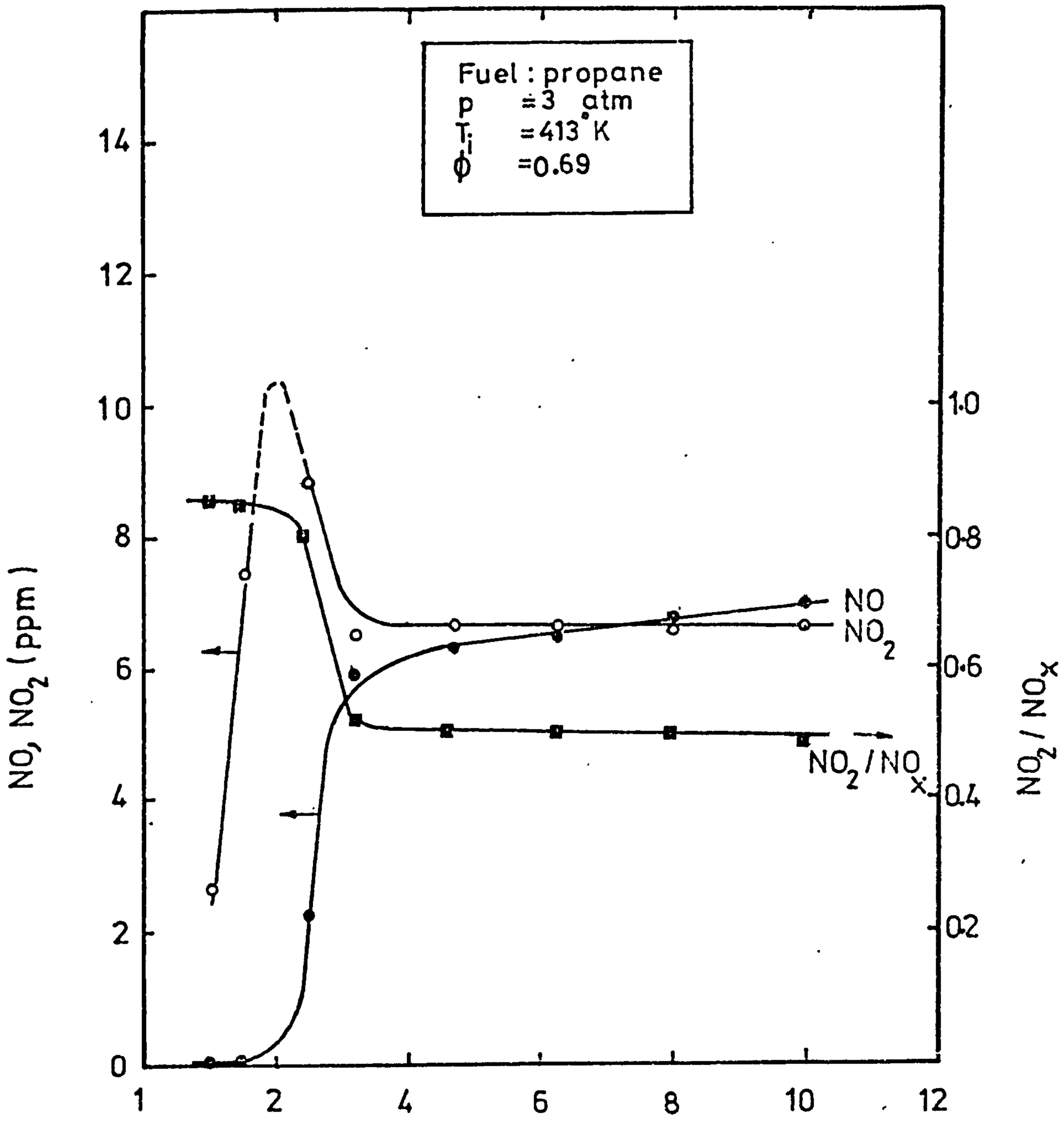

FIGURE 9.3 NO_2 and NO levels in a high pressure propane-air flame

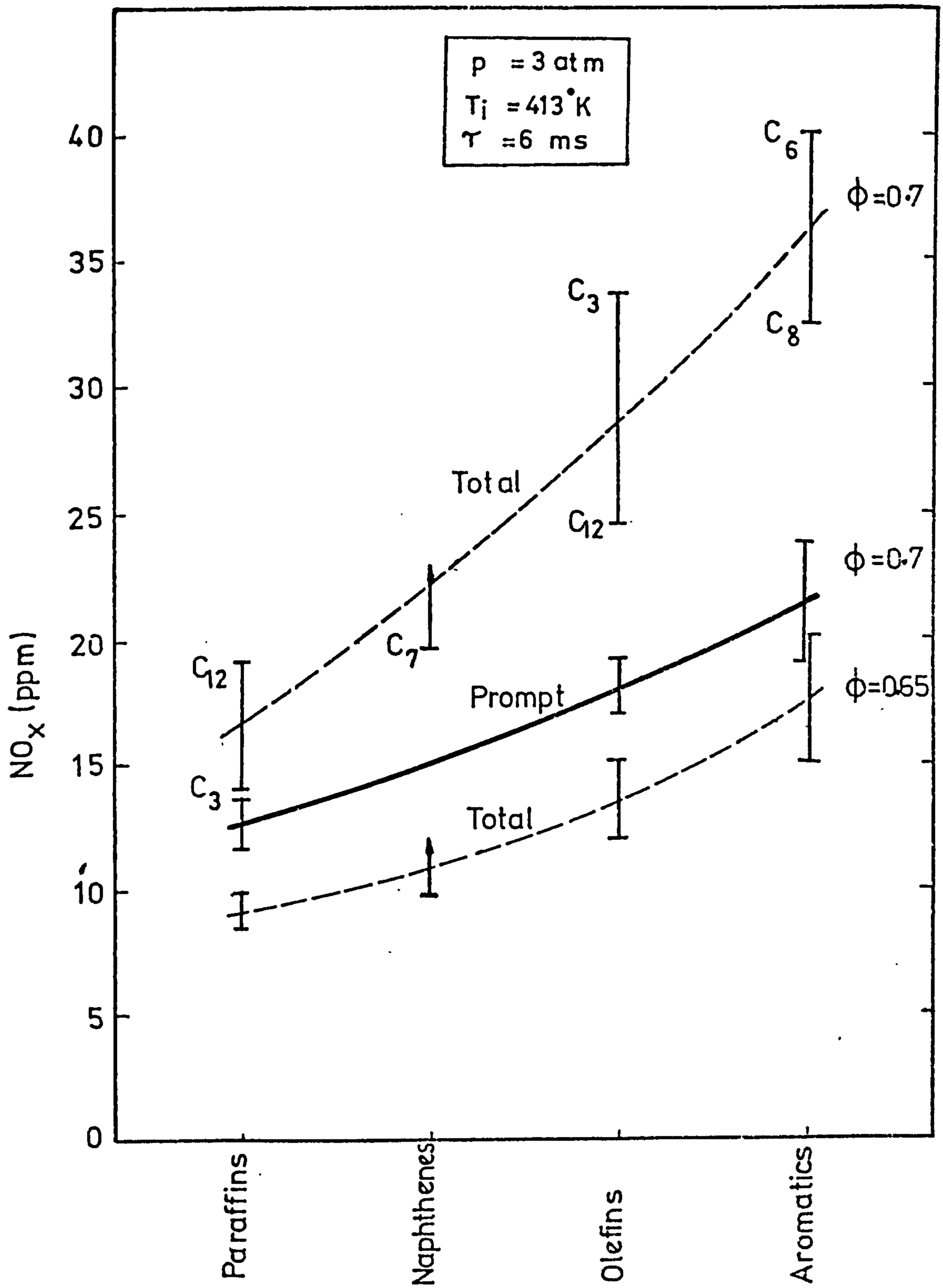

FIGURE 9.4 Variation of NO_X with fuel type

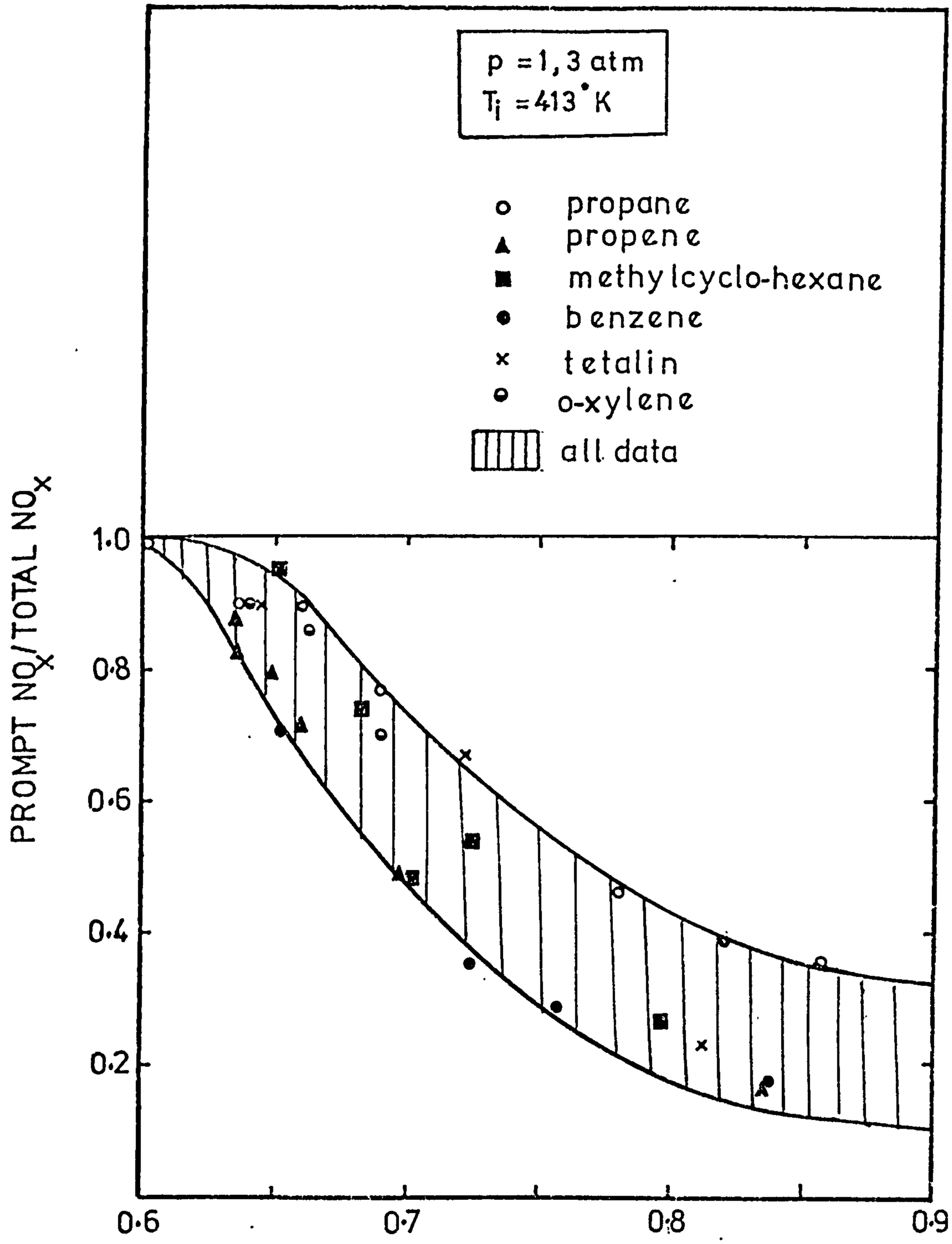

FIGURE 9.5 Variation of the prompt NO_X ratio with the equivalence ratio for different hydrocabon-air flames

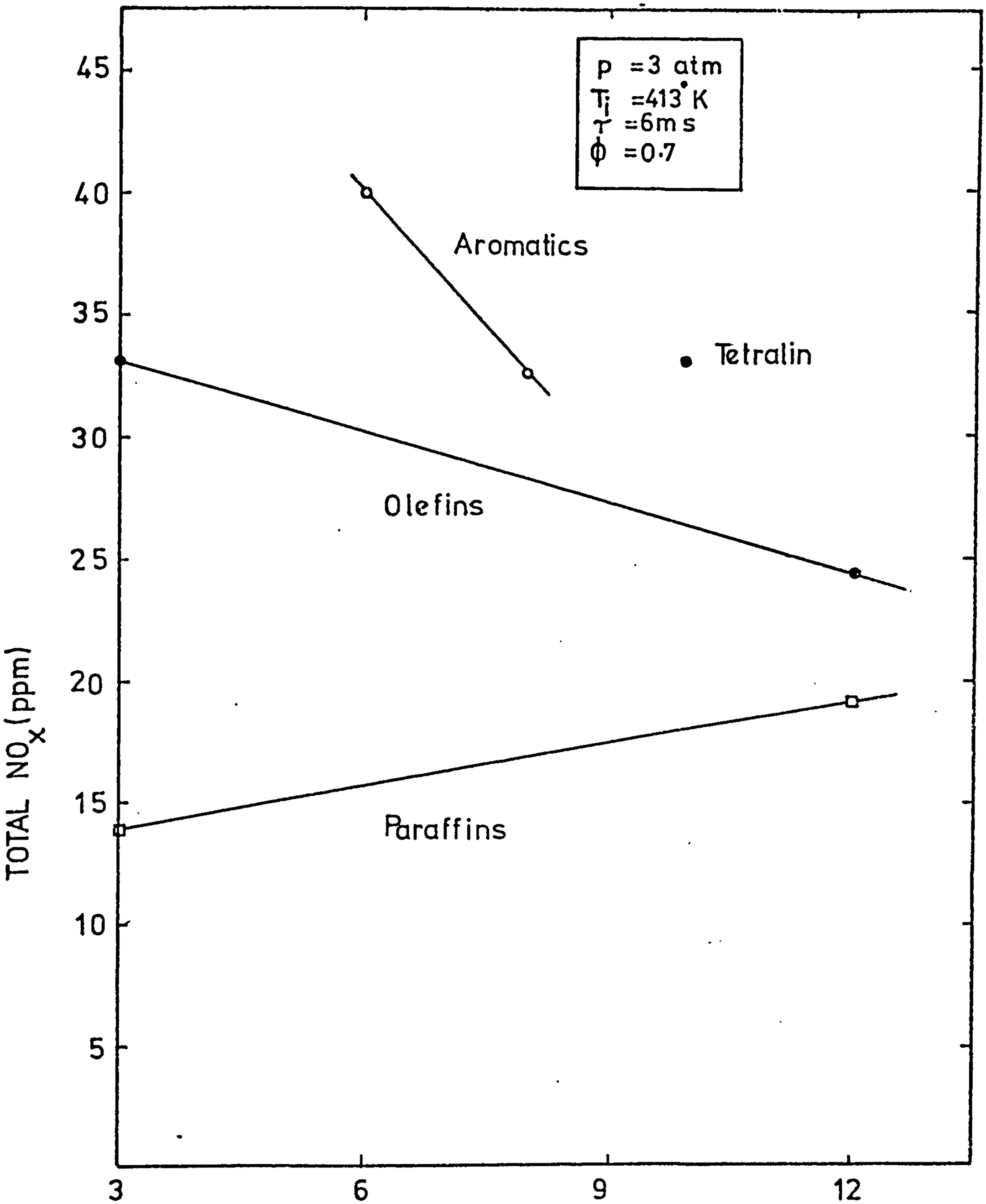

FIGURE 9.6 Variation of total NO_x with the carbon number

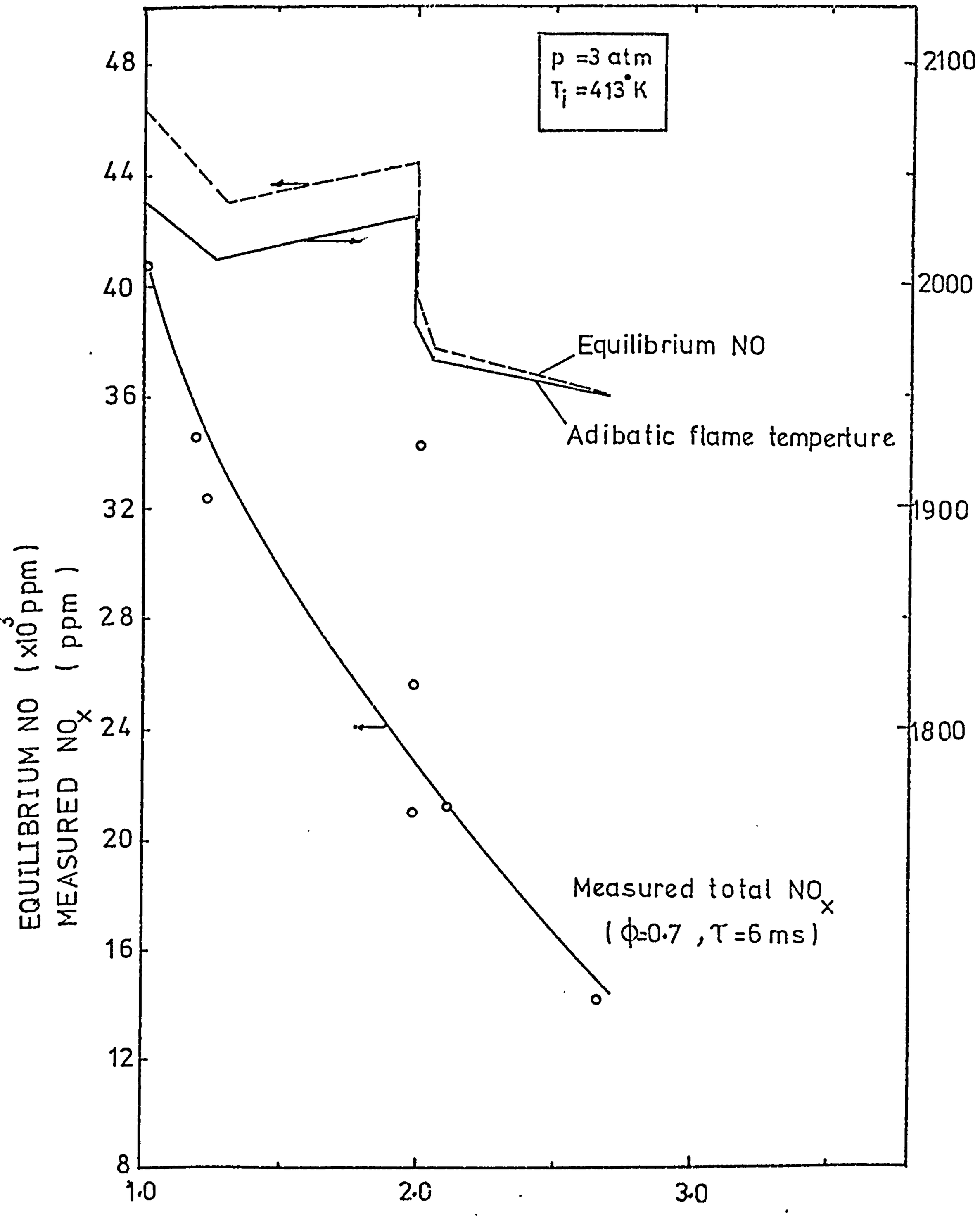

FIGURE 9.7 Variation of NO_X with H/C ratio

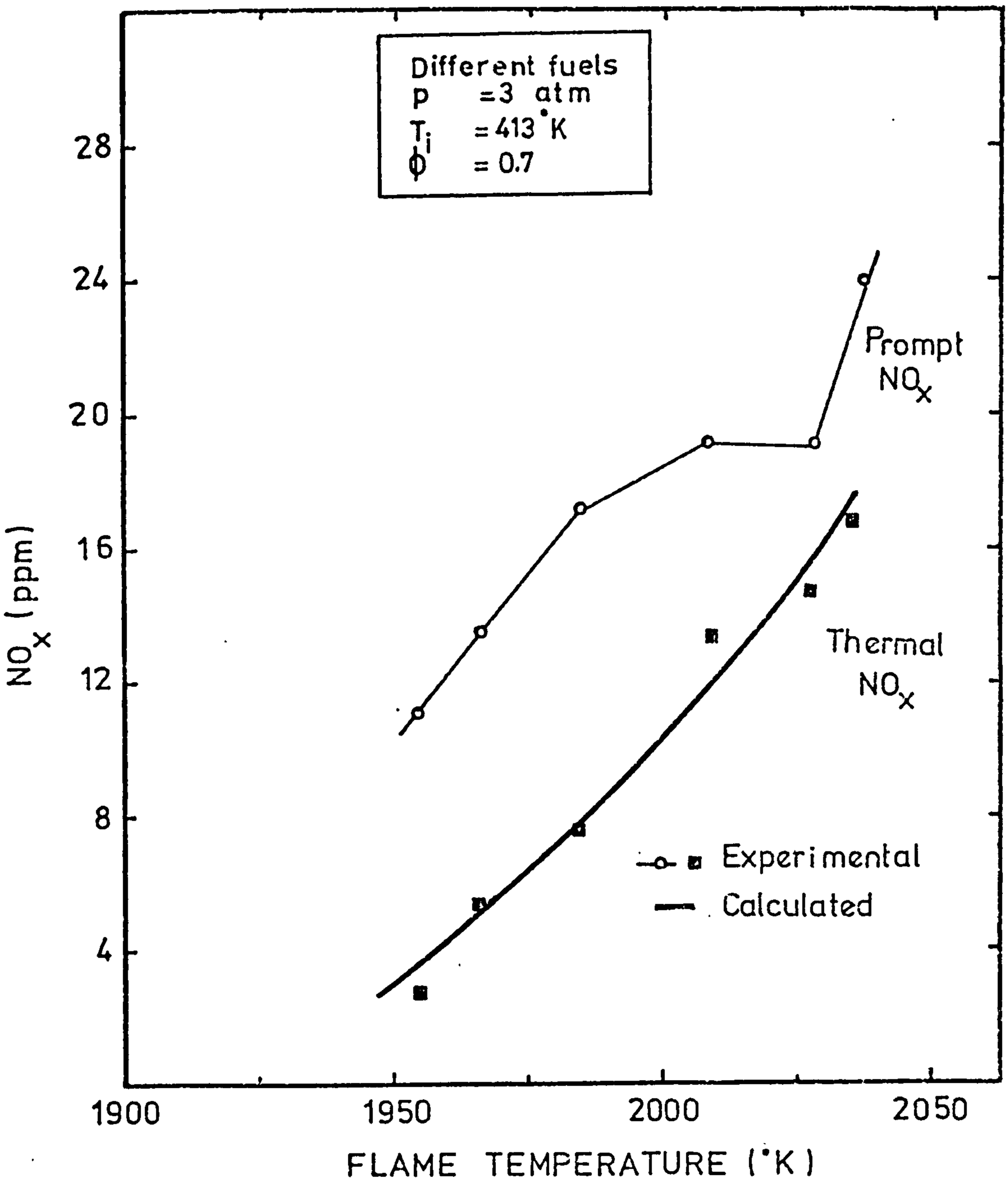

FIGURE 9.8 Influence of the flame temperature on NO_x levels.

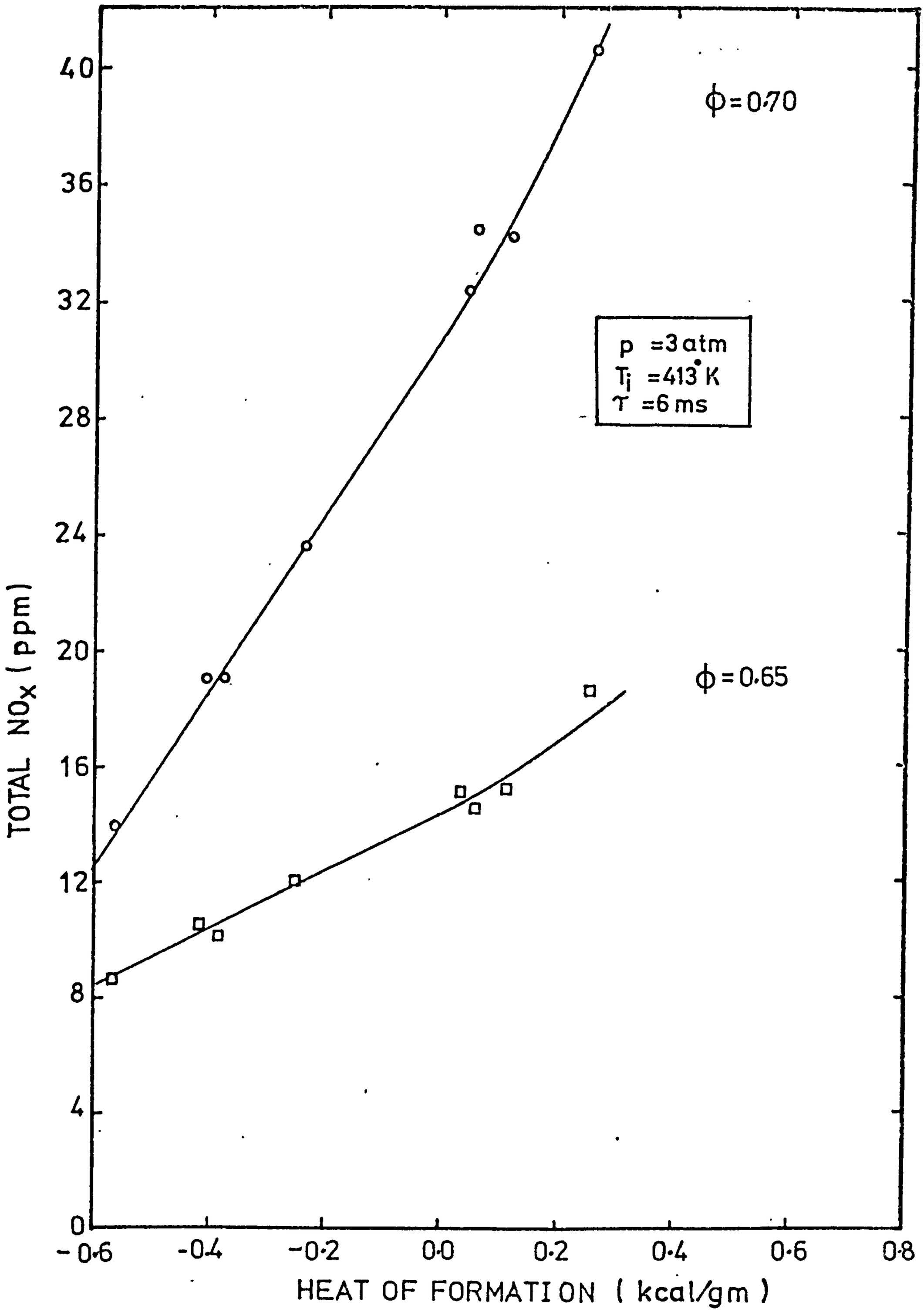

FIGURE 9.9 Variation of NO_x with the standard heat of formation of fuel at high pressure.

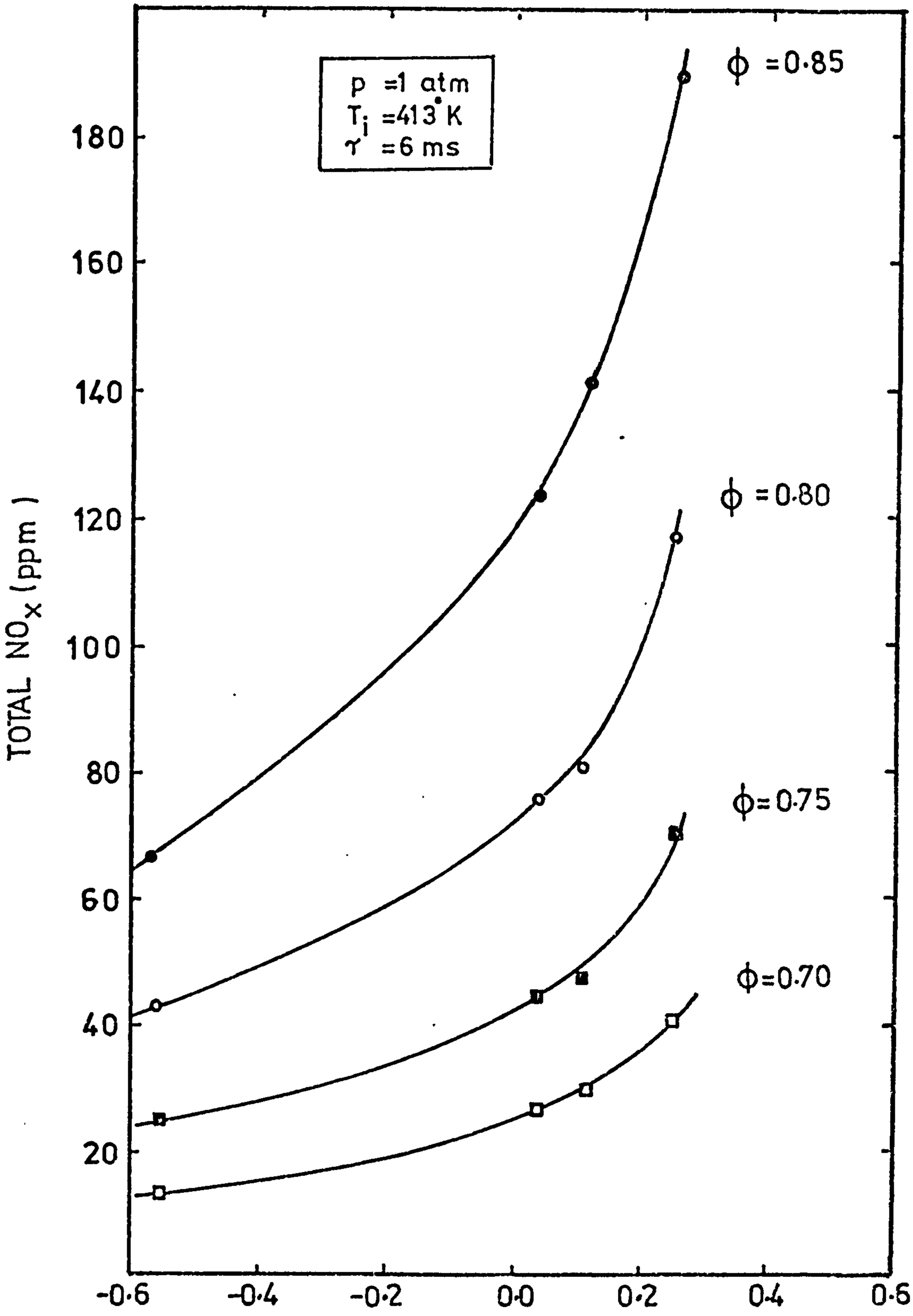

FIGURE 9.10 Variation of NO_x with the fuel heat of formation at atmospheric pressure.

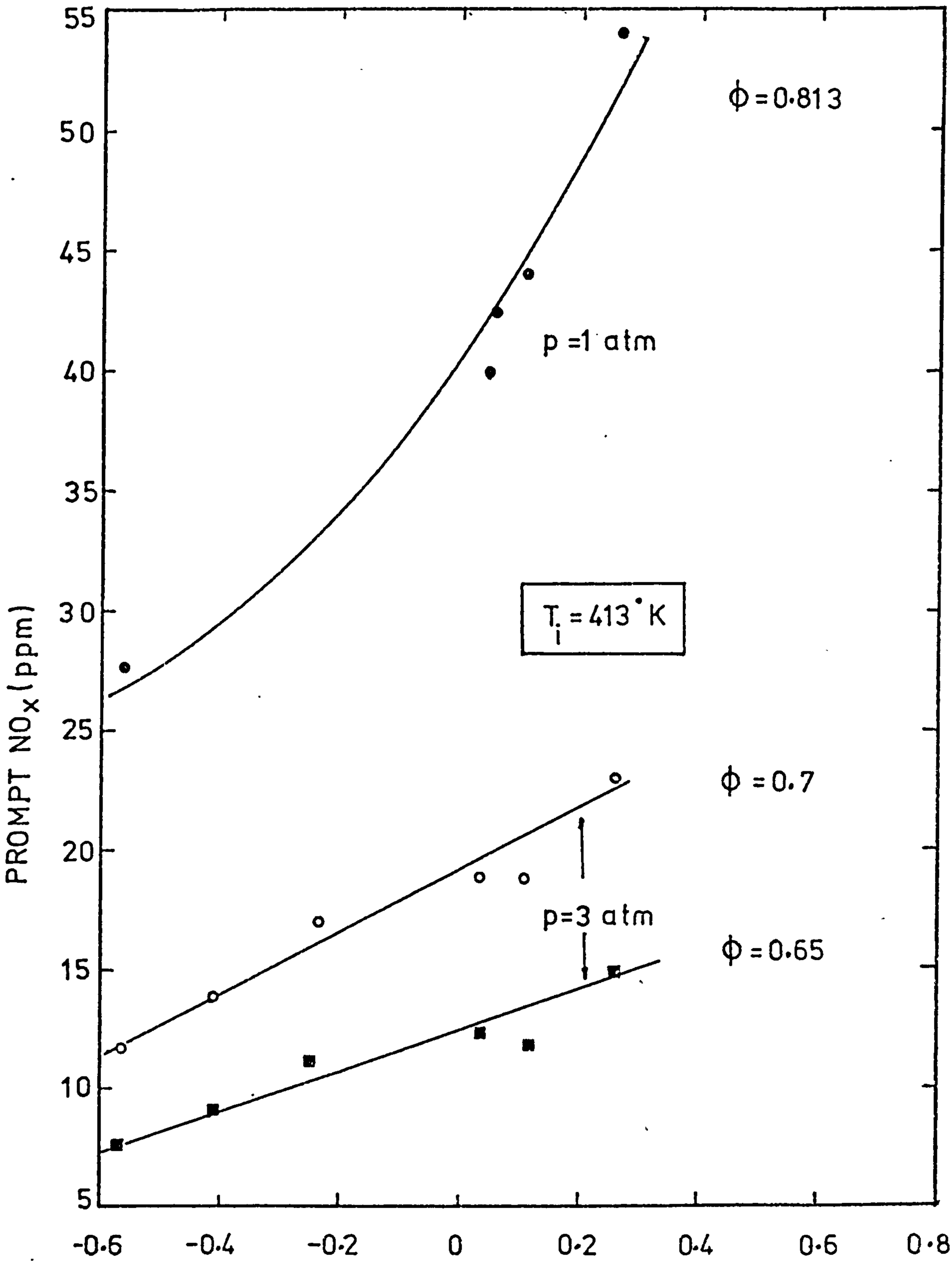

FIGURE 9.11 Variation of prompt NO_x with the fuel heat of formation.

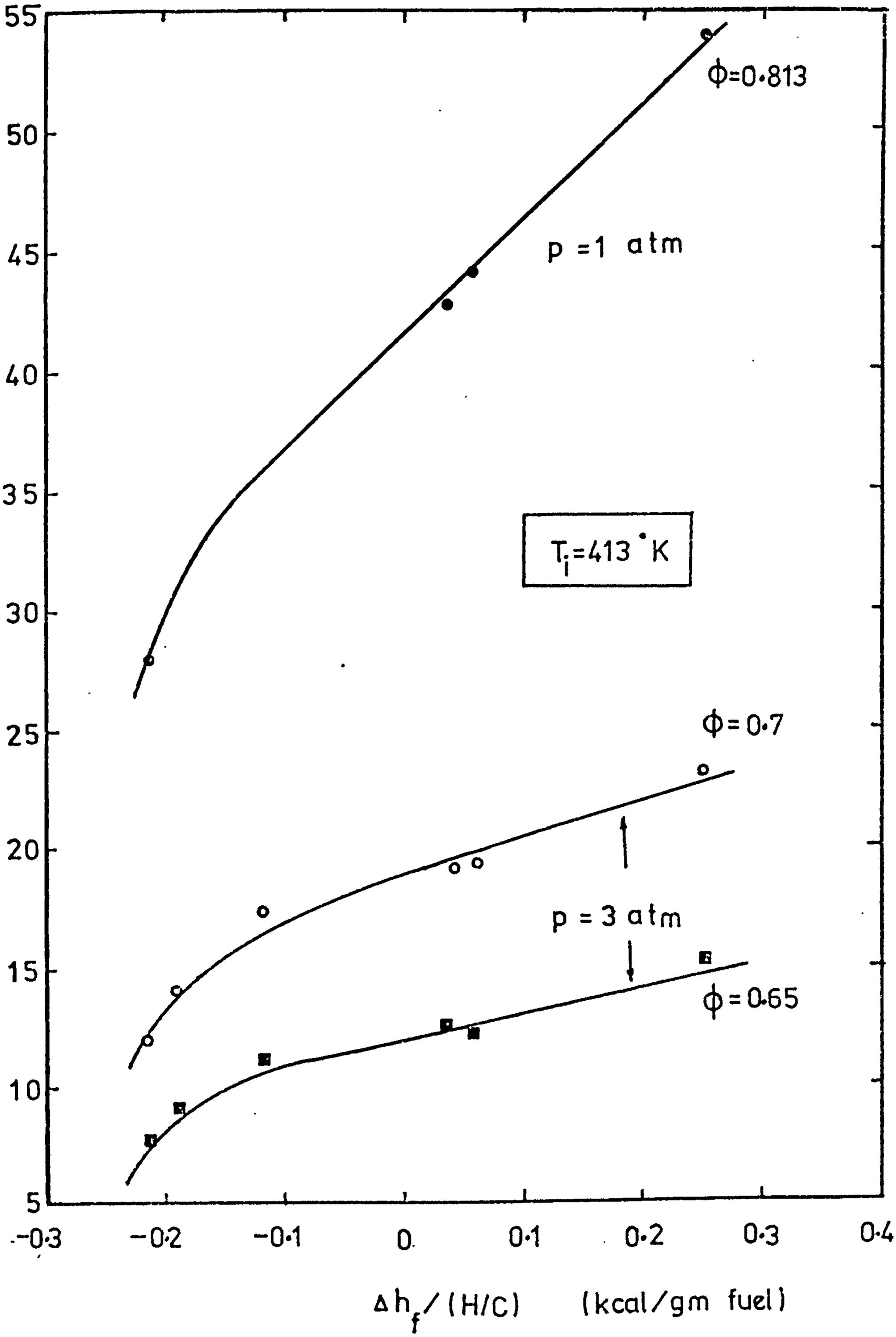

FIGURE 9.12 Variation of prompt NO_x with the parameter $h_f/(H/C)$

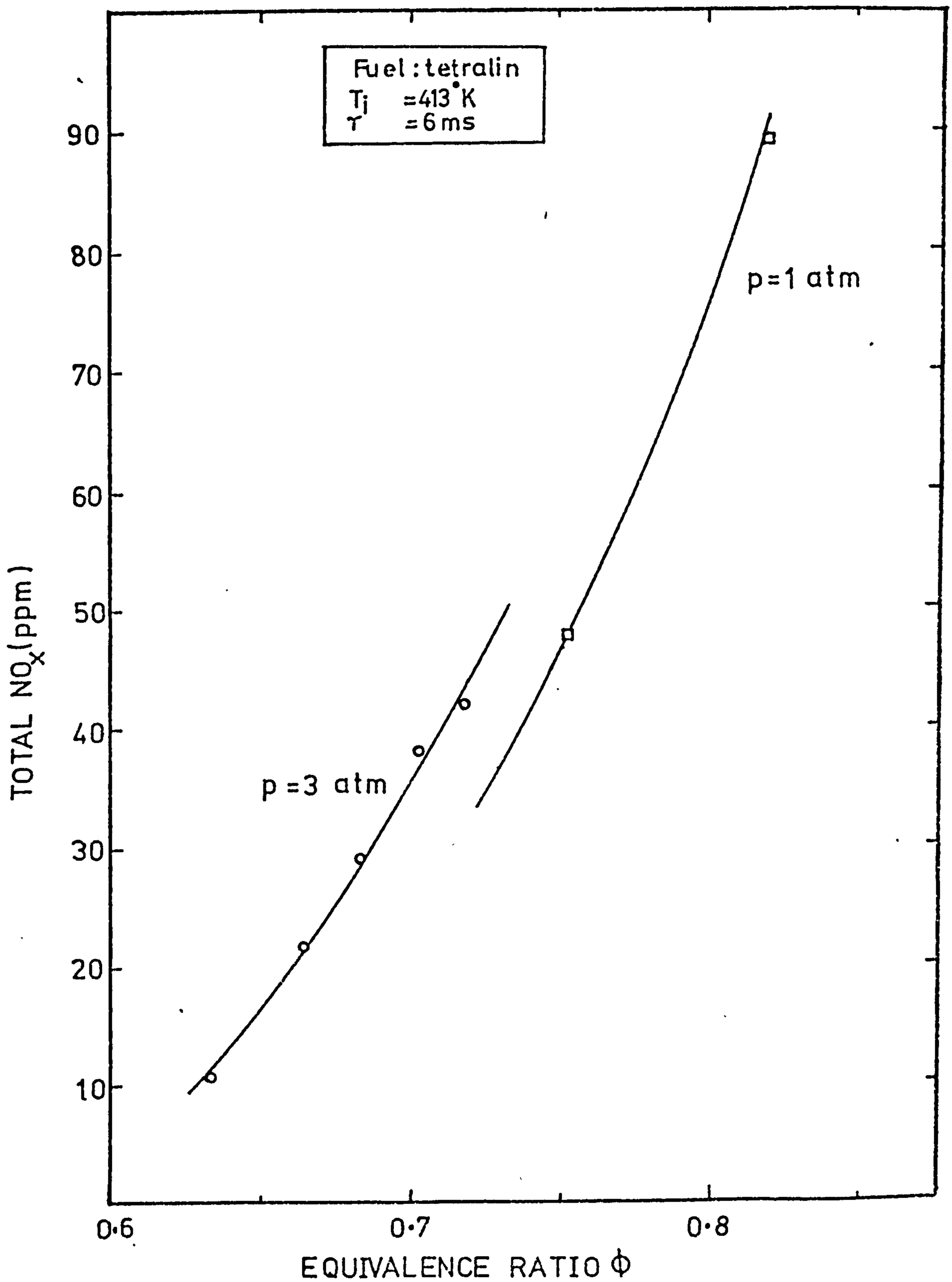

FIGURE 9.13 Effect of pressure on NO_x levels formed in tetralin–air flames.

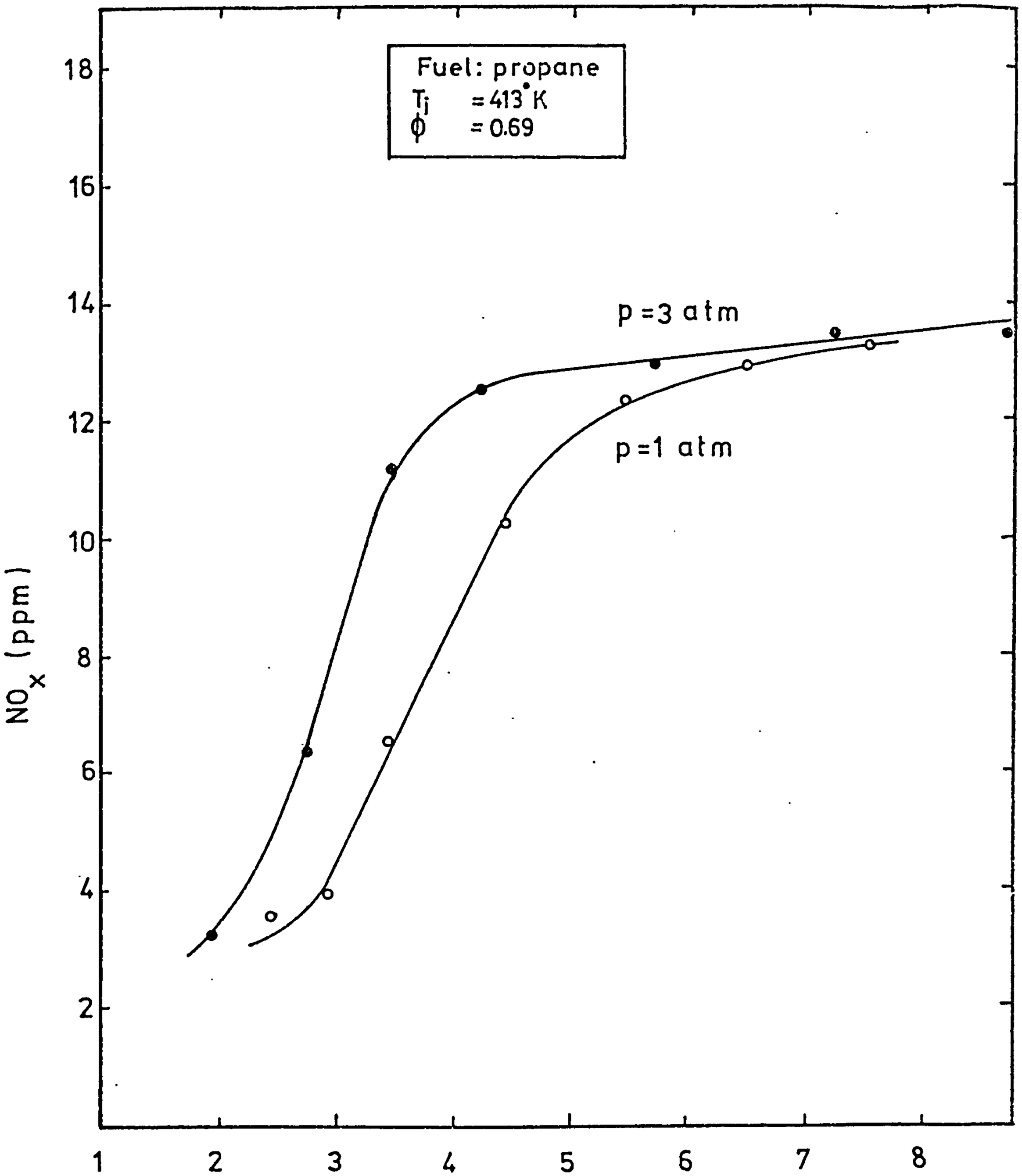

FIGURE 9.14 Effect of pressure on NO_x profiles in propane — air flames.

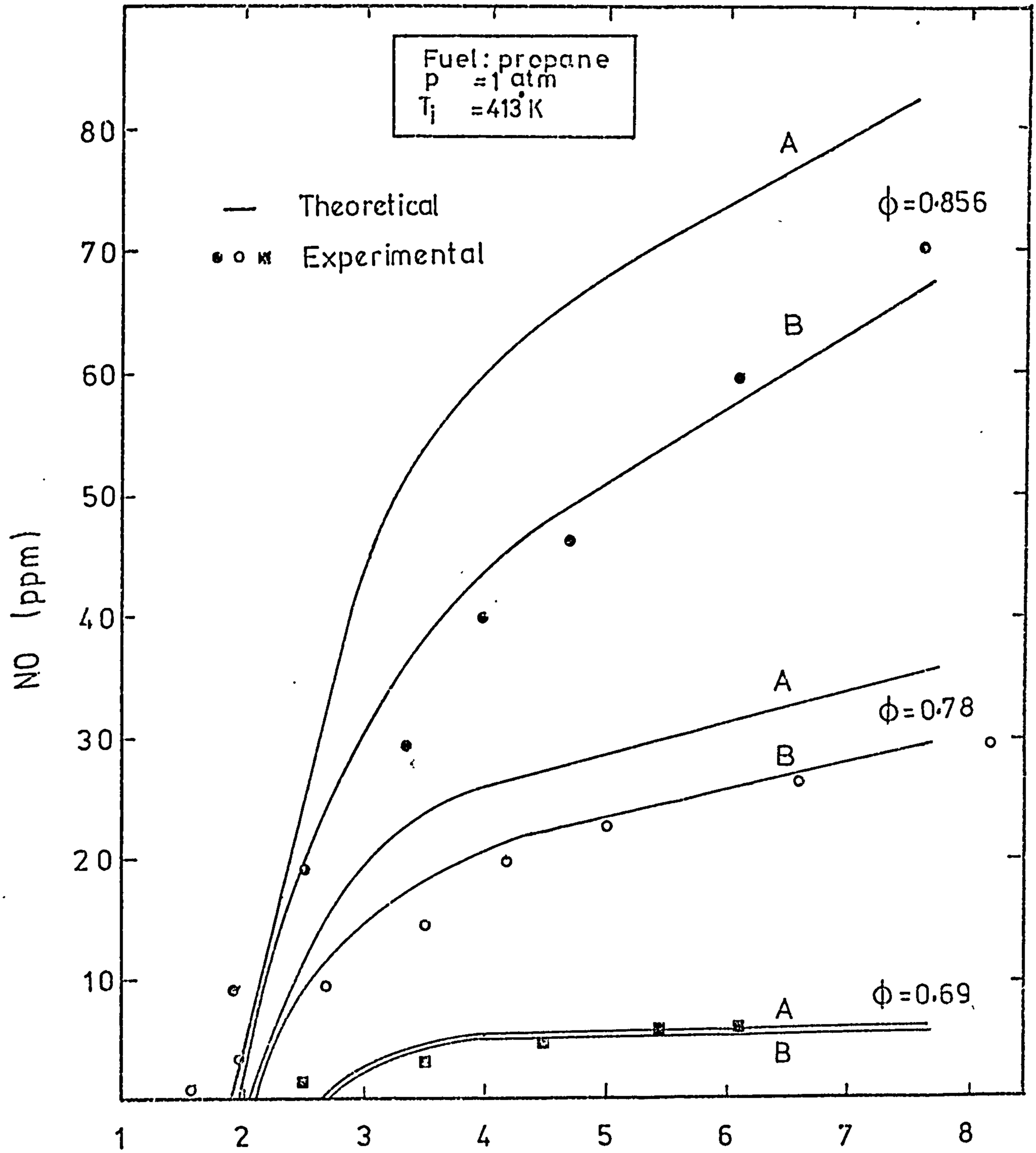

FIGURE 9.15. Measured and predicted NO profiles in atmospheric propane-air flames.

A: 90% of fuel consumed at NO=0

B: 95% of fuel consumed at NO=0

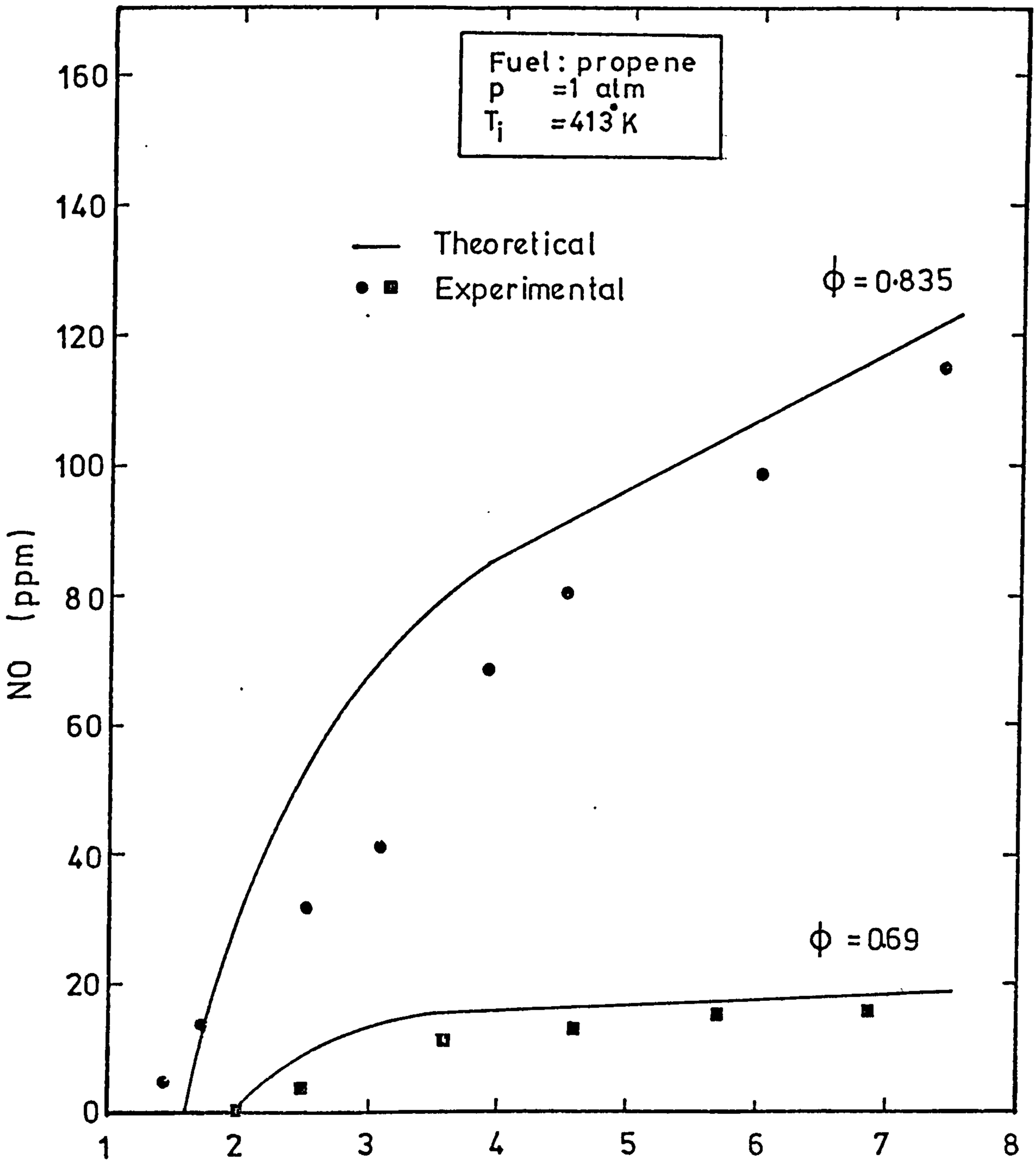

FIGURE 9.16. Measured and predicted NO profiles in propene-air flames

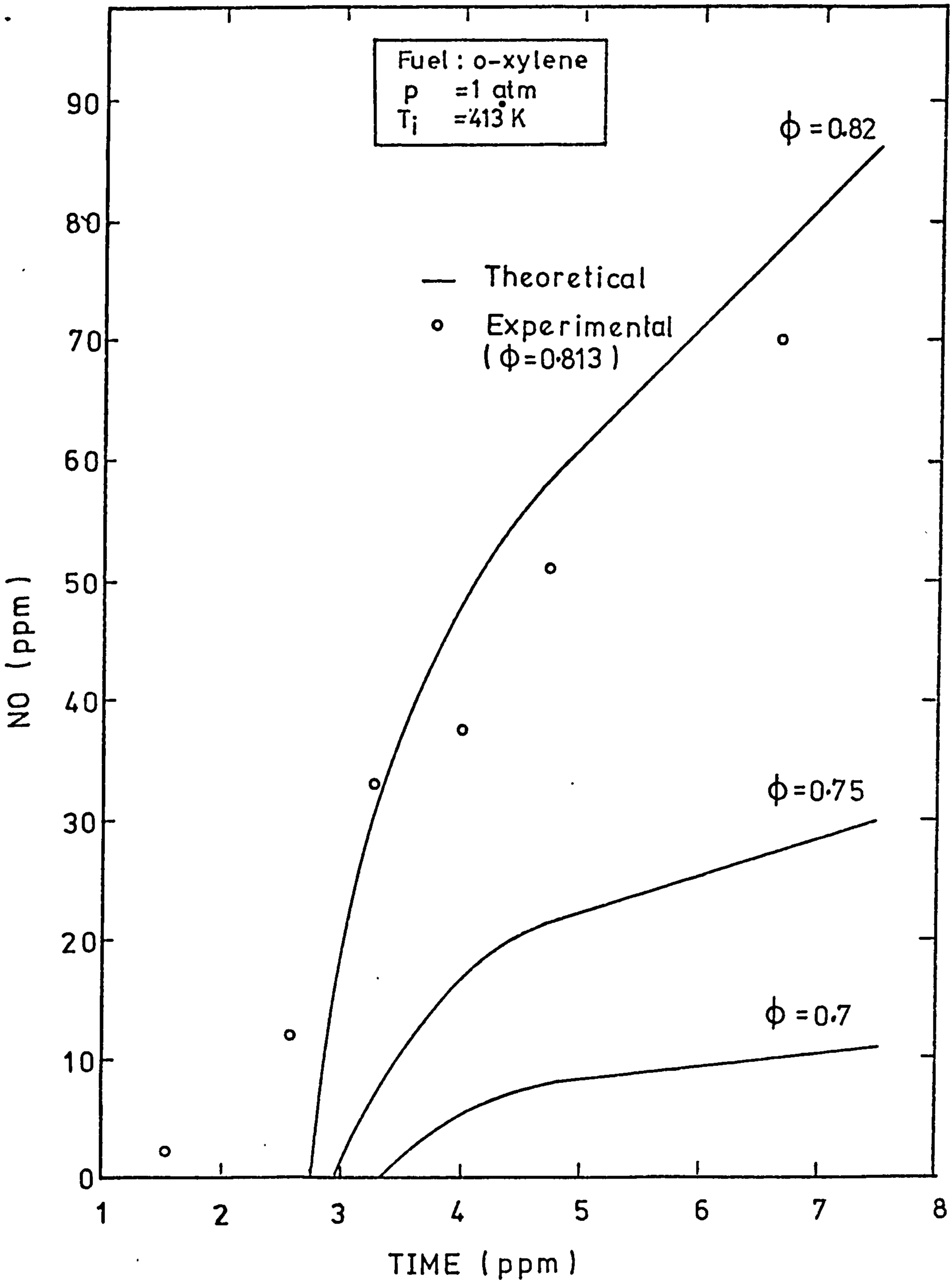

FIGURE 9.17. Measure and predicted NO profiles in o-xylene-air flames

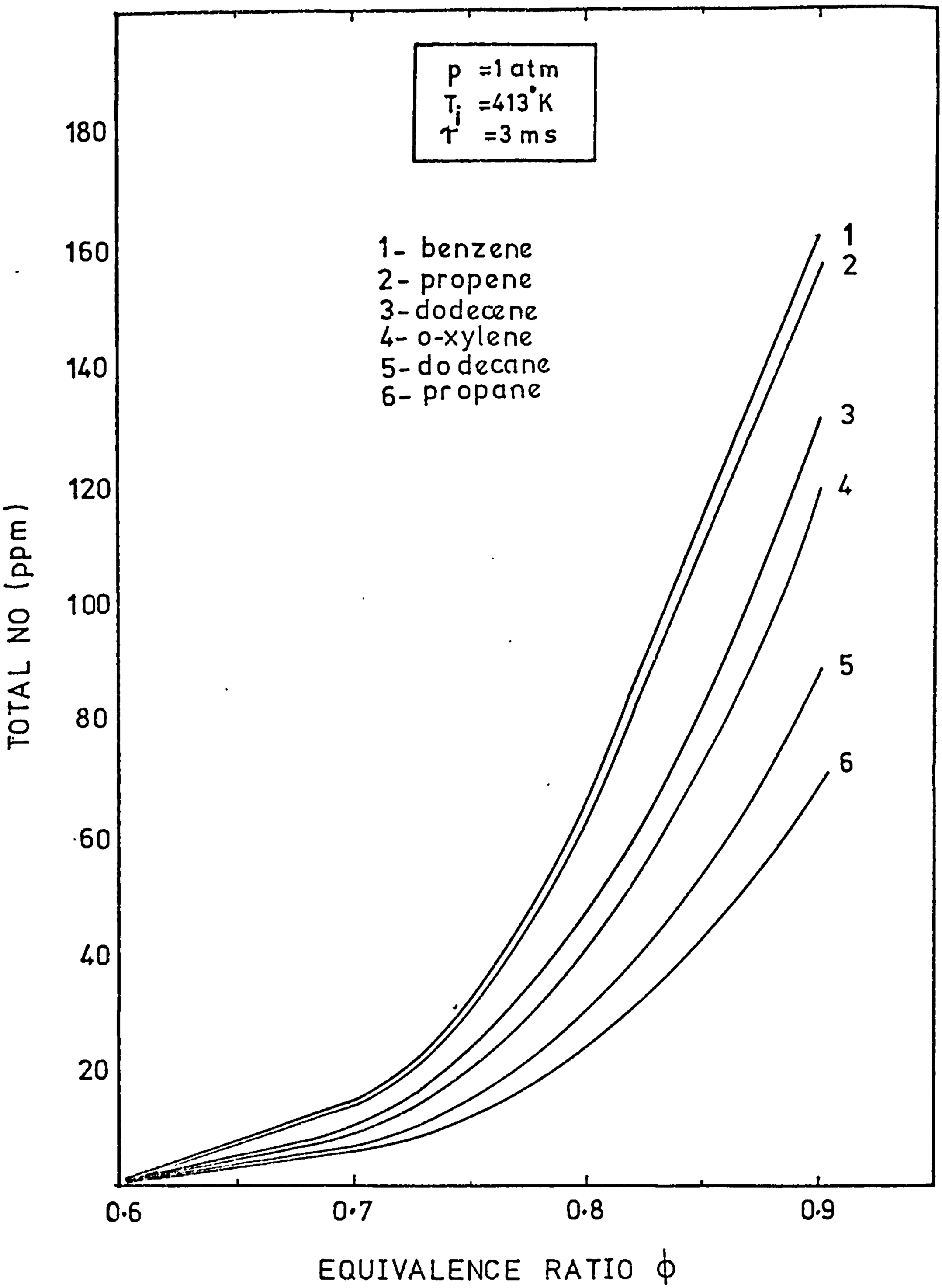

FIGURE 9.18. Predicted NO levels in different hydrocarbon - air flames after 3ms residence time in the post-flame zone.

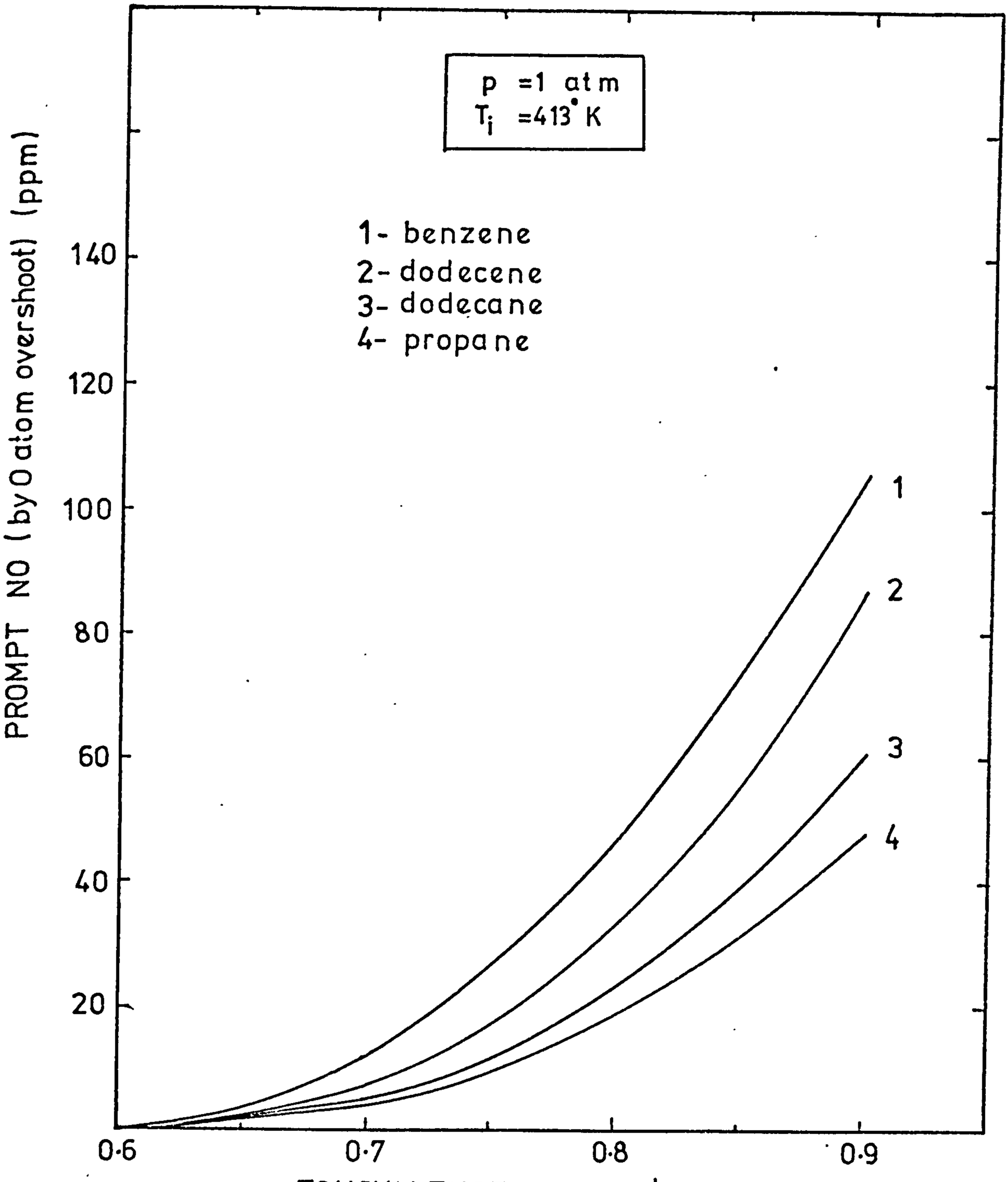

FIGURE 9.19 Predicted prompt NO levels for different hydrocarbon - air flames at atmospheric pressure.

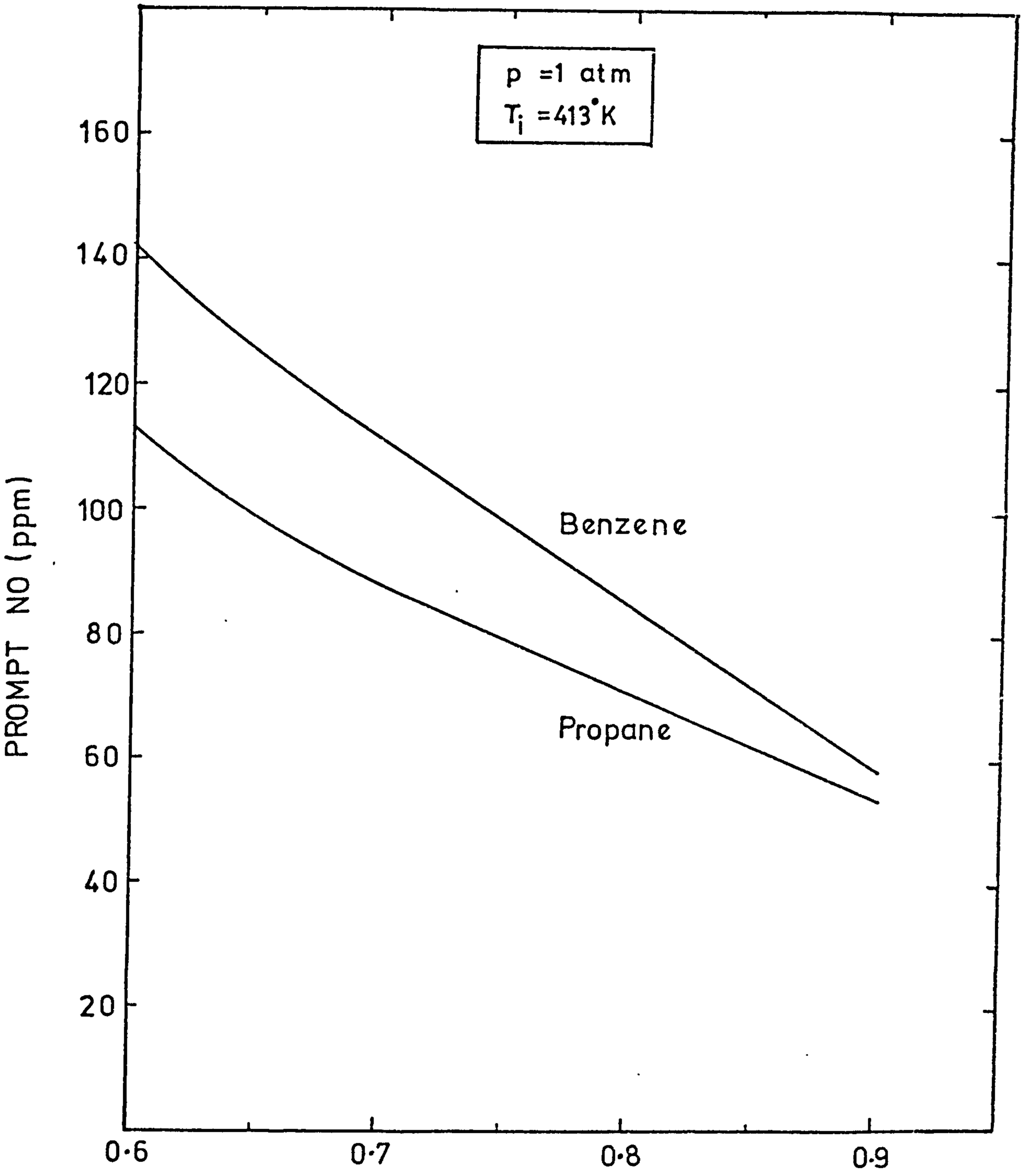

FIGURE 9.20. Predicted prompt NO at constant flame temperature for different hydrocarbon - air flames

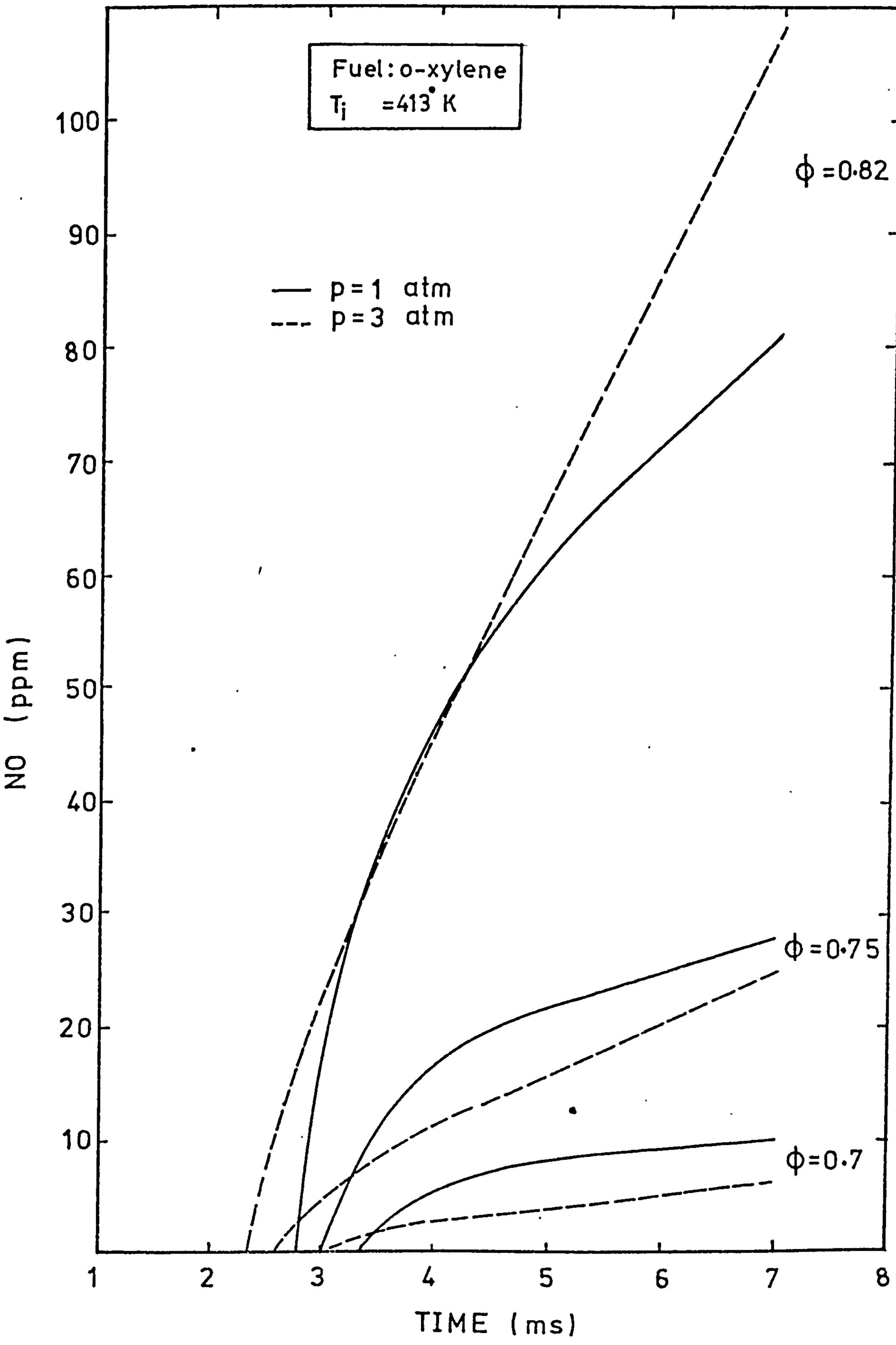

FIGURE 9.21 Predicted NO profiles in o-xylene/air flames at different pressures

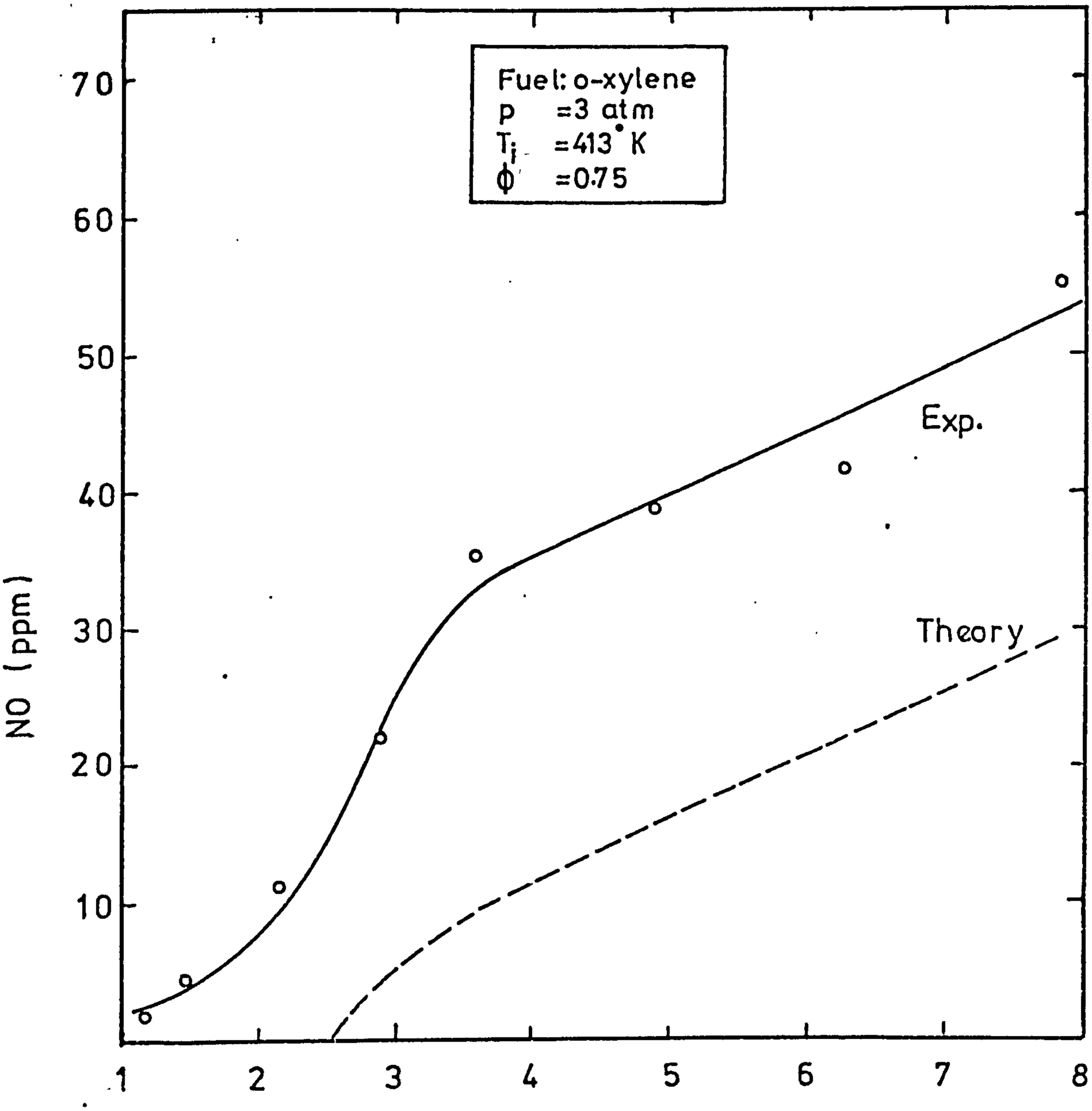

FIGURE 9.22. Measured and predicted NO profiles in o-xylene/air flame at high pressure.

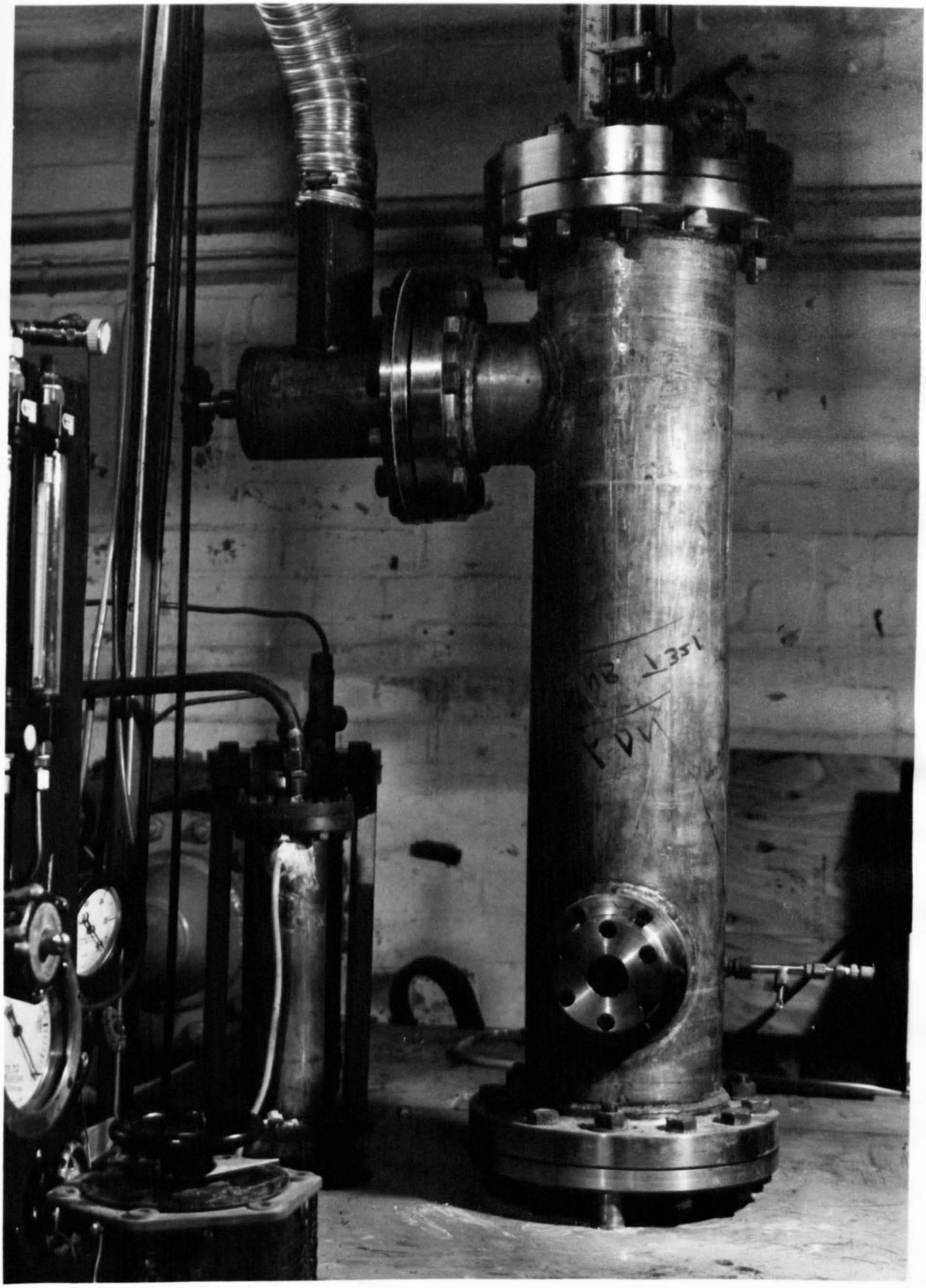

PLATE1 General view of burner assembly

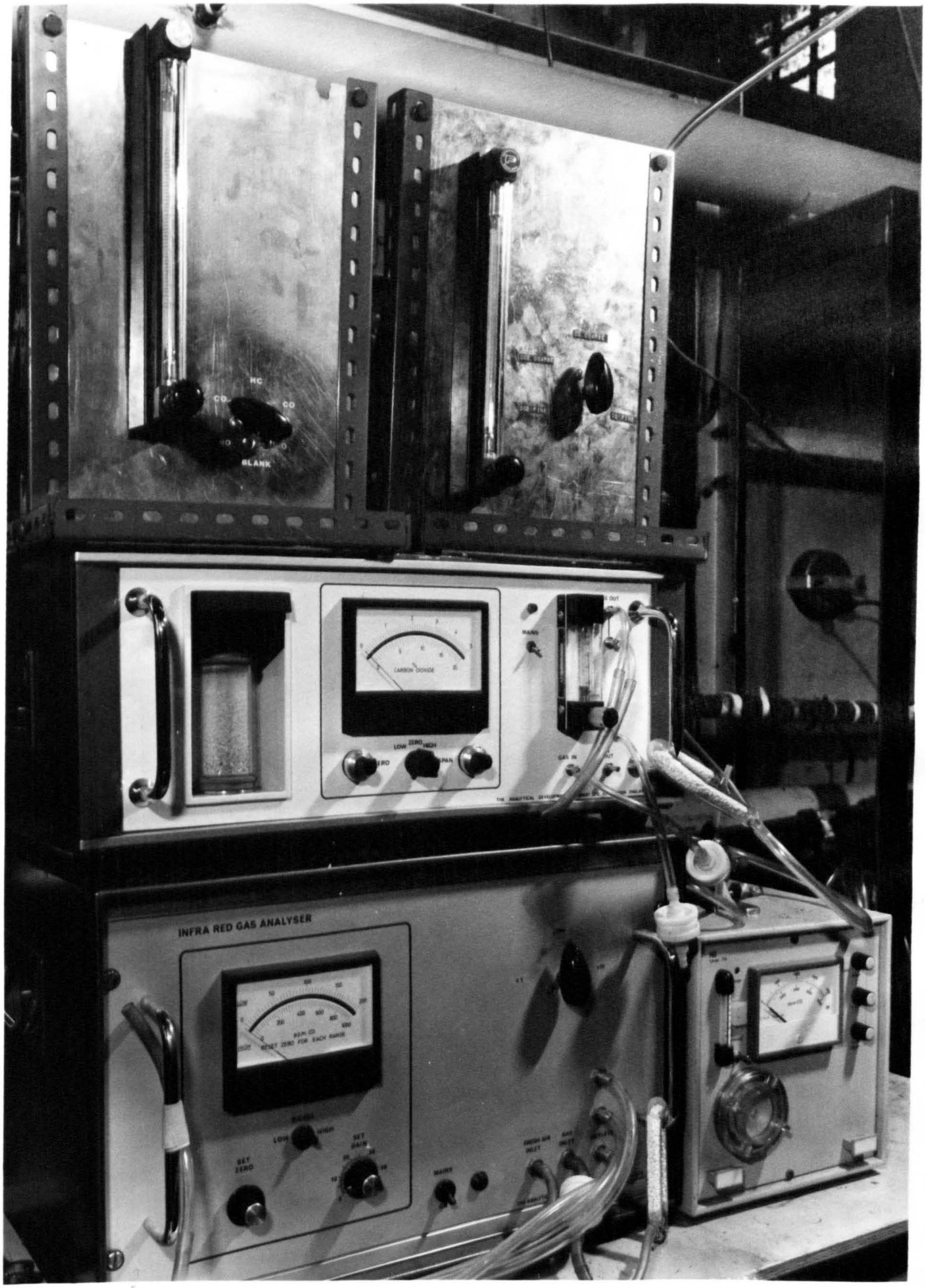

PLATE 2 CO and CO_2 gas analysers

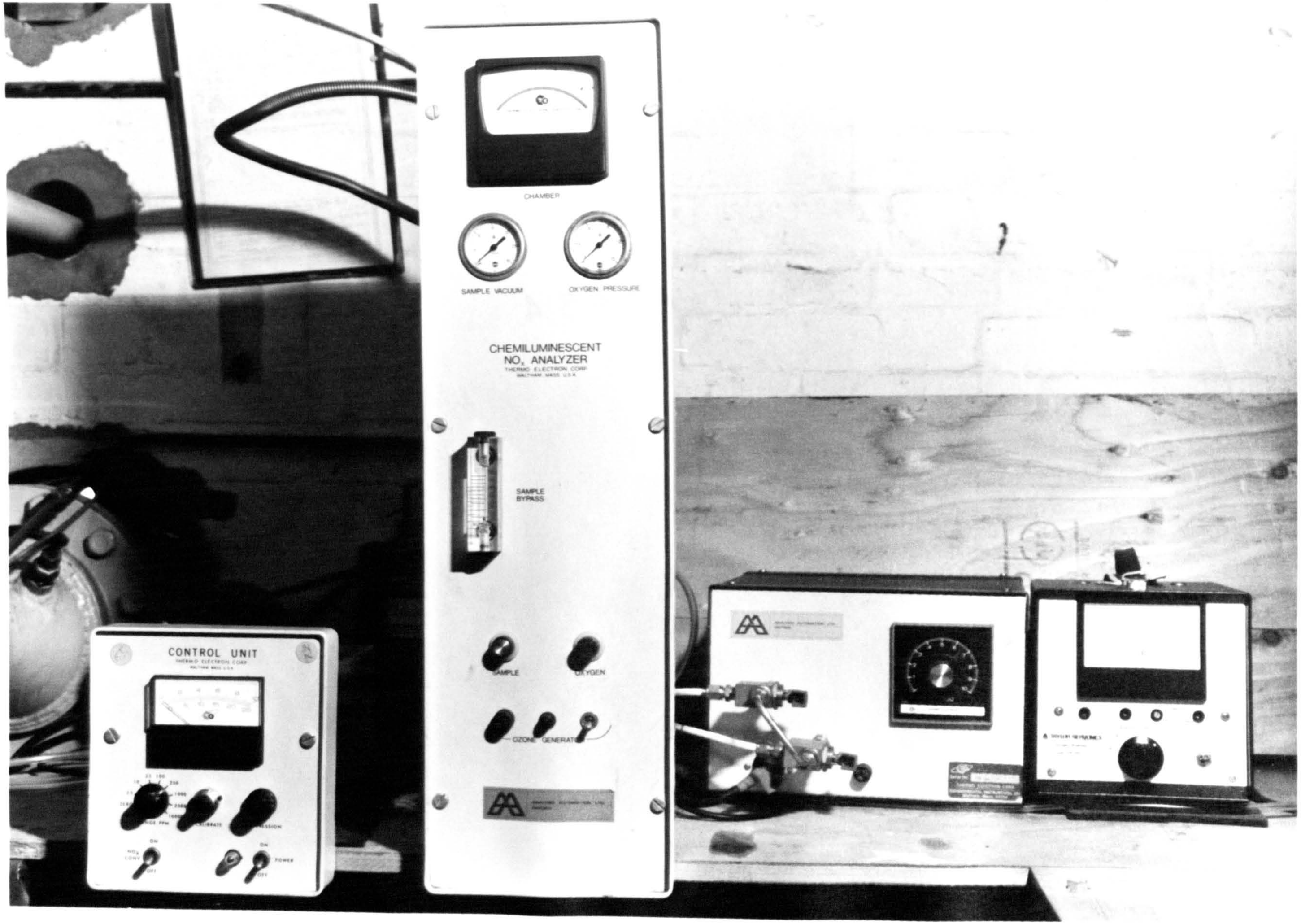

PLATE 3 NO_x and O_2 gas analysers